ISOLATION AND CHARACTERIZATION OF MUTANTS WITH ALTERED SENSITIVITY TO THE NATURAL ANTIMICROBIAL *TRANS*-CINNAMALDEHYDE IN *LISTERIA MONOCYTOGENES*

Lei Sun

Supervisor:
Prof. Chris Michiels, KU Leuven

Co-supervisor:
Prof. Abram Aertsen, KU Leuven

Members of the Examination Committee:

Prof. Erik Smolders, Chairman, KU Leuven
Prof. Hans Steenackers, KU Leuven
Prof. Dirk Springael, KU Leuven
Prof. Aurélie Crabbé, Universiteit Gent
Prof. Pierre Cornelis, Vrije Universiteit Brussel

Dissertation presented in partial fulfilment of the requirements for the degree of Doctor of Bioscience Engineering

August, 2022

Uitgegeven in eigen beheer, Lei Sun, Kasteelpark Arenberg 22 box 2457, B-3001 Leuven (Belgium)

Preface and acknowledgments

Four and half years ago, I officially started my scientific research life as a Ph.D. student in the Laboratory of Food Microbiology and now I am writing my Ph.D. thesis! This achievement would be unfeasible without all the support from many awesome people that I have met during my Ph.D. study.

First, I would like to sincerely acknowledge my supervisor Prof. Chris Michiels for providing me the great opportunity to join his research team. I have experienced a fulfilled and memorable research experience in the last four years, even during the COVID-19 pandemic period. He gave me a new and challenging topic to investigate the antimicrobial mechanism of thiol-reactive essential oil in *Listeria monocytogenes*. Before I joined his team, I had little experience in microbiology research, but he always explicitly explained my doubts and supported me through all the challenges. In addition, I thank him for the great input that he has done to review and edit my manuscripts. I learned a lot from his incredible writing skills and critical thinking. His sincere support and continuous guidance contributed immensely to my research and personal development and will certainly help me to further grow as a research scientist in the future.

Next, I would like to express my gratitude to my co-supervisor Prof. Abram Aertsen. His enthusiasm for research and creative thinking has inspired me tremendously. In addition, he provided numerous practical suggestions for my project and gave critical advice during each lab meeting. I also thank him for all the critical comments in reviewing my manuscript and for valuable suggestions to make it better.

Next to my supervisors, I would like to show my appreciation to all other members of the examination committee for their interest in my work and their precious input to comment on the manuscript. I thank Prof. Erik Smolders, for being a perfect Chairman, and Prof. Hans Steenackers, Prof. Dirk Springael, Prof. Aurélie Crabbé, and Prof. Pierre Cornelis for their valuable and critical comments, which undoubtedly meliorated the scientific quality of my Ph.D. thesis.

Then I want to express my thanks to a previous colleague, Gil Rogers. He was the first researcher in our laboratory who explicitly investigate *Listeria monocytogenes*. I

appreciate all the techniques and methods that he developed during his work to study *Listeria monocytogenes*, which paved the path of my research and saved mine time astronomically. In addition, his work also inspired my project tremendously and some of my initial ideas were established based on his extraordinary findings.

I would like to specifically thank Maarten Goedseels, who was in the lab the day I came to the laboratory. I am very grateful for all his assistance when I started my research life and all the experience of working with *Listeria monocytogenes* he shared with me. We discussed research questions together, exchanged our ideas, and overcame many obstacles. I also thank him for all the nice chats and fun times in the office.

A deep appreciation also goes to Kristof Vanoirbeek, the perfect lab manager. I thank him for his critical comments on my work and the numerous practical solutions he suggested when I met new challenges. I had asked so many stupid questions, but he always tried his best to come up with rapid and efficient solutions to keep my work on the right track. A heartfelt thanks also go to Lut for all the administration work.

Furthermore, I would like to express my deepest gratitude to those friendly, brilliant, and lovely colleagues! A special thanks to Marijke Poortmans, the perfect bench-mate in the world. Thank Dr. Elisa Gayán, Dr. Kim Tom Dongmin, Rafik Benhachemi, Sanne Wolput, Dr. Ines Staes, Dr. Julien Mortier, Alexander Cambré, Pinyi She, Leon Bäcker, Sadhana Khanal, Ronald Van Eyken, and Stefanie Van Riet for all the assistance in the laboratory. Thank you for all the help and discussions about work and life. I am glad to have you as my colleagues and good friends.

As an international student, my life in Leuven would be hard without the accompany of many important friends. I want to express my profound gratitude to all my friends in Leuven. Here, I would like to especially thank Xinlong Luo, who has given me so much encouragement and useful suggestions in both research and life and always acted like a big brother during my difficult times.

My imperishable gratitude goes to my parents and my sister for everything they have done to support me. Their encouragement and unconditional love are the power source to support my achievements during the last four years. I would also like to thank my lovely girl, Zhu Caiying, for all her unconditional support and encouragement during my Ph.D. study.

Last but not the least, I would like to appreciate the financial support from the Chinese Scholarship Council under grant #201607650020 and from *KU Leuven* during my Ph.D. study.

Lei Sun

August 2022

Summary

Listeria monocytogenes is a Gram-positive, rod-shaped, non-sporulating, and facultative aerobic member of the bacterial Firmicutes phylum, that causes relatively rare but severe foodborne infections. Foodborne listeriosis has a high hospitalization rate and case-fatality rate, particularly among susceptible persons such as elderly persons, immunocompromised individuals, pregnant women, and newborns. Furthermore, *L. monocytogenes* is a versatile and resilient organism that thrives well in many natural and man-made environments because of its capacity to grow over a wide range of adverse conditions including temperatures below 0°C and salt concentrations up to 10%. The organism is frequently found in raw materials of plant and animal origin used for food production, but it can also establish in the resident house microbiota of food production facilities, and as such, it is a common contaminant during food production and distribution. Prevention of foodborne listeriosis therefore aims at either eradicating the pathogen by heat treatment or preventing its outgrowth to high concentrations in unheated foods or foods that are subject to recontamination after heating.

To prevent the outgrowth of *L. monocytogenes*, but also other pathogens and spoilage organisms, artificial preservatives are widely used, especially in ready-to-eat foods. However, artificial preservatives are increasingly perceived by the consumer as foreign and undesirable additions. Some, like nitrites, are even under scrutiny for possible adverse health effects. In response to these concerns, plant essential oils and their constituents have attracted increased attention as possible alternatives because of their remarkable and broad antimicrobial properties. The present work focuses on *trans*-cinnamaldehyde (t-CIN), the major antimicrobial compound of cinnamon bark essential oil, which is known to inhibit many foodborne pathogens including *L. monocytogenes*, and that displays synergetic effects in combination with other food preservatives or processes. The antimicrobial capacity of t-CIN is thought to stem at least partially from its thiol-reactive α,β-unsaturated aldehyde moiety, but the antimicrobial mechanisms and cellular targets of t-CIN are not well established. An in-depth elucidation of these mechanisms and targets can provide a basis for developing more rational and effective food preservation strategies utilizing t-CIN.

A genome-wide random *Himar1* transposon mutant library of *L. monocytogenes* Scott A was previously constructed and screened in our laboratory, yielding several mutants with increased t-CIN sensitivity. Two of these mutants, *yvcK::Himar1* and *asnB::Himar1*, manifested severe cell shape deformation that was exacerbated by t-CIN. Also, a fraction of the cells in wild-type *L. monocytogenes* populations showed distortions upon exposure to a sub-lethal concentration of t-CIN. Although the functions of YvcK and AsnB in *L. monocytogenes* were not yet known, these observations suggested a possible role in the adaptation of *L. monocytogenes* to t-CIN by maintaining the cell wall integrity and homeostasis, and both mutants were therefore further studied.

The vulnerability of the *yvcK::Himar1* mutant to sublethal concentrations of t-CIN was demonstrated to be caused by increased bacterial lysis invoked by severely impaired cell wall integrity. Evolution experiments to restore t-CIN tolerance in the *yvcK* mutant resulted in suppressor mutations in several genes involved in the biosynthesis of the peptidoglycan precursor uridine-diphosphate-N-acetylglucosamine (UDP-GlcNAc), including the small RNA rli73 that locates immediately upstream of the *glmU-prs* operon, and *nagR*. GlmU catalyzes the last two steps of UDP-GlcNAc biosynthesis and NagR represses the uptake and utilization of GlcNAc. Overexpression of UDP-GlcNAc biosynthetic enzymes or supplying GlcNAc restored the t-CIN tolerance of the *yvcK* mutant, pointing to a pivotal role of YvcK in UDP-GlcNAc biosynthesis in *L. monocytogenes*, similar to its homolog in *B. subtilis*. An insufficient substrate flux into the UDP-GlcNAc biosynthesis pathway leading to a peptidoglycan synthesis defect can probably explain the hypersensitivity of the *yvcK* mutant towards t-CIN.

Loss of AsnB functionality resulted in the absence of amidated *meso*-Diaminopimelic acid (*m*DAP) residues in peptidoglycan, confirming that AsnB, like several of its homologs in Gram-positive bacteria, is a Gln-hydrolyzing amidotransferase that mediates the amidation of the ε-carboxyl group of *m*DAP. Deficiency in *m*DAP amidation caused several peptidoglycan- and cell surface-related phenotypes in the *asnB* mutant, including susceptibility to lysozyme, loss of flagellation and motility, and a strong reduction in biofilm formation. Moreover, AsnB inactivation also abrogated the proper cell wall anchoring of internalin A (InlA), an LPXTG motif-containing surface-exposed protein that normally cross-links to peptidoglycan via the free ε-amino group of *m*DAP, and that mediates host cell entry

during the infection process. As a result, the *asnB* mutant showed reduced invasion of human epithelial JEG-3 and Caco-2 cells.

As a complementary approach to the screening of the transposon mutant library, evolutionary experiments were performed by repeated passaging wild-type *L. monocytogenes* in a sublethal concentration of t-CIN to acquire spontaneous mutants with increased t-CIN resistance. All isolated mutants were found to contain amino acid substitutions in YhfK, a predicted oxidoreductase of the short-chain dehydrogenases/reductases superfamily that has homologs in several Gram-positive bacteria but whose function was unknown. Analysis of a *yhfK* deletion mutant demonstrated that this protein conferred tolerance of *L. monocytogenes* to several α,β-unsaturated aldehydes besides t-CIN. The mutant forms of YhfK obtained from the evolution experiment, however, elevated the tolerance to t-CIN, but not to other α,β-unsaturated aldehydes. Using GC-MS analysis, YhfK was shown to be required for the conversion of t-CIN to the less toxic 3-phenylpropanal in *L. monocytogenes* cultures, suggesting that it is an ene reductase. Deletion of the *yhfK* homolog also sensitized *Bacillus subtilis* to both t-CIN and *trans*-2-hexenal, suggesting a conserved function of YhfK in bacteria, possibly to cope with reactive and toxic α,β-unsaturated aldehydes in their environment. Ene reductases like YhfK may also have applications as stereoselective biocatalysts for the synthesis of valuable chemicals.

In conclusion, this work has generated novel insights into the effects of t-CIN and other α,β-unsaturated aldehydes on the foodborne pathogen *L. monocytogenes*. The biosynthesis of peptidoglycan precursors was identified as a target, and peptidoglycan *m*DAP amidation was demonstrated to be important for tolerance to these toxic compounds. Furthermore, a bacterial degradation pathway was identified that detoxifies the compounds. Finally, the work also for the first time implicates the amidation of peptidoglycan *m*DAP residues in cell wall anchoring of InlA and bacterial virulence, and as such illustrates that studying how bacteria cope with stress can result in unexpected novel fundamental insights.

Samenvatting

Listeria monocytogenes is een Gram-positieve, staafvormige, niet-sporulerende en facultatief aerobe bacterie van het Firmicutes phylum, die relatief zeldzame maar ernstige voedselinfecties veroorzaakt. Voedselgebonden listeriose kent een hoog aantal ziekenhuisopnames en een hoog sterftecijfer, met name bij gevoelige personen zoals ouderen, immuungecompromitteerde personen, zwangere vrouwen en pasgeborenen. Bovendien is *L. monocytogenes* een veelzijdig en robust organisme dat goed gedijt in veel natuurlijke en door de mens gemaakte omgevingen vanwege zijn vermogen om te groeien onder een breed scala aan ongunstige omstandigheden, waaronder temperaturen beneden 0°C en zoutconcentraties tot 10%. Het organisme wordt vaak aangetroffen in grondstoffen van plantaardige en dierlijke oorsprong die worden gebruikt voor voedselproductie, maar kan zich ook vestigen in de huismicrobiota van voedingsmiddelenbedrijven, en is daardoor een veel voorkomende contaminant tijdens voedselproductie en -distributie. Preventie van listeriose is daarom gericht op het elimineren van de ziekteverwekker door warmtebehandeling, of het voorkomen van uitgroei tot hoge concentraties in onverwarmde voedingsmiddelen of voedingsmiddelen die na verhitting opnieuw worden gecontamineerd.

Om de uitgroei van *L. monocytogenes*, maar ook andere pathogenen en bederforganismen, te voorkomen, worden vaak kunstmatige conserveermiddelen toegepast, vooral in kant-en-klare voedingsmiddelen. Kunstmatige conserveermiddelen worden echter door de consument steeds vaker gezien als vreemde en ongewenste toevoegingen. Sommige, zoals nitrieten, worden zelfs onder de loep genomen voor mogelijke nadelige gezondheidseffecten. Als reactie op deze zorgen krijgen plantaardige essentiële oliën en hun bestanddelen toenemende aandacht als mogelijke alternatieven vanwege hun opmerkelijke en brede antimicrobiële eigenschappen. Het huidige werk richt zich op *trans-cinnamaldehyde* (t-CIN), de belangrijkste antimicrobiële component van de etherische olie van kaneelbast, waarvan bekend is dat het veel voedselpathogenen inhibeert, waaronder *L. monocytogenes*, en dat synergetische effecten vertoont in combinatie met andere conserveermiddelen of -processen. De antimicrobiële capaciteit van t-CIN wordt verondersteld ten minste gedeeltelijk voort te komen uit de thiol-reactieve α,β-onverzadigde aldehydegroep, maar de antimicrobiële mechanismen en cellulaire doelwitten van t-CIN zijn niet goed gekend. Een diepgaande kennis van deze mechanismen en doelwitten kan een basis bieden voor het

ontwikkelen van meer rationele en effectieve strategieën voor het bewaren van voedsel met behulp van t-CIN.

Een genoombrede random *Himar1* transposon mutantenbibliotheek van *L. monocytogenes* Scott A werd eerder geconstrueerd en gescreend in ons laboratorium, wat verschillende mutanten met verhoogde t-CIN-gevoeligheid opleverde. Twee van deze mutanten, *yvcK::Himar1* en *asnB::Himar1*, vertoonden een ernstige celvervorming die werd versterkt door t-CIN. Ook een fractie van de cellen in wild-type *L. monocytogenes* populaties vertoonde vervormingen bij blootstelling aan een sub-letale concentratie van t-CIN. Hoewel de functies van YvcK en AsnB in *L. monocytogenes* nog niet bekend waren, suggereerden deze waarnemingen een mogelijke rol in de aanpassing van *L. monocytogenes* aan t-CIN door het behoud van de celwandintegriteit en -homeostase, en beide mutanten werden daarom verder bestudeerd.

De gevoeligheid van de *yvcK::Himar1* voor subletale concentraties van t-CIN bleek te worden veroorzaakt door verhoogde bacteriële lysis als gevolg van verminderde celwandintegriteit. Evolutie-experimenten om de t-CIN-tolerantie in de *yvcK-mutant* te herstellen resulteerden in suppressormutaties in verschillende genen die betrokken zijn bij de biosynthese van de peptidoglycan-precursor uridine-difosfaat-N-acetylglucosamine (UDP-GlcNAc), waaronder het “small RNA” rli73 dat zich onmiddellijk stroomopwaarts van het *glmU-prs* operon bevindt, en *nagR*. GlmU katalyseert de laatste twee stappen van de UDP-GlcNAc biosynthese, en NagR represseert de opname en het gebruik van GlcNAc. Overexpressie van UDP-GlcNAc biosynthetische enzymen of supplementatie met GlcNAc herstelde de t-CIN-tolerantie van de *yvcK* mutant, wat wijst op een centrale rol van YvcK in de UDP-GlcNAc biosynthese in *L. monocytogenes*, vergelijkbaar met het homoloog in *B. subtilis*. Een onvoldoende substraatflux in de UDP-GlcNAc biosyntheseroute met als gevolg een peptidoglycaansynthesedefect kan waarschijnlijk de overgevoeligheid van *yvcK-mutant* ten opzichte van t-CIN verklaren.

Verlies van AsnB functionaliteit resulteerde in de afwezigheid van geamideerde meso-diaminopimelzuur (mDAP) residuen in het peptidoglycan, wat bevestigt dat AsnB, net als verschillende van zijn homologen in Gram-positieve bacteriën, een Gln-hydrolyserend amidotransferase is dat de amidatie van ε -carboxylgroep van mDAP katalyseert. Deficiëntie in mDAP amidatie veroorzaakte verschillende peptidoglycaan- en celoppervlakgerelateerde fenotypen in de *asnB* mutant, waaronder gevoeligheid voor lysozym, verlies van flagellatie

en motiliteit en een sterke vermindering van biofilmvorming. Bovendien gaat AsnB inactivatie ook gepaard met een verlies van de celwandverankering van internaline A (InlA), een celoppervlakeiwit met een LPXTG motief dat normaalgezien crosslinks vormt met peptidoglycaan via de vrije ε-aminogroep van mDAP, en dat invasie van de gastheercel medieert tijdens het infectieproces. Als gevolg hiervan vertoonde de *asnB* mutant een verminderde invasie van menselijke epitheliale JEG-3 en Caco-2 cellen.

Als een complementaire benadering van de screening van de transposon mutantenbibliotheek, werden evolutionaire experimenten uitgevoerd door herhaalde passage van wild-type *L. monocytogenes* in een subletale concentratie van t-CIN, om spontane mutanten met verhoogde t-CIN-resistentie te isoleren. Alle bekomen mutanten bleken aminozuursubstituties te bevatten in YhfK, een voorspeld oxidoreductase van de “short-chain dehydrogenases/reductases” superfamilie dat homologen heeft in verschillende Gram-positieve bacteriën, maar waarvan de functie onbekend was. Analyse van een *yhfK* deletiemutant toonde aan dat dit eiwit in *L. monocytogenes* tolerantie verleende ten opzichte van verschillende α,β-onverzadigde aldehyden naast t-CIN. De gemuteerde vormen van YhfK verkregen uit het evolutie-experiment verhoogden echter enkel de tolerantie voor t-CIN, maar niet voor andere α.β-onverzadigde aldehyden. Met behulp van GC-MS analyse kon aangetoond worden dat YhfK nodig is voor de omzetting van t-CIN naar het minder toxische 3-fenylpropanal in *L. monocytogenes* culturen, wat suggereert dat het een 'ene-reductase' is. Deletie van de *yhfK* homoloog sensitiseerde ook *Bacillus subtilis* voor zowel t-CIN als t-hexenal, wat een geconserveerde functie van YhfK in bacteriën suggereert, mogelijk om zich te wapenen tegen reactieve en toxische α,β-onverzadigde aldehyden in hun omgeving. Ene-reductasen zoals YhfK kunnen ook toepassingen hebben als stereoselectieve biokatalysatoren voor de synthese van waardevolle chemicaliën.

Samengevat heeft dit werk nieuwe inzichten opgeleverd in de effecten van t-CIN en andere α,β-onverzadigde aldehyden op de voedselpathogeen *L. monocytogenes*. De biosynthese van peptidoglycaanprecursoren werd geïdentificeerd als een doelwit en mDAP-amidatie van peptidoglycaan bleek belangrijk te zijn voor de tolerantie voor deze toxische verbindingen. Bovendien werd een bacteriële afbraakroute geïdentificeerd die de verbindingen detoxificeert. Ten slotte wijst het werk ook voor het eerst op een rol van de amidatie van peptidoglycan mDAP-residuen in de celwandverankering van InlA en in

bacteriële virulentie, en illustreert als zodanig dat het bestuderen van hoe bacteriën omgaan met stress kan resulteren in onverwachte nieuwe fundamentele inzichten.

List of abbreviations

μmax	Maximum growth rate
4-HNE	4-hydroxy-2-nonenal
ATP	Adenosine triphosphate
ADH	Alcohol dehydrogenase
ALDH	Aldehyde dehydrogenase
Amp	Ampicillin
BHI	Brain Heart Infusion
cfu	Colony-forming units
Cm	Chloramphenicol
EOs	Essential oils
Ery	Erythromycin
FMN	Flavin mononucleotide
FtsZ	Filamenting temperature-sensitive mutant Z
FDA	Food and Drug Administration
GAPDH	Glyceraldehyde 3-phosphate dehydrogenase
GC-MS	Gas chromatography-mass spectrometry
GFP	Green fluorescent protein
GlcN-1-P	Glucosamine-1-phosphate
GlcNAc	N-acetylglucosamine
GlmM	Phosphoglucosamine mutase
GlmS	Glucosamine-6-phosphate synthase
GlmU	Bifunctional glucosamine-1-phosphate acetyltransferase/GlcNAc-1-phosphate uridyltransferase
GRAS	Generally recognized as safe
GrxA	Glutaredoxin
GSH	Glutathione
HS-SPME-GC-MS	Headspace solid phase micro-extraction gas chromatography mass spectrometry
IPTG	Isopropyl β-D-1-thiogalactopyranoside
Km	Kanamycin

LB	Luria-Bertani
LMW	Low-molecule-weight
MALDI	Matrix-assisted laser desorption ionization
MALDI-TOF MS	MALDI - time of flight mass spectrometry
*m*DAP	*meso*-Diaminopimelic acid
MEM	Minimum Essential Medium
MIC	Minimum inhibitory concentration
MOI	Multiplicity of infection
NAC	N-acetyl-L-cysteine
NADPH	Reduced nicotinamide adenine dinucleotide phosphate
NCBI	National Centre for Biotechnology Information database
ODmax	Maximal OD
OYE	Old Yellow Enzyme
PBS	Phosphate-buffered saline
PPB	Potassium phosphate buffer
PRPP	Phosphoribosyl pyrophosphate
Ribose-5-P	Ribose-5-phosphate
ROS	Reactive oxygen species
RP-UHPLC	Reverse phase-ultra high-pressure liquid chromatography
RT-qPCR	Reverse transcription-quantitative polymerase chain reaction
SD	Standard deviation
SDRs	Short-chain dehydrogenases/reductases
SEM	scanning electron microscopy
SOD	Superoxide dismutase
SrtA	Sortase A
t-CIN	*trans*-Cinnamaldehyde
t-HEX	*trans*-2-Hexenal
Trx	Thioredoxin
UDP-GlcNAc	Uridine-diphosphate-N-acetylglucosamine
WGS	Whole genome sequencing
WT	Wild-type
λ	Lag phase time

Table of contents

Chapter 1 Introduction and Scope of the Research

Trans-cinnamaldehyde (t-CIN), together with several other antimicrobial plant essential oils (EOs) constituents, has attracted tremendous attention in recent times for their potential as natural food preservatives. In this regard, the introduction chapter will mainly describe: (i) the current knowledge on the antimicrobial properties and potential antimicrobial mechanisms of t-CIN; (ii) the various protective strategies that might be employed by microorganisms to detoxify t-CIN as well as other α,β-unsaturated aldehydes; (iii) the scope and objective of this thesis.

1.1 t-CIN, a plant essential oil component and promising natural food preservative

Because microorganisms are omnipresent in the food production chain, their presence is inevitable in foods that are not sterilized, and preservatives are therefore used in some foods to prevent the outgrowth of spoilage organisms and pathogens to high numbers, especially in ready-to-eat foods. Acetic acid and acetates, sorbic acid and sorbates, sulfur dioxide and sulfites, benzoic acid and benzoates, propionic acid and propionates, and nitrites and nitrates are among the most commonly utilized preservatives in the food industry [1]. Despite their effectiveness, most of these preservatives are perceived by the consumer to be foreign and undesirable additions to the food because they are produced synthetically or derived from non-food sources. Moreover, several preservatives are suspected of causing adverse health effects [1]. Nitrites, in particular, are under scrutiny because they can react with secondary amines to form potentially carcinogenic nitrosamines, and food producers are exploring natural and safer alternatives to replace them [2].

Plant essential oils are aromatic and volatile plant extracts that have a long history of use in the flavors and fragrances industry for various applications including foods, but their potential as natural food preservatives has attracted increased attention over the last decades [3–6]. Many EOs are active against a wide range of foodborne microorganisms, and because of their complex composition, they compose an immense reservoir of natural antimicrobial compounds with potential applications [3–5]. More specifically, EOs are composed of a range of low-molecular-weight (LMW) organic metabolites with vast differences in structure,

chemical properties, and antimicrobial activity. The constituents are often classified according to their chemical structure and biosynthesis into terpenes, terpenoids (enzymatically modified terpenes), phenylpropenes, and those falling outside the aforementioned three groups (Fig. 1.1) [3,4]. Compounds that occur in many different EOs and whose antimicrobial properties have been extensively documented include thymol, carvacrol, citral, *trans*-cinnamaldehyde, eugenol, and allyl isothiocyanate (Fig. 1.1), and for some of these compounds, the mode of action has also been addressed and partly elucidated [4,5,7–11]. Knowledge of the mode of action can facilitate the regulatory approval and the development of highly effective applications of EOs and their constituents as natural food preservatives.

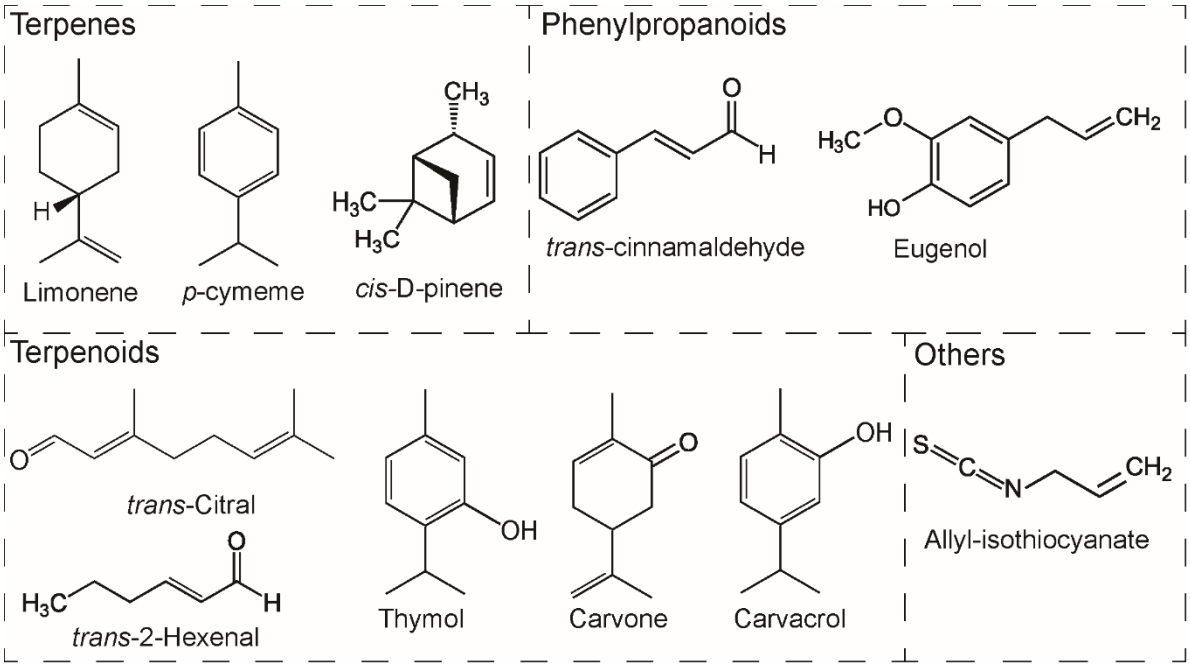

Figure 1.1 Chemical structures of selected constituents of EOs that have been demonstrated to exhibit pronounced antimicrobial properties [3,4].

1.2 t-CIN exhibits broad antimicrobial activity against food-borne pathogens

One of the best-studied antimicrobial essential oils constituents is t-CIN, the major component of cinnamon bark essential oil [12]. The cinnamon tree has long been used in traditional medicine in some Asian countries and as a source of spices for cooking all over the world [13]. Moreover, t-CIN is classified as GRAS (generally recognized as safe) by the

U.S. Food and Drug Administration (FDA) for use in foods (Code of Federal Regulations Title 21 Chapter 1). The most notable structural feature of t-CIN is the presence of an α,β-unsaturated aldehyde functional group, which confers electrophilic properties to the compound (Fig. 1.2) [14]. Besides t-CIN, a number of other plant EO compounds also contain the α,β-unsaturated carbonyl functional group and exhibit a broad and promising antimicrobial activity, such as *trans*-2-hexenal, citral, and carvone [3–5,10,15,16] (Fig. 1.2). Like t-CIN, these compounds impart typical flavors to several plants or plant parts, and they have applications in the perfumery, food, and flavor industry.

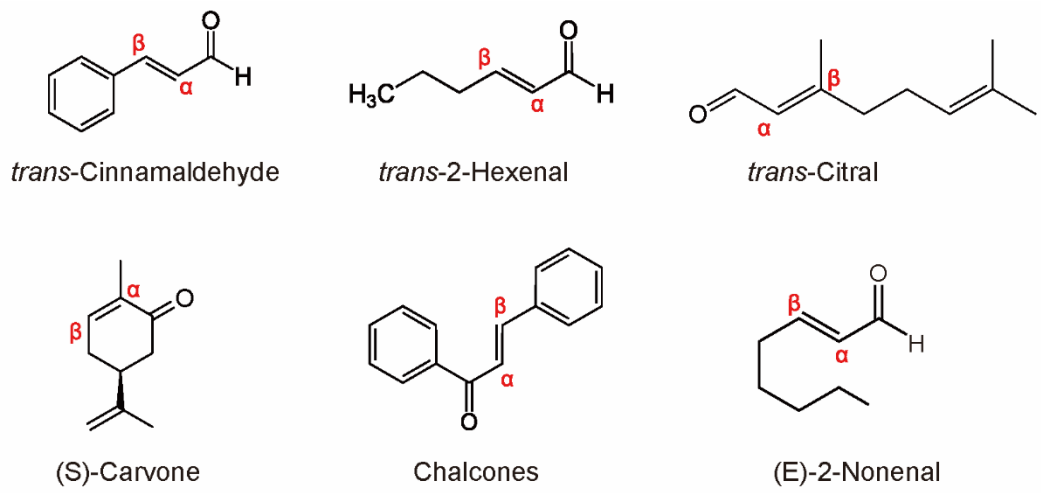

Figure 1.2 Chemical structures of selected plant essential oil constituents with α,β-unsaturated carbonyl functional group and showing promising antimicrobial activity.

The antimicrobial properties of t-CIN have been demonstrated across an array of foodborne Gram-positive and Gram-negative bacteria, and fungi (Table 1.1). Regarding *L. monocytogenes*, previous work in our laboratory showed that the growth inhibition by t-CIN is typically characterized by a dose-dependent elongation of the lag phase when the pathogen was cultivated in Brain Heart Infusion (BHI) broth [17] (Fig. 1.3). An elongated lag phase was also observed for *Escherichia coli* at a sublethal concentration of t-CIN [18]. Furthermore, the exposure of *L. monocytogenes* to t-CIN also induced reduced μmax and ODmax when grown in BHI. The t-CIN-induced growth suppression provides a prospect of the compound in extending the shelf-life of food products, especially for ready-to-eat foods. It should be underlined that the optical density measurements used in Fig. 1.3 have a lower sensitivity limit of approximately 10^7 cfu/mL or above, while the growth assays were conducted with an

initial cell density of approximately 10^6 cfu/mL, resulting in a blind spot for the lag phase period.

Efforts were taken in our laboratory to identify the primary causes of the lag phase extension when exposed to t-CIN [19]. Possible causes include: (i) the gradual degradation of t-CIN to sub-inhibitory concentrations in BHI broth that allow bacterial growth resumption; (ii) the emergence of t-CIN resistant mutants; (iii) the adaptation of bacterial cells to t-CIN. The evolution of t-CIN concentration (the initial concentration was 1 mM) in BHI broth was monitored with headspace solid-phase micro-extraction gas chromatography-mass spectrometry analysis. A stable but slow t-CIN degradation was observed and about 90% of t-CIN still remained in the culture of wild-type strain at the end of the lag phase. The 10% loss of t-CIN was speculated to be at least partly due to the conjugation with nucleophiles present in the medium since it also occurred in sterile BHI broth (described in [19], p64). However, evaporation, adhesion to the container surface, and uptake and metabolization by bacteria might also contribute to the reduced t-CIN concentration in the culture. Furthermore, the appearance of t-CIN resistant mutants was ruled out by comparing the growth of parental wild-type strain with their progeny that had been subcultured (1:1000 dilution) for four consecutive rounds in BHI broth with 4 mM t-CIN. Lastly, plate count analysis demonstrated steady cell numbers of *L. monocytogenes* wild-type strain during the lag phase in BHI broth with 4 mM t-CIN, excluding the transient killing upon exposure to t-CIN. Taken together, the extended lag phase and the subsequent resumption of growth were hypothesized to be most likely because of bacterial adaption [19].

The minimum inhibitory concentrations (MICs) have frequently been adopted to evaluate the resistance or vulnerability of specific microbial strains to certain antimicrobial compounds and are commonly defined as the lowest dose of the antimicrobial that prevents the visible growth of the tested microorganism after incubating overnight [20]. The determined MIC values of t-CIN against various microorganisms fall in a wide range (0.6 - 7.6 mM). Notably, MIC values can vary between different studies even for the same microorganism because of differences in methods, experimental conditions like growth medium and temperature, and interpretation of the results [3]. The disk diffusion, agar dilution, and broth dilution (via measuring the turbidity or enumerating the colonies) methods have been repeatedly applied to determine MICs of EOs [3].

Like many other antimicrobial EO components, t-CIN has many different effects on microbial cells, including alteration of the cell morphology [21–23], inhibition of cell division [21,22] and growth [14,17,24–26], suppression of biofilm-forming ability [24,26–28] and damaged cell membrane integrity [17,18,23,25,29]. These effects against various foodborne microorganisms, both prokaryotic and eukaryotic, will be extensively reviewed in the next section.

Table 1.1 Selected studies of the antimicrobial properties of t-CIN against foodborne microorganisms.

Microorganism	MIC*	Reported antimicrobial effect
Gram-positive		
Listeria monocytogenes	MIC: 0.9 mM [30]; 640 μg/mL(4.8 mM) [28].	Inhibition of bacterial growth [17]; inhibition of swimming and swarming motility [28]; reduced intracellular adenosine triphosphate (ATP) content [31]; damaged membrane integrity [17,23,32] ; inhibition of biofilm formation [28].
Staphylococcus aureus	MIC: 250 μg/mL (1.9 mM) [33,34]; 0.31 mg/mL (2.4 mM)[23]; 1 g/L (7.6 mM) [25].	Inhibition of bacterial growth [34]; damaged bacterial cell morphology [23]; alteration of cell membrane fatty acids composition [35]; damaged membrane integrity and permeability [23].
Bacillus cereus	n.a.	Inhibition of bacterial growth and strong inhibition of cell separation (0.3 mL/L, i.e. 2.4 mM t-CIN) [21].
Clostridium difficile	MIC: 80 μg/mL (0.61 mM) [36].	Inhibition of bacterial proliferation [36].
Gram-negative		
Salmonella Typhimurium	MIC: 312 μg/mL (2.4 mM) [27].	Inhibition of bacterial growth and disruption of preformed biofilm [27]; alteration of cell membrane fatty acids composition [35].
Pseudomonas fluorescens	MIC: 0.125 μL/mL (1 mM) [37].	Inhibition of bacterial growth, swimming and swarming motility, quorum sensing, and biofilm formation [37]; alteration of cell membrane fatty acids composition [29].
Campylobacter jejuni	MIC: 2.27 mM [26].	Inhibition of bacterial growth, motility, and biofilm formation; inactivation of mature biofilm [26].
Escherichia coli	MIC: 240 mg/L (1.9 mM) [11]; 310 mg/L (2.4 mM) [18,23,38]; 500 mg/L (3.8 mM) [39]; 1 g/L (7.6 mM) [25].	Inhibition of bacterial growth [11,18,22,38]; inhibition of bacterial motility [7]; reducing intracellular ATP content [31]; alteration of cell membrane fatty acids composition [29]; inducing damaged membrane integrity and permeability [18,23,25]; damaged bacterial cell morphology [23,25].
Fungi		
Aspergillus flavus	MIC: 78 mg/L (0.6 mM) [38]; 0.065 mg/mL (0.5 mM) [39]; 0.8 mM [40].	Inhibition of mycelial growth, biomass production, spore production and germination, and aflatoxin biosynthesis [9,40–42].
Penicillium italicum	MIC: 313 μg/mL (2.4 mM) [43].	Inhibition of mycelial growth, increased membrane permeability, damaged membrane integrity, and cell wall integrity [43].
Geotrichum citri-aurantii	MIC: 0.5 μL/mL (4 mM) [44]	Inhibition of the cell growth and disruption of the cell wall integrity [44].

*MIC: the lowest dose of an antimicrobial compound that prevents the visible growth of the tested microorganism after incubating overnight [3]. MICs are determined in standardized laboratory growth conditions that support the good growth of the tested organism. However, conditions like temperature, culture medium, etc. may vary.

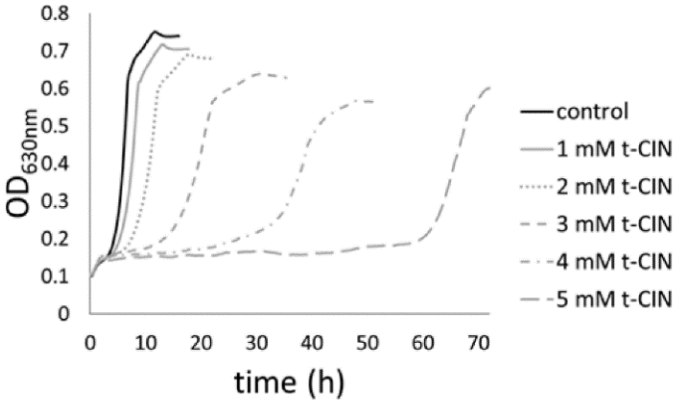

Sample	λ (h)	μ_{max} (1/h)	OD_{max}
Control (t-CIN)	4.4 ± 0.1	0.187 ± 0.002	0.754 ± 0.020
1 mM t-CIN	5.5 ± 0.2	0.137 ± 0.001	0.718 ± 0.021
2 mM t-CIN	7.9 ± 0.2	0.096 ± 0.001	0.693 ± 0.027
3 mM t-CIN	14.9 ± 0.6	0.054 ± 0.004	0.641 ± 0.018
4 mM t-CIN	31.2 ± 0.2	0.033 ± 0.002	0.568 ± 0.015
5 mM t-CIN	61.8 ± 0.2	0.053 ± 0.001	0.587 ± 0.014

Figure 1.3 Growth curves of *L. monocytogenes* Scott A in BHI broth with different concentrations of t-CIN (obtained from [19]). Lag phases (λ), growth rates (μmax), and maximum optical densities (ODmax) are represented as means ± standard deviation (SD).

t-CIN was also demonstrated to exert inhibitory activities against a wide variety of fungi, and some studies reporting on these effects are listed in Table 1.1. In *Aspergillus flavus*, dose-dependent inhibition of spore germination and mycelial growth was reported, and t-CIN also suppressed spore production and germination [41]. Interestingly, the production of mycotoxins was also suppressed in some fungi such as this of aflatoxin B_1 in *A. flavus* [9,40,42]. In *A. flavus,* for example, aflatoxin B_1 production by mycelia was reduced by 68.9 % after 5 days in 0.4 mM t-CIN (~53 mg/L), a concentration that did not significantly inhibit mycelial growth. Analysis by real-time PCR analysis showed that the expression of the key aflatoxin biosynthesis genes *aflM*, *aflD*, *aflR*, *aflP*, and *aflT* was significantly suppressed [42]. In a follow-up study from the same research group, a genome-wide transcriptomic analysis confirmed the downregulation of most of the structural genes of the aflatoxin biosynthesis cluster and proposed a complex regulatory cascade to explain this effect [9].

1.3 The antimicrobial effects of t-CIN

In general, the antimicrobial capacity of t-CIN is thought to stem at least partially from its electrophilic and lipophilic character, but the specific intracellular targets of t-CIN in microorganisms are not well established. To dissect the antimicrobial mode of t-CIN, dozens of studies have been conducted with different methods and in various Gram-positive and Gram-negative bacteria as well as in fungi. These studies, of which a selection are listed in Table 1.2, have reported the perturbance of different cellular structures, homeostatic systems and functional properties, including an increased cell membrane permeability resulting in intracellular content leakage [18,23,25,32], inhibition of the membrane-associated ATPase activity [31], the elevation of intracellular redox stress [7,11,18,39], inhibition of filamenting temperature-sensitive mutant Z (FtsZ, a cell division protein) polymerization and cell division [21,22], suppression of the expression of motility-associated genes [11,26,30,45] and quorum sensing system-related genes [28,37,46–48], and disruption of cell wall homeostasis [23] (Fig 1.4). It is important to note that these effects may depend on the target organism, the t-CIN concentration, and other experimental conditions [14]. Nevertheless, the wide variety of observed effects suggests that t-CIN, unlike typical antibiotics, does not have a very specific target but interferes with multiple structures and/or processes in the cell. It is also important to note that many of the reported effects of t-CIN,

like cellular leakage and induction of redox stress, are quite general and may be secondary effects resulting from damage to the primary cellular targets that still need to be identified.

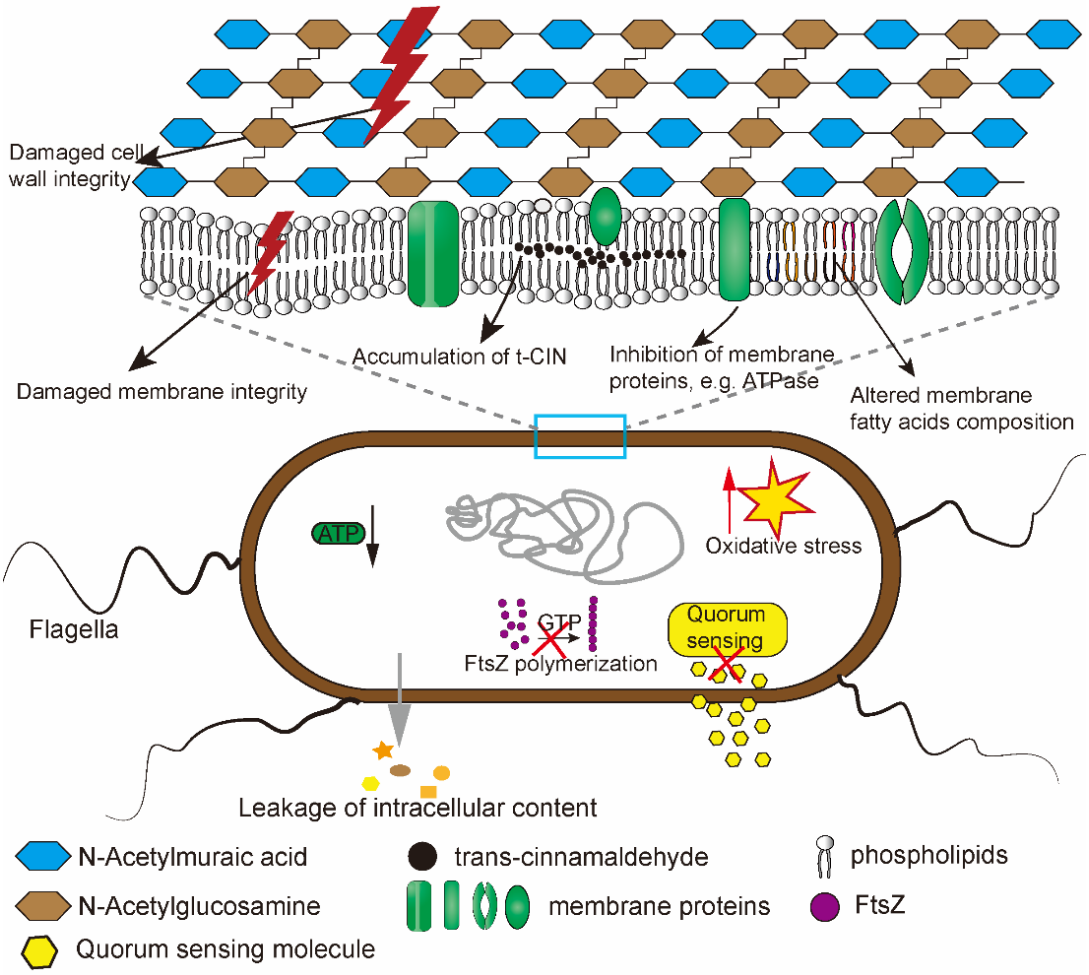

Figure 1.4 Summary scheme showing reported effects of t-CIN on bacterial cellular structure and function.

Table 1.2 Proposed antimicrobial mechanisms of t-CIN against foodborne pathogens. The concentrations of t-CIN applied in the studies are specified between brackets.

Microorganism	Mode of action
Bacteria	
Listeria monocytogenes	Depletion of intracellular ATP by inhibition of membrane-bound ATPase (10 mM) [31]; repression of bacterial motility-associated genes (0.75 mM) [30]; alteration of membrane fatty acid profile and reduction of membrane fluidity (2 mM) [17].
Staphylococcus aureus	Increase in cell membrane permeability and intracellular content leakage; perturbation of cell wall integrity (0.31 mg/mL, i.e. 2.4 mM) [23].
Bacillus cereus	Inhibition of cell separation (0.3 mL/L, i.e. 2.4 mM t-CIN) [21].
Escherichia coli	Depletion of intracellular ATP by inhibition of membrane-bound ATPase (> 0.1 mM) [31]; increase in cell membrane permeability and intracellular content leakage (0.31 mg/mL, i.e. 2.4 mM) [23]; perturbation of cell wall integrity (0.31 mg/mL, i.e. 2.4 mM) [23]; disruption of FtsZ polymerization and inhibition of cell separation (100 µM) [22]; elevation of intracellular oxidative stress (0.6 - 1.5 mM) [7,11,39]; interference with carbohydrate metabolism (80 mg/L, i.e. 0.6 mM) [11]; repression of bacterial motility-associated genes (80 mg/L, i.e. 0.6 mM) [11].
Salmonella Enteritidis	Repression of bacterial motility-associated genes (0.75 mM) [45].
Campylobacter jejuni	Repression of bacterial motility-associated genes (0.75 mM) [26].
Pseudomonas fluorescens; Pseudomonas aeruginosa	Repression of quorum sensing system and motility (0.025 – 0.1 µL/mL, i.e. 0.2 – 0.8 mM) [35]; repression the expression of quorum-sensing regulatory genes (2.27 mM) [47].
Fungi	
Aspergillus flavus	Damage to plasma membrane integrity, increased cell membrane permeability and intracellular content leakage (> 0.065 mg/mL, i.e. 0.5 mM) [41]; decreased mitochondrial membrane potential and attenuated mitochondrial function (> 0.065 mg/mL, i.e. 0.5 mM) [41]; elevation of intracellular ROS and depletion of NADPH (> 0.5 mM) [9,40,41]; interference with cell wall biosynthesis (0.6 mM) [9].
Aspergillus niger;	Damage to membrane integrity and cell ultrastructure; induction of intracellular oxidative stress (> 50 µg/mL, i.e. 0.38 mM) [49].

Penicillium italicum	Damage to plasma membrane integrity, increased cell membrane permeability, and intracellular content leakage; damage to cell wall integrity; accumulation of ROS and disruption of mitochondrial function (> 0.313 µg/mL, i.e. 2.4 mM) [43].
Geotrichum citri-aurantii	Interference with cell wall biosynthesis, repression of cell wall integrity-related genes, and damage to cell wall integrity (0.25 µL/mL, i.e. 2 mM) [44].

1.3.1 Inhibition of cell division by t-CIN

Defects in cell division as a result of t-CIN exposure have been reported in *E. coli* and *Bacillus cereus*. Scanning electron microscope analysis revealed a filamentous morphology when exponential phase *B. cereus* cells were incubated with t-CIN (0.3 mL/L, i.e. 2.4 mM t-CIN) at 37°C for 1 h in 0.85% NaCl [21]. Although septa were formed between the cells, their formation seemed to be incomplete, and the cells did not separate. Remarkably, no important morphology difference was induced in *Staphylococcus aureus* cells in the same conditions [21]. This might be because of a higher tolerance of *S. aureus* to t-CIN or because of differences in the cell division process (*B. cereus* is rod-shaped and *S. aureus* is coccus-shaped). Elongated cell morphology was also induced in *E. coli* treated for 75 min with 100 µM t-CIN, which is a sub-inhibitory concentration for bacterial growth [22]. The average cell length of the treated cells was doubled compared to the untreated controls. Confocal imaging showed that t-CIN at this concentration disrupted the Z-ring morphology and reduced the Z-ring occurrence per unit cell length of *E. coli* cells. The same authors further found that t-CIN at a similar concentration significantly suppressed the bundling of FtsZ protofilaments and FtsZ GTPase activity in a dose-dependent manner *in vitro* experiments. The FtsZ inhibitory activity of t-CIN is probably the most specific mode of action suggested for t-CIN in the literature, but unfortunately, it has not been confirmed since the study conducted by Domadia et al. [22].

1.3.2 Morphological disruption and cell wall damage

Shen et al. [23] found that treating *E. coli* or *S. aureus* cells with t-CIN at the MIC (0.31 mg/mL, i.e. 2.3 mM) for 6 - 8 h elicited cell wall and cell membrane changes, including separation of the cytoplasmic membrane from the cell wall, cell shape distortion and deterioration of the cell wall and cell membrane. In contrast, no obvious morphological changes of *S. aureus* were revealed by Kwon et al. [21] at a similar concentration, but these authors applied a much shorter exposure time to t-CIN. Morphological alterations and cell wall integrity damage are also frequently reported in fungal cells treated with t-CIN. Deformed mycelium ultrastructure and disrupted cell wall integrity were induced in *Aspergillus ochraceus* treated with a subinhibitory concentration of t-CIN [50]. OuYang et al. [44] also revealed that treatment of *Geotrichum citri-aurantii* with 1/2x MIC (0.25 mL/L, i.e. 2 mM) of t-CIN induced a disrupted cell wall structure. Furthermore, an uneven distribution of chitin and a dramatic decrease of chitin content in the cell wall in line with a

significant repression of chitin synthases genes (*chsA*, *chsB*, *chsG*, and *UAP1* and *CHS2*) were induced in *G. citri-aurantii* after a 30 min exposure to 1/2x MIC t-CIN, suggesting a potential interference of t-CIN in fungal cell wall construction. Chitin is a β(1,4)-linked N-acetylglucosamine polymer that is indispensable in the cell wall of many fungi including all major human pathogens [51]. An *in vitro* study showed that t-CIN inhibited the activity of *β*-(1,3)-glucan synthase and chitin synthase I, two cell wall synthesizing enzymes of *Saccharomyces cerevisiae*, with a 50% inhibitory concentration of 0.84 and 1.44 mM respectively [52].

1.3.3 Cell membrane damage

The bacterial cytoplasmic membrane is composed of a phospholipid bilayer in which proteins with various functions are embedded. It is a selective permeability barrier that controls molecular transport in and out of the cell, and it supports the establishment of a transmembrane electrochemical gradient that generates ATP and powers many important cell functions, coordinates cell division, and supports the function of various membrane-attached proteins. While the cell membrane is one of the most important barriers against the access of antimicrobial molecules to the cytoplasm, it is at the same time a target of hydrophobic EO compounds such as t-CIN [3–5]. The adverse effects of these compounds include changes to the membrane fatty acid composition and fluidity, disruption of the membrane integrity leading to increased membrane permeability and leakage of cytoplasmic content, and loss of membrane potential [3–5,29]. Unlike Gram-positive bacteria, Gram-negative bacteria possess a distinct bilayer outer membrane that acts as an additional selective permeability barrier and protects the bacteria from detergent-like molecules and hydrophobic antimicrobials [53,54]. This outer membrane might affect the resistance of bacteria against hydrophobic antimicrobial EO compounds as well. Nowotarska et al. [55] evaluated the interaction of three EO compounds, namely t-CIN, geraniol and carvacrol, with monolayers composed of bacterial phospholipids as a membrane model and found that all three EOs integrated into the monolayers and formed aggregates with lipids which consequently altered the membrane fluidity and packing effectiveness of lipids. Therefore, it can be anticipated that lipophilic EO compounds accumulate in the hydrophobic core of the cell membrane, and from there diffuse to the aqueous-phase extracellular space and cytosol. The compounds can thus impair the integrity and composition of the membrane as well as membrane proteins as a result of direct interactions between the membrane and hydrophobic parts of the proteins or an altered

hydrophobic environment around these proteins. Importantly, the compounds may also affect targets in the cytosol.

The membrane-perturbing activity of t-CIN has been noted in a number of studies on both Gram-positive and Gram-negative bacteria (Table 1.1). Our research group observed a modulated membrane fatty acid composition in *L. monocytogenes* Scott A upon addition of 2 mM t-CIN (sub-MIC concentration) during growth at 30°C with GC-MS analysis of whole-cell fatty acids [17]. More specifically, t-CIN decreased the fraction of the *anteiso* branched-chain fatty acids (from 63.4% to 32.9%) and increased the *iso*-branched-chain fatty acids fraction (from 20.1% to 33.9%), resulting in an overall reduction of branched-chain fatty acids fraction by 17%. Furthermore, inactivation of *ilvE*, a key gene involved in the biosynthesis of branched-chain fatty acids in rich culture media, confers hypersensitivity of *L. monocytogenes* to t-CIN, manifested as a significantly extended lag phase [17]. Further analysis suggested a direct link of the t-CIN sensitivity of the *ilvE* mutant with its altered membrane fatty acid composition, featuring an almost complete absence of *anteiso* branched-chain fatty acids and elevated levels of unbranched saturated fatty acids and *iso*-branched-chain fatty acids. Exposure of the *ilvE* mutant to a sub-MIC concentration (2 mM) of t-CIN further reduced the percentage of branched-chain fatty acids in the membrane by nearly 30%. Since branched-chain fatty acids, in particular the *anteiso* fraction, are essential in maintaining the fluidity of the cell membrane in *L. monocytogenes*, the *ilvE* mutant's membrane can be predicted to be more rigid. Since t-CIN was suggested to be capable of integrating into the membrane and altering the membrane fluidity and packing effectiveness of lipids [55], the adaptive changes in the fatty acid composition of *L. monocytogenes* in the presence of t-CIN may be considered as a response of the bacteria to counteract this effect [17]. Altogether, these results suggested a crucial role of membrane fatty acid composition in the bacterial sensitivity to sub-lethal concentrations of t-CIN. Alterations of unsaturated fatty acids composition in the cell membrane of different bacteria by sublethal concentrations (~ 0.64 - 2.38 mM) of t-CIN were reported by Di Pasqua et al. [29] as well. In *E. coli* O157:H7 and *Brochothrix thermosphacta*, t-CIN elevated the content of unsaturated fatty acids while no significant change on the degree of saturation was observed in *Salmonella enterica* serovar Typhimurium and *Pseudomonas fluorescens*. For *S. aureus*, however, t-CIN even reduced the unsaturated fatty acid content in the membrane. In addition to t-CIN, several other hydrophobic EO compounds such as thymol, hexenal and carvacrol were shown to influence membrane fatty acid composition in different bacteria species [29,56]. These findings suggest

that the modulation of membrane fatty acid composition might be a common response of bacteria species to the presence of small hydrophobic EO components.

While the modulation of cytoplasmic membrane composition has been well documented at sub-lethal concentrations of t-CIN, higher concentrations -near or above the MIC value, lead to changes in membrane integrity and permeability, increased leakage of cytoplasmic content, and ultimately cell death [14]. The membrane permeability of microorganisms is often monitored by measuring leakage of cytoplasmic components such as potassium, protein, ATP, or genetic material (DNA and RNA), which indicates membrane integrity disruption [3–5]. A significant release of cytoplasmic content was noted when *E. coli* was treated with Chinese cinnamon oil or t-CIN at or above their MIC [23,25,32]. A more recent study also reported cell membrane permeabilization based on the elevated electrical conductivity of *E. coli* ATCC 25922 suspensions after exposure to relatively high concentrations (1x, 2x, 4x MIC) of t-CIN for several hours [18]. In contrast, t-CIN at sub-inhibitory concentration (1/8x, 1/4x, 3/8x, 1/2x MIC) only slightly raised the electrical conductivity. An enhanced release of the cytoplasmic content was revealed when *L. monocytogenes* was treated with cinnamon oil at MIC as well [32]. Furthermore, loss of membrane permeability and membrane integrity were recorded when *S. aureus* was treated with t-CIN at MIC (0.3 - 1 mg/mL, i.e. ~ 2.4 - 7.6 mM), as indicated by the significant leakage of proteins, increased electrical conductivity of the culture supernatant, and abnormal cell membrane morphology [23,25].

The effects of t-CIN on the fungal plasma membrane were also studied. Significant leakage of intracellular proteins and potassium ions was induced when *Penicillium italicum* mycelium was treated with t-CIN at 1/2x MIC and MIC for a short time (0.5 h - 2 h), indicating an elevated membrane permeability [43]. Likewise, t-CIN also caused a perturbation of the cytoplasmic membrane in *A. flavus* and *A. niger* cells [41,49]. Up to 0.52 mg/mL (3.9 mM) (MIC = 0.065 mg/mL, i.e. 0.5 mM), the release of intracellular contents and the uptake of propidium iodide increased, suggesting dose-dependent damage on the membrane integrity by t-CIN [41]. Notably, the content of ergosterol, a key component for controlling the fluidity and permeability in fungal cell membranes [57], decreased in a dose-dependent manner in *A. flavus*, *A. niger* and *A. ochraceus* at different concentrations of t-CIN [41,49,58]. Further supporting this observation, transcription of several genes related to the ergosterol biosynthesis pathway was repressed when *A. flavus* was treated with t-CIN [9].

Also in *A. ochraceus*, 100 µg/mL (0.76 mM) of t-CIN and 200 µg/mL (1.31 mM) of citral completely inhibited the ergosterol biosynthesis [58]. However, in contrast to these observations, the treatment of *G. citri-aurantii* with 0.25 mL/L (1/2x MIC, 2 mM) of t-CIN induced an increased content of total lipids and ergosterol [44].

1.3.4 Suppression of cellular ATP level

A reduction of the intracellular ATP level that was not due to membrane leakage has been reported in several studies with both bacteria and fungi, but the underlying mechanism is unclear. When *E. coli* and *L. monocytogenes* cells were exposed to 1/2x MIC of cinnamon EO, a 44% and 36% decline of intracellular ATP concentration was induced, respectively, while the extracellular ATP concentration remained constant and at a low level, indicating that the intracellular ATP did not leak away through the membrane [32]. However, whether the growth retardation of bacteria at the sublethal concentration of t-CIN was directly related to the reduced intracellular ATP supply remains undetermined. Using an *in vitro* assay, Gill and Holley [31] demonstrated that t-CIN inhibited the activity of the membrane-bound ATPase of *E. coli* in a dose-dependent manner, even at concentrations that are subinhibitory for growth (0.1 - 1 mM). Nevertheless, whether this inhibition was due to a specific or non-specific interaction between t-CIN and the ATPase remains unknown. In *L. monocytogenes*, the inhibition of the membrane ATPase was only observed at t-CIN concentrations of 5 - 10 mM [31], which are bactericidal in our experience. Therefore, cellular ATP depletion in *L. monocytogenes* at the sublethal concentration (< 2 mM) is unlikely due to direct interference of t-CIN with the membrane-bound ATPase. However, the t-CIN-induced membrane damage and membrane permeability, as discussed above, may exert an indirect effect on the intracellular ATP levels by disturbing cellular homeostasis and thus elevating the cellular energy expenditure. A more recent study of late exponential phase *E. coli* cells treated with 1/3x MIC (80 mg/L, i.e. 0.6 mM) of t-CIN for 1 and 2 h also observed a decline of ATP concentration after the treatment, but no differential expression of genes involved in the assembly of the ATP synthetase complex was noticed by the proteomic analysis [11]. This is inconsistent with the proteomic analysis conducted by Silva et al. [27] who claimed that the expression of F0F1 ATP synthase subunits beta and alpha in *S.* Typhimurium biofilm were significantly downregulated by the t-CIN treatment (624 mg/L (2x MIC, i.e. 4.72 mM), at 37°C for 1 h). However, since this observation was made at a t-CIN concentration well above

the MIC, macromolecular synthesis is unlikely to occur, and the results may reflect selective protein degradation rather than differential expression.

In fungi, mitochondria generate most of the intracellular ATP, and damage to these organelles by t-CIN was noted in several studies, especially at a relatively high concentration (≥ MIC). More specifically, a dose-dependent release of cytochrome c from the mitochondria to the cytoplasm was observed when *A. flavus* was treated with t-CIN up to 0.52 mg/mL (3.9 mM) (MIC = 0.065 mg/mL, i.e. 0.5 mM) [41]. Even at a sub-MIC concentration (0.033 mg/mL, i.e. 0.25 mM) of t-CIN, the level of cytochrome c in the mitochondria was significantly decreased, which could affect the functionality of mitochondria given the role of this protein in the mitochondrial electron transport chain. At a relatively higher concentration of t-CIN (> 2x MIC), additional effects were induced in *A. flavus* cells, including a dramatically elevated Ca^{2+} content in mitochondria, a high degree of mitochondrial membrane depolarization, and the accumulation of reactive oxygen species (ROSs) [41]. These effects are not only expected to interfere with mitochondrial function but also to contribute to cell apoptosis.

1.3.5 Disturbance of intracellular redox balance

Being an electrophilic and thiol-reactive compound, t-CIN is assumed to interfere with the intracellular redox balance in bacterial cells. Visvalingam et al. [7] evaluated the transcriptional response of *E. coli* O157:H7 at 37°C, 2 and 4 h after exposure to 200 mg/L (1.51 mM) t-CIN, a concentration that inhibited growth but did not reduce viability. The treatment elevated the transcription of several oxidative stress-associated genes, including *gshA*, *katE*, *sodA* and *sufA*, encoding a glutathione synthetase, catalase, superoxide dismutase (SOD), and iron-sulfur cluster insertion protein respectively, reminiscent of an intracellular redox stress response. The total superoxide dismutase activity in *E. coli* also increased with increasing concentrations (0, 1/2x, 3/4x, 1x MIC) of t-CIN, implying that t-CIN triggered oxidative damage [18]. In another study, the transcription of several oxidative stress-associated genes, encoding glutaredoxin (GrxA), thioredoxin 2 (TrxC), and manganese transport protein (MntH), were found to be upregulated in *E. coli* O157:H7 treated with t-CIN at 1/2x MIC [38]. The different transcriptional responses reported in these two studies may be due to the different t-CIN exposure times after which the analysis was done, i.e. 2 h [7] and 17 h [38]. Furthermore, Du et al. [11] reported that supplementation of the antioxidant N-acetyl-L-cysteine (NAC) in the medium significantly reversed the growth inhibition of t-

CIN on *E. coli*. *E. coli* cells previously treated with t-CIN at 1/2x MIC also exhibited a relatively faster adaption to oxidative stress (50 mM H_2O_2) than the untreated control [38].

Elevated oxidative stress was also reported in fungal cells after t-CIN exposure, and in this case may be attributed to t-CIN-induced damage to the mitochondria, the primary intracellular source of ROS (mainly hydrogen peroxide and superoxide) [41,59]. Exposure of *P. expansum* to a combination of t-CIN and citral at 1/2x MIC induced the accumulation of H_2O_2 and other ROS, enhanced SOD activity, and elevated expression of the SOD gene and other genes related to the response to oxidative stress [60,61]. In addition, transcriptomic analysis of *A. flavus* treated with a subinhibitory concentration (0.6 mM) of t-CIN also revealed a pronounced upregulation of the pentose phosphate pathway genes [9]. The pentose phosphate pathway plays a vital role to counteract oxidative stress by boosting NADPH generation [62,63]. Pentose phosphate pathway genes were also induced in *E. coli* treated with t-CIN [11]. Moreover, superoxide dismutase (*sod1* and *mnsod*) and catalase (*cat1* and *catA*) genes were all up-regulated in the presence of t-CIN in *A. flavus* [9]. ROS are well known to affect the oxidative phosphorylation and membrane permeability of mitochondria, which further exacerbates ROS accumulation [64]. Excessive accumulation of ROS could cause direct injury to proteins, lipids, and nucleic acids, leading to cellular dysfunction and cell death [65], and this may well explain the t-CIN-induced mitochondrial damage that has been reported in fungi including *A. ochraceus, A. flavus* and *C. albicans* [41,50,59] (see previous sections). Besides t-CIN, other natural α,β-unsaturated carbonyl compounds were also reported to trigger the release of ROS in fungal cells. In a study of the antifungal mechanism of citral against *Penicillium digitatum*, it was found that citral at 1/2x MIC induced ROS formation, a reduction of the mitochondrial membrane potential, a decreased glutathione content, and an elevated glutathione S-transferase activity [66].

1.3.6 Anti-quorum sensing activity

Quorum sensing is a cell-to-cell communication system that detects and responds to cell-population density changes by coordinating bacterial gene expression [67]. A variety of physiological activities, including virulence, motility, and biofilm formation are controlled by quorum sensing in bacteria. In general, Gram-positive and Gram-negative bacteria use processed oligo-peptides and acylated homoserine lactones as their signaling molecules, respectively [67]. In *L. monocytogenes*, quorum sensing is regulated by the accessory gene regulator (Agr) system in which *agrD* encodes a pro-peptide that is processed by AgrB into

a mature autoinducing peptide, and *agrA* encodes the response component of the system [68]. The Agr system was reported to affect biofilm formation, virulence, and global gene expression profiles in *L. monocytogenes*, and attenuation of *agrA* and *agrD* genes significantly suppressed biofilm formation [69,70]. In a recent study, Liu et al. [28] showed that the presence of t-CIN at 1/4x MIC significantly repressed the expression of three quorum sensing-associated genes, and this was proposed to explain the t-CIN induced biofilm formation inhibition. Anti-quorum sensing activity of t-CIN has also been reported in *Vibrio fischeri* [46], *P. fluorescens* [37] and *Pseudomonas aeruginosa* [48]. Using green fluorescent protein (GFP) based reporters, Niu et al. [46] showed that 26 ppm t-CIN, which exerted no inhibitory effect on bacterial growth, suppressed the LuxR-mediated transcription from the *PluxI* promoter by 70% in *E. coli*. LuxR is a representative acylated homoserine lactone-dependent transcription factor which senses 3-oxo-hexanoyl-homoserine lactone and regulates quorum sensing genes including the *luxCDABE* operon in *V. fischeri* [67]. In addition, 8 ppm of t-CIN also reduced the 3-hydroxy-butanoyl-homoserine lactone mediated bioluminescence of *Vibrio harveyi* by 55% [46]. Subinhibitory concentrations of t-CIN also exerted an inhibitory effect on quorum sensing in *P. fluorescens*, resulting in inhibition of biofilm formation and swimming and swarming motility, while the production of acylated homoserine lactones was not affected [37]. In summary, t-CIN at low concentrations appears to exert anti-quorum sensing activity in various bacteria, but a full understanding of the underlying mechanism will require further research.

1.3.7 Biofilm inhibition by t-CIN

Biofilms consist of surface-associated microorganisms that are embedded within a slimy self-produced extracellular matrix composed of polymeric substances [71]. The biofilm-inhibiting activity of t-CIN and cinnamon EOs has been intensively investigated across a range of bacteria including *E. coli*, *S.* Typhimurium, *Streptococcus pyogenes*, *Cronobacter sakazakii*, *Pseudomonas spp*, *L. monocytogenes*, and *S. aureus* by methods such as microscopy observation and crystal violet staining [14]. This property of t-CIN may provide the potential for applications to control biofilms in the food industry.

Biofilm-formation by *L. monocytogenes* was significantly suppressed by t-CIN as revealed by scanning electron microscopy (SEM) and confocal laser-scanning microscopy [28]. Even at 1/8x MIC, a 41% biofilm inhibition was recorded on the polystyrene surface, and the biofilm formed in the presence of t-CIN showed a significantly inhibited metabolic

activity. Since no obvious growth inhibition of *L. monocytogenes* was exerted by t-CIN at 1/8x MIC and only a very slight growth attenuation was observed at 1/4x MIC, the inhibition appeared to be specific for biofilm formation. In addition, the swimming motility and the quorum sensing system were strongly suppressed by t-CIN, and since these are known to play critical roles in biofilm formation in *L. monocytogenes* [69,70,72], the results obtained by Liu et al. [28] suggested that inhibition of *L. monocytogenes* biofilm formation by t-CIN can be at least partially attributed to attenuation of the quorum sensing system and motility. Similarly, the anti-biofilm activity of t-CIN on *L. monocytogenes* at subinhibitory concentrations (0.50 mM and 0.75 mM, no growth inhibition of *L. monocytogenes* at these concentrations) was observed by Upadhyay et al. [73]. Transcription of genes known to be critical for biofilm formation, including the quorum sensing-associated genes *agrA*, *agrB*, and *agrC*, the motility gene repressor *mogR*, and the transcriptional regulatory gene *degU*, was significantly repressed by subinhibitory concentrations of t-CIN. Subinhibitory concentrations of t-CIN (1/8 - 1/2x MIC) also reduced biofilm biomass and metabolic activity of *Streptococcus mutans*, in line with down-regulated expression of genes involved in extracellular polysaccharide synthesis (*gtfB*, *gtfC*, *gtfD*, and *gbpB*) [74].

In *P. aeruginosa*, t-CIN at 1/8x -1/2x MIC inhibited biofilm formation and eradicated preformed biofilm [48]. At 1/4x MIC (no growth attenuation for planktonic bacteria), 37.9% inhibition of biofilm formation was reported and was accompanied by significantly decreased intracellular concentrations of cyclic di-GMP, a signalling compound that is critical for *P. aeruginosa* biofilm formation. Furthermore, swarming motility, which is also key to the biofilm-forming ability of *P. aeruginosa*, was also suppressed by t-CIN in a concentration-dependent manner. In a separate study, cinnamon oil was also found to suppress biofilm formation and swarming motility of *P. aeruginosa* at a subinhibitory concentration (1.6 - 4.0 mM) [75]. In *S.* Typhimurium, the biomass of preformed biofilm on a polypropylene surface was reduced by 21%, and the number of attached cells declined from 8.03 $\log_{10}$ CFU/cm^2 to 6.90 $\log_{10}$ CFU/cm^2, after 1 h of exposure to t-CIN at MIC (0.312 mg/mL, i.e. 2.4 mM) [27].

1.4 Synergy of t-CIN with other antimicrobials

Currently, one of the obstacles to applying some EO constituents such as t-CIN in food preservation is that they lose much of their activity in real food matrices and therefore lack potency when used alone at low doses [3,4]. Furthermore, increasing their concentration

to achieve the desired antimicrobial effect often has a negative organoleptic impact. Exploiting synergies between EO and other antimicrobial compounds or treatments has been proposed as a solution to this problem [4]. However, little is known about which interactions lead to synergistic, additive, or antagonistic effects. Synergistic approaches for boosting the effectiveness of t-CIN have been investigated in many studies and these insights can support the development of more effective hurdle technology applications of t-CIN. Inactivation of several Gram-positive and Gram-negative bacteria by high-pressure treatment was found to be strongly enhanced in the presence of electrophilic EO compounds such as t-CIN, *trans*-2-hexenal, and allyl isothiocyanate, while compounds lacking an electrophilic character generally did not exhibit synergy [76]. Since the t-CIN concentration used in this study (10 mM) is lethal for many bacteria, it would be worthwhile to extend the experiments to sub-MIC concentrations of t-CIN. Further evidence that this synergistic interaction stems from the thiol-reactivity of the compounds, was provided by demonstrating that the effects were abolished in the presence of cysteine, and that a glutathione synthesis-deficient *E. coli* strain showed increased sensitivity to the combined treatment with high-pressure and t-CIN [76].

Combination with antimicrobial EOs was also proposed to enhance the efficacy of antibiotics and overcome the increased emergence of antibiotic-resistant bacteria [77]. A group of EOs including t-CIN act synergistically with some antibiotics, which offers a perspective for reducing antibiotic usage. For example, the combination of t-CIN (1/16x and 1/8x MIC) with streptomycin (1/8x MIC) synergistically inhibited the planktonic cells as well as preformed biofilms of *L. monocytogenes* and *S.* Typhimurium [78]. Karumathil et al. [79] found that t-CIN and eugenol decreased the resistance of multi-drug resistant *Acinetobacter baumannii* to the β-lactam antibiotics ampicillin, methicillin, meropenem, penicillin, aztreonam, amoxicillin, and piperacillin. Reverse transcription-quantitative polymerase chain reaction (RT-qPCR) revealed that the EOs repressed the genes encoding resistance to β-lactam antibiotics (*blaP*) and efflux pumps (*adeABC*), which might explain the synergy. Significant synergistic effects of t-CIN with amikacin, gentamicin, vancomycin, and amoxicillin at sub-inhibitory concentrations against methicillin-resistant *S. aureus* strains were revealed recently [33]. Furthermore, sub-inhibitory concentrations (1/8 - 1/2x MIC) of t-CIN suppressed the transcription of *mecA, mecR1, and mecI,* which are critical for the resistance of *S. aureus* to penicillin-like antibiotics including methicillin [33].

1.5 Chemical properties of t-CIN

As depicted in Fig. 1.2, t-CIN contains a conjugated C=C double bond and C=O carbonyl group, a feature that accounts for most of its reactivity. The electronegative carbonyl oxygen atom withdraws electrons from the carbonyl carbon atom, causing a local electron deficiency [80]. The partial positive charge of the carbonyl carbon can be transferred to the β-carbon of the double bond because of the presence of a resonance system. As a result, nucleophiles may react with α,β-unsaturated aldehydes via either the 1,2-addition or 1,4-addition (Michael addition) reaction (Fig. 1.5) depending on the nature of the nucleophile. For biological thiol or amine nucleophiles, the competition between 1,2- and 1,4-addition is under thermodynamic control and 1,4-addition prevails in this case because the stable carbonyl group is retained.

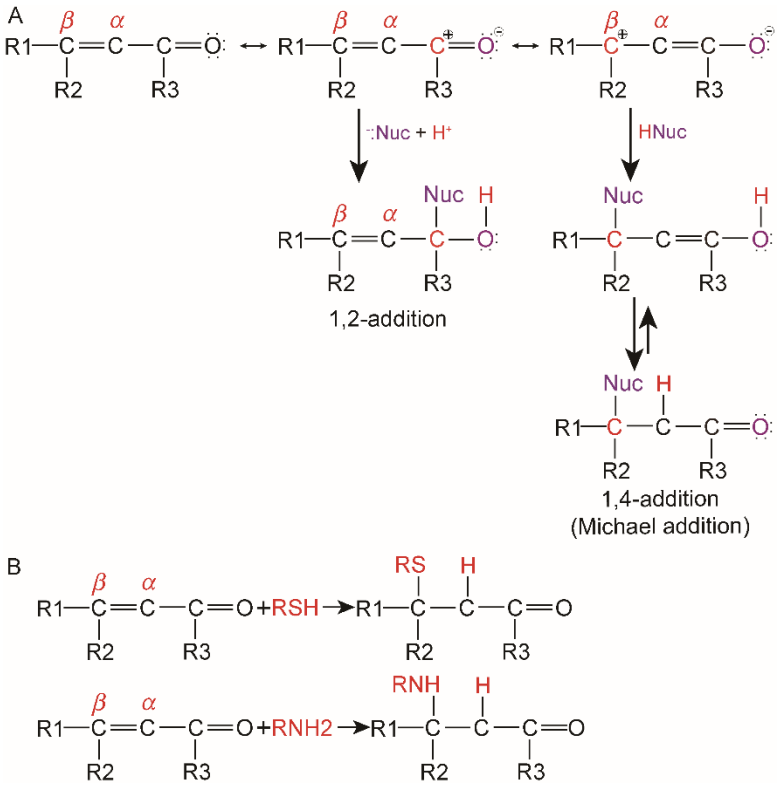

Figure 1.5 (A) α, β-unsaturated carbonyl resonance system and the scheme of 1,2 and 1,4 (Michael-type) nucleophilic addition reactions; (B) Michael-type addition reaction of an α,β-unsaturated carbonyl compound with a thiol and amine compound [80].

The relationship between electrophilicity and the antimicrobial activity of various t-CIN derivatives has been studied [81]. The effect of t-CIN against *S. aureus* and *E. coli* were compared to a family of derivatives with either electron-donating (–OCH_3, –CH_3, –$N(CH_3)_2$) or electron-withdrawing groups (–Br, –Cl, –NO_2, –CN, –CO_2CH_3) substituted at the para-position of the phenyl ring. Electron-donating groups decreased the electrophilicity of the parental compound, resulting in a significantly reduced inhibitory effect against both *S. aureus* and *E. coli*. Conversely, electron-withdrawing substituents increased the electrophilicity of t-CIN and enhanced the antimicrobial ability towards *S. aureus*. Remarkably, only t-CIN substituted with –Br, –NO_2, and –CN groups exhibited a stronger inhibitory activity towards *E. coli* while introducing –Cl and –CO_2CH_3 slightly reduced the inhibitory effect. Overall, this work strongly suggests that the antimicrobial activity of α,β-unsaturated aldehydes stems at least partly from their electrophilic properties.

Besides, the lipophilicity of t-CIN contributes to its biological activity as well [82]. The logKow (logarithm of the partition coefficient of the compound between n-octanol and water) of t-CIN is about 1.97 (https://pubchem.ncbi.nlm.nih.gov/). As previously mentioned, the hydrophobicity of t-CIN allows it to interact with the hydrophobic core of the cytoplasmic membrane, where it may also distort lipid-protein interactions and attenuate the functionality of membrane-associated proteins or enzymes by directly interacting with their hydrophobic regions [83]. An example is the reported inhibition of the membrane-bound ATPase activity of *E. coli* by t-CIN [31].

1.6 Chemical reactivity and potential cellular targets

The intracellular nucleophilic targets of α,β-unsaturated carbonyl compounds can generally be categorized into proteins and LMW compounds including glutathione (L-γ-glutamyl-L-cysteinyl-glycine, GSH), nucleophilic amino acids such as cysteine and histidine, and hemiacetal and hemi-thioacetal compounds (Fig. 1.6) [84]. Cysteine sulfhydryl groups are believed to be the primary nucleophilic targets of t-CIN while lysine and histidine residues are less reactive targets [84,85].

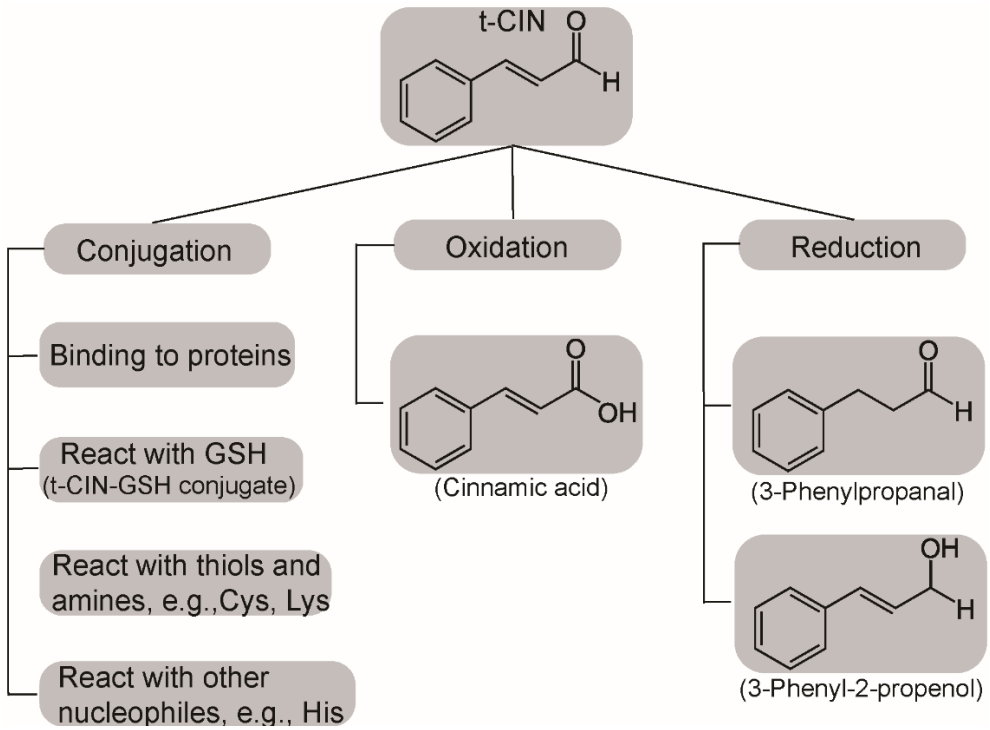

Figure 1.6 Potential interactions of t-CIN with cellular biochemistry. t-CIN can be oxidized, reduced, or conjugated with proteins or other LMW nucleophiles. The reaction products may be further metabolized or excreted.

Conjugation with GSH is an important detoxification pathway for electrophilic toxic compounds including α,β-unsaturated carbonyl compounds, generating products that are less reactive than the parent electrophiles [84–86]. In addition, GSH also plays a pivotal role in protecting bacteria from t-CIN-induced ROS and maintaining the intracellular thiol redox homeostasis. Many organisms can produce GSH, including eukaryotes and most Gram-negative bacteria [87]. However, only few Gram-positive bacteria can synthesize GSH independently and *L. monocytogenes* is one of them [87–89]. Alternatively, the redox buffer bacillithiol (the α-anomeric glycoside of L-cysteinyl-D-glucosamine with L-malic acid) is employed by other Firmicutes bacteria species such as *Bacillus* and *Staphylococcus*, and Actinomycetes utilize mycothiol (1-d-*myo*-inosityl-2-(N-acetyl-l-cysteinyl)amido-2-deoxy-α-d-glucopyranoside), for maintaining the reducing environment [87]. The Cys thiol group of bacillithiol and mycothiol can react with electrophilic α,β-unsaturated carbonyl compounds via the Michael-type addition. In *L. monocytogenes*, dysfunction of bifunctional GshF abolishes GSH biosynthesis and results in an accumulation of the intermediate γ-

glutamylcysteine and hypersensitivity to oxidative agents such as diamide, hydrogen peroxide, and tert-butyl alcohol hydroperoxide [88,89].

Electrophilic α,β-unsaturated aldehydes and ketones can undergo either nonenzymatic or enzymatically catalyzed conjugation with GSH by Michael-type addition (Fig. 1.5) [90,91]. Using ultra-performance liquid chromatography, Kiwamoto et al. [92] demonstrated the formation of t-CIN-GSH conjugate catalyzed by glutathione S-transferases in rat liver and intestine tissue S9 fractions at 37°C and pH 7.4. Additionally, the aldehyde dehydrogenase mediated oxidation and aldose reductase mediated reduction, which will be discussed below, were also revealed to be essential t-CIN detoxification pathways. Kiwamoto et al. also examined the chemical (non-enzymatic) reaction of GSH with t-CIN and five other α,β-unsaturated aldehydes (*trans*-2-pentenal, *trans*-2-hexenal, *trans*-2-octenal, *trans*-2-decenal, and *trans*-2-dodecenal) and reported second-order rate constants (k_{GSH}) ranging from 0.10 to 0.26 $M^{-1}s^{-1}$ [92,93]. A rapid conjugation of *trans*-2-hexenal with GSH *in vitro* in rat liver tissue with mixtures of *trans*-2-hexenal and GSH at 37°C and pH 7.4 was also revealed [94]. However, at higher *trans*-2-hexenal concentrations, the aldehyde dehydrogenase mediated conversion to 2-hexenoic acid and the aldose reductase mediated reduction to *trans*-2-hexenol became the main detoxification pathways of *trans*-2-hexenal in the rat liver tissue in the presence of sufficient cofactors.

In another study, the reactivity of several electrophiles including t-CIN with GSH was assessed with a kinetic GSH chemoassay at 25°C and pH 7.4 [95], and second-order rate constants k_{GSH} ($M^{-1}s^{-1}$) were quantified including corrections for oxidative GSH loss (GSSG formation) [82,96]. Under the applied experimental conditions, the k_{GSH} of the t-CIN-GSH conjugation reaction was 0.092 ± 0.003 $M^{-1}s^{-1}$ while the values for some aliphatic aldehydes such as *trans*-2-hexenal (0.418 ± 0.032 $M^{-1}s^{-1}$), *trans*-2-pentenal (0.472 ± 0.028 $M^{-1}s^{-1}$), *trans*-2-nonenal (0.252 ± 0.005 $M^{-1}s^{-1}$) and methyl acrolein (3.383 ± 0.100 $M^{-1}s^{-1}$) were considerably greater, indicating a weaker reactivity of t-CIN [82]. These results somewhat disaccord with findings from the report by Kiwamoto et al., which showed much smaller differences between the k_{GSH} of t-CIN, *trans*-2-pentenal, and *trans*-2-hexenal. These inconsistent results between studies might be because of different experimental conditions like temperature and solvent. While the electrophilicity and reactivity of α,β-unsaturated aldehydes is an important parameter determining their biological activity, also their ability to pass through the cell membrane, which varies between compounds, has to be taken into

account. This could explain why the smaller k_{GSH} of t-CIN was not reflected by lower toxicity compared to methyl acrolein and *trans*-2-pentenal in terms of their 48-h EC50 values, which represented the effective doses yielding 50% growth retardation of the ciliate *Tetrahymena pyriformis* within 48 h [82,96]. The 48 h-EC50 value of t-CIN was comparable to that of *trans*-2-hexenal, but significantly larger than the value of *trans*-2-nonenal [82]. Regression analysis of the k_{GSH} and Kow values of 18 α,β-unsaturated aldehydes revealed that both hydrophobicity and electrophilic reactivity contribute to the toxicity of α,β-unsaturated aldehydes to ciliates, and that the impact of hydrophobicity on the toxicity is particularly pronounced for aldehydes with smaller k_{GSH} like t-CIN [82].

As mentioned, glutathione S-transferases, which are widely distributed in eukaryotic cells and Gram-negative bacteria (e.g., *E. coli* and *Vibrio cholerae*), significantly promote the conjugation of GSH with electrophiles by catalyzing the binding of the sulfhydryl group of GSH to electrophilic centers of nucleophilic substrates [90,97,98]. Given the ability to synthesize GSH and the presence of glutathione S-transferase in many foodborne Gram-negative pathogens and fungi, the glutathione S-transferase mediated conjugation with GSH might be a relevant detoxification pathway for α,β-unsaturated carbonyls in these microorganisms. Information about the occurrence of these enzymes in Gram-positive bacteria is limited, and they may be less abundant. In particular, no predicted glutathione S-transferase gene was found in the genome *of L. monocytogenes* [98,99].

Aside from GSH, other LMW compounds with reactive thiol, imidazole, or amine groups may also be targeted by t-CIN. One such compound that has been studied is cysteamine (2-aminoethanethiol), a compound that has both a thiol and an amino group and that can be synthesized by degradation of coenzyme A. The second-order rate constant k_2 of cysteamine with t-CIN was determined to be $0.636 \pm 0.019\ M^{-1}\ s^{-1}$, while cinnamic acid, caffeic acid, and cinnamic acid ethyl ester showed either no reaction or exceedingly slow rates of covalent adduct formation ($k_2 < 0.001\ M^{-1}s^{-1}$) [100]. Autelitano et al. [101] also examined the *in vitro* reactivity of t-CIN and related compounds with cysteamine (in DMSO) utilizing a quick NMR assay. Their work confirmed that t-CIN derivatives lacking the α,β-unsaturated aldehyde group, like cinnamoyl esters and amides, as well as cinnamyl ketones, demonstrated no detectable reactivity, while t-CIN reacted efficiently with cysteamine mainly via Michael-type addition. To our best knowledge, no direct *in vivo* evidence showing the

conjugation of t-CIN with intracellular GSH or Cys residue in microorganisms has been reported yet.

Besides LMW nucleophiles, proteins, in particular those containing active Cys residues, also represent important intracellular targets of electrophilic α,β-unsaturated carbonyls [85]. The pKa values of sulfhydryl groups in free Cys and reduced GSH are above 8, while these values can be lower in proteins because of the molecular environment, and this leads to a significantly elevated $-S^-$/-SH ratio at physiological pH for these Cys residues [102]. Compared to undissociated thiol groups (-SH), thiolates ($-S^-$) are more potent nucleophiles and much more vulnerable to the attack of electrophilic species under physiological conditions [102]. In particular, enzymes with nucleophilic Cys residue in their active site may be vulnerable targets for electrophilic compounds. Examples include glyceraldehyde 3-phosphate dehydrogenase (GAPDH) and various thiol enzymes (e.g. thioredoxins and glutaredoxins) [103–105]. In GAPDH, the thiolate group of the conserved active Cys moiety (Cys151 for GAPDH of *L. monocytogenes* EGD-e) attacks the aldehyde carbon of glyceraldehyde 3-phosphate, forming a thiohemiacetal adduct [103]. Because of its nucleophilic character, this active Cys residue of GAPDH is also highly sensitive to ROS and RNS which can result in the inactivation of this enzyme [62,63]. The active site Cys of GAPDH was also indicated to be targeted by several reactive α,β-unsaturated carbonyl toxicants [106,107]. Purified human GAPDH was inhibited by acrylamide, acrolein, and methylvinyl ketone in a concentration- and time-dependent manner, and the inhibitory effect was correlated to the electrophilicity of tested α,β-unsaturated carbonyl compounds [107]. Moreover, Sauerland et al. [84] reported adduct formation between the α,β-unsaturated carbonyl compounds acrolein, crotonaldehyde, dimethylfumarate, cyclohexenone, and Cys residues in GAPDH, bovine serum albumin, and creatine kinase. Among these electrophiles, acrolein reacted most rapidly. Overall, these studies indicate that Cys-containing proteins are potential targets of electrophilic α,β-unsaturated carbonyls and that the biological function of these proteins may be attenuated or abrogated, especially for enzymes with active site Cys residues. However, adduct formation with proteins is a complex reaction, and its efficiency depends on many factors, including structure, hydrophobicity, and electrophilicity of the electrophile, as well as pKa and accessibility of the reactive Cys residues in the protein [84,107]. Unlike the highly toxic acrolein, the ability of t-CIN to react with proteins has been rarely studied, especially in microorganisms.

Thioredoxin reductase, a component of the cellular thioredoxin systems, was inhibited by t-CIN and its derivatives 2-hydroxycinnamaldehyde and 2-benzoyloxycinnamaldehyde in human cancer cells [108]. Thioredoxin reductase catalyzes the NADPH-dependent reduction of the dithiol/disulfide active site of thioredoxin, and the reduced thioredoxin will then in its turn reduce the disulfides of a wide range of substrates [109,110]. Both thioredoxin and glutaredoxin systems play pivotal roles in maintaining the thiol homeostasis in many organisms and profound consequences might be expected if thioredoxin reductase or thioredoxins were targeted by α,β-unsaturated carbonyls. Thus far, evidence for the inhibition of microbial thioredoxin systems by t-CIN or other EO components containing an α,β-unsaturated aldehyde group is lacking, but within the genome of *L. monocytogenes* EGD-e, six thioredoxin-like proteins (lmo1233, lmo1609, lmo1903, lmo2152, lmo2424, lmo2830) and one thioredoxin reductase (lmo2478) were detected [111,112]. However, few of them have been characterized to date except for lmo1233 (thioredoxin reductase A), which was shown to be essential for maintaining a highly reducing environment in the bacterial cytosol, and the deletion of which markedly compromised the tolerance of the pathogen to the thiol reagent diamide [113].

1.7 Enzymatic degradation of t-CIN

The enzymatic routes of detoxification of α,β-unsaturated aldehydes have been mostly documented in humans and rats, and remain largely unclarified in microorganisms. Transformation to less electrophilic and toxic molecules takes place via three major pathways: conjugation with GSH, oxidation, and reduction (Fig. 1.7) [92,114–116]. The oxidation is mediated by NAD+-dependent aldehyde dehydrogenases, which catalyze the formation of carboxylic acids from the corresponding α,β-unsaturated aldehydes (Fig. 1.7) [92]. The reduction of α,β-unsaturated aldehydes is facilitated by NAD(P)H-dependent aldehyde reductases, generating α,β-unsaturated alcohols [92,117,118]. However, these alcohols may be re-oxidized to the corresponding unsaturated aldehydes by alcohol dehydrogenases [92]. As a result, when exposed to t-CIN, mammalian cells produce a mixture of cinnamyl alcohol, cinnamic acid, and GSH conjugates in varying proportions depending on the tissue type and the dose of t-CIN [92]. In what follows, the major known enzymatic detoxification reactions of t-CIN in microorganisms will be described.

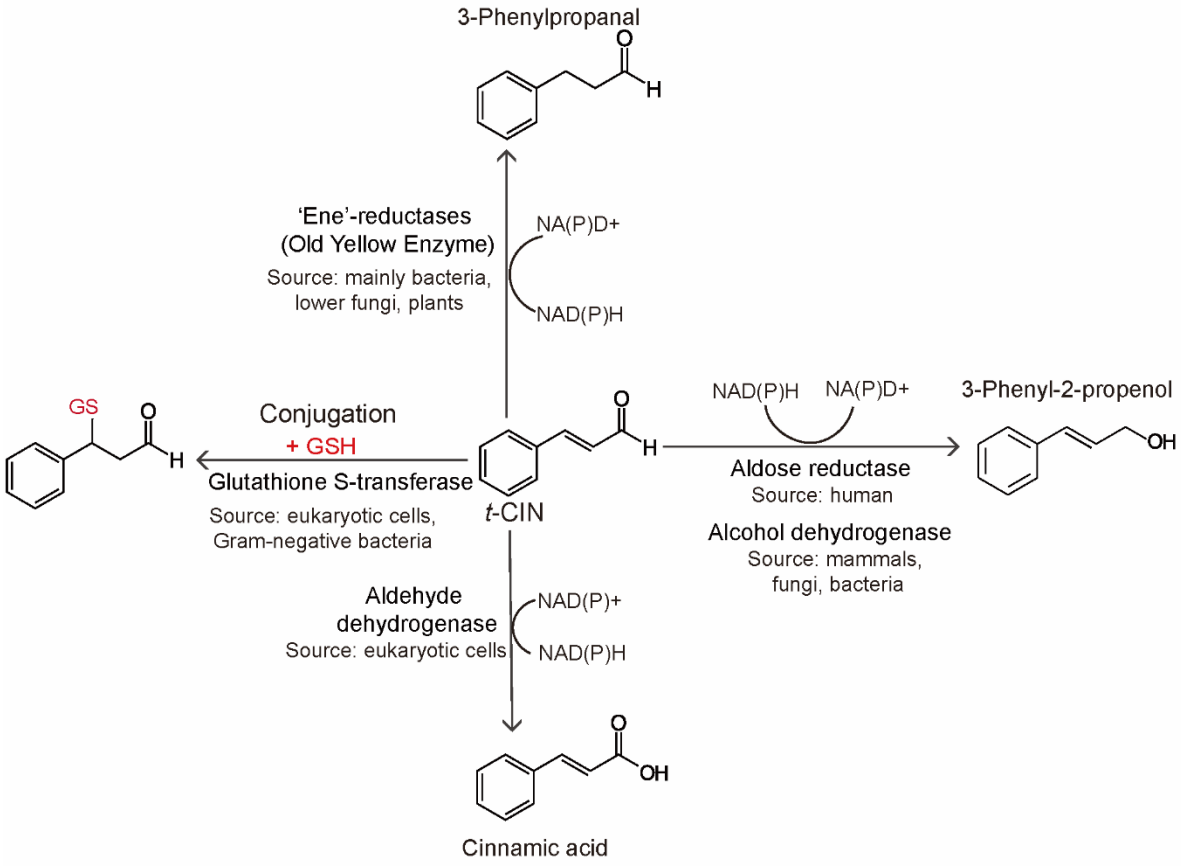

Figure 1.7 Scheme of enzyme-catalyzed detoxification process of t-CIN.

1.7.1 Aldehyde reductases

Aldose reductases (synonym aldehyde reductases; systematic name alditol:NAD(P)+ 1-oxidoreductase; EC 1.1.1.21) are oxidoreductases belonging to the aldo-keto reductases that can catalyze the reduction of a variety of physiological aldehydes or ketones, such as sugars and some intermediates of the retinoids, lipids, steroids, and prostaglandins biosynthesis pathways to the corresponding alcohols, with the concomitant oxidation of NADPH [119]. Bander Jagt et al. [118] and Srivastava et al. [117] demonstrated that a human aldose reductase efficiently catalyzed the reduction of a series of α,β-unsaturated aldehydes such as *trans*-2-nonenal, 4-hydroxy-nonenal and *trans*-2-octenal and t-CIN. Notably, it was also revealed that, in the absence of NADPH, the α,β-unsaturated aldehydes could covalently modify the Cys298 active-site residue of the enzyme, thereby altering its activity [117]. This modification did not take place in the presence of NADPH. Reduction of t-CIN or other α,β-unsaturated aldehydes by microbial aldo-keto reductases has not been reported in the literature yet.

The α,β-unsaturated aldehydes can also be metabolized by members of the well-characterized alcohol dehydrogenase family (ADHs) (alternative name aldehyde reductase, systematic name alcohol:NADP+ oxidoreductase; EC 1.1.1.2), including the short-chain and medium-chain dehydrogenases/reductases family proteins [120]. Klibanov and Giannousis [121] reported that NADH-dependent ADH from yeast, horse liver, and *Leuconostoc mesenteroides* preferably catalyzed the reduction of α-methylcinnamaldehyde and the *trans* isomer of cinnamaldehyde rather than its *cis* counterpart. ADH6 and ADH7, two NADPH-dependent alcohol dehydrogenases from *S. cerevisiae*, exhibited pronounced substrate specificity and activity towards t-CIN [122,123]. The kinetic study of both proteins at 25°C and pH 7.0 with t-CIN and cinnamyl alcohol showed that the efficiencies of reductive reactions were around 50-fold higher than the corresponding oxidations. Furthermore, the thermostable NAD+-dependent ADH from *Sulfolobus solfataricus* (SsADH) also manifested remarkable activity towards t-CIN at 65°C [124]. Kinetic assays also showed that *Lactococcus lactis* ADH (LladhA) exhibited high NADH-dependent activity towards t-CIN, 2-furaldehyde, and acetaldehyde, with catalytic efficiencies of $3.9x10^4$ $M^{-1}s^{-1}$, and $5.7x10^4$ $M^{-1}s^{-1}$ and $9.4x10^4$ $M^{-1}s^{-1}$, respectively [125].

Of special relevance, Visvalingam et al. [7] demonstrated that t-CIN was mostly converted to cinnamic alcohol after 4 h incubation with *E. coli* O157:H7 cells at 37°C, while no conversion occurred in the cell-free control. Subsequently, transcriptional response analysis of *E. coli* O157:H7 exposed to sublethal concentration of t-CIN showed significant upregulation of *yqhD* and *dkgA*, encoding an ADH and a 2,5-diketo-D-gluconate reductase respectively [7,11]. Furthermore, the inactivation of YqhD significantly reduced the tolerance of *E. coli* to the toxicity of t-CIN [11]. This led the authors to speculate that one or both of these enzymes detoxify t-CIN by converting it to cinnamic alcohol in *E. coli*. In support of this hypothesis, YqhD was previously reported to play a role in the resistance of *E. coli* to a broad range of short-chain aldehydes, such as acrolein, isobutyraldehyde, glycolaldehyde, butanaldehyde, malondialdehyde, and propanaldehyde, and purified YqhD can catalyze the conversion of these aldehydes to the corresponding alcohols in an NADPH-dependent manner [126,127]. DkgA, on the other hand, is an aldo-keto reductase family enzyme with NADPH as the cofactor and broad substrate specificity [128]. However, no direct evidence has ever confirmed the activity of either YqhD or DkgA towards t-CIN. Several fungal species, including *A. ochraceus* [58] and *P. expansum* [60] are also able to transform t-CIN to cinnamic alcohol, presumably by means of aldehyde reductase enzymes. In summary,

ADHs are widely distributed in virtually all organisms and have versatile biological functions in many metabolic processes including xenobiotic detoxification. Some ADHs have a relaxed substrate selectivity and therefore can detoxify a variety of exogenous toxic aldehydes including t-CIN.

1.7.2 Aldehyde dehydrogenases

Several studies have reported that aldehyde dehydrogenases (ALDH, systematic name aldehyde:NAD+ oxidoreductase; EC 1.2.1.3), can also mediate the metabolism of t-CIN, primarily in eukaryotes. This is not surprising given the broad specificity of many ALDHs on a wide range of exogenous and endogenous aldehydes [129]. *In vitro* incubation of 0.005 to 3 mM t-CIN with mixtures of rat liver tissue fraction and NAD+ (2 mM) at 37°C resulted in the conversion of t-CIN to cinnamic acid, and this was suggested to be mediated by ALDH [92]. Indeed, human mitochondrial ALDH (ALDH-2) and human liver ALDH isozyme (ALDH-1) were previously reported to catalyze the oxidation of t-CIN and t-CIN derived aldehydes [130]. Another study also showed that purified human liver ALDH1 and ALDH2 and yeast mitochondrial ALDH2 detoxified exogenous/endogenous aliphatic and aromatic aldehydes including phenylacetaldehyde, 2-phenylpropionaldehyde, benzaldehyde, 2-furaldehyde, and t-CIN in the presence of NAD^+ [131].

1.7.3 'Ene'-reductases

Not only the aldehyde group but also the double bond of α,β-unsaturated carbonyl compounds can be enzymatically reduced, and a prominent group of enzymes mediating this reaction are the flavin-dependent 'ene' reductases from the old yellow enzyme family (OYE, systematic name NADPH:acceptor oxidoreductase; EC 1.6.99.1), which are renowned for containing a non-covalently bound flavin mononucleotide (FMN) [132,133]. Numerous members of the OYE family have been identified and they are widely distributed in plants and microorganisms, particularly in bacteria and lower fungi [132]. Many OYEs can selectively catalyze the reduction of a wide spectrum of α,β-unsaturated ketones, aldehydes, nitroalkenes, and carboxylic acids (Fig. 1.8). Primarily, these flavoenzymes typically catalyze the *trans*-hydrogenation of the C=C double bond of α,β-unsaturated aldehydes and ketones, through the so-called reductive half-reaction, in which NAD(P)H serves as the reductant of FMN [133,134] (Fig. 1.8A).

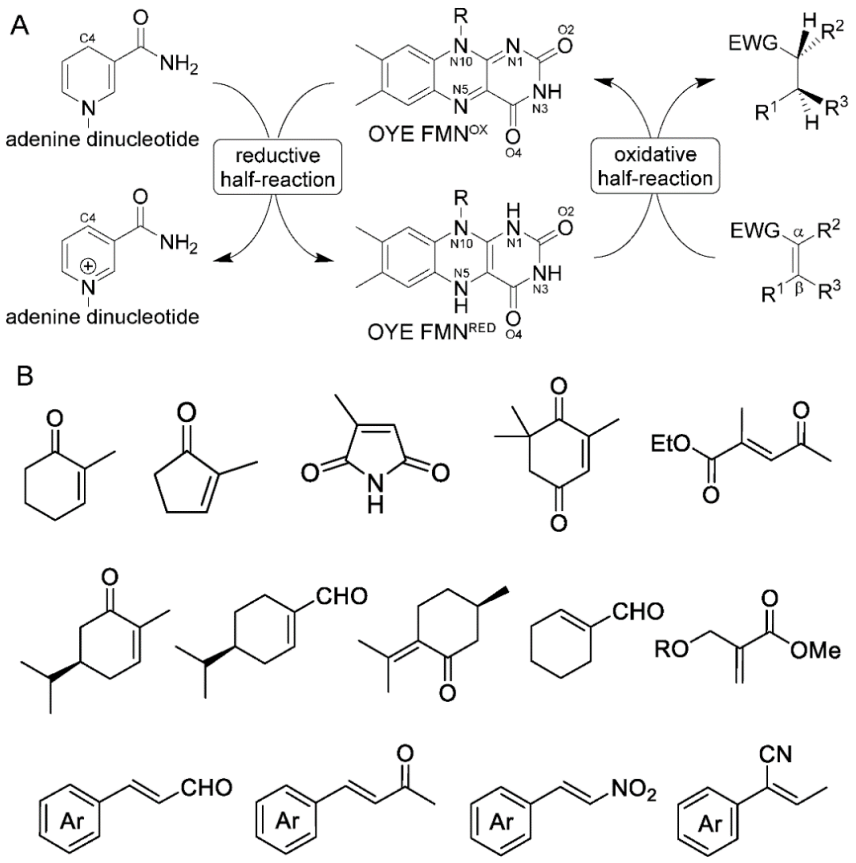

Figure 1.8 (A) OYE-catalyzed hydrogenation of the C=C bond of α,β-unsaturated carbonyl compounds (adapted from [134] and [135]). An enzyme-bound FMN is firstly reduced by NADPH and the generated $FMNH_2$ subsequently reduces the substrate by transferring the hydride to the β-carbon atom of the C=C bond in a Michael-type reaction. The resulting anion is then protonated through a tyrosine moiety of the flavoenzyme from the opposite face of the C=C bond and the saturation process of the C=C bond is therefore closed. (B) Typical substrates of OYEs. R, ribose phosphate; EWG, electron-withdrawing group.

The structure, enzyme kinetics, and substrate specificity of various prokaryotic OYEs have been in-depth characterized and reviewed, including YqjM from *Bacillus subtilis*, LacER from *Lactobacillus casei*, the pentaerythritol tetranitrate reductase (PETNR) from *Enterobacter cloacae*, and XenA from *Pseudomonas putida* [133,135–139]. Despite the similarity in the catalytic mechanisms and used cofactors, these enzymes exhibit a wide diversity in substrate specificity, secondary protein structure, and stereoselectivity.

B. subtilis YqjM, one of the best-studied OYEs of Firmicutes origin, catalyzes the *trans*-hydrogenation of the double bond from an array of α,β-unsaturated aldehydes and

ketones including *trans*-2-hexenal, N-ethylmaleimide, and cyclohexen-1-one [136,137]. A recent study investigated the reduction of t-CIN by YqjM and the OYE homologue (TsOYE) from *Thermus scotoductus* [140]. The OYEs were activated by transferring photo-activated electrons from a photosensitizer (xanthene dyes) to the flavin moiety of OYEs instead of utilizing NAD(P)H as the source of reducing equivalents. Both enzymes displayed reductive activity towards t-CIN with a product yield of around 30%. The moderate yield was attributed to the poor solubility of t-CIN in the aqueous medium and the inhibitory effect of the product on the enzymes [140]. An additional OYE from *B. subtilis* str.168 (YqiG) was characterized and showed considerable activity towards α,β-unsaturated aldehydes and ketones such as carvone, alpha-methyl cinnamaldehyde, citral, and cyclohexen-1-one [141]. A YqjM homolog (GkOYE, 66% amino acid sequence identity with YqjM) from the thermophile *Geobacillus kaustophilus* also reduced the C=C bond of a number of α,β-unsaturated compounds [142]. However, neither YqiG nor GkOYE were tested towards t-CIN.

Also in Gram-negative bacteria and fungi, OYEs acting on t-CIN and derivatives have been reported. Kohli and Massey [134] studied the oxidative half-reaction (Fig. 1.8A) of OYE1 (*Saccharomyces pastorianus*) with t-CIN as a substrate and a tight binding of t-CIN to the reduced OYE1 was noted. Moreover, an additional electron-withdrawing 4-nitro substituent weakened the binding of t-CIN to OYE1 while the interaction was enhanced by the electron-donating 4-dimethylamino and 4-methoxy substituents [134]. Like OYE1, the purified native and recombinant estrogen binding protein 1 (EBP1), an OYE homolog from *Candida albicans*, displayed NADPH-dependent activity towards *trans*-2-hexenal, t-CIN, and many other α,β-unsaturated ketones or aldehydes [143]. In addition, the OYEs KYE1 from *Kluyveromyces lactis*, XenA from *P. putida*, and Yers-ER from *Yersinia bercovieri* displayed broad but different substrate specificities towards a set of α,β-unsaturated carbonyl compounds, although t-CIN, 2,4-hexadienal, 2-cyclohexen-1-one and citral were converted equally well by all three enzymes [144]. In another study, the PETNR of *E. cloacae* st. PB2 displayed a relatively low preference (k_{cat}/K_m = 8) towards t-CIN compared to the specificity for maleimides (k_{cat}/K_m = 2468) [145]. For carboxylic acid derivatives of t-CIN, including *trans*-cinnamide, *trans*-cinnamic acid, methyl *trans*-cinnamate, and *trans*-cinnamonitrile, no activity of PETNR was detected. Finally, an OYE from the thermophilic *Thermus scotoductus* SA-01 designated as chromate reductase was active towards essential oils compounds such as t-CIN, *trans*-2-hexenal, and carvone but not to citral at 65°C [146].

Although the presence of functional OYEs has not been documented in *L. monocytogenes,* they are likely to exist given their general widespread occurrence in the bacterial kingdom, particularly in closely related bacteria like *B. subtilis*. To confirm this assumption, we used a BLAST search to look for homologs of the well-known OYEs YqjM and YqiG from *B. subtilis* (NCBI accession #: NP_390263 and NP_390301 respectively), in the genome of *L. monocytogenes* EGD-e (NCBI accession #: NC_003210). Two proteins, namely NamA (NCBI accession #: WP_003732493) and Lmo0489 (NCBI accession #: WP_010989492) showed significant similarities (> 30% identity) to these two OYE homologs. The functions of NamA and Lmo0489 have not been characterized and it will therefore be interesting to investigate whether they provide resistance of *L. monocytogenes* to antimicrobial α,β-unsaturated aldehydes, in particular t-CIN.

1.8 Summary

Cinnamon essential oil and its main constituent t-CIN are being investigated for their potential as natural antimicrobials to control foodborne pathogens such as *L. monocytogenes*, individually or in combination with other food preservatives or food processing techniques. Our previous work showed that the growth inhibition by t-CIN against *L. monocytogenes* is typically characterized by a dose-dependent elongation of the lag phase and reduction of growth rate when the pathogen was cultivated in BHI broth supplemented with t-CIN. Several studies have addressed the effects of t-CIN in a wide range of bacteria and fungi, and it can be concluded that many cellular structures and processes are affected, including cell membrane structure and function, redox homeostasis, cell division, motility, and quorum sensing. To obtain a deeper understanding of the mode of action of t-CIN, several studies have employed genome-wide transcriptomic or proteomic approaches to elucidate the transcriptional response induced by t-CIN, but the results of such analyses are often complex and difficult to interpret. In addition, the conclusions of some studies should be interpreted with caution, since they used concentrations of t-CIN above the MIC which most likely inhibit transcription and translation.

The antimicrobial properties of t-CIN are believed to stem at least partly from its characteristic α,β-unsaturated aldehyde group, which is an electrophile that can react with thiol and amino groups of a wide range of cellular compounds. Both eukaryotic and prokaryotic organisms have evolved different protective enzymes that detoxify α,β-

unsaturated aldehydes by conjugation with intracellular nucleophilic molecules (e.g. proteins, glutathione, and cysteine), oxidation to carboxylic acids mediated by aldehyde dehydrogenases, reduction to alcohols mediated by aldehyde reductases, and hydrogenation of the double bond by 'ene-reductases'. While some of the above detoxifying enzymes have been demonstrated to exist (with varying levels of evidence) in a few Gram-negative and Gram-positive bacteria and yeasts, no information is available about the metabolism of α,β-unsaturated carbonyl compounds in *L. monocytogenes* and several other foodborne pathogens.

Scope of the Research

L. monocytogenes is a Gram-positive, rod-shaped, non-sporulating and facultative aerobic member of the Firmicutes and a major foodborne pathogen [147]. Epidemiological data indicate that the majority of human outbreaks are associated with the *L. monocytogenes* serovars 1/2a, 1/2b, and 4b [148,149]. Although some foodborne infections by *L. monocytogenes* cause only mild gastrointestinal symptoms, the infection can also spread to different organs and it is this systemic listeriosis that is of most concern because it has a high hospitalization rate (more than 95%) and case-fatality rate (approximately 20 - 30% worldwide) [147,150]. With about 2,500 confirmed listeriosis cases in the EU/EEA in 2017, listeriosis has a much lower incidence than salmonellosis or campylobacteriosis, but it is worrying that the disease shows an increasing trend in recent years in the EU/EEA, which calls for greater attention to the prevention and control of *L. monocytogenes* infection outbreaks [151]. Although *L. monocytogenes* is considered to have a high infective dose, low doses ($\sim 10^2$-10^4 CFU) can cause invasive listeriosis among susceptible persons such as immunocompromised individuals, pregnant women, new-borns and elderly persons [150,152]. *L. monocytogenes* is a versatile and resilient organism that thrives well in a wide range of natural and man-made environments, including soil, freshwater, decaying plant material, and the gastrointestinal tract of various animals [153]. It can also establish in the resident house microbiota of food production facilities, and as such, it is a common contaminant during food production and storage [150]. Foods such as milk, fish, meat, vegetables, and in particular fresh ready-to-eat foods are linked to most outbreaks of human listeriosis [147,154,155]. The ability of *L. monocytogenes* to grow in adverse environments, over a wide range of temperatures (from -1.5 to 45°C) and pH conditions (pH 4.0 - 9.6), at high osmotic stress (up to 10% NaCl) and low water activity (aw $\geqslant$ 0.9), further challenge the control of this organism in the food production chain [156,157]. In particular, the capacity to proliferate at low temperatures is held accountable for the frequent implication of refrigerated ready-to-eat foods in listeriosis [158].

To prevent the outgrowth of spoilage organisms and pathogens in foods and hence extend the shelf-life, artificial preservatives such as acetic acid, sorbic acid, benzoic acid, and nitrites are widely used in the food industry, especially in ready-to-eat foods. Despite their effectiveness, most artificial preservatives are perceived by the consumer to be foreign and

undesirable additions to the food. Some conventional preservatives such as nitrites are even increasingly under scrutiny for possible adverse health effects [1]. To accommodate the increasing demand of consumers for natural foods that are free from artificial preservatives, natural antimicrobials such as essential oils and their constituents have attracted wide attention over the last decades as potential natural alternatives to those 'synthetic' preservatives because of their remarkable and broad range of antimicrobial properties [3–6] (Chapter 1, section 1).

One of the best-studied antimicrobial EO constituents is t-CIN, a compound that exhibits pronounced antimicrobial activity across a wide array of foodborne microbes including *L. monocytogenes*. Being the major component of cinnamon bark essential oil, t-CIN is classified as GRAS by the U.S. FDA for use in foods (Code of Federal Regulations Title 21 Chapter 1). In general, the antimicrobial capacity of t-CIN is believed to stem from its lipophilic properties and reactive α,β-unsaturated aldehyde moiety, but detailed knowledge on the mode of action of t-CIN is still lacking. Dozens of studies have been conducted to describe the effects and identify the targets of t-CIN in various microbial species, but the findings have so far been mainly descriptive, including alteration of the cell morphology [21–23], inhibition of cell division [21,22], suppression of biofilm-forming ability [24,26–28], and damaged cell membrane integrity [17,18,23,25,29] (Chapter 1, section 3).

Like many other EO compounds, t-CIN has undesirable side effects (e.g. sensory and smell) at the concentrations that are needed for food preservation. The implementation of the hurdle technology concept, which works by combining low doses of t-CIN with other natural antimicrobials or with mild food preservation processes such as mild heat or pressure treatment, provides a promising solution to this restriction without compromising the food quality. Yet, most efforts in developing hurdle technology rely on trial and error to probe extraordinary synergistic combinations, which is time-consuming and labor-intensive. Knowledge of the mode of action of t-CIN could provide explanations why some combinations are synergistic while others are not, and could thereby support the rational integration of t-CIN in the hurdle concept to develop more effective hurdle applications. The knowledge of the antimicrobial mechanisms can also facilitate the regulatory approval of t-CIN as an innovative natural food preservative. Moreover, applying t-CIN at lower concentrations can also slow down the development of resistance among foodborne pathogens. Since natural antimicrobials are present in the natural environment of the pathogen,

studying the mode of action and the tolerance mechanisms in the bacteria may provide novel insights into the physiology, ecology, and evolution of the pathogens. Therefore, the main goal of this work was to explore the antimicrobial mechanisms of t-CIN as well as other EO compounds with *L. monocytogenes* as the model organism.

The reported antimicrobial effects and proposed modes of action of t-CIN in literature were summarised in Chapter 1. In addition, the potential t-CIN detoxification pathways in microorganisms were also described in Chapter 1, including the conjugation with cellular nucleophiles (e.g., proteins, glutathione, and cysteine) and the enzymatic oxidation or reduction into less toxic molecules. However, these studies have not identified the primary cellular targets of t-CIN. Previous work in our laboratory showed that t-CIN induced a dose-dependent elongation of the lag phase in *L. monocytogenes* grown in BHI broth [17] and that t-CIN could be degraded by *L. monocytogenes*. The t-CIN-induced growth suppression provides a prospect of the compound in extending the shelf-life of food products while maintaining the food quality, especially for ready-to-eat foods. However, the intracellular targets of t-CIN and the enzymes involved in its metabolism remained unidentified.

In an attempt to identify these antimicrobial targets and/or the degradative enzymes, a genome-wide random *Himar1* transposon mutant library of *L. monocytogenes* Scott A was previously constructed and screened, resulting in the isolation of multiple mutants with increased t-CIN sensitivity [17]. Two of the t-CIN hypersensitive transposon mutants, *yvcK::Himar1* and *asnB::Himar1*, manifested severe cell shape deformation that was exacerbated in the presence of t-CIN. The cell shape of some cells in wild-type *L. monocytogenes* populations was also noted to be distorted after incubation with a sub-lethal concentration of t-CIN. Since bacterial cell shape and integrity are maintained by the rigid peptidoglycan cell wall of bacterial cells, particularly in hypoosmotic environments that would otherwise be conducive to cell lysis [159], we hypothesized that a disrupted cell wall homeostasis could be accountable for the hypersensitivity of *yvcK::Himar1* and *asnB::Himar1* towards t-CIN, despite the hitherto unknown function of both YvcK and AsnB in *L. monocytogenes*. Further characterization of *yvcK::Himar1* and *asnB::Himar1* is reported in Chapter 2 and Chapter 3, respectively, and confirmed that both YvcK and AsnB play pivotal roles in the adaptation of *L. monocytogenes* to t-CIN by maintaining the cell wall integrity and homeostasis.

As a complementary approach to the screening of the transposon mutant library, evolutionary experiments were conducted by repeated passaging of wild-type *L. monocytogenes* in sublethal t-CIN concentrations to select for spontaneous t-CIN resistant mutants. The characterization of these mutants reported in Chapter 4 revealed a t-CIN detoxification pathway in *L. monocytogenes* mediated by YhfK, an oxidoreductase of the short-chain dehydrogenases/reductases superfamily. More specifically, YhfK was critical for the transformation of t-CIN to 3-phenylpropanal, demonstrating the ene-reductase function of YhfK. Inactivation of YhfK also increased the sensitivity of *L. monocytogenes* to several other reactive α,β-unsaturated aldehydes such as *trans*-2-hexenal and 4-hydroxy-2-nonenal. YhfK homologs exist in several other Gram-positive bacteria, but our work is the first to reveal the role of this protein in metabolizing α,β-unsaturated aldehydes like t-CIN. Taken together, our work provides novel insights into the effects of t-CIN and other α,β-unsaturated aldehydes on *L. monocytogenes* and in the bacterial detoxification of these compounds. The findings of this work and further perspectives are summarized and discussed in Chapter 5.

Chapter 2 The Natural Antimicrobial *trans*-Cinnamaldehyde Interferes with UDP-N-acetylglucosamine Biosynthesis and Cell Wall Homeostasis in *Listeria monocytogenes* [§]

2.1 Abstract

t-CIN, an antimicrobial compound from cinnamon essential oil, is of interest because it inhibits various foodborne pathogens. In the present work, we investigated the antimicrobial mechanisms of t-CIN in *L. monocytogenes* using a previously isolated *yvcK::Himar1* transposon mutant which shows hypersensitivity to t-CIN. Time-lapse microscopy revealed that t-CIN induces a bulging cell shape followed by lysis in the mutant. Complementation with wild-type *yvcK* gene completely restored the tolerance of *yvcK::Himar1* strain to t-CIN and the cell morphology. Suppressor mutants that partially reversed the t-CIN sensitivity of the *yvcK::Himar1* mutant were isolated from evolutionary experiments. Three out of five suppression mutations were in the *glmU-prs* operon and in *nagR* gene, which are linked to the biosynthesis of the peptidoglycan precursor uridine-diphosphate-N-acetylglucosamine (UDP-GlcNAc). GlmU catalyzes the last two steps of UDP-GlcNAc biosynthesis and NagR represses the uptake and utilization of N-acetylglucosamine. Feeding N-acetylglucosamine or increasing the production of UDP-GlcNAc synthetic enzymes fully or partially restored the t-CIN tolerance of the *yvcK* mutant. Together, these results suggest that YvcK plays a pivotal role in diverting substrates to UDP-GlcNAc biosynthesis in *L. monocytogenes* and that t-CIN interferes with this pathway, leading to a peptidoglycan synthesis defect.

[§] This chapter is based on the following publication: Sun, L.; Rogiers, G.; Michiels, C.W. The natural antimicrobial *trans*-cinnamaldehyde interferes with UDP-N-acetylglucosamine biosynthesis and cell wall homeostasis in *Listeria monocytogenes*. *Foods* **2021**, *10*, 1666.

2.2 Introduction

Because of its widespread occurrence, contamination of foods with *L. monocytogenes* cannot always be prevented, and preservatives are used in some foods to prevent the outgrowth of the pathogen to high numbers [3,156]. Despite their effectiveness, traditional preservatives are increasingly under scrutiny for possible adverse health effects, and food producers are exploring natural alternatives to replace them. Plant essential oils have received much attention in this respect since they constitute an immense reservoir of compounds that are active against a wide range of microorganisms [3]. A well-studied compound is t-CIN, one of the major components of cinnamon essential oil [13]. The most notable structural feature of t-CIN is the presence of an α,β-unsaturated aldehyde functional group, which confers electrophilic and thiol-reactive properties to the compound [13]. Our previous analysis showed that growth inhibition of *L. monocytogenes* by t-CIN is typically characterized by elongation of the lag phase [17]. Several studies have addressed the antimicrobial mechanisms of t-CIN and multiple hypotheses have been proposed including the inhibition of cell division [22], alteration of cell membrane composition and permeability [29], and reduction in intracellular ATP levels [31]. However, these effects are quite general secondary effects and precise insight into the primary cellular targets are not provided; hence, more specific approaches are therefore necessary.

In our previous work, a genome-wide random *Himar1* transposon mutant library was constructed in *L. monocytogenes* Scott A, and one of the mutants showing increased t-CIN sensitivity had a transposon insertion in the *yvcK* gene (*yvcK::Himar1*) [17]. However, the precise function of YvcK in *L. monocytogenes* was obscure. Loss of YvcK increased the sensitivity of *L. monocytogenes* to lysozyme and cell wall targeting antibiotics such as ampicillin, bacitracin, and ceftriaxone, and caused severe growth and morphology defects when growing the bacteria in minimal media with glycerol as the primary carbon source [160]. Similarly, deletion of *yvcK* in *B. subtilis* and *Mycobacterium smegmatis* induced deformed cell shape, attenuated growth on non-glycolytic carbon sources, and an elevated sensitivity to cell wall targeting antibiotics [161–163]. The similar phenotypes caused by loss-of-function mutations suggest a conserved function of YvcK in cell wall integrity and optimal carbon utilization in a broad range of Gram-positive bacteria, but its detailed cellular function needs to be further clarified.

A study of suppression mutations that restored either the attenuated growth on gluconeogenic carbon sources or the sensitivity to cefuroxime of a Δ*yvcK* mutant was recently conducted in *B. subtilis* [162]. Several mutations induced elevated expression of glucosamine-6-phosphate synthase (GlmS) and phosphoglucosamine mutase (GlmM), two key enzymes of the UDP-GlcNAc biosynthesis pathway [164]. Moreover, supplementation of N-acetylglucosamine (GlcNAc) to a growth medium with a non-glycolytic carbon source alleviated the attenuated morphology of a *B. subtilis yvcK* null mutant [162]. Furthermore, YvcK has been demonstrated to stimulate the activity of GlmS, depending on the intracellular concentration of UDP-GlcNAc [162,165]. Therefore, YvcK in *B. subtilis* was suggested to play a role in diverting carbon sources from central metabolism to the synthesis of UDP-GlcNAc [162,165].

In this work, we have characterized the t-CIN hypersensitive transposon mutant *yvcK::Himar1* to generate a deeper insight into the mode of action of t-CIN in *L. monocytogenes*. The mutant showed cell shape deformations which were exacerbated in the presence of t-CIN. Suppressor mutants of *yvcK::Himar1* with partially reversed t-CIN sensitivity were isolated and had mutations residing in the promoter region of the *glmU-prs* operon and in the coding region of *nagR*, which are both connected to UDP-GlcNAc biosynthesis. Overproduction of UDP-GlcNAc biosynthetic enzymes [GlmU (bifunctional glucosamine-1-phosphate acetyltransferase/GlcNAc-1-phosphate uridyltransferase), GlmS, and GlmM] and supplementation of GlcNAc to the growth medium restored at least partially the tolerance of the *yvcK* mutant to t-CIN. These findings suggest that YvcK plays a pivotal role in UDP-GlcNAc biosynthesis in *L. monocytogenes*, similar to its role in *B. subtilis* [162,165], and that t-CIN interferes with the UDP-GlcNAc homeostasis, probably by limiting the availability of the substrate Fru-6-P.

2.3 Materials and methods

2.3.1 Bacterial strains and growth conditions

Bacterial strains and plasmids used in this work are listed in Table 2.1. *L. monocytogenes* Scott A wild-type (WT) strain was acquired from the International Life Sciences Institute North America [166]. *E. coli* DH5α [167] and S17-1 λpir [168] were employed as the host for cloning constructs and as donor strain for conjugational plasmid

transfer, respectively. *L. monocytogenes* strains were grown at 30°C in Brain Heart Infusion (Oxoid, Hampshire, UK). *E. coli* strains were grown in Luria-Bertani (LB; 10 g/L tryptone, 5 g/L yeast extract, 5 g/L NaCl) at 37°C. Antibiotics were used when appropriate in the following concentrations: 50 µg/mL erythromycin (Acros Organics, Fair Lawn, NJ, USA) (Ery), 50 µg/mL kanamycin (AppliChem GmbH, Darmstadt, Germany) (Km), 100 µg/mL ampicillin (Thermo Fisher Scientific, Waltham, MA, USA) (Amp), 20 µg/mL polymyxin B sulfate (AppliChem GmbH) and 10 µg/mL chloramphenicol (Acros Organics) (Cm). Other chemicals used in this work include t-CIN (Acros Organics), N-Acetylglucosamine (Sigma-Aldrich, Saint Louis, MO, USA), and isopropyl β-D-1-thiogalactopyranoside (Acros Organics) (IPTG, 1 mM).

2.3.2 Evolutionary study to isolate *yvcK::Himar1* suppression mutants with regained t-CIN tolerance

An experimental evolution experiment was conducted as illustrated in Fig. 2.1. Independent colonies of the *yvcK::Himar1* strain were inoculated in six parallel test tubes with 4 mL BHI broth. After overnight incubation at 30°C with shaking (250 rpm), the cultures were diluted 1000-fold in BHI containing 1 mM, 2 mM, or 3 mM t-CIN (the stock solution of t-CIN at 1 M was prepared by dissolving t-CIN in ethanol). In BHI with 3 mM t-CIN, the *yvcK::Himar1* mutant failed to resume growth. A culture in BHI without t-CIN, to which only the equivalent amount of ethanol was added, was included as the control without selection pressure. Two hundred µL portions of diluted cultures were transferred into a 96-well microplate, covered with a transparent adhesive foil (Greiner Bio-One EASYseal™ Adhesive Microplate Sealer, Thermo Fisher Scientific) to protect against evaporation and contamination, and incubated at 30°C with continuous shaking (250 rpm) to reach stationary phase (OD_{630} ~ 0.7, determined with an automated microplate reader). Cultures were then again diluted 1:1000 in the same medium and passed to a fresh microplate for another round of growth. In each round, a portion of the stationary cultures was diluted $10^{\wedge 5}$ fold and 100 µL was spread on BHI agar. A 6 mm sterile Whatman® filter paper disc impregnated with 10 µL pure t-CIN was then placed in the center of the agar plate. An inhibition halo was formed around the paper disc after incubating the plate at 30°C for two days and 16 colonies near the inhibition zone were streaked. The resistance of the isolates against 2 mM t-CIN was evaluated by a growth assay in the microplate reader. The evolution experiment was continued until isolates with (partially) restored t-CIN tolerance emerged. No resistant colony

was picked when *yvcK::Himar1* mutant cells evolved in BHI or BHI with 1 mM t-CIN. A selection of these isolates from independent cultures was sent for whole-genome-sequencing (WGS) to analyze mutations.

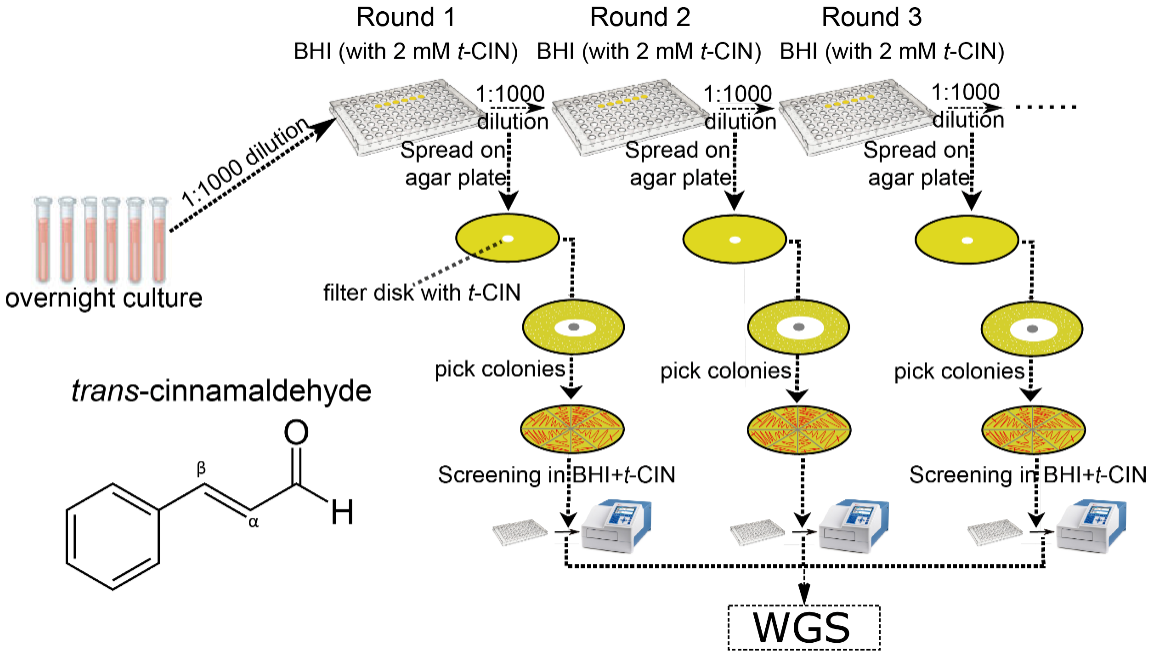

Figure 2.1 Scheme of the evolutionary experiment setup with *yvcK::Himar1* in BHI supplemented with 2 mM t-CIN as described in Materials and Methods. Isolates that recovered t-CIN tolerance were identified in all six independent lineages with t-CIN supplementation after three rounds of subculture, while no recovery of t-CIN tolerance was observed in control cultures without t-CIN. The molecular structure of t-CIN is also shown.

2.3.3 Whole-genome-sequencing

Genomic DNA was extracted from overnight cultures of *L. monocytogenes* with the GeneJET Genomic DNA purification kit (Thermo Fisher Scientific). The quality and concentration of genomic DNA were determined by gel electrophoresis, NanoDrop™ photometric, and Qubit fluorometric analysis (Thermo Fisher Scientific). Paired-end libraries were constructed with the NEBNext Ultra DNA Library Prep Kit (NEB, Ipswich, MA, USA) and sequenced at VIB Nucleomics Core (Leuven, Belgium) with an Illumina MiSeq sequencer (Illumina, San Diego, CA, USA). Reads were analyzed with CLC Genomic Workbench software (QIAGEN, Hilden, Germany) to determine mutations in the evolved strains compared to the *yvcK::Himar1* parental strain. All detected mutations were

subsequently checked by targeted amplification and Sanger sequencing (Macrogen Europe, Amsterdam, The Netherlands).

2.3.4 Growth assay

Growth curves were established by turbidity measurement (OD_{620} or OD_{630}) with an automated microplate reader (Multiskan Ascent® or Multiskan™ FC, Thermo Fisher Scientific). Firstly, the OD_{600} of overnight cultures was determined with an Ultrospec™ 10 Cell Density Meter (Biochrom, Cambridge, UK) and slightly adjusted by supplying additional BHI to obtain the same value ($OD_{600} \approx 2$) for all the cultures within a single experiment. The suspensions were then diluted 1000-fold in BHI to which 1 mM IPTG and/or 2 (3) mM t-CIN had been added if necessary. Then, 200 µL aliquots were transferred to a 96-well microplate, the plate was sealed with a transparent adhesive foil and incubated at 30°C in an automated microplate reader. Every 15 or 30 min, the plate was shaken at 960 rpm and OD_{620} was recorded. The Excel add-in package DMFit (Quadram Institute Bioscience, Norwich, United Kingdom) was used to determine the maximum growth rate (µmax), the lag phase time (λ), and the maximal OD (ODmax) value at stationary phase through the Baranyi and Roberts model [169].

Table 2.1 Strains and plasmids used in this work, the superscript "R" above antibiotics denotes the resistance to the corresponding antibiotic.

Bacterial Species	**Designation in This Work**	**Description**	**Reference**
L. monocytogenes	WT	WT strain Scott A; WGS accession number at NCBI: CM001159	[166]
	WT/pIMK2	WT with pIMK2 integrated, Km^R	This work
	yvcK::Himar1	Transposon insertion in *yvcK*, Em^R	This work
	yvcK/pIMK3	*yvcK::Himar1* with pIMK3 integrated, Km^R Em^R	This work
	yvcK/pIMK3::yvcK	*yvcK::Himar1* with pIMK3-yvcK integrated, Km^R Em^R	This work
	yvcK/pIMK3::glmU	*yvcK::Himar1* with pIMK3-glmU integrated, Km^R Em^R	This work
	yvcK/pIMK2::glmM	*yvcK::Himar1* with pIMK2-glmM integrated, Km^R Em^R	This work
	yvcK/pIMK2::glmS	*yvcK::Himar1* with pIMK2-glmS integrated, Km^R Em^R	This work
	yvcK::Himar1 ΔnagR	In-frame deletion of *nagR* in *yvcK::Himar1* strain, Em^R	This work
	yvcK::Himar1 ΔnagR/pIMK2	*yvcK::Himar1 ΔnagR* with pIMK2 integrated, Km^R Em^R	This work
	yvcK/pIMK2::nagR	*yvcK::Himar1* with pIMK2-nagR (WT allele) integrated, Km^R Em^R	This work
	yvcK/pIMK2::nagR^M	*yvcK::Himar1* with pIMK2-nagR (mutated allele from *M 2.2* suppression mutant) integrated, Km^R Em^R	This work
E. coli	S17-1 λpir	Donor strain for plasmid conjugation	[168]
	DH5-α	Host strain for plasmid constructs	[167]
Plasmids	Description		Reference
pIMK2	Site-specific listerial integrative vector, Phelp constitutive promoter, 6.2 kb, Km^R		[170]
pIMK3	Site-specific listerial integrative vector, Phelp IPTG inducible promoter, 7.5 kb, Km^R		[170]
pIMK3-yvcK	pIMK3 with *yvcK* gene (locus tag: LMOSA_4390) from Scott A		This work
pIMK3-glmU	pIMK3 with *glmU* gene (locus tag: LMOSA_10910) from Scott A		This work
pIMK2-glmM	pIMK2 with *glmM* gene (locus tag: LMOSA_1060) from Scott A		This work
pIMK2-glmS	pIMK2 with *glmS* gene (locus tag: LMOSA_16310) from Scott A		This work
pIMK2-nagR	pIMK2 with *nagR* gene (locus tag: LMOSA_18480) from Scott A		This work
pIMK2-nagR^M	pIMK2 with mutated *nagR^M* gene from *M 2.2* suppression mutant strain		This work
pKSV7-oriT	Temperature-sensitive shuttle vector for making gene deletion in *L. monocytogenes*, 6742 bp, Amp^R, Cm^R		[171,172]
pKSV7-oriT-ΔnagR	pKSV7-oriT with 1 kb flanking fragments upstream and downstream of *nagR* inserted		This work

2.3.5 Microscopy and cell dimension measurement

To measure cell dimensions, one µL of an appropriately diluted late exponential culture ($OD_{600} \approx 1$) was applied to 2% agarose pads deposited on a microscopy slide on which a cover glass was mounted using a Gene Frame (Thermo Fisher Scientific). Observations were made with an Eclipse Ti-E inverted microscope (Nikon, Champigny-sur-Marne, France) equipped with a CoolSnap HQ2 FireWire CCD-camera. Images were acquired using NIS-elements software (Nikon), and cell width and length were determined with the MicrobeTracker image analysis software [173], with manual curation to remove false segmentation. For the time-lapse phase-contrast microscopy, the agarose pads were prepared with BHI supplemented with 1 mM t-CIN. Overnight stationary cultures were diluted 50-fold in BHI with 1 mM t-CIN and one µL diluted culture was applied to the BHI agarose pad. The observation was performed at the temperature set at 30°C and an image was acquired every 30 min for 24 h.

2.3.6 Genetic complementation of mutant strains

For genetic complementation of the *yvcK::Himar1* mutant, the WT *yvcK* gene was amplified using primer pair yvcK_NcoI/yvcK_SalI (Table 2.2), cleaved with the restriction enzymes NcoI and SalI, and cloned in pIMK3 restricted with the same enzymes, using standard cloning procedures. After verification with Sanger sequencing, the construct was conjugated from *E. coli* S17-1 λpir into *L. monocytogenes yvcK::Himar1*. Successful chromosomal integration was confirmed via PCR with primers yvcK_NcoI and NC16(II) (Table 2.2) (which anneal left and right of the integration site and point inwards) and Sanger sequencing with pIMK_FW/pIMK_REV (Table 2.2) primer pair, which point towards the *yvcK* gene from both sides of the pIMK3 cloning site. The complementation strain was designated as *yvcK/pIMK3-yvcK*. Control strains were constructed by integration of the empty pIMK2 and pIMK3 plasmid into WT and *yvcK::Himar1* strains, respectively, and were designated as *WT/pIMK2* and *yvcK/pIMK3*, respectively.

The same strategy was used to overexpress *glmU*, *glmM*, *glmS*, and the WT and mutant allele of *nagR* in *L. monocytogenes*, using glmU_NcoI/glmU_SalI, glmM_NcoI/glmM_SalI, glmS_NcoI/glmS_SalI, and nagR_BspHI/nagR_SalI primer pairs, respectively (Table 2.2). The integration vectors used were pIMK2 (*glmM, glmS,* and *nagR*) or pIMK3 (*glmU*) [170]. The plasmid constructs and strains are listed in Table 2.1.

Table 2.2 Primers used in this work.

Primer	Sequence (5′–3′) *	Reference
yvcK_NcoI	GCATCCATGGGAAAAAAGGAAATGAAACC	This work
yvcK_SalI	CACTGTCGACTCACTCCTTTTCAATAG	This work
glmU_NcoI	ATATCCATGGAATCAAAACGATATGCTGTAGTGC	This work
glmU_SalI	ATATGTCGACTTATTTACCGTGATTCAAATGTTTTGC	This work
glmM_NcoI	ATATATCCATGGGTAAATATTTTGGTACGGATGGAGT	This work
glmM_SalI	ATATATGTCGACTGTTGTTTTAATCGTTAAGTGCCAT	This work
glmS_NcoI	ATATATCCATGGAATGTGGAATCGTTGGATATATTGGAA	This work
glmS_SalI	ATATATGTCGACTTATTCTACTGTGACACTTTTTGCTA	This work
nagR-KO-A	ATATGGTACCGGCTGGTAAGGATGCAGATTT	This work
nagR-KO-B	CATTTTCCCGCCCTCTTCTT	This work
nagR-KO-C	AAGAAGAGGGCGGGAAAATGATGAAACTCAGGCAGATTACAACA	This work
nagR-KO-D	ATATCTGCAGCAAGTGTCCCAGCGATTAACA	This work
nagR_BspHI	ATATATTCATGATCGATAAACAATCAGGAATAC	This work
nagR_SalI	ATATATCTGCAGTTATTGTTTAATCCTAGCTACAAATTGAA	This work
pIMK_FW	GAGTCAGTGAGCGAGGAAGC	[17]
pIMK_REV	CCTATCACCTCAAATGGTTCG	[17]
NC16(II)	GTCAAAACATACGCTCTTATCGATTC	This work
pKSV7-CK-F	TAGCTCACTCATTAGGCAC	This work
pKSV7-CK-R	TAAGGAGAAAATACCGCATCA	This work

* Restriction sites are underlined: NcoI (CCATGG), SalI (GTCGAC), BspHI (TCATGA), KpnI (GGTACC), and PstI (CTGCAG).

2.3.7 Construction of *nagR* deletion mutant

The pKSV7-oriT plasmid [171] was utilized to generate in-frame deletions of *nagR* as described [171,172]. Firstly, approximately 1 kb fragments from upstream and downstream of *nagR* were amplified with nagR-KO-A/B and nagR-KO-C/D primer pairs (Table 2.2). The obtained PCR products were diluted 100-fold, mixed in a ratio of 1:1, and employed as a template for overlapping extension PCR utilizing nagR-KO-A/D primer pair. The obtained ~ 2 kb PCR fragment and pKSV7-oriT were then digested with KpnI and PstI restriction enzymes and ligated overnight. Following transformation to *E. coli* DH5α, constructs were extracted and checked by PCR and Sanger sequencing with pKSV7-CK-F and pKSV7-CK-R primers. The construct was then electro-transformed to *L. monocytogenes* as described [170]. After recovery in BHI broth at 30°C for three hours, the cells were spread on BHI agar plates with Cm (10 μg/mL) and incubated at 30°C for two days. The allelic exchange was performed with a colony picked from the plate as previously described [172]. Mutants were identified by colony PCR with nagR-KO-A and nagR-KO-D primers and Sanger sequencing was then performed to identify a successful deletion mutant.

2.3.8 Statistical analysis

Growth parameters calculated from the growth assay are presented as means ± SD of three biological replicates. The significance of mean differences was calculated by Tukey's honestly significant difference (Tukey's HSD) test using GraphPad PRISM 7.0 (GraphPad, San Diego, CA, USA). p values < 0.05 were considered statistically significant.

2.4 Results

2.4.1 Characterization of the t-CIN hypersensitive *yvcK::Himar1* mutant

As aforementioned, a t-CIN hypersensitive mutant *yvcK::Himar1* was isolated in a screening of an *L. monocytogenes* Scott A transposon mutant library [17]. The *Himar1* transposon is inserted at 655 bp from the start codon of *yvcK* (Fig. 2.2A) and WGS analysis demonstrated no additional mutation. The *yvcK* gene is part of an operon comprising the ORFs *yvcJ*, *yvcK*, *whiA*, and a gene predicted to encode an NADH dehydrogenase [174] (Fig. 2.2A). However, their intracellular functions are poorly characterized.

In BHI broth with 2 mM t-CIN, the *yvcK::Himar1* mutant showed attenuated growth, with a significantly extended lag phase compared to WT (48.2 h vs. 8.9 h) (Fig. 2.2B&C). In addition, the mutant also exhibited a lower OD_{max} and growth rate. Complementation with the WT *yvcK* allele (designated as *yvcK/pIMK3::yvcK*), but not with the two downstream genes of *yvcK* (data not shown), completely restored the phenotype, confirming the role of YvcK in t-CIN tolerance. Time-lapse microscopy confirmed the attenuated growth of the WT strain in the presence of 1 mM t-CIN and revealed a filamentous shape with swellings at the pole of some bacteria (Fig. 2.3, 15 h). More pronounced pole bulging and cell lysis were observed for the *yvcK* mutant (Fig. 2.3, bottom panel, 15 h and 20 h). This bulging cell shape and cell lysis indicate a severe disruption of cell wall integrity and can explain the attenuated growth of the *yvcK* mutant in the presence of t-CIN. Although the *yvcK* mutant grew almost like a WT strain in the absence of t-CIN (Fig. 2.2B&C), its cells at late log phase (OD_{600} = 1 by a cell density meter) are on average 0.07 µm (p < 0.05) thicker and 0.36 µm (p < 0.05) shorter than those of the WT strain (Fig. 2.4), indicating that YvcK might play a role in cell wall biosynthesis or regulation of *L. monocytogenes*. Normal cell shape was restored upon complementation with the WT *yvcK* allele (Fig. 2.4).

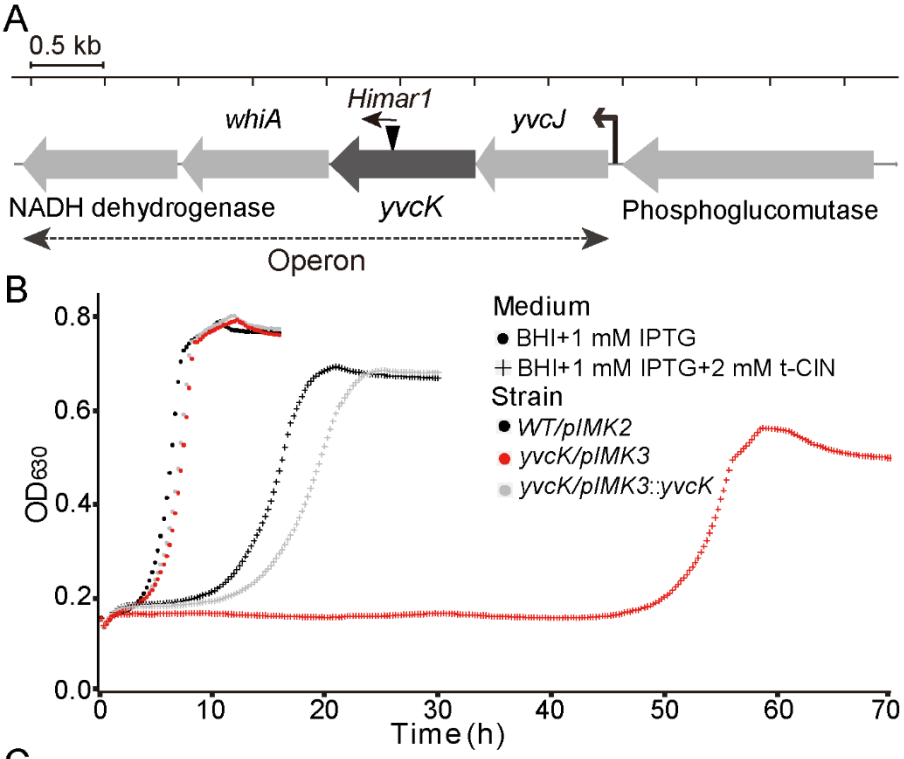

C

Strain	*WT/pIMK2*	*yvcK/pIMK3*	*yvcK/pIMK3::yvcK*
Medium	BHI		
lag phase (h)	3.9 ± 0.2^{A}	4.3 ± 0.1^{A}	4.1 ± 0.1^{A}
ODmax	0.78 ± 0.02^{A}	0.79 ± 0.01^{A}	0.79 ± 0.01^{A}
µmax (/h)	0.170 ± 0.002^{A}	0.169 ± 0.001^{A}	0.170 ± 0.000^{A}
Medium	BHI + 2 mM *t*-CIN + 1mM IPTG		
lag phase (h)	8.9 ± 0.2^{A}	48.2 ± 0.5^{B}	9.6 ± 0.2^{A}
ODmax	0.68 ± 0.02^{C}	0.55 ± 0.04^{D}	0.68 ± 0.04^{C}
µmax (/h)	0.068 ± 0.002^{C}	0.056 ± 0.005^{D}	$0.065 \pm 0.005^{C,D}$

Figure 2.2 The transposon mutant *yvcK::Himar1* is hypersensitive to t-CIN. (**A**) The gene context of *yvcK* in the genome of *L. monocytogenes* Scott A, with the insertion of the *Himar1* transposon (black triangle) indicated. The arrow on top of the transposon indicates the orientation of the erythromycin resistance gene (*ermC*). Four genes, including *yvcJ*, *yvcK*, *whiA*, and the gene predicted to encode an NADH dehydrogenase, form an operon [174]. A putative transcription start site is indicated with a black arrow. (**B**) Growth curves of *WT/pIMK2* (black), *yvcK/pIMK3* mutant (red), and the complemented strain *yvcK/pIMK3::yvcK* (grey) in BHI broth (dot) and BHI broth with 2 mM t-CIN and 1 mM IPTG (cross). All curves represent the mean values of three independent cultures. (**C**) Values of λ, µmax, and ODmax from the growth curves in (**B**) are listed in the table. Values are mean ± SD (n = 3) and those followed by a common letter are not significantly different at the 5% level of significance.

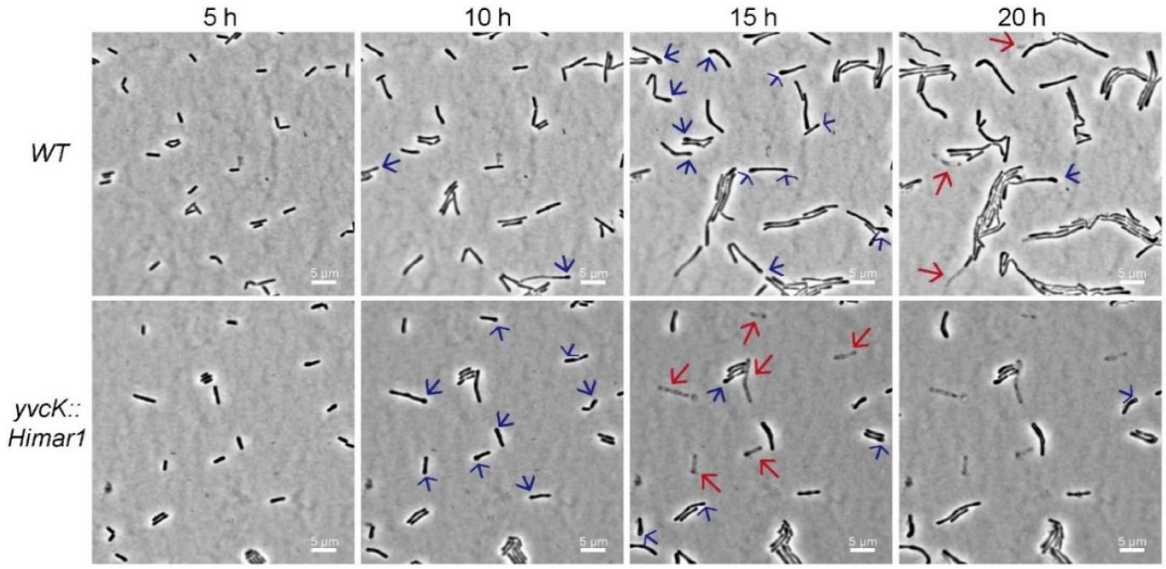

Figure 2.3 Time-lapse observation of WT and *yvcK::Himar1* in BHI supplemented with 1 mM t-CIN at 30°C. Phase-contrast images were acquired every 0.5 h and images of a representative specific field at 5 h, 10 h, 15 h, and 20 h are presented. The red arrows indicate cell lysis of *yvcK::Himar1*. Polar bulging (blue arrows) can be observed at 10 h, 15 h, and 20 h, and is more pronounced for the *yvcK* mutant cells at 10 h.

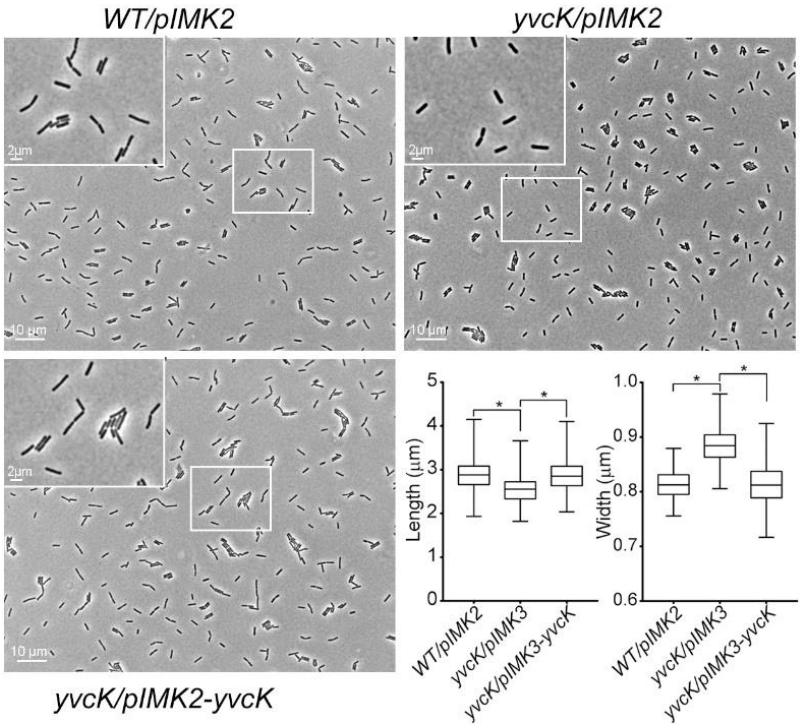

Figure 2.4 Microscopic cell dimension measurement of *L. monocytogenes* WT and *yvcK::Himar1* mutant strain grown in BHI to exponential phase (OD_{600} = 1) without t-CIN (but containing 1 mM

IPTG). The cell width and length were analyzed with MicrobeTracker software [173] and are depicted in the box and whisker plots (displaying Min and Max at the whiskers, 25 to 75 percentiles at the box, and median in the centre line). n = 300. *, the significant difference at $p < 0.0001$ by two-tailed Student's t-test.

2.4.2 Suppressor mutations reverse the sensitivity of *yvcK::Himar1* to t-CIN

To gain insight into the role of YvcK in t-CIN tolerance, an evolutionary experiment was performed as depicted in Fig. 2.1, and several isolates with partially restored t-CIN tolerance were obtained from the *yvcK::Himar1* mutant. These suppression mutants exhibited lag phases intermediate to those of the *yvcK* mutant and the WT strain when grown in BHI with 2 mM t-CIN (Fig. 2.5). In contrast, no strains with restored t-CIN tolerance were isolated from the control culture in BHI. Five independent suppressor mutants were subjected to WGS analysis and mutations they have incurred compared to their parental *yvcK::Himar1* strain are listed in Table 2.3. Two suppression mutants (M 3.3 and M 4.1) had a point mutation immediate upstream of the *glmU-prs* operon, in a region reported to encode the small RNA rli73 [174] (Fig. 2.6A). GlmU is a bifunctional protein, whose C-terminal and N-terminal domain catalyze the sequential conversion of glucosamine-1-phosphate (GlcN-1-P) to GlcNAc-1-P and then to UDP-GlcNAc [164] (Fig. 2.6B). Moreover, M 4.1 had an additional point mutation causing an amino acid replacement in *fbaA*, which encodes a class II fructose-bisphosphate aldolase. This protein catalyzes the reversible conversion of fructose-1,6-bisphosphate to glyceraldehyde-3-phosphate and dihydroxyacetone phosphate in the glycolysis and gluconeogenesis pathways [175]. Within the *glmU-prs* operon, a point mutation was also found in the coding region of *prs* in suppression mutant M 6.1 (Fig. 2.6A, Table 2.3). The *prs* gene encodes the ribose-phosphate pyrophosphokinase which converts ribose-5-phosphate (Ribose-5-P) into phosphoribosyl pyrophosphate (PRPP), an essential reaction connecting the pentose phosphate pathway with biosynthesis pathways of nucleotides as well as some amino acids and other compounds [176].

Another mutation directly linked to the biosynthesis of UDP-GlcNAc is the 6 bp in-frame insertion in *nagR* in mutant M 2.2 (Fig. 2.6A, Table 2.3), whose product functions as the repressor for GlcNAc utilization (Fig 2.6B) [177–179]. As depicted in Fig. 2.6, *nagR* forms an operon with *nagA* and *nagB* that is under the direct control of NagR. Among all the isolates from the evolution experiment, this suppression mutant exhibited the strongest reversion of t-CIN sensitivity of the *yvcK* mutant (the lag phase from 56 h to 13.6 h), with a

lag phase approaching that of the WT strain (Fig. 2.5). Finally, the growth of mutant M 5.1, which has a 6 bp in-frame deletion in *rpoA*, encoding the RNA polymerase subunit alpha, resembled the growth of mutant M 2.2 in the presence of 2 mM t-CIN. However, how the mutated RpoA affects transcription and whether it has a specific impact on the UDP-GlcNAc biosynthesis pathway is unclear and was not further investigated here.

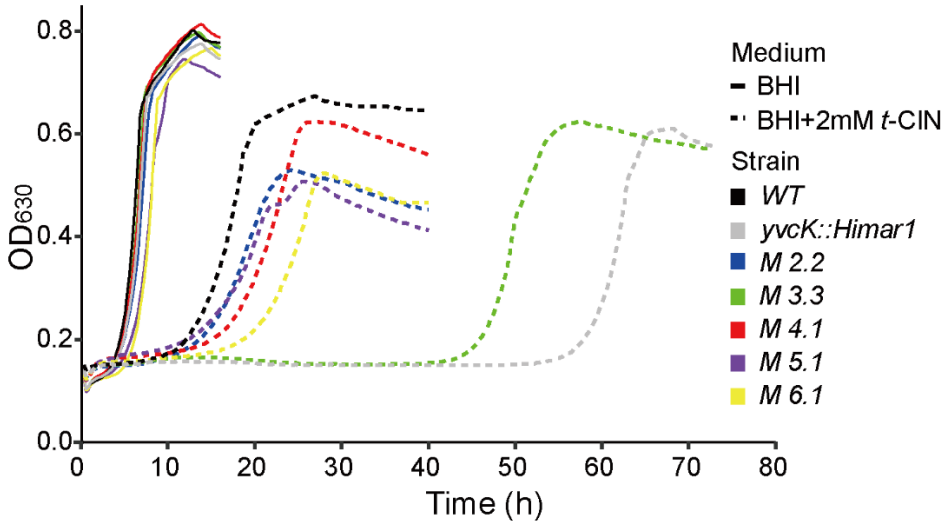

	BHI			BHI + 2 mM t-CIN		
Strain	lag phase (h)	ODmax	μmax (/h)	lag phase (h)	ODmax	μmax (/h)
WT	4.2 ± 0.0^{A}	0.74 ± 0.00^{A}	0.170 ± 0.002^{A}	12.9 ± 0.3^{A}	0.64 ± 0.00^{A}	0.070 ± 0.000^{A}
yvcK::Himar1	4.5 ± 0.2^{B}	$0.72 \pm 0.01^{A,B}$	0.168 ± 0.001^{A}	55.0 ± 1.2^{D}	0.59 ± 0.06^{A}	$0.064 \pm 0.005^{A,B}$
M 2.2	5.2 ± 0.0^{C}	$0.70 \pm 0.02^{A,B}$	0.162 ± 0.002^{A}	13.6 ± 0.2^{A}	0.50 ± 0.00^{B}	0.043 ± 0.014^{B}
M 3.3	$4.3 \pm 0.2^{A,B}$	$0.71 \pm 0.02^{A,B}$	0.167 ± 0.004^{A}	41.7 ± 1.3^{C}	0.59 ± 0.03^{A}	$0.059 \pm 0.009^{A,B}$
M 4.1	$4.4 \pm 0.1^{A,B}$	$0.71 \pm 0.02^{A,B}$	0.165 ± 0.001^{A}	14.2 ± 0.1^{A}	0.61 ± 0.04^{A}	$0.054 \pm 0.006^{A,B}$
M 5.1	6.1 ± 0.2^{D}	0.65 ± 0.02^{C}	0.145 ± 0.004^{C}	13.1 ± 0.6^{A}	0.49 ± 0.02^{B}	0.039 ± 0.017^{B}
M 6.1	5.7 ± 0.1^{D}	$0.68 \pm 0.02^{B,C}$	0.149 ± 0.005^{C}	19.3 ± 2.1^{B}	0.48 ± 0.04^{B}	$0.045 \pm 0.005^{A,B}$

Figure 2.5 Growth curves and parameters of suppression mutants that partially restore the tolerance of *yvcK::Himar1* to t-CIN, in BHI and BHI with 2 mM t-CIN. Growth curves represent the average of measurements of three independent cultures. Values of λ, μmax, and ODmax are shown in the table as mean ± SD; $n = 3$. Values followed by a common letter are not significantly different at the 5% level of significance.

Table 2.3 Mutations identified by WGS in the suppression mutants that partially restore t-CIN tolerance of *yvcK::Himar1*.

Strain	Mutations	Coding Region Change	Location in Gene	Affected Gene	Encoded Product
M 3.3	C-A		−108 b from *glmU* start codon	*rli73*	Small RNA rli73
	T-C		243 b downstream of peroxide-responsive repressor gene *perR*		Noncoding region
M 6.1	A-G	Y97C	+290 b from *prs* start codon	*prs*	Ribose-phosphate pyrophosphokinase
M 2.2	In frame insertion ATAAAG	Insertion of I K between L165-Y166	between +495 b–+496 b of *nagR* start codon	*nagR*	Transcriptional regulator NagR
M 4.1	T-C		−111 bp from *glmU* start codon	*rli73*	Small RNA rli73
	C-A	W239L	+716 bp from *fbaA* start codon	*fbaA*	Fructose-bisphosphate aldolase
M 5.1	In-frame deletion ACCACG	Deletion of R144-G145	from +430 b to +435 b of *rpoA*	*rpoA*	DNA-directed RNA polymerase subunit alpha

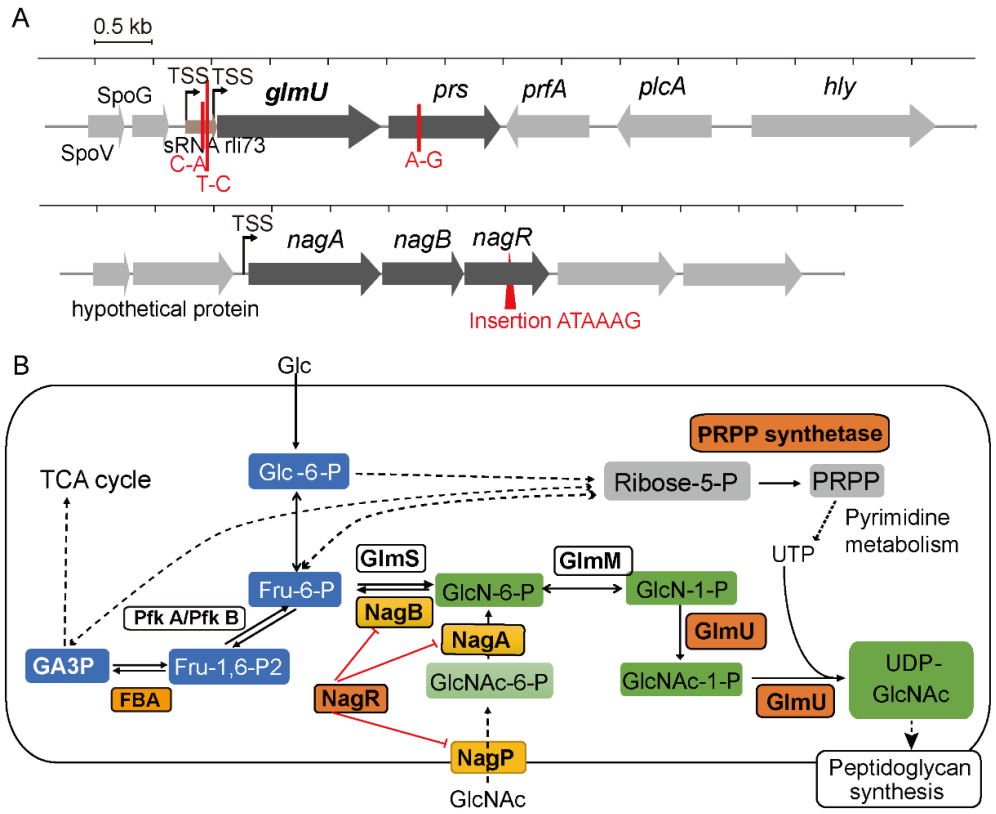

Figure 2.6 (**A**) Locations of *yvcK* suppression mutations in the *glmU-prs* and *nagABR* operon. Single nucleotide variations are depicted as red bars and the in-frame insertion in *nagR* as a red triangle. Transcription start sites (TSSs) [174] of operons are indicated with a black arrow. (**B**) Scheme of the UDP-GlcNAc biosynthesis pathway with the indication of the functions of GlmU and NagR [164,177]. Proteins affected by suppression mutations identified in this work are colored in orange. NagR-suppressed proteins are colored yellow. Intermediates of the glycolysis, the UDP-GlcNAc pathway, and the pentose phosphate pathway are shown in blue, green, and grey, respectively. PRPP, phospho-alpha-D-ribosyl-1-pyrophosphate; PRPP synthetase, ribose-phosphate pyrophosphokinase; Pfk, phosphofructokinase; and FBA, fructose-bisphosphate aldolase.

2.4.3. GlcNAc supplementation reverses the t-CIN sensitivity of the *yvcK::Himar1* mutant

Since several of the identified suppression mutations were linked to the biosynthesis of UDP-GlcNAc, we tested whether supplementation of the growth medium with GlcNAc could suppress the growth defect of the *yvcK* mutant in the presence of t-CIN. Depending on the concentration, GlcNAc indeed partially (10 mM) or completely (50 mM) reduced the lag phase of the *yvcK* mutant to WT level (Fig. 2.7). The growth of the WT strain in BHI with 2 mM t-CIN was also slightly improved by 50 mM GlcNAc, with a slightly higher growth rate and ODmax. The ability of GlcNAc to suppress the t-CIN sensitivity of the *yvcK* mutant is

consistent with the idea that YvcK regulates UDP-GlcNAc biosynthesis in *L. monocytogenes*. Microscopy also revealed reduced cell lysis of the *yvcK* mutant in the presence of 1 mM t-CIN upon GlcNAc supplementation, although the cells retained their characteristic shape deformation both with and without t-CIN (Fig. S2.1 and Fig. 2.2).

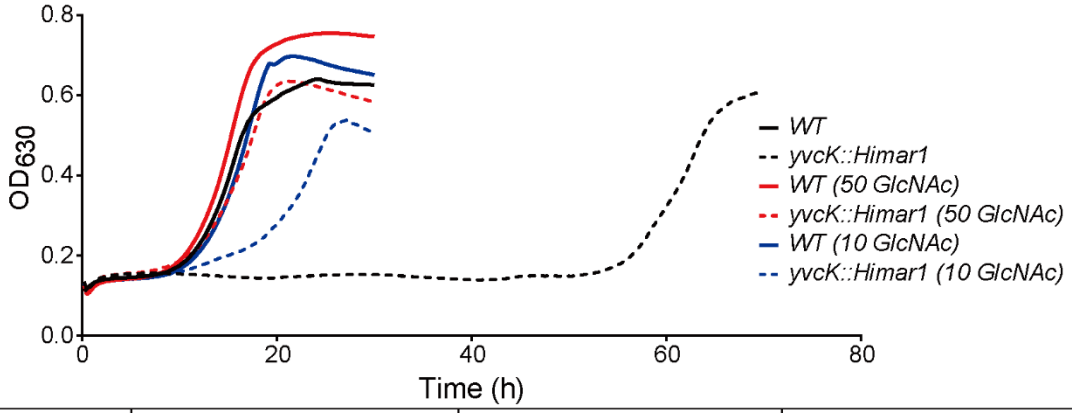

	BHI		BHI + 50 mM GlcNAc		BHI + 10 mM GlcNAc	
Strain	*WT*	*yvcK::Himar1*	*WT*	*yvcK::Himar1*	*WT*	*yvcK::Himar1*
lag phase (h)	12.7 ± 0.9^{A}	54.0 ± 2.2^{B}	12.0 ± 0.5^{A}	13.6 ± 1.7^{A}	13.4 ± 1.4^{A}	14.4 ± 1.1^{A}
ODmax	$0.65 \pm 0.01^{A,B}$	0.61 ± 0.03^{B}	0.75 ± 0.01^{C}	0.62 ± 0.01^{B}	0.67 ± 0.01^{A}	0.49 ± 0.01^{D}
μmax (/h)	0.075 ± 0.002^{A}	0.021 ± 0.003^{B}	0.090 ± 0.002^{C}	0.023 ± 0.006^{B}	$0.069 \pm 0.015^{A,C}$	0.0012 ± 0.000^{D}

Figure 2.7 Growth curves and parameters of *L. monocytogenes* WT and *yvcK::Himar1* in BHI broth with 2 mM t-CIN, and with or without 50 mM or 10 mM GlcNAc supplementation. Growth curves represent the average of three independent cultures. Values of λ, μmax, and ODmax are shown in the table as mean ± SD; $n = 3$. Values followed by a common letter are not significantly different at the 5% level of significance.

The catabolism of GlcNAc is well elucidated in *B. subtilis* [177]. The uptake of GlcNAc into the bacteria is mediated by the GlcNAc-specific phosphoenolpyruvate phosphotransferase system protein NagP, which concomitantly phosphorylates GlcNAc to GlcNAc-6-phosphate (GlcNAc-6-P) [177,180] (Fig. 2.6B). GlcNAc-6-P is then converted to GlcN-6-phosphate (GlcN-6-P) by the GlcNAc-6-P deacetylase NagA [177,181]. GlcN-6-P can either be converted to Fru-6-P by GlcN-6-P deaminase NagB [182] or feed into the UDP-GlcNAc biosynthesis pathway [177]. The capacity of GlcNAc to suppress the t-CIN sensitivity of the *yvcK* mutant may implicate an insufficient availability of substrate (GlcN-6-P) for UDP-GlcNAc biosynthesis in this mutant under these conditions.

2.4.4. Overexpression of UDP-GlcNAc biosynthetic enzymes reduce the t-CIN sensitivity of the *yvcK* mutant

As aforementioned, two suppression mutations were found immediately upstream of *glmU-prs* operon, in a region demonstrated by transcriptome analysis to encode a small RNA (sRNA) [174] (Fig. 2.6A). Since the provision of GlcNAc restored the attenuated growth of the *yvcK* mutant, we hypothesize that transcription of *glmU-prs* is affected by these mutations, leading to increased UDP-GlcNAc biosynthesis. To test whether increased expression of UDP-GlcNAc biosynthetic enzymes suppresses the t-CIN sensitivity of the *yvcK* mutant, *glmU*, *glmM* and *glmS* were cloned into pIMK2 or pIMK3 plasmids [170] and introduced into *yvcK* mutant. When the expression of *glmU* was induced by IPTG, the sensitivity of *yvcK* mutant to t-CIN was effectively restored to almost WT level (Fig. 2.8A). Expression of *glmM and glmS* also restored the t-CIN tolerance of the *yvcK* mutant, but only partially (Fig. 2.8B). These results suggest that increased levels of these UDP-GlcNAc biosynthetic enzymes promote the flux of substrate into the UDP-GlcNAc biosynthetic pathway. In contrast, overexpression of these proteins in the WT strain did not further increase t-CIN resistance (Fig. S2.3), indicating that the growth-limiting factor of WT in the presence of t-CIN is not UDP-GlcNAc homeostasis.

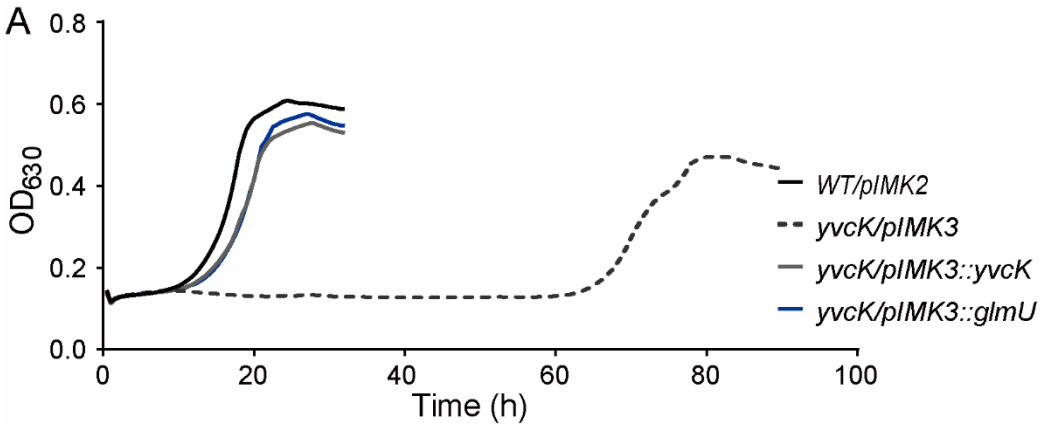

Strain	*WT/pIMK2*	*yvcK/pIMK3*	*yvcK/pIMK3::yvcK*	*yvcK/pIMK3::glmU*
lag phase (h)	11.6 ± 0.1^{A}	63.0 ± 1.1^{C}	14.0 ± 0.2^{B}	13.8 ± 0.1^{B}
ODmax	0.61 ± 0.00^{A}	0.51 ± 0.05^{B}	0.60 ± 0.04^{A}	0.58 ± 0.02^{A}
µmax (/h)	0.070 ± 0.000^{A}	0.057 ± 0.001^{B}	0.065 ± 0.010^{A}	0.071 ± 0.009^{A}

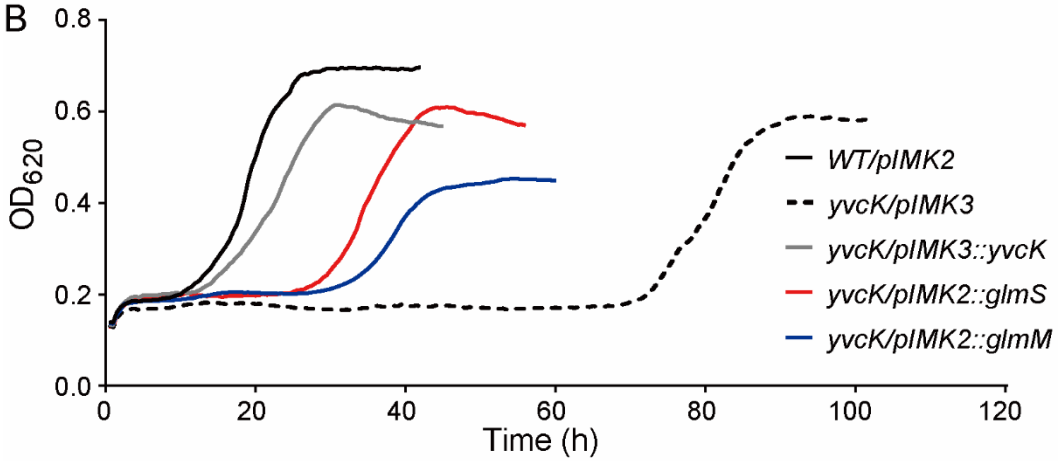

Strain	*WT/pIMK2*	*yvcK/pIMK3*	*yvcK/pIMK3:: yvcK*	*yvcK/pIMK2:: glmM*	*yvcK/pIMK2:: glmS*
lag phase (h)	13.7 ± 0.2^{A}	72.4 ± 1.2^{D}	14.9 ± 0.9^{A}	32.0 ± 1.1^{C}	25.1 ± 1.7^{B}
ODmax	0.66 ± 0.05^{A}	0.55 ± 0.01^{B}	$0.59 \pm 0.05^{A,B}$	0.34 ± 0.03^{C}	$0.57 \pm 0.04^{A,B}$
µmax (/h)	0.045 ± 0.003^{A}	0.022 ± 0.008^{B}	0.044 ± 0.008^{A}	0.015 ± 0.001^{B}	0.042 ± 0.010^{A}

Figure 2.8 Effect of overproduction of UDP-GlcNAc biosynthetic enzymes on t-CIN sensitivity of the *yvcK* mutant. (**A**) Expression of *glmU* on the pIMK3 plasmid was induced by 1 mM IPTG in the *yvcK::Himar1* strain and growth in BHI with 2 mM t-CIN and 1 mM IPTG was monitored at 30°C by measuring OD_{630}. (**B**) *glmS* and *glmM* were constitutively expressed from the pIMK2 plasmid in the *yvcK::Himar1* strain and growth curves in BHI with 2 mM t-CIN were monitored at 30°C by measuring OD_{620}. The curves represent the average of three independent cultures. Values of λ, µmax, and ODmax are specified in the tables as mean ± SD; $n = 3$. Values followed by a common letter are not significantly different at the 5% level of significance.

2.4.5 Complementation with mutated *nagR* allele from strain M 2.2 partially restores sensitivity of *yvcK::Himar1* to t-CIN

Since NagR acts as the repressor of GlcNAc utilization genes, we anticipated that deletion of *nagR* might cure the t-CIN sensitivity of the *yvcK* mutant. However, unexpectedly, the opposite effect was observed, with a further lag time extension by several hours (Fig. 2.9). Medium supplementation with GlcNAc also did not suppress t-CIN sensitivity of the *yvcK-nagR* double mutant, unlike what was the case for the *yvcK* mutant (Fig. S2.4). A possible explanation of this behavior is the derepression of *nagB* expression in absence of NagR [177], which routes the incoming GlcNAc to glycolysis rather than to UDP-GlcNAc synthesis (Fig. 2.6B). Likewise, in *B. subtilis*, GlcNAc supplementation only slightly lowered the sensitivity of a *yvcK* null mutant to the beta-lactam antibiotic cefuroxime, while disruption of the route from GlcNAc to Fru-6-P by disruption of *nagB* reduced the sensitivity of this mutant to WT level [162]. Interestingly, overexpression of the mutated $nagR^M$ allele (the mutated *nagR* from strain M 2.2) in the *yvcK* mutant (designated as *yvcK/pIMK2::*$nagR^M$*)* significantly reduced the sensitivity of the bacteria to t-CIN, with a reduction in the lag time from 58 h to 32 h (Fig. 2.9). However, the strain remained more sensitive than the suppression mutant M 2.2 in which the $nagR^M$ mutation was identified (Fig. 2.5). Overexpression of WT *nagR*, in contrast, showed no impact on the t-CIN sensitivity of the *yvcK* mutant (Fig. 2.9). Also, neither inactivation of NagR nor overproduction of NagR or $NagR^M$ affected the resistance of WT bacteria to t-CIN (Fig. S2.3). Altogether, we suspect that the mutation in $NagR^M$ modulates its repression of target genes.

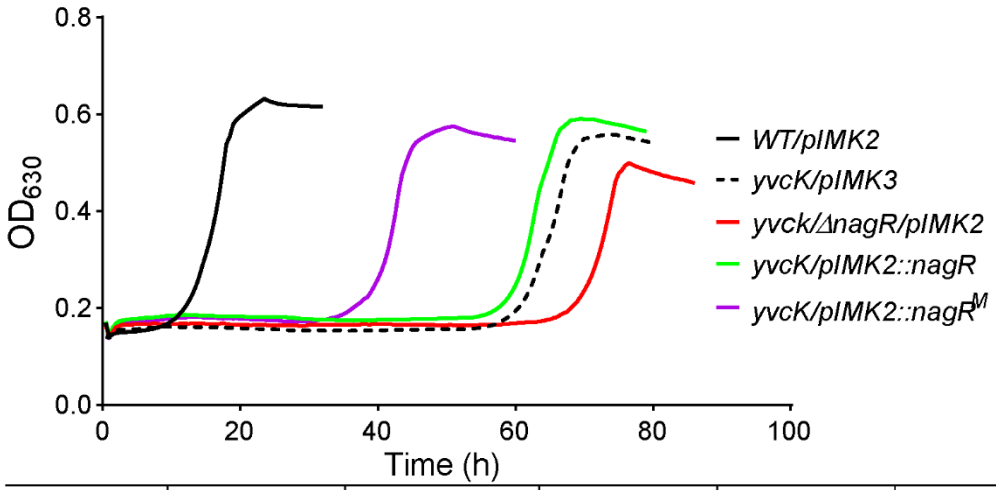

Strain	*WT/pIMK2*	*yvcK/pIMK3*	*yvcK/ΔnagR/ pIMK2*	*yvcK/pIMK2:: nagR*	*yvcK/pIMK2:: nagR^M*
lag phase (h)	9.9 ± 0.1^A	57.5 ± 1.6^C	66.8 ± 1.8^D	54.5 ± 3.4^C	32.0 ± 0.7^B
ODmax	0.62 ± 0.00^A	0.56 ± 0.01^B	0.48 ± 0.00^C	0.59 ± 0.00^{A,B}	0.59 ± 0.04^{A,B}
µmax (/h)	0.040 ± 0.000^A	0.040 ± 0.005^A	0.042 ± 0.005^A	0.035 ± 0.007^A	0.034 ± 0.006^A

Figure 2.9 Growth curves and parameters of *yvcK::Himar1* mutant with *nagR* or *nagR^M* allele expressed from integrated pIMK2 plasmid (designated as *yvcK/pIMK2::nagR* and *yvcK/pIMK2::nagR^M*, respectively). Bacterial growth in BHI supplemented with 2 mM t-CIN was monitored at 30°C by measuring OD_{630}. In addition, the *nagR* deletion strain (*yvcK/ΔnagR/pIMK2*) was included in the growth assay. All curves represent the mean values of three independent cultures. Values of λ, µmax, and ODmax are listed in the table and represented as mean ± SD, *n* = 3. Values followed by a common letter are not significantly different at the 5% level of significance.

2.5 Discussion

In this work, we investigated a previously isolated t-CIN hypersensitive *yvcK::Himar1* mutant and link the vulnerability of the mutant to t-CIN to elevated cell lysis invoked by impaired cell wall integrity (Fig. 2.4). Evolutionary experiments led to the identification of suppression mutations in genes involved in the biosynthesis of the major peptidoglycan precursor UDP-GlcNAc (Table 2.3). Chemical supplementation of GlcNAc restored the attenuated growth of *yvcK* mutant in the presence of t-CIN (Fig. 2.7), suggesting an insufficient substrate availability for UDP-GlcNAc biosynthesis in the *yvcK* mutant when grown in the presence of t-CIN. This idea was further supported by the observation that overproduction of UDP-GlcNAc biosynthetic enzymes in the *yvcK* mutant fully or partially restored the resistance to t-CIN (Fig. 2.8). Together, this collective evidence validates the role of YvcK in UDP-GlcNAc biosynthesis in *L. monocytogenes*. A similar role has been recently proposed for YvcK in *B. subtilis*, but based on different evidence [162]. In *B. subtilis*,

suppressor mutations were identified that reversed the sensitivity of a *yvcK* mutant to cefuroxime or the growth defect on gluconeogenic carbon sources, and these mutations were shown to elevate the expression of *glmS* and *glmM* [162]. Moreover, supplementation of GlcNAc also reversed the phenotypes of YvcK deficiency in *B. subtilis* [162]. These results suggest a conservative function of YvcK in UDP-GlcNAc biosynthesis in both bacteria.

In *B. subtilis*, the function of YvcK has been studied in greater detail and depends on the availability of glycolytic carbon sources; a Δ*yvcK* mutant exhibited attenuated growth and altered cell morphology when grown on non-glycolytic carbon sources, but the provision of glucose, which drives glycolytic carbon flux and thus generates an elevated level of intracellular glycolytic intermediates, revitalized the growth of the mutant [162,163]. The *L. monocytogenes yvcK* mutant also displayed altered cell morphology when grown in BHI (Fig. 2.4). However, since BHI has a complex nutrient composition and contains 2 g/L added glucose, our data do not allow us to assess the role of glycolytic carbon sources on the phenotypes of the *L. monocytogenes yvcK* mutant.

Being an electrophilic and thiol-reactive compound, t-CIN is anticipated to induce an intracellular redox disbalance [11,183]. This is indeed reflected by the induction of oxidative-stress-related genes upon t-CIN exposure, as demonstrated in *E. coli* [7,11,38]. Maintenance of the bacterial intracellular redox homeostasis depends on various enzymatic antioxidant systems and reducing agents such as glutathione [104,184]. Another critical molecule for the antioxidant defense is NADPH, which fuels the regeneration of glutathione and diverse enzymatic antioxidant systems [104]. The cellular NADPH, in turn, is predominantly replenished via the oxidative pentose phosphate pathway into which the glycolytic carbon flux will be rerouted when cells are exposed to oxidative stress [62,185,186]. Thus, *L. monocytogenes* might respond to an oxidative t-CIN challenge by driving glycolytic substrates to the oxidative pentose phosphate pathway to stabilize the intracellular redox state and alleviate the damage caused by t-CIN. Proteomic analysis of *E. coli* treated with a sublethal concentration of t-CIN showed that the expression of genes involved in the pentose phosphate pathway is indeed highly upregulated [11], implying an increased carbon flux to the pentose phosphate pathway. While it increases the production of NADPH, this reallocation of carbon flux at the same time decreases the glycolytic production of Fru-6-P, which is the basis of the UDP-GlcNAc biosynthetic reactions (Fig. 2.6B). This mechanism can explain the cell shape deformations induced by t-CIN (Fig. 2.3). It also explains the

hypersensitivity of the *yvcK* mutant, given the role of YvcK to control the carbon flux into the UDP-GlcNAc biosynthesis pathway. However, cell shape deformations could alternatively also be explained by interference of t-CIN with cytoskeletal elements [187]. In fact, one specific study has claimed t-CIN inhibited the polymerization of FtsZ protein and cell separation in *E. coli*, thus inducing cell filamentation [22].

Furthermore, t-CIN may not only destabilize the overall cellular redox balance, but it may also have one or more specific thiol-containing targets in the pathways mentioned above. For example, it may inhibit the activity of GAPDH (Chapter 1), a glycolytic enzyme that exhibits sensitivity to electrophilic attack due to its Cys active site [62], and hence block the glycolytic and gluconeogenetic flux. Also, GlmS, the first enzyme of the UDP-GlcNAc pathway (Fig. 2.6B), has a Cys active site in its N-terminal glutaminase domain that may be targeted by electrophiles [188,189].

The reaction connecting glycolysis and UDP-GlcNAc biosynthesis is mediated by GlmS [190]. In many Gram-positive bacteria, the intracellular concentration of GlmS is post-transcriptionally regulated by *glmS* ribozyme, a *cis*-regulatory structure in the 5′ untranslated region of *glmS* mRNA which activates the degradation of *glmS* transcript by RNase upon binding to GlcN-6-P [191,192]. This mechanism thus provides feedback inhibition on the production of GlcN-6-P from Fru-6-P by GlmS. Recent work in *B. subtilis* indicated that YvcK provides an additional level of control, by stimulating the activity of GlmS in a UDP-GlcNAc dependent manner [162,165]. When the intracellular UDP-GlcNAc content is high (> 0.1 mM), the activation of GlmS by YvcK will be inhibited [165], probably by the binding of UDP-GlcNAc to YvcK [193].

Furthermore, YvcK was reported to interact with YvcJ, encoded by the gene immediately upstream of *yvcK*, also in a UDP-GlcNAc concentration-dependent manner [165], but the precise role of YvcJ is still unclear. *L. monocytogenes* also has a *yvcJ* homolog upstream of *yvcK*, whose product shares a 67% identity with YvcJ of *B. subtilis* 168, and thus a similar interaction between YvcK and YvcJ may exist in *L. monocytogenes* as well. YvcJ of both *L. monocytogenes* and *B. subtilis* share a high sequence identity with RNase adapter protein RapZ of *E. coli*, which interacts with two small RNAs, GlmY and GlmZ, to regulate the intracellular GlmS concentration in response to the intracellular GlcN-6-P level [194,195]. The exact role of YvcJ in regulating GlmS activity and UDP-GlcNAc biosynthesis in *B. subtilis* and *L. monocytogenes* demands further investigation.

In *B. subtilis*, the NagR repressor was shown to bind to specific operator sites called *dre*-sites, in the promoter region of *nagP* and the *nagABR* operon [177,196,197]. Upon binding to the *dre*-sites, transcription of downstream genes is blocked by NagR [177]. The binding affinity of NagR is tuned by its interaction with ligands, in particular, GlcN-6-P and GlcNAc-6-P [197]. Crystal structure analysis of the NagR-ligand complex showed that the phosphate group ligand is coordinated by multiple residues including Thr90, Ser165, Ile166, Tyr167, Arg 133, and Arg135, all of which are conserved in *L. monocytogenes* Scott A NagR (considering the substitution of the Ile by a Leu residue as conservative). Also, five out of seven residues proposed to interact with the sugar moiety of the ligands (Ser88, Phe89, Glu145, Arg 211, Glu222, Ala 224, and Tyr 228) are conserved between *B. subtilis* and *L. monocytogenes* NagR [196,197] (Fig. S2.5). Interestingly, the $NagR^{M}$ mutant allele has an Ile and Lys insertion that interrupts the three consecutive residues (Ser-Leu-Tyr) proposed to interact with the phosphate group. This mutation is therefore likely to modify the interaction of $NagR^{M}$ with its ligands, and thus modulate the expression of *nagP* and the *nagABR* operon. A reduced ligand affinity would maintain the repressor activity of $NagR^{M}$ at higher ligand concentration, and thus in particular reduce the expression of NagB, and thereby favor the synthesis of UDP-GlcNAc over the breakdown of GlcN-6-P (Fig. 2.6B). This hypothesis explains the failure of *nagR* deletion to cure the t-CIN sensitivity of the *yvcK* mutant (Fig. 2.9) and the inability of GlcNAc supplementation to suppress t-CIN sensitivity of the *yvcK-nagR* double mutant (Fig. S2.4). Furthermore, this gain-of-function hypothesis also rationalizes the incapacity of GlcNAc supplementation (50 mM GlcNAc) to confer a stronger resistance of M 2.2 to t-CIN, evidenced by the growth in the nutrient-rich BHI broth with 2 mM t-CIN (Fig. S2.6).

Suppressor mutations of *yvcK::Himar1* were also identified in genes whose products do not relate directly to UDP-GlcNAc biosynthesis. One point mutation was located in *prs* (Table 2.3), encoding PRPP synthetase which catalyzes the reversible conversion of Ribose-5-P to PRPP, thereby connecting the pentose phosphate pathway with the biosynthesis of nucleotides [176]. Ribose-5-P is a key metabolite of the pentose phosphate pathway and can be produced by the oxidative and nonoxidative part of the pathway [198] (Fig. 2.6B). Fru-6-P and glyceraldehyde-3-phosphate can be reversibly converted to Ribose-5-P (and Xylulose-5-P) through different steps of the nonoxidative pentose phosphate pathway reactions without NADPH generation [198]. In contrast, the unidirectional oxidative pentose phosphate pathway reactions oxidize Glu-6-P to Ribulose-5-P (and CO_2), with the generation of

NADPH [104,185,186]. Ribulose-5-P is then further converted to Ribose-5-P (and Xylulose-5-P) [198]. As aforementioned, *L. monocytogenes* might divert the glycolytic carbon flux into the oxidative pentose phosphate pathway to generate NADPH and counteract the oxidative stress induced by t-CIN, and this would be accompanied by the synthesis of Ribose-5-P. If the mutation in *prs* compromises the activity of the PRPP synthetase, this could push more Ribose-5-P through the nonoxidative pentose phosphate pathway to produce glyceraldehyde-3-phosphate and Fru-6-P, the substrate for UDP-GlcNAc synthesis. On the other hand, reduced PRPP activity would potentially also limit the biosynthesis of UDP and other nucleotides (Fig. 2.6B), and could in this way also prevent UDP-GlcNAc production. Given that mutant M 6.1 shows a mild growth attenuation in BHI, characterized with a smaller growth rate and 1.2 h extended lag phase compared to the parental strain (Fig. 2.5), it is, therefore, hard to exclude the assumption that nucleotides are limiting the growth of the mutant in this medium.

Interestingly, two suppressor mutants (M 3.3 and M 4.1) have a mutation in Rli73, a presumed small RNA immediately upstream of the *glmU-prs* operon. The function of Rli73 has not been identified, but our result strongly suggests that it may affect the expression of the downstream operon. The precise effect remains open to speculation because both suppressor strains also have a second mutation that can potentially interfere. Of note, mutant M 4.1 contains a mutated fructose-biphosphate aldolase that could increase the cellular pool of Fru-6-P and thus account for the higher t-CIN resistance compared to mutant M 3.3 (Fig. 2.5). Likewise, suppression mutations of a *B. subtilis yvcK* null mutant were found in genes involved in the glycolysis, pentose phosphate pathway, or gluconeogenesis when bacteria were grown on nonpreferred carbon sources [162,163]. One suppression mutation was found in the glycolytic gene regulator CggR [163], which represses the transcription of the *gapA* operon encoding five glycolytic enzymes [199]. Suppression mutations were also commonly found in *zwf*, encoding the glucose-6-phosphate dehydrogenase [162,163]. This enzyme catalyzes the conversion of Glu-6-P into gluconate 6-phosphate and connects the glycolysis pathway with the pentose phosphate pathway [200]. These suppression mutations might all enrich the cellular Fru-6-P levels and thus the flux into UDP-GlcNAc biosynthesis, thereby alleviating the metabolic defect of a *yvcK* null mutant.

In conclusion, this study identifies peptidoglycan synthesis, and more specifically biosynthesis of the UDP-GlcNAc precursor, as a pathway that limits the tolerance of *L.*

monocytogenes to t-CIN, and possibly to thiol-reactive antimicrobials. In addition, the work sheds light on the role of YvcK in diverting glycolytic intermediates into UDP-GlcNAc biosynthesis pathway, especially when the glycolytic intermediate Fru-6-P is running low. However, the precise regulatory activity of YvcK remains ambiguous and needs further investigation. A detailed structural analysis would help to clarify the interaction of YvcK with its suspected target proteins such as GlmS and YvcJ, and the modulation of this interaction by chemical effectors. Given the high conservation of YvcK in Gram-positive bacteria, uncovering its function will improve our understanding of peptidoglycan precursor biosynthesis in a wide variety of pathogens. Since the presence of t-CIN significantly attenuates the growth and morphology of the *yvcK* mutant, we anticipate that this compound and other thiol-reactive essential oil compounds may act synergistically with antibiotics targeting peptidoglycan precursor biosynthesis.

2.6 Supplementary materials

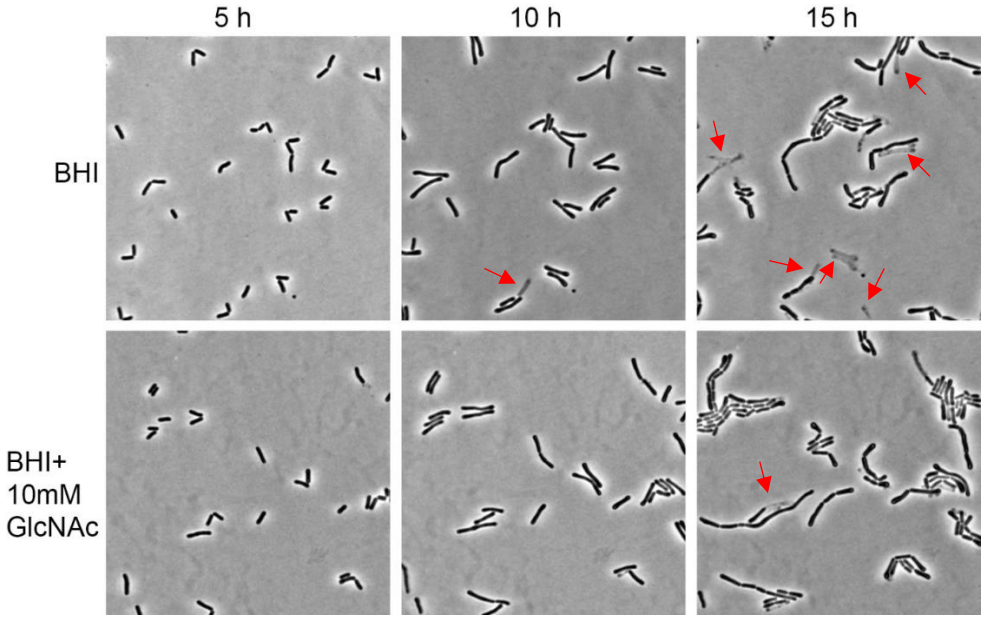

Figure S2.1 Time-lapse observation of *yvcK::Himar1* cells in BHI supplemented with 1 mM t-CIN and with or without 10 mM GlcNAc at 30°C. Phase-contrast images of a representative field at 5 h, 10 h, and 15 h are presented. The red arrow indicates cell lysis of *yvcK::Himar1*. The addition of GlcNAc (bottom series) clearly reduced the occurrence of cell lysis at 15 h.

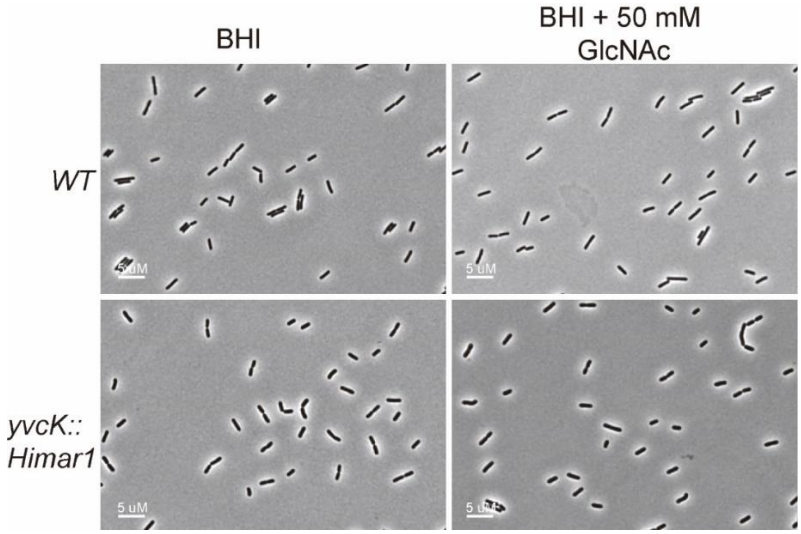

Figure S2.2 Phase contrast microscopy of WT and *yvcK::Himar1* in BHI with and without 50 mM GlcNAc (in absence of t-CIN). Cultures were grown at 30°C till OD_{600} = 1.0. Images are representative of three biological replicates.

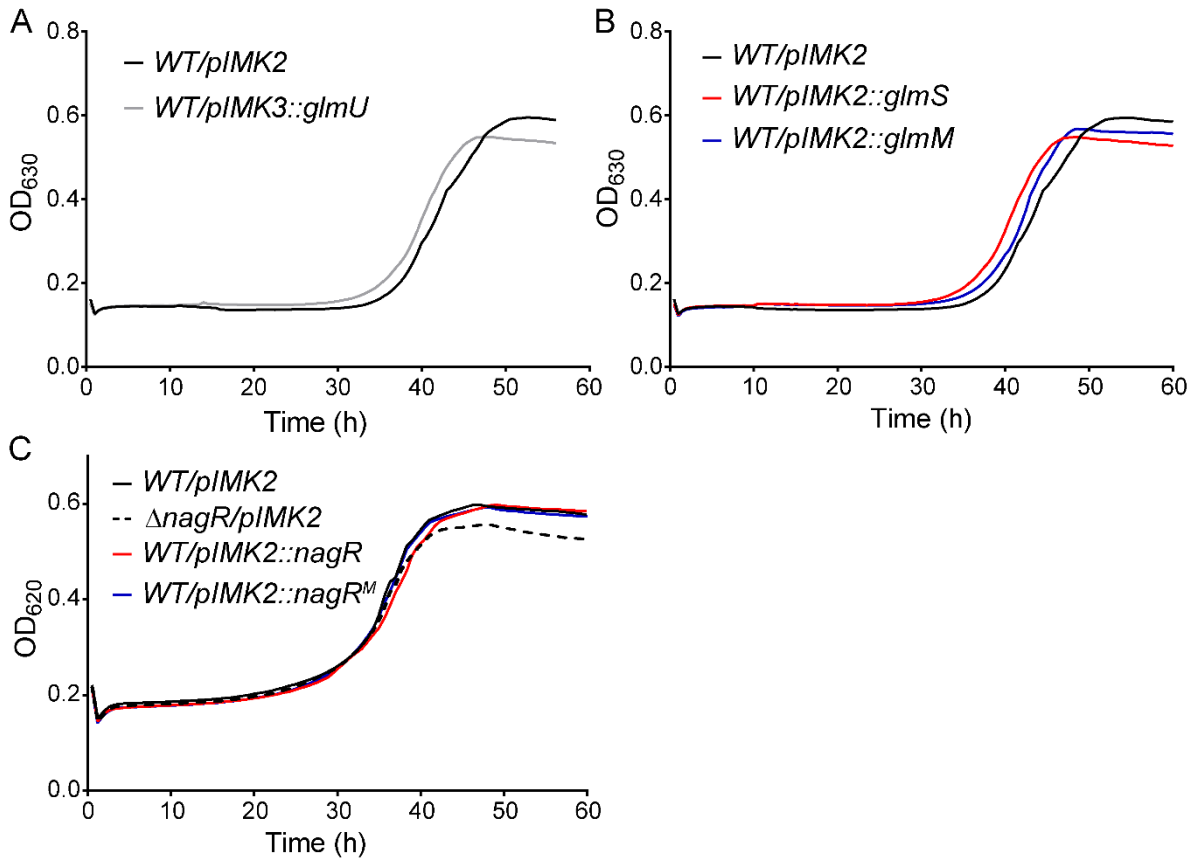

Figure S2.3 Effect of overexpression of enzymes involved in GlcNAc metabolism on t-CIN sensitivity of WT *L. monocytogenes*. A Δ*nagR* strain was included for comparison. Where pIMK2 was used, (over)expression was constitutive, while in case pIMK3 was used, it was induced by 1 mM IPTG. Bacterial growth was monitored by OD_{620} in BHI with 3 mM t-CIN at 30°C. All curves represent the average of three independent cultures. The SD is omitted for clarity.

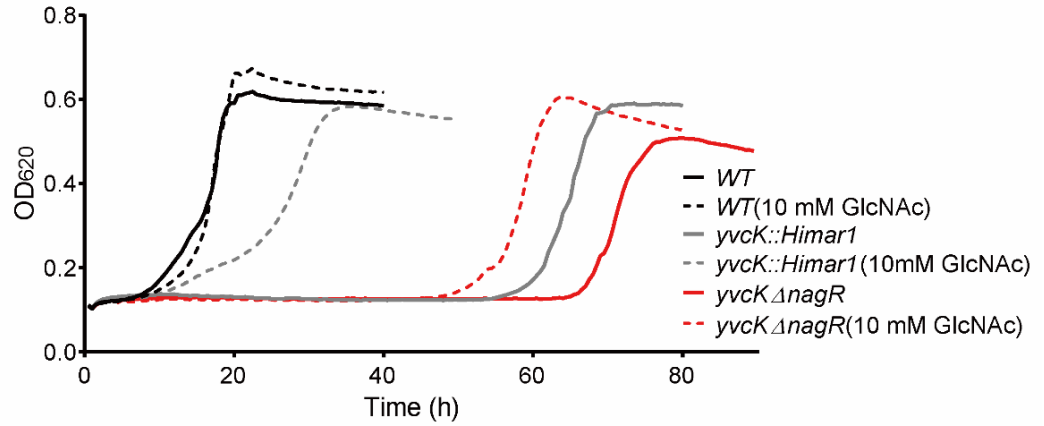

Figure S2.4 Growth curves of *yvcK::Himar1/ΔnagR* at 30°C in BHI with 2 mM t-CIN, with or without 10 mM GlcNAc. Curves represent the average of three independent cultures. The SD is omitted for clarity. Supplementation of GlcNAc almost fully restored the tolerance of *yvcK::Himar1* to t-CIN, but only slightly reduced the sensitivity of *yvcK::Himar1*/Δ*nagR* to t-CIN.

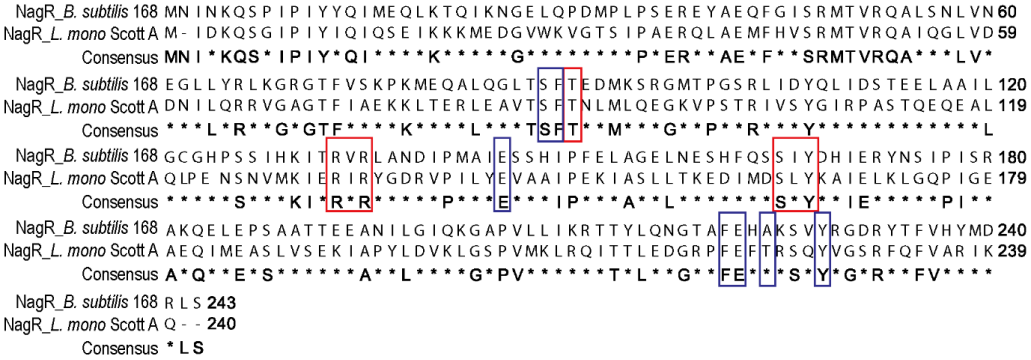

Figure S2.5 Alignment of NagR amino acid sequences from *L. monocytogenes* Scott A (GenBank accession no.: EGJ24460.1) and *B. subtilis* 168 (GenBank accession no.: WP_003228089.1). Both sequences show 35% identity. Residues of *B. subtilis* NagR that are proposed to interact with the phosphate group of the ligands (GlcN-6-P and GlcNAc-6-P) and the corresponding positions in *L. monocytogenes* NagR are highlighted in red boxes. Residues proposed to interact with the sugar moieties of the ligands are shown in blue boxes.

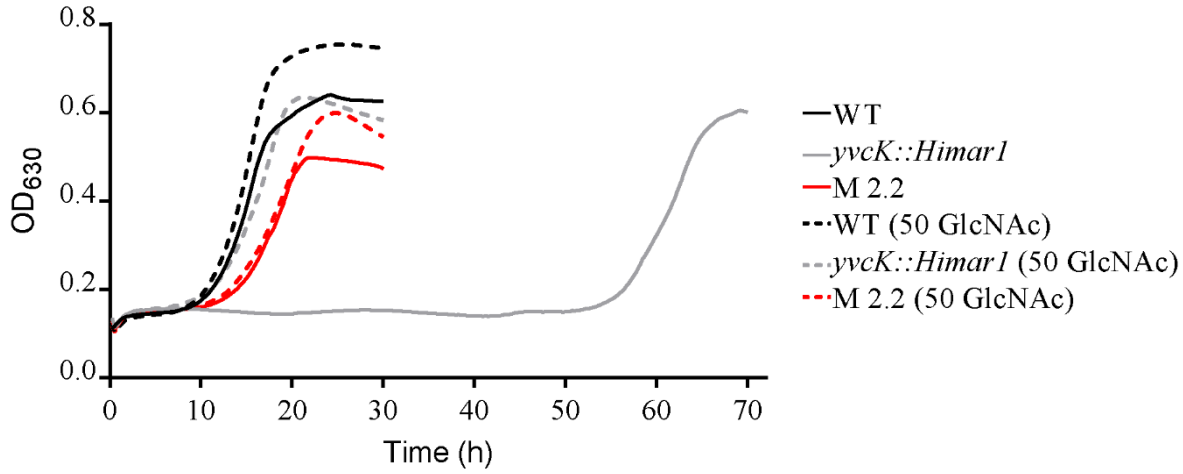

Figure S2.6. Growth curves of mutant M 2.2 at 30°C in BHI with 2 mM t-CIN, with or without 50 mM GlcNAc. Curves represent the average of three independent cultures. The SD is omitted for clarity. Supplementation of GlcNAc almost did not affect the tolerance of mutant M 2.2 to t-CIN.

2.7 Author contribution

Conceptualization: Lei Sun[1] and Chris W. Michiels[1]; methodology: Lei Sun; investigation: Lei Sun and Gil Rogers[1]; writing—original draft preparation: Lei Sun; writing—review and editing: Lei Sun and Chris W. Michiels; supervision: Chris W. Michiels; project administration: Chris W. Michiels; funding acquisition: Chris W. Michiels. All authors have read and agreed to the published version of the manuscript.

Affiliations:

[1] Laboratory of Food Microbiology, Department of Microbial and Molecular Systems (M2S) and Leuven Food Science and Nutrition Research Center (LFoRCe), KU Leuven, Leuven, Belgium.

2.8 Funding

This work was supported by research grants from the Research Foundation-Flanders (FWO) (G.0C77.14N) and from the KU Leuven Research Fund (METH/14/03).

2.9 Acknowledgments

We thanked Sanne Wolput for the assistance of microscopic observation and Julien Mortier for help with the MicrobeTracker software.

Chapter 3 Role of Diaminopimelic Acid Amidation on Cell Wall Homeostasis and Cell Invasion in *Listeria monocytogenes* [§]

3.1 Abstract

A mutant of *L. monocytogenes* Scott A with a transposon in the 5' untranslated region of the *asnB* gene was identified to be hypersensitive to the antimicrobial t-CIN. Here, we report the functional characterization of AsnB in peptidoglycan modification and intracellular infection. While AsnB of *Listeria* is annotated as a glutamine-dependent asparagine synthase, sequence alignment showed that this protein is closely related to a subset of homologs that catalyze the amidation of *meso*-diaminopimelic acid (*m*DAP) residues in the peptidoglycan of other bacterial species. Structural analysis of peptidoglycan from an *asnB* mutant, compared to that of isogenic WT and complemented mutant strains, confirmed that AsnB mediates *m*DAP amidation in *L. monocytogenes*. Deficiency in *m*DAP amidation caused several peptidoglycan- and cell surface-related phenotypes in the *asnB* mutant, including the formation of shorter but thicker cells, susceptibility to lysozyme, loss of flagellation and motility, and a strong reduction in biofilm formation. In addition, the mutant showed reduced invasion of human epithelial JEG-3 and Caco-2 cells. Analysis by immunofluorescence microscopy revealed that *asnB* inactivation abrogated the proper display at the listerial surface of the invasion protein InlA, which normally gets cross-linked to *m*DAP. Together, this work shows that AsnB of *L. monocytogenes*, like several of its homologs in related Gram-positive bacteria, mediates the amidation of *m*DAP residues in the peptidoglycan and, in this way, affects several cell wall and cell surface-related properties. It also for the first time implicates the effects of amidation of peptidoglycan *m*DAP residues on the virulence and attachment of surface proteins, in particular the LPXTG containing protein, in *L. monocytogenes*.

[§] This chapter is based on the following publication: Sun, L.; Rogiers, G.; Courtin, P.; Chapot-Chartier, M.-P.; Bierne, H.; Michiels, C.W. AsnB mediates amidation of *meso*-diaminopimelic acid residues in the peptidoglycan of *Listeria monocytogenes* and affects bacterial surface properties and host cell invasion. *Frontiers in Microbiology* **2021**, *12*, 3119.

3.2 Introduction

Bacterial cells are surrounded by a rigid peptidoglycan cell wall whose primary universal function is to maintain cell shape and preserve cell integrity, particularly in hypo-osmotic environments that would otherwise be conducive to cell lysis [159]. The tensile strength required for this function is derived from the mesh-like structure of peptidoglycan, which consists of long N-acetylglucosamine, N-acetylmuramic acid heterodisaccharide polymers crosslinked via peptide side chains. While this basic architecture has been well conserved, there is a wide variety of peptidoglycan chemical structures in different bacteria. This variation stems mainly from differences in the amino acid composition and cross-linking of side chains, but also from the presence or removal of modifying substituents on the sugar and amino acid units [201]. Differences in peptidoglycan structure have also been observed depending on the growth stage and growth conditions in several bacteria, and are developmentally regulated in spore-forming bacteria, where a distinct and unique δ-lactam peptidoglycan modification exists in the so-called spore cortex, a thick protective peptidoglycan layer surrounding the germ cell wall which lacks this modification. This allows specific hydrolases embedded on the spore's surface to selectively cleave the cortex without compromising the germ cell wall upon spore germination.

Besides having a structural role, peptidoglycan is also a scaffold anchoring surface proteins with various functions [202], and peptidoglycan or peptidoglycan fragments also serve as a molecular signal in several symbiotic or pathogenic interactions with animal or plant hosts [203,204]. The high specificity required for such signaling is made possible by the presence of some unique or rare building blocks including N-acetylmuramic acid, *m*DAP, and D-amino acids, and by the large structural variation in peptidoglycan which is generated in part by enzymatic modifications. peptidoglycan modifications are widespread in Gram-positive and -negative bacteria and are often important for virulence in pathogens [201]. N-deacetylation of N-acetylglucosamine, for example, occurs in pathogens including various streptococci and *L. monocytogenes*, prevents peptidoglycan hydrolysis by lysozyme, and helps cells to evade the immune response during infection [205–207]. The most widespread and best-studied modification is probably O-acetylation of N-acetylmuramic acid, and this modification has also been implicated in conferring lysozyme resistance and virulence in pathogens like *Neisseria gonorrhoeae* and *Staphylococcus aureus* [208]. Even more variations exist in the stem peptide as compared to the sugar backbone. These include the addition of substituents, with the most widespread and best-documented examples being the

amidation of D-*iso*-Glu and *m*DAP residues, on their α-carboxyl and ε-carboxyl groups respectively. These amidation modifications occur in several genera and species of Gram-positive bacteria, while the only example reported in Gram-negative bacteria thus far is the amidation of the α-carboxyl group of *m*DAP in *Acetobacteraceae* [209].

Stem peptide amidation has been reported to affect different bacterial properties and functions. The amidation of D-*iso*-Glu is mediated by MurT/GatD and is essential in *S. aureus* and *Streptococcus pneumoniae*, and reduced expression of the *murT-gatD* operon enhanced the sensitivity to β-lactam antibiotics and lysozyme in *S. aureus* [210,211]. The ε-carboxyl amidation of *m*DAP is mediated by an enzyme that is homologous to the glutamine-dependent asparagine synthetase found in various organisms, such as AsnB of *E. coli*. At least some of these enzymes are promiscuous, being able to catalyze the amidotransfer from glutamine not only to aspartate for the synthesis of asparagine, but also to *m*DAP for modification of the peptidoglycan stem peptide. *B. subtilis* encodes three homologs, designated AsnB, AsnO and AsnH, and while each of these can complement the asparagine deficiency of an *E. coli* asparagine auxotroph, none of them is essential for Asn synthesis in *B. subtilis*, since even a triple knockout mutant could still grow without Asn, albeit at a reduced rate [212]. It was later shown that AsnB, but neither of its two homologs, mediates *m*DAP amidation [213]. Furthermore, *asnB* was essential unless excess Mg^{2+} was provided in the growth medium, and its deletion rendered cells sensitive to antibiotics targeting the cell wall and to lysozyme [213]. *Lactobacillus plantarum* has two homologs, AsnB1 and AsnB2, of which the former was shown to mediate *m*DAP amidation [214]. Mutants in which AsnB1 was deactivated were affected in growth and showed filamentation, suggesting a role of amidation in the cell septation process. In addition, amidation also controlled the activity of the L,D-carboxypeptidase DacB that trims the stem peptide. A similar situation - two homologs of which one specifically mediates *m*DAP amidation - exists in *Clostridioides difficile*, but a remarkable feature in this organism is that the expression of *asnB* gene and *m*DAP amidation are specifically induced by vancomycin [215]. Somewhat unexpectedly, amidation slightly reduced vancomycin resistance but did not affect lysozyme resistance, and its role in *C. difficile* therefore remains unclear. While *B. subtilis*, *L. plantarum* and *C. difficile* belong to the *Firmicutes* (low GC) phylum of Gram-positive bacteria, an AsnB homolog mediating *m*DAP amidation has also been identified in *Corynebacterium glutamicum*, which belongs to the (high GC) *Actinobacteria* phylum [216]. *C. glutamicum* encodes only one AsnB homolog (designated LtsA), and deletion of the gene resulted in the loss of *m*DAP amidation,

attenuated growth, morphological changes, and sensitivity to cell wall-targeting antibiotics and lysozyme, thus mirroring the phenotype of an *asnB* knock-out mutant in *B. subtilis.* Mycobacteria, finally, also belong to the *Actinobacteria* and have amidated *m*DAP residues as well. Although there is no direct evidence for a role of their AsnB homologs in *m*DAP amidation, knockout mutants have been isolated and partially characterized. In *M. smegmatis*, a transposon insertion mutant in *asnB* showed a delayed onset of growth and displayed sensitivity to multiple antibiotics [217]. In *M. tuberculosis*, *in vitro* enzymatic assay demonstrated that *m*DAP amidation was required for the formation of cross-links between neighboring stem peptides by the L,D-transpeptidase Ldt, and the construction of a conditional *asnB* knock-out led to the conclusion that the gene was essential [218].

In the present work, we report the isolation of *asnB* mutant from a screen of a genome-wide *L. monocytogenes* transposon insertion library with the natural antimicrobial t-CIN. *L. monocytogenes* is a foodborne pathogen that occasionally causes systemic infections with a high mortality rate, primarily in immunocompromised individuals. The organism is widespread and thrives in a variety of terrestrial and aqueous natural environments as well as in man-made environments like food production plants, while it can also engage in a highly specialized and complex pathogenic interaction with the human host, involving receptor-mediated endocytosis by nonphagocytic cells in the gut epithelium, escape from the vacuole, cell to cell spread facilitated by actin polymerization, sepsis, and infection of various organs including the fetus of pregnant women [219]. Like many other *Bacilli*, *L. monocytogenes* peptidoglycan contains *m*DAP in the third position of the stem peptide, and at least in some strains, the residue is also amidated [206,220]. However, while several peptidoglycan modifications have been implicated in virulence in several pathogens, including N-deacetylation and O-acetylation in *L. monocytogenes* [206,221], a similar role has not yet been demonstrated for *m*DAP amidation in any pathogen. Therefore, the goal of this study was to conduct a detailed functional analysis of AsnB in *L. monocytogenes.* Our results confirm that AsnB catalyzes *m*DAP amidation and provide evidence for a role in cell wall homeostasis, flagellum-mediated motility, and bacterial pathogenicity.

3.3 Materials and methods

3.3.1 Bacterial strains and plasmid construction

The bacterial strains and plasmids used in this work are listed in Table 3.1. *L. monocytogenes* Scott A WT strain was acquired from the International Life Sciences Institute North America [166]. Strain *asnB::Himar1* was identified as a sensitive mutant from a random Scott A transposon mutant collection [17] in a screen with the natural antimicrobial t-CIN (Acros Organics). *E. coli* DH5α [167] was employed as the host for cloning constructs. *E. coli* S17-1 λpir [168] was utilized as the donor strain for conjugational plasmid transfer. *L. monocytogenes* strains were grown at 30°C or 37°C in BHI (Oxoid) medium. *E. coli* strains were grown in LB medium at 37°C. Growth media were supplemented with Em (Acros Organics) (50 µg/mL) or Km (AppliChem GmbH) (50 µg/mL) when appropriate.

For genetic complementation of the *asnB::Himar1* mutant, the *asnB* gene was amplified using primers asnB_NcoI and asnB_SalI (Table 3.2) and cloned in pIMK2 [170] restricted with NcoI and SalI. The construct was verified with Sanger sequencing and then conjugated from *E. coli* S17-1 λpir into the *asnB::Himar1* mutant. Successful integration in the chromosome was confirmed via PCR with primers asnB_NcoI and NC16 (which anneals near, and point towards, the plasmid integration site) and Sanger sequencing with primers pIMK_FW and pIMK_REV, which point towards the *asnB* gene from both sides of the pIMK2 cloning site. The complemented strain was designated *asnB/pIMK2::asnB*. Control strains were constructed by integration of the empty pIMK2 plasmid into the WT and *asnB::Himar1* strains, and were designated as *WT/pIMK2* and *asnB/pIMK2* respectively.

Table 3.1 Strains and plasmids in this work**.**

Bacterial species	Designation in this work	Description/Construction	Reference
L. monocytogenes	*WT*	Wild-type strain Scott A	[166]
	WT/pIMK2	WT with pIMK2 integrated, Km^R	This work
	asnB::Himar1	Transposon insertion at 5' end of *asnB*, Em^R	This work
	asnB/pIMK2	*5' asnB::Himar1* with pIMK2 integrated, Km^R Em^R	This work
	asnB/pIMK2::asnB	*5' asnB::Himar1* with pIMK2-asnB integrated, Km^R Em^R	This work
E. coli	S17-1 λpir	Donor for plasmid conjugation	[168]
	DH5-α	Host strain for plasmid constructs	[167]
Plasmids	Description		Reference
pIMK2	Site-specific listerial integrative vector, Phelp promoter for constitutive overexpression, 6.2 kb, Km^R		[170]
pIMK2-*asnB*	pIMK2 with *asnB* gene from Scott A under control of pHelp promotor		This work

Table 3.2 Primers used in this work.

Primer	Sequence (5' – 3')*	Reference
asnB_NcoI	GCATCCATGGGATGTGGATTTGTAGGATGCGTAC	This work
asnB_SalI	CACTGTCGACTTATTTTCCAAAATCGTATTTATCTGC	This work
pIMK_REV	CCTATCACCTCAAATGGTTCG	[17]
pIMK_FW	GAGTCAGTGAGCGAGGAAGC	[17]
NC16	GTCAAAACATACGCTCTTATC	[17]
Ylinker	CTGCTCGAATTCAAGCTTCT	[17]
Marq269	GCTCTGATAAATATGAACATGATGAGTGAT	[17]

*Restriction sites: NcoI (CCATGG) and SalI (GTCGAC).

3.3.2 Growth assay

Growth curves of strains *WT/pIMK2*, *asnB/pIMK2*, and *asnB/pIMK2::asnB* were established by measuring the turbidity (OD_{630}) with an automated microplate reader (Multiskan Ascent®, Thermo Fisher Scientific). In general, the OD_{600} of overnight cultures was determined firstly with an Ultrospec™ 10 Cell Density Meter (Biochrom, Cambridge, UK) and slightly adjusted by supplying additional BHI to obtain the same value ($OD_{600} \approx 2$) for all the cultures within a single experiment. Diluted cultures were diluted 1000-fold in BHI

or BHI with 3- or 4-mM t-CIN, and 200 µL aliquots were transferred into a 96-well microplate, which was then covered with a transparent adhesive foil and incubated at 30°C or 37°C in the automated microplate reader. Every 15 min the plates were shaken at 960 rpm and OD_{630} was measured. The Excel add-in package DMFit was used to determine the μ_{max}, λ, and OD_{max} values at stationary phase through the Baranyi and Roberts model [169].

3.3.3 Sensitivity to Lysozyme

Lysozyme sensitivity was evaluated by disc diffusion assay and broth growth inhibition assay as previously described [222] with minor modifications. The lysozyme (Sigma Aldrich, Saint Louis, USA) stock was prepared in 10 mM potassium phosphate buffer (PPB) pH 7.0. For the disc diffusion assay, 5 µL of an overnight culture was evenly spread on a BHI agar plate, and a 6 mm sterile Whatman paper disc was placed in the center and impregnated with 10 µL of a 10 mg/mL lysozyme solution. The formation and size of an inhibition halo were registered after incubation at 30°C for 24 h. For the broth inhibition assay, overnight cultures were diluted 1000-fold in BHI broth supplemented with 1 mg/mL lysozyme, and 200 µL aliquots of the cell suspension were loaded into 96-well microplates. The OD_{630} was monitored at 15-min intervals in the microplate reader at 30°C. Additionally, a lysozyme lysis assay was conducted using cells from overnight cultures that were washed and resuspended in 10 mM PPB pH 7.0 to an OD_{450} of 0.6-0.8. Two hundred and seventy µL of the suspension were then dispensed into a 96-well microplate and 30 µL of the 1000-fold diluted lysozyme stock (1 mg/mL) (or water for control) was added. The OD_{450} was recorded at 30-min intervals in the microplate reader at 25°C.

3.3.4 Flagellar staining and swimming motility assay

Overnight stationary cultures were diluted 100-fold in BHI medium and grown to exponential phase (2 - 3 h) at 30°C with shaking. Crystal violet flagellar staining was performed as described [30], and cells were observed with a Leica SFL4000 microscope. Swimming motility was evaluated by picking colonies from a BHI plate and stab-inoculating them into BHI soft agar (0.2%) with a toothpick [223]. Plates were incubated at 30°C for 24 h, and motility was assessed by measuring the migration distance of bacteria from the center to the periphery of the colony.

3.3.5 High-Resolution SEM and cell dimension measurement

Cells were harvested from BHI broth at $OD_{600} \approx 1$, washed once with 0.1 mM PPB pH 7.0, and diluted appropriately. Fifty µL of cell suspension was applied to a coverslip mounted to an AI stub by carbon adhesive discs and dried in the oven at 37°C. HR SEM was performed on a Nova NanoSEM450 (FEI) scanning electron microscope.

To measure the cell dimension, one µl of an appropriately diluted exponential culture ($OD_{600} \approx 1$) was applied to 2% agarose pads, which were deposited on a microscopy slide. A Gene Frame (Thermo Fisher Scientific) was used to mount a cover glass on the microscopy slide. Observations were performed with an Eclipse Ti-E inverted microscope (Nikon Instruments Europe BV, Netherlands) in phase contrast modus at a total magnification of 100x, and images were acquired using NIS-elements software (Nikon). Image analysis (cell width and cell length) was conducted with the MicrobeTracker software [173], with manual curation to remove false segmentation and tracking.

3.3.6 Bioinformatics analysis

The amino acid sequences of putative AsnB from *L. monocytogenes* Scott A and its homologs from other bacteria were acquired from the National Centre for Biotechnology Information database (NCBI) and listed in Table S3.1. Amino acid sequence alignment was conducted with MUSCLE [224], and a phylogeny tree was constructed with CLC Genomic Workbench (QIGEN, Hilden, Germany) using the Neighbour-joining (NJ) method with 100 bootstrap replicates.

3.3.7 Peptidoglycan extraction and structural analysis

Peptidoglycan was purified as described [225] with minor modifications. Overnight cultures were diluted 100-fold in 0.5 L BHI broth and grown to $OD_{600} \approx 1$ at 30°C. After cooling in ice water (20-30 min), cells were collected by centrifugation (5000 rpm, 10 min, 4°C), resuspended in 40 ml cold H_2O, boiled (10 min), cooled again, and centrifuged. After suspending the cell pellet in 1 mL H_2O, 1 mL SDS solution (10% SDS, 100 mM Tris-HCl pH 7.0) at 60°C was added and the suspension was boiled (30 min) and centrifuged (10 min, 14000 rpm, RT). The pellet was resuspended in 2 mL lysis solution (4% SDS, 50 mM Tris-HCl pH 7.0), boiled (15 min), and washed 6 times with H_2O preheated to 60°C. Afterward, the pellets were treated with 2 mg/mL pronase from *Streptomyces griseus* (Roche, Basel, Switzerland) in 50 mM Tris-HCl pH 7 for 1.5 h at 60°C, and with 10 µg/mL DNase (Thermo

Fisher Scientific), 50 µg/mL RNase (Thermo Fisher Scientific) and 50 µg/mL lipase from *Aspergillus niger* (Sigma Aldrich) in 20 mM Tris-HCl pH 7.0, 1 mM $MgCl_2$, 0.05% sodium azide for 4 h at 37°C. Then the suspensions were washed with H_2O and treated with 200 µg/mL trypsin (Sigma Aldrich) in 20 mM Tris-HCl pH 8.0 at 37°C with agitation overnight. Finally, after inactivating trypsin by boiling for 3 min, the suspensions were incubated with 48% hydrofluoric acid (Merck, Kenilworth, NJ, USA) overnight at 4°C. After centrifugation (10 min, 14000 rpm, RT), the pellet was washed twice with 250 mM Tris-HCl (pH 7.0) and four times with H_2O to reach a pH close to 5. The extracted peptidoglycan was eventually lyophilized and resuspended in H_2O to 10 mg/mL.

For structural analysis, 50 µL of purified peptidoglycan was digested by adding 50 µL 25 mM NaHPO4 pH 5.5 and 2 µL 10 mg/mL mutanolysin from *Streptomyces globisporus* (Sigma Aldrich) and incubating overnight at 37°C with shaking. The resulting soluble muropeptides were reduced with sodium borohydride and separated by reverse phase-ultra high-pressure liquid chromatography (RP-UHPLC) with a 1290 chromatography system (Agilent Technologies, Santa Clara, CA, USA) and a Zorbax Eclipse Plus C18 RRHD column (100 by 2.1 mm; particle size, 1.8 µm) (Agilent Technologies) at 50°C using ammonium phosphate buffer and methanol linear gradient as described previously [225]. One µL of collected muropeptides was then spotted directly on the matrix-assisted laser desorption ionization (MALDI) target and thoroughly mixed with 1 µL of α-cyano-4-hydroxycinnaminic acid solution (5 mg/mL in 50% acetonitrile containing 0.1% trifluoroacetic acid). Muropeptides were analyzed by matrix-assisted laser desorption ionization MALDI - time of flight mass spectrometry (MALDI-TOF MS) with an UltrafleXtreme instrument (Bruker Daltonics, Billerica, Massachusetts, USA) (located at Université Paris Saclay, CEA, INRAE, Médicaments et Technologies pour la Santé (MTS), MetaboHUB, Gif-sur-Yvette, France). MS spectra were acquired at 2 kHz laser repetition rate in the positive reflector ion mode, with a 20-kV acceleration voltage and an extraction delay of 130 ns. The spectra were obtained by accumulating 1000 to 5000 shots (depending on the samples) over the 500-5000 m/z range. MS/MS spectra were acquired in LIFT mode, at 1 kHz laser repetition rate applying 7.5 kV for the initial acceleration of ions and 19 kV for a reacceleration of fragments in the LIFT cell.

3.3.8 Human cell lines and invasion assays

Human JEG-3 placental cells (ATCC HTB-36) and Caco-2 intestinal cells (ATCC HTB-37) were grown following ATCC recommendations at 37°C in a humidified 10% CO_2 atmosphere. The invasion of *L. monocytogenes* strains was assessed by the gentamicin assay, as described [226] with some modifications. To prepare bacterial inoculums, bacterial cultures were grown to early exponential or stationary phase at 37°C, washed with 10 mM phosphate-buffered saline (PBS) pH 7.4, and diluted in Eagle's Minimum Essential Medium (MEM). JEG-3 and Caco-2 cells at 80% confluency were infected with bacterial inoculums at a multiplicity of infection (MOI) of about 0.05 to 0.1 bacteria per cell, and centrifuged at 300 x g for 2 minutes to synchronize bacterial entry. For JEG-3 cells, after 1 h incubation, cells were washed with MEM and incubated with complete culture media containing 25 µg/mL gentamicin for 3 h to kill the extracellular bacteria. For Caco-2 cells, after 0.5 h incubation, cells were washed with MEM and incubated with 25 µg/mL gentamicin for 0.5 h to kill the extracellular bacteria while minimizing the intracellular replication of the infected bacteria. Subsequently, infected cells were washed twice in MEM and lysed in cold distilled water. The number of bacteria in bacterial inoculums and cell lysates were determined by serial dilutions plated on BHI agar and counting colony-forming units (cfu) after 48 h incubation at 37°C. The relative entry efficiency was expressed as the ratio of cfu recovered after cell lysis to inoculated cfu.

3.3.9 Immunofluorescence microscopy

Immunofluorescent staining was performed as described [226]. Briefly, overnight bacterial cultures were washed twice with PBS, fixed on a coverslip with 4% paraformaldehyde in PBS, and stained for 1 h with a mixture of mouse monoclonal InlA antibodies L7.7 and G6.1 [226] and a rabbit polyclonal *L. monocytogenes* antibody in 2% bovine serum albumin, at 1:500 dilution. Coverslips were then washed several times with PBS and incubated with Alexa 488-labeled goat anti-rabbit (1:400 dilution; Molecular Probes, Eugene, OR, USA) and Cy3-labeled goat anti-mouse (Jackson ImmunoResearch, West Grove, PA, USA) secondary antibodies for 1 h, followed by mounting with 10 µL of Fluoromount G (Interchim, Montluçon, France).

3.3.10 Statistical analysis

Data for the growth assay and intracellular infection assay are presented as means ± SD from three independent repetitions. The significance of mean differences of growth parameters was calculated by Tukey's honestly significant difference (Tukey's HSD) test using GraphPad PRISM 7.0. Bacterial cell width and length are means ± SD of 300 cells and the significance of mean differences were calculated by Student's t-test (two-tailed). For the lysozyme lysis assay, linear regression was applied to fit straight lines through the data points and the slopes are presented as means ± SD from five independent repetitions. The significance of mean differences was calculated by analysis of variance (two-way ANOVA) using GraphPad Prism software. P values < 0.05 were considered statistically significant.

3.4 Results

3.4.1 *asnB* mutants show increased sensitivity to the antimicrobial t-CIN and have altered cell shape

Several mutants with increased sensitivity to t-CIN, an antimicrobial from cinnamon bark essential oil, were previously isolated from a random *Himar1* transposon insertion library of *L. monocytogenes* Scott A [17]. One mutant had the transposon inserted 22 bp upstream of the start codon of *asnB* (NCBI accession no. and locus tag are CM001159 and LMOSA_25850), which is predicted to encode an asparagine synthetase (Fig. 3.1A), and this mutant was designated *5'asnB::Himar1*. The transcription start site of *asnB* has been reported to be located at -47 bp relative to the start codon in *L. monocytogenes* EGD-e and at -50 bp in *L. innocua* [174], making it likely that transcription of *asnB* is disrupted in this mutant. The gene downstream of *asnB* encodes a putative rRNA methylase, and is encoded on the opposite strand. An S-adenosylmethionine synthetase gene is located upstream of *asnB* and its stop codon is 136 bp away from the start codon of *asnB*. Given their position and orientation, the expression of these flanking genes is unlikely to be strongly affected by the transposon. The genome of the *5'asnB::Himar1* mutant was sequenced and no other mutations were identified. To further study the function of the *asnB* gene, a genetically complemented mutant strain was constructed by chromosomal insertion of an intact *asnB* copy under the control of a constitutive promoter (strain *asnB/pIMK2::asnB*), and the WT and *asnB* mutant strain were equipped with an empty pIMK2 vector at the same chromosomal

insertion site. A more detailed analysis of the t-CIN sensitivity indicated that the mutant displayed an extended lag phase (56 h vs 23 h for the WT strain), but not a reduced exponential growth rate or stationary phase level (Fig. 3.1C). Furthermore, t-CIN tolerance was restored to WT level (20 h lag phase) by genetic complementation (Fig. 3.1C), but not by supplementation of the growth medium with asparagine (Fig. 3.1D), suggesting that t-CIN sensitivity of the *asnB* mutant is not related to an Asn deficiency that could be the result of impaired Asn synthetase activity.

Although the *asnB* mutant showed normal growth in BHI broth without t-CIN at 30°C, it grew at a lower rate and to a lower stationary phase level at 37°C (Fig. 3.1B). Furthermore, both SEM and optical microscopic observations of exponential and stationary phase cells grown at 30°C revealed that the *asnB* mutant produced 'fat rods' that were shorter and thicker than WT cells, and also the presence of some club-shaped cells (Fig. 3.2). Both the growth at 37°C and cell morphology were largely restored by genetic complementation. The observed defects in growth and cell morphology are reminiscent of the phenotype of *asnB* mutant of *B. subtilis* [212]. Interestingly, *B. subtilis* has two additional paralogs of *asnB*, designated *asnH* and *asnO*. However, while the three paralogs could restore Asn prototrophy to an *E. coli asnB* mutant, none was essential for producing Asn in *B. subtilis*, and *asnB* was later shown to mediate amidation of the ε-carboxyl group of *m*DAP residues in the peptidoglycan peptide stem [213]. The role of *asnB* homologs in *m*DAP amidation has also been demonstrated in other Gram-positive bacteria, including *Lactobacillus plantarum* [214] and *Clostridioides difficile* [215]. However, unlike these bacteria, which have two or three *asnB* paralogs, *L. monocytogenes* contains only one. This unique constellation triggered us to further study the function(s) of *asnB in L. monocytogenes*, including its possible role in virulence, since such a role had not been previously reported in any pathogen.

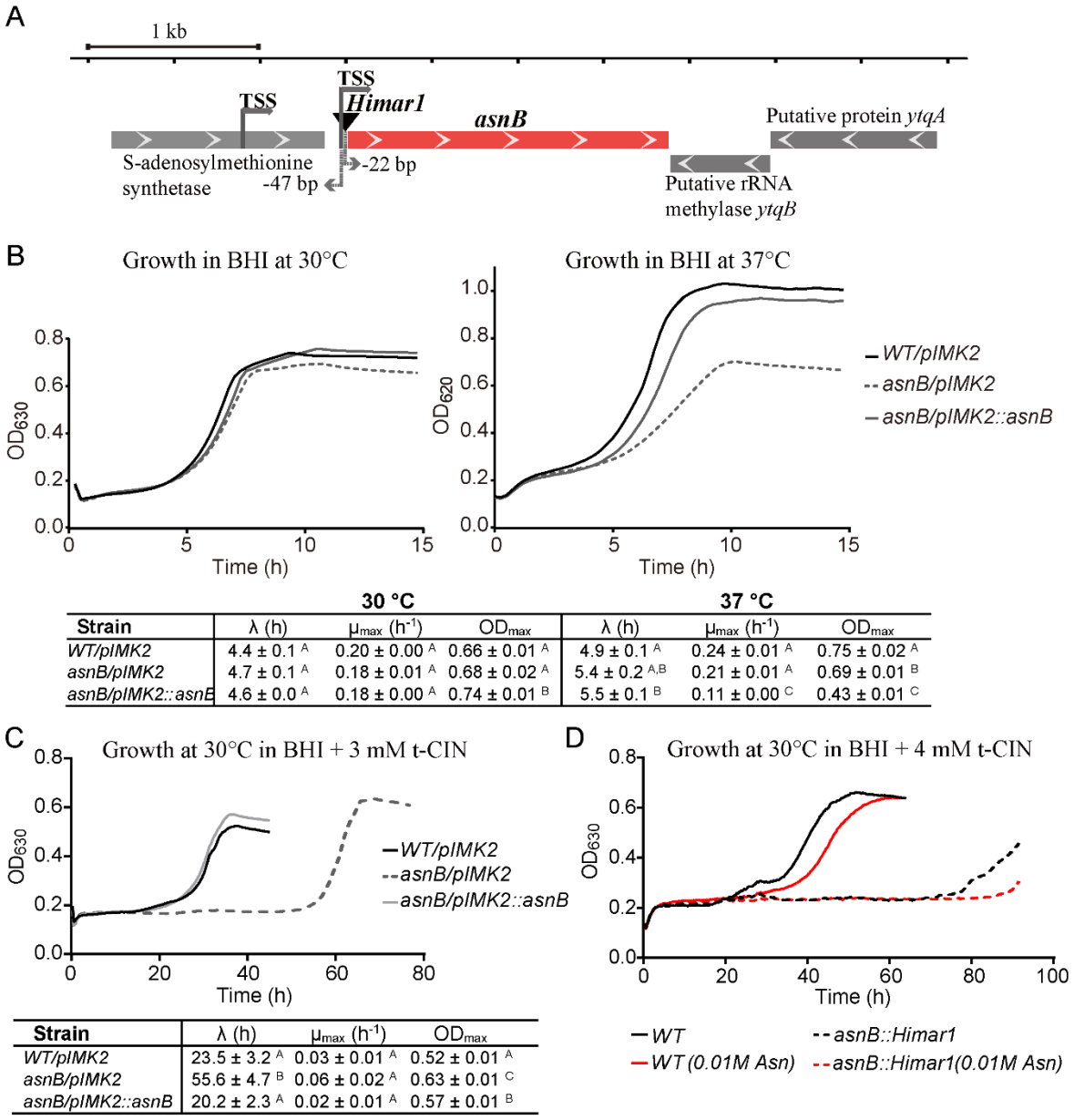

	30 °C			37 °C		
Strain	λ (h)	μ_{max} (h^{-1})	OD_{max}	λ (h)	μ_{max} (h^{-1})	OD_{max}
WT/pIMK2	4.4 ± 0.1 ^{A}	0.20 ± 0.00 ^{A}	0.66 ± 0.01 ^{A}	4.9 ± 0.1 ^{A}	0.24 ± 0.01 ^{A}	0.75 ± 0.02 ^{A}
asnB/pIMK2	4.7 ± 0.1 ^{A}	0.18 ± 0.01 ^{A}	0.68 ± 0.02 ^{A}	5.4 ± 0.2 ^{A,B}	0.21 ± 0.01 ^{A}	0.69 ± 0.01 ^{B}
asnB/pIMK2::asnB	4.6 ± 0.0 ^{A}	0.18 ± 0.00 ^{A}	0.74 ± 0.01 ^{B}	5.5 ± 0.1 ^{B}	0.11 ± 0.00 ^{C}	0.43 ± 0.01 ^{C}

Strain	λ (h)	μ_{max} (h^{-1})	OD_{max}
WT/pIMK2	23.5 ± 3.2 ^{A}	0.03 ± 0.01 ^{A}	0.52 ± 0.01 ^{A}
asnB/pIMK2	55.6 ± 4.7 ^{B}	0.06 ± 0.02 ^{A}	0.63 ± 0.01 ^{C}
asnB/pIMK2::asnB	20.2 ± 2.3 ^{A}	0.02 ± 0.01 ^{A}	0.57 ± 0.01 ^{B}

Figure 3.1 Characterization of the t-CIN sensitive *L. monocytogenes asnB* mutant. (**A**) Genomic context of the *asnB* gene. Gene orientations are indicated by white arrows in the gene boxes. The *Himar1* transposon (black inverted triangle) is inserted at -22 bp of the *asnB* start codon. Transcription start sites (TSSs) [174] of *asnB* are indicated with grey arrows. (**B**) Growth curves and growth parameters of *WT/pIMK2*, *asnB/pIMK2* and *asnB/pIMK2::asnB* in BHI broth at 30°C (left) and 37°C (right). (**C**) Growth curves and growth parameters of the same strains in BHI broth with 3 mM t-CIN at 30°C. (**D**) Growth curves of the *asnB::Himar1* mutant compared to the WT strain in BHI broth with 4 mM t-CIN with and without the addition of Asn. The growth parameters (λ, μmax, and ODmax) represent mean ± SD; n = 3. Values of different strains followed by a common letter are not different at the 5% level of significance.

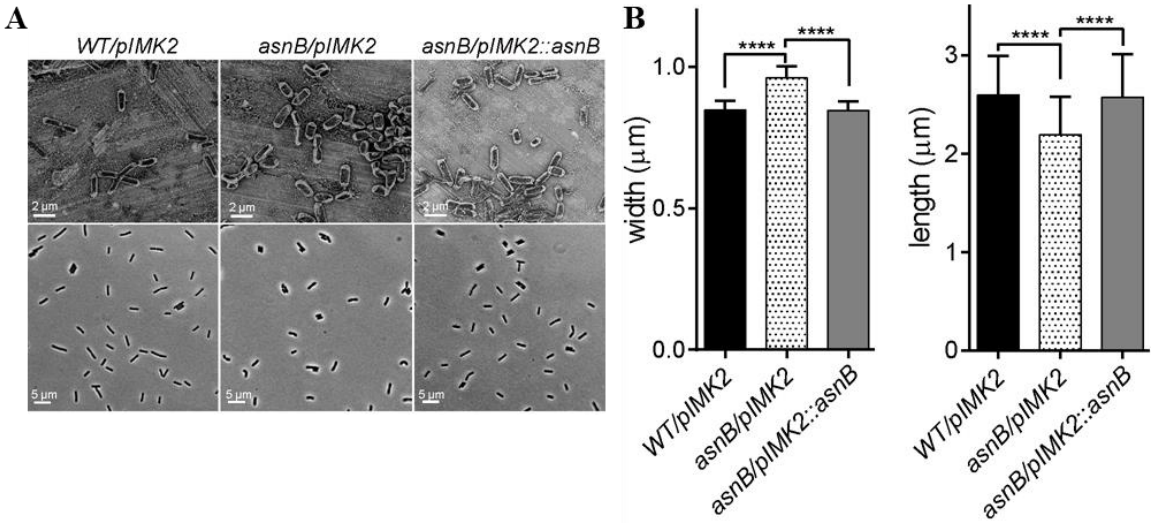

Figure 3.2 Analysis of cell morphology of the *L. monocytogenes asnB* mutant grown to exponential phase (OD600 = 1) at 30°C. (**A**) SEM (top row) and phase-contrast light microscopy images (bottom row) of *WT/pIMK2*, *asnB/pIMK2* and *asnB/pIMK2::asnB* strains. (**B**) Analysis of cell dimensions of the same strains from phase-contrast images using MicrobeTracker software [173]. The data represent mean ± SD of cell length and width; n = 300. ****, $p < 0.0001$ by two-tailed Student's t-test.

3.4.2 The *asnB* mutant is flagella-less, defective in biofilm formation, and exhibits increased sensitivity to lysozyme

In view of the observed cell shape defects of the *asnB* mutant and the possible role of AsnB in *m*DAP amidation, we analyzed some additional phenotypes that could be affected by cell wall perturbation. Swimming motility in 0.2% BHI agar at 30°C was completely lost for the *asnB* mutant, and flagellar staining indicated that this was due to the complete absence of flagella (Fig. 3.3A-B). Motility and flagella production were almost fully restored for the complemented mutant. Since flagellar motility was previously shown to play an essential role in *L. monocytogenes* biofilm formation [72], we subsequently determined the biofilm-forming capacity of the *asnB* mutant using the crystal violet staining method. The data showed a complete loss of biofilm-forming capacity of the *asnB* mutant (Fig. 3.3C).

Finally, we investigated the sensitivity of the *asnB* mutant to lysozyme, since *m*DAP amidation had been linked to lysozyme resistance in some bacteria [213,216]. Both the disc diffusion assay and the broth growth inhibition assay revealed lysozyme sensitivity of the *asnB* mutant during growth, while the WT was fully resistant (Fig. 3.4A-B). Furthermore, the *asnB* mutant was also more sensitive to lysozyme in a lysis assay with non-growing cells

suspended in a buffer (Fig. 3.4C). Genetic complementation restored WT, or almost WT, lysozyme tolerance in all these assays.

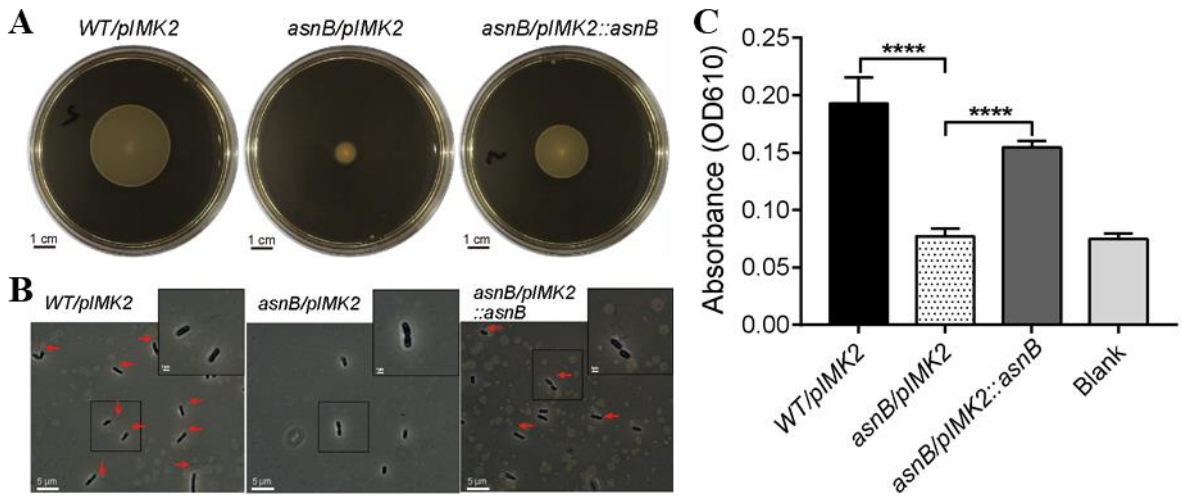

Figure 3.3 Flagellation, motility, and biofilm formation of the *L. monocytogenes asnB* mutant. (**A**) Swimming motility at 30°C of *WT/pIMK2*, *asnB/pIMK2*, and *asnB/pIMK2::asnB* stabbed in 0.2% BHI agar. Images are representative of three independent tests. (**B**) Detection of flagella by flagellar staining and phase-contrast microscopy, in the same strains. For each strain, more than 300 cells from three independent analyses were observed, and flagella were never seen in the *asnB* mutant. (**C**) Biofilm forming capacity of the same strains in a 96-well polystyrene microplate, determined by crystal violet staining. The data represent mean ± SD; $n = 4$; ****, $P < 0.0001$ by two-tailed Student's t-test.

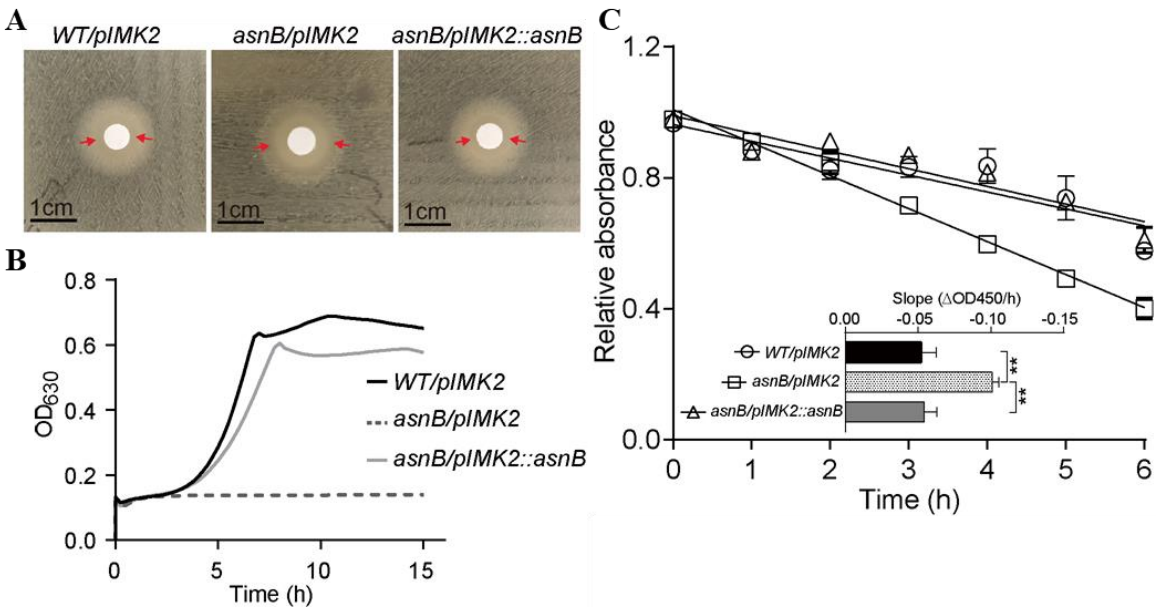

Figure 3.4 Lysozyme sensitivity of the *L. monocytogenes asnB* mutant. (**A**) Disk diffusion assay of *WT/pIMK2*, *asnB/pIMK2* and *asnB/pIMK2::asnB* strains. The zone of clearance is indicated with red arrows. Images are representative of at least three independent experiments. (**B**) Growth of the same strains in BHI broth with 1 mg/mL lysozyme at 30°C. Graphs are means of three independent experiments. (**C**) Lysis of cell suspensions of the same strains in potassium phosphate buffer in the presence of 0.1 µg/mL lysozyme. The relative absorbance on the y-axis represents the ratio of absorbance (OD_{450}) in the presence of lysozyme versus water as a control. The inset shows the slopes of linear regression curves from the main graph. Data represents mean ± SD; $n = 5$; **, $P < 0.0021$ by two-tailed Student's t-test.

3.4.3 AsnB mediates amidation of *meso*-diaminopimelic acid residues in peptidoglycan

The aberrant cell shape, absence of flagellation, and lysozyme sensitivity suggested a role in *m*DAP amidation rather than in Asn biosynthesis for AsnB in *L. monocytogenes*. To further investigate this possible function, the AsnB amino acid sequence was compared with homologs in other Gram-positive bacteria (Fig. 3.5A). The analysis reveals three major clades, of which one contains no representatives with proven *m*DAP amidation activity. Among the members of this clade are AsnH and AsnO from *B. subtilis*, but also homologs from *Actinobacteria* and AsnB from *E. coli*, which was included for comparison because it is known to be an Asn-producing enzyme. The other two clades, which are more closely related to each other than to the first clade, contain proteins from *Actinobacteria* and *Firmicutes*, respectively, and both contain representatives with demonstrated *m*DAP amidation activity. With 68% sequence identity, *L. monocytogenes* AsnB is most closely related to AsnB from

B. subtilis (Fig. 3.5B), which was recently shown to mediate peptidoglycan *m*DAP amidation [213]. Another highly similar homolog is AsnB1 of *Geobacillus stearothermophilus*, whose *m*DAP in peptidoglycan is amidated as well [227]. In the same clade, AsnB1 of *L. plantarum* was also demonstrated to mediate *m*DAP amidation [214]. The same holds for AsnB1 from *C. difficile* [215], but this sequence, together with that of its AsnB2 paralog from the same organism, forms a small distinct clade.

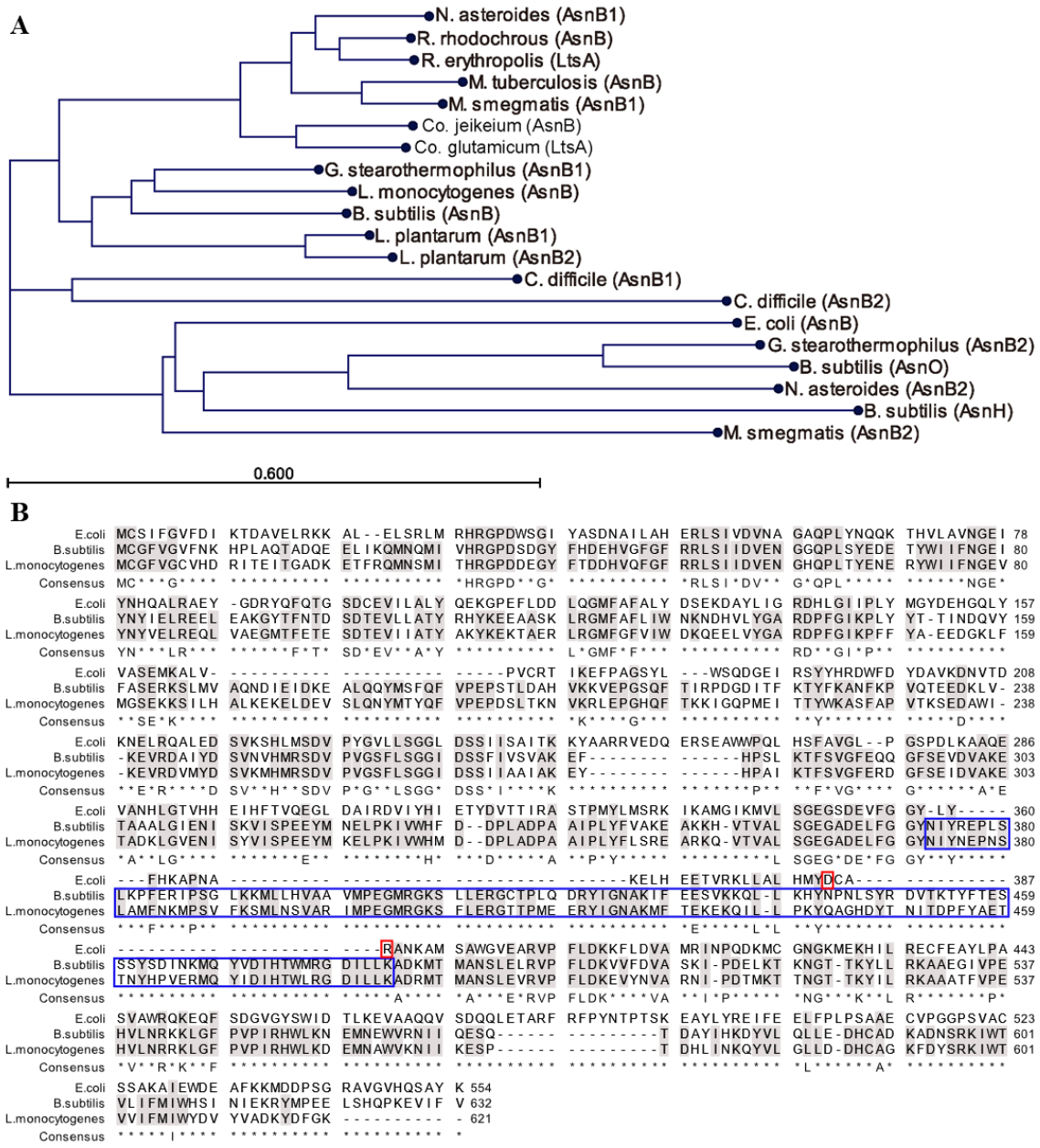

Figure 3.5 Sequence comparison of AsnB proteins from selected bacteria. (**A**) Phylogenetic tree of AsnB homologs from several Gram-positive bacteria and from *E. coli*, all of which contain *m*DAP in

their peptidoglycan. Bacterial genera: B, *Bacillus*; C, *Clostridioides*; Co, *Corynebacterium*; E, *Escherichia*; G, *Geobacillus*; L, *Lactobacillus*; M, *Mycobacterium*; N, *Nocardia*; R, *Rhodococcus*. (**B**) Sequence alignment of AsnB from *L. monocytogenes*, *B. subtilis*, and *E. coli*. Identical residues between the three proteins and between AsnB from *B. subtilis* and *L. monocytogenes* are highlighted in gray color. Conserved Asp-binding residues [228] in AsnB of *E. coli* are highlighted with a red box. The extra amino acid loop characteristic of *m*DAP-amidating AsnB homologs is highlighted with a blue box.

To provide direct evidence for the involvement of AsnB in *m*DAP amidation, the peptidoglycan structure of the *WT/pIMK2*, *asnB/pIMK2*, and *asnB/pIMK2::asnB* strains was analyzed by enzymatic hydrolysis followed by RP-HPLC and mass spectrometry. The muropeptide profiles of *WT/pIMK2* and *asnB/pIMK2::asnB* by RP-HPLC were almost indistinguishable (Fig. 3.6). In contrast, the profile of *asnB/pIMK2* was strikingly different from the major peaks shifted towards lower retention times.

MALDI-TOF analysis was conducted to identify the muropeptides corresponding to peaks in the chromatogram and indicated the presence of about one amide group per stem peptide in WT (and complementation strain) peptidoglycan (Table S3.2). In contrast, no amidation was detected in the mutant strain. Since amidation can not only occur on the ε-carboxyl group of *m*DAP, but also the α-carboxyl groups of D-Glu, tandem mass spectrometry was performed on the major monomer muropeptide (disaccharide tripeptides), which corresponds to peak b and peak 1 in the chromatogram of *WT/pIMK2* and *asnB/pIMK2*, respectively (Fig. S3.1). This confirmed that only *m*DAP in the peptidoglycan peptide is amidated. In addition, the analysis showed that some GlcNAc residues were deacetylated, and some MurNAc residues were O-acetylated, which is consistent with previous studies [206,220]. Altogether, these results provide convincing evidence that *L. monocytogenes* AsnB is an amidotransferase that amidates *m*DAP of the peptidoglycan peptide.

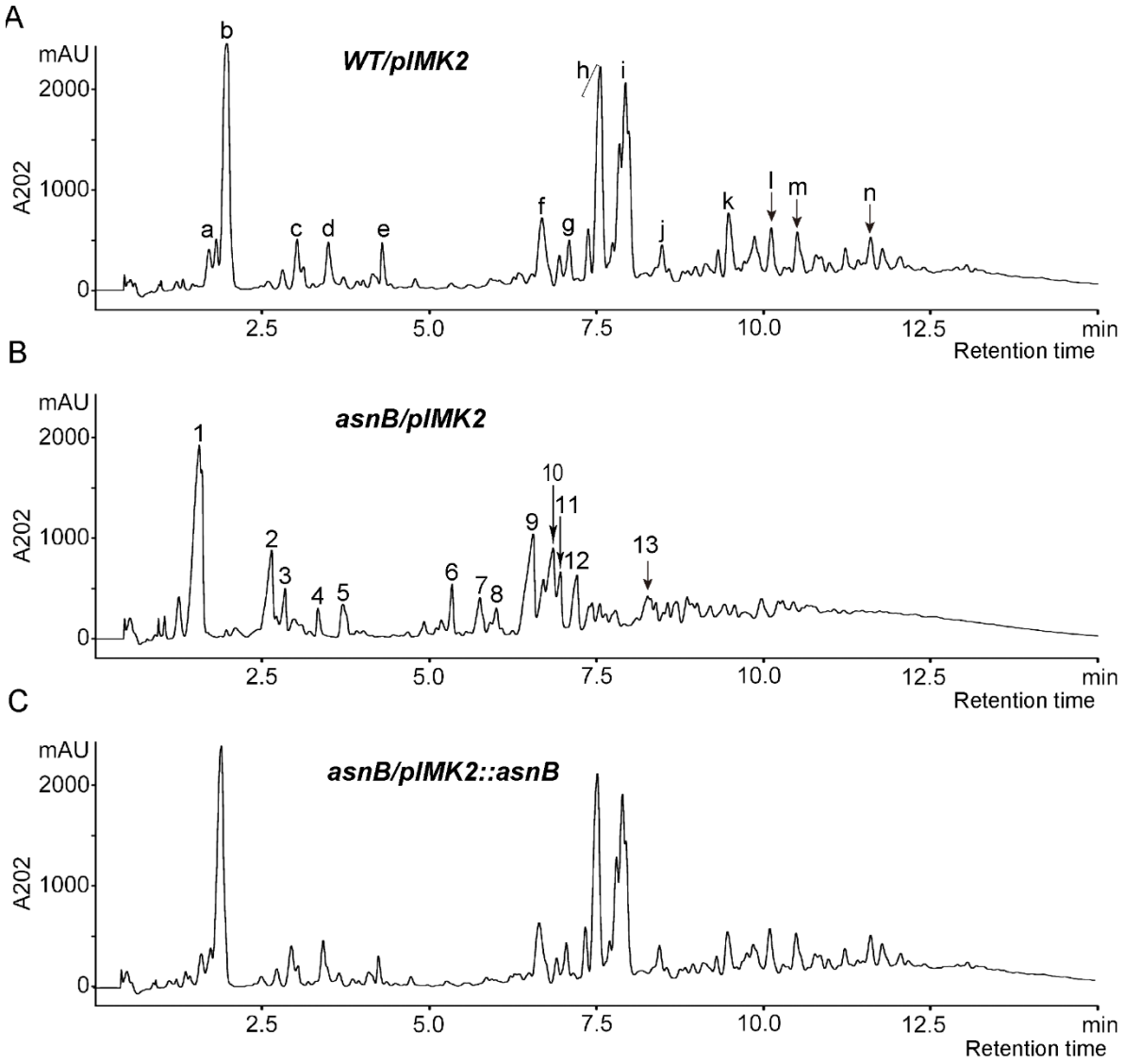

Figure 3.6 RP-HPLC chromatograms of muropeptides generated by mutanolysin hydrolysis of peptidoglycan from (**A**) *WT/pIMK2*, (**B**) *asnB/pIMK2* and (**C**) *asnB/pIMK2::asnB*. The major muropeptide peaks of the chromatogram are annotated with letters and numbers for *WT/pIMK2* and *asnB/pIMK2*, respectively. The mass and identity of the labeled peaks are listed in Table S3.2. Disaccharide tripeptides identified in peak b of *WT/pIMK2* and peak 1 of *asnB/pIMK2* were further analyzed by MS-MS (Figure S3.1).

3.4.4 The *m*DAP amidation is required for cell invasion

Peptidoglycan N-deacetylation and O-acetylation are critical for the virulence of *L. monocytogenes* by mediating escape of the immune response [206,221,222]. However, the possible role of *m*DAP amidation in virulence has not yet been studied in *L. monocytogenes*, nor in any other pathogen, and was therefore addressed here by using a gentamicin cell invasion assay. Firstly, human JEG3 placental cells were infected with stationary phase

bacteria for 1 h, followed by incubation with gentamicin for an additional 3 h, and the invasion efficiency was expressed as the ratio of the number of recovered bacteria to the number of bacteria initially applied. The results highlighted an important defect in the cellular invasion of the *asnB/pIMK2* mutant, with a reduction in invasion efficiency to less than 2% of the level of the wild-type strain, while complementation resulted in a restoration of invasion efficiency to about 30% of that of the WT strain (Fig. 3.7A). To determine whether the attenuation of cell invasion caused by *asnB* inactivation also occurred in another cell type, we next performed invasion assays in human Caco-2 intestinal cells. The assay was modified to test bacteria in either stationary or exponential phase and to shorten the duration of the infection, in order to avoid the intracellular replication of bacteria, which might be impacted by AsnB deficiency. Caco-2 cells were thus exposed to bacteria for only one hour, of which 30 min was allocated for the entry of bacteria into the cells, and another 30 min to the elimination of the extracellular bacteria with gentamicin. Entry efficiency was expressed as the ratio of bacteria recovered after 1 h of infection to the initial number of bacteria applied (Fig. 3.7B-C). Compared to the WT strain, the entry efficiency of the *asnB/pIMK2* mutant at exponential and stationary phase was ten and six times lower, respectively (Fig. 3.7B-C). Furthermore, the entry efficiency was fully restored by complementation. Taken together, these results indicate that *asnB* inactivation impairs *L. monocytogenes* entry into epithelial cells.

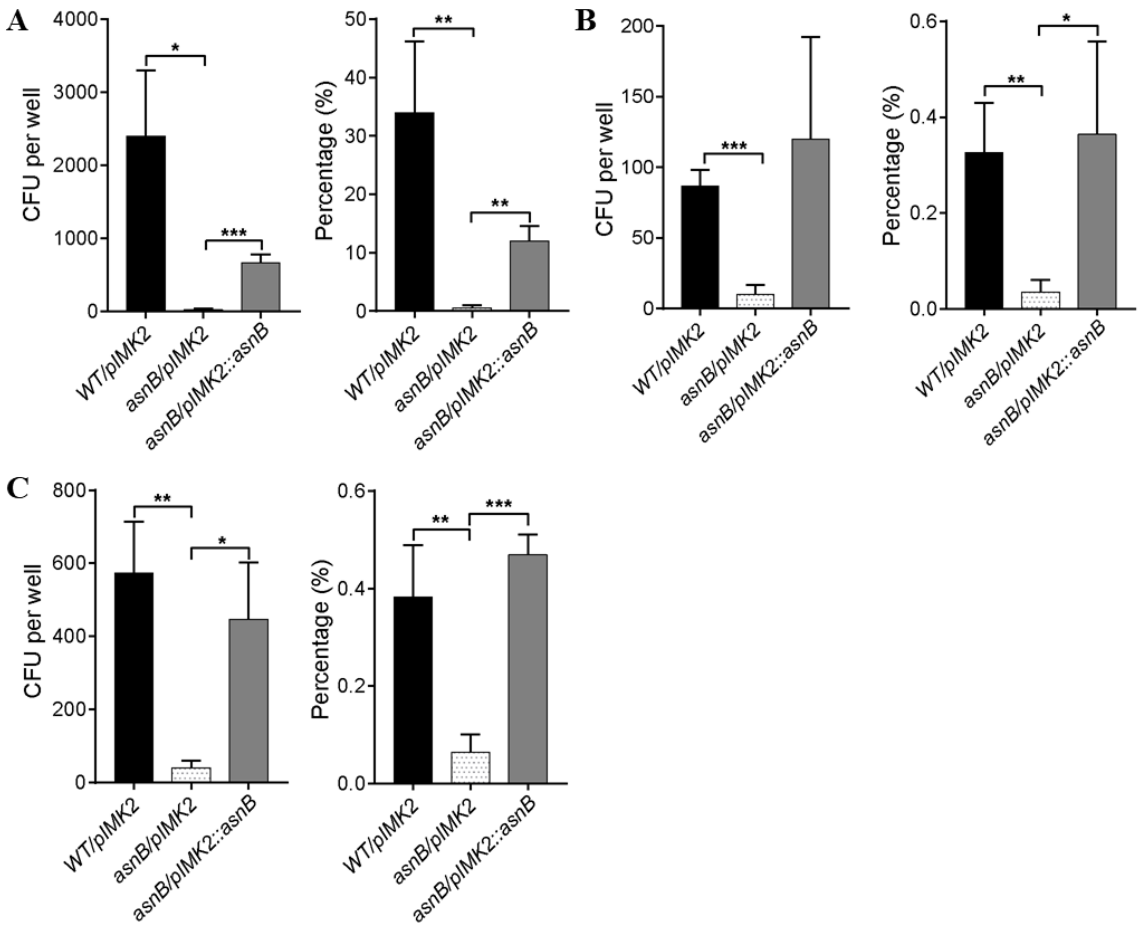

Figure 3.7 Analysis of cell invasion by the *L. monocytogenes asnB* mutant using gentamicin invasion assays. The number of intracellular bacteria was enumerated by CFU counts (left panel) and the invasion efficiency was expressed as the percentage of intracellular bacteria relative to the bacterial inoculum (right panel). **(A)** Human JEG-3 placental cells were infected with *WT/pIMK2*, *asnB/pIMK2*, or *asnB/pIMK2::asnB* bacteria for 4h (1 h to allow bacterial entry and 3 h of treatment with gentamicin, which kills extracellular bacteria). **(B** and **C)** Human Caco-2 intestinal cells were infected with *WT/pIMK2*, *asnB/pIMK2*, or *asnB/pIMK2::asnB* bacteria at either exponential (**B**) or stationary (**C**) phase, for 1h (0.5 h to allow bacterial entry and 0.5 h of treatment with gentamicin). All data represent mean ± SD; $n = 3$; *, $P < 0.05$; **, $P < 0.01$; ***, $P < 0.001$ by two-tailed Student's t-test.

3.4.5 Loss of *m*DAP amidation reduces anchoring of invasion InlA to the cell surface

Internalins are a family of leucine-rich repeat proteins that play an important role in the *Listeria* infection process [229]. The majority of internalins are LPxTG proteins covalently bound to the bacterial cell wall by the Sortase A (SrtA) enzyme, the best characterized being InlA, which mediates the adhesion and internalization of

L. monocytogenes into epithelial cells [230,231]. Interestingly, InlA is anchored to the bacterial surface by covalent linkage to *m*DAP in the peptidoglycan stem peptide [232]. Therefore, and because the *asnB* mutant has a defect in cell entry, we tested whether the *asnB* mutant is defective in the cell wall anchoring of InlA. The presence of InlA on the bacterial surface was analyzed by immunofluorescence using InlA-specific monoclonal antibodies, as previously described for the study of a sortase A mutant [226]. In comparison with the WT strain, detection of InlA on the surface of the *asnB/pIMK2* mutant cells was considerably reduced (Fig. 3.8). In contrast, InlA was clearly detected on the surface of the complemented strain, indicating that expression of *asnB* in the mutant restored surface anchoring. Thus, amidation at the ε-carboxyl group of *m*DAP appears to be required for efficient cross-linking of InlA to *m*DAP.

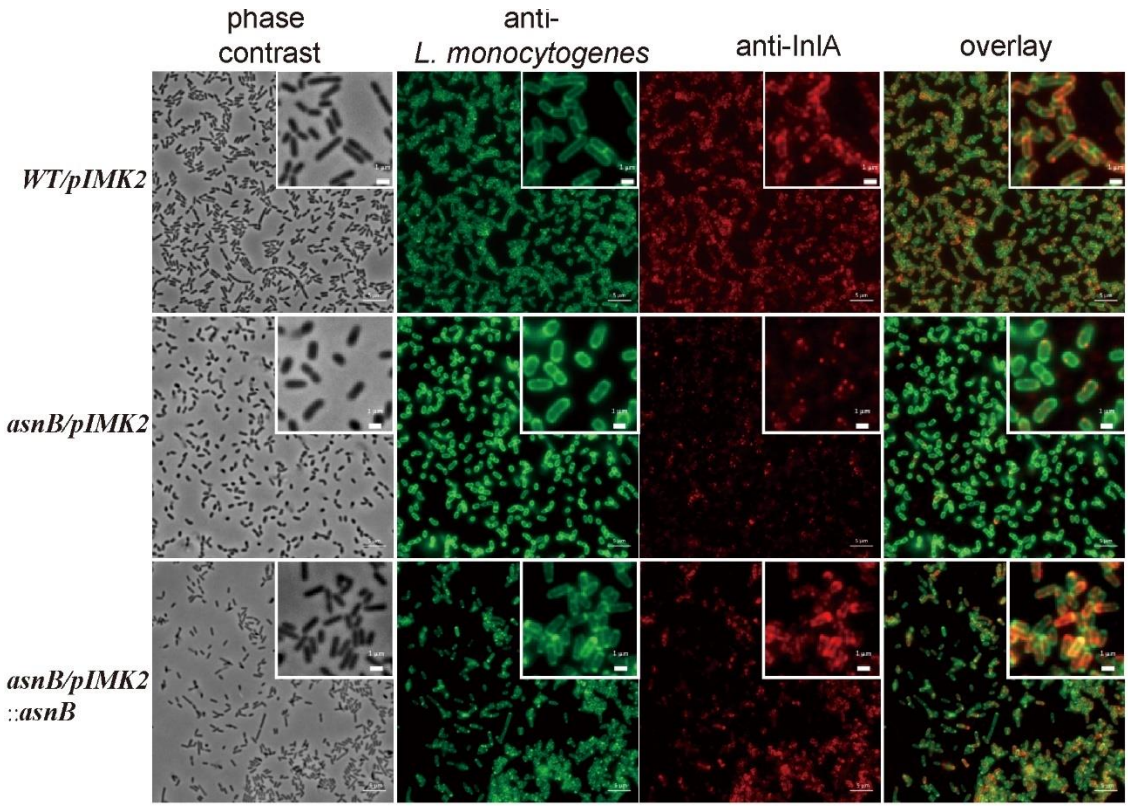

Figure 3.8 Immunofluorescence microscopy analysis of the invasion protein InlA on the surface of *L. monocytogenes WT/pIMK2*, *asnB/pIMK2*, and *asnB/pIMK2::asnB* strains. Bacteria were visualized using phase-contrast microscopy (first lane) and with immunofluorescence staining with a polyclonal anti-*L. monocytogenes* antibody (second lane) and a mixture of two monoclonal anti-InlA antibodies

(third lane). Bacteria (in green) and InlA (in red) are shown together in an overlay composition (last lane). Scale bar 5 µM. A higher magnification is shown in the upper right corner. Scale bar 1 µM.

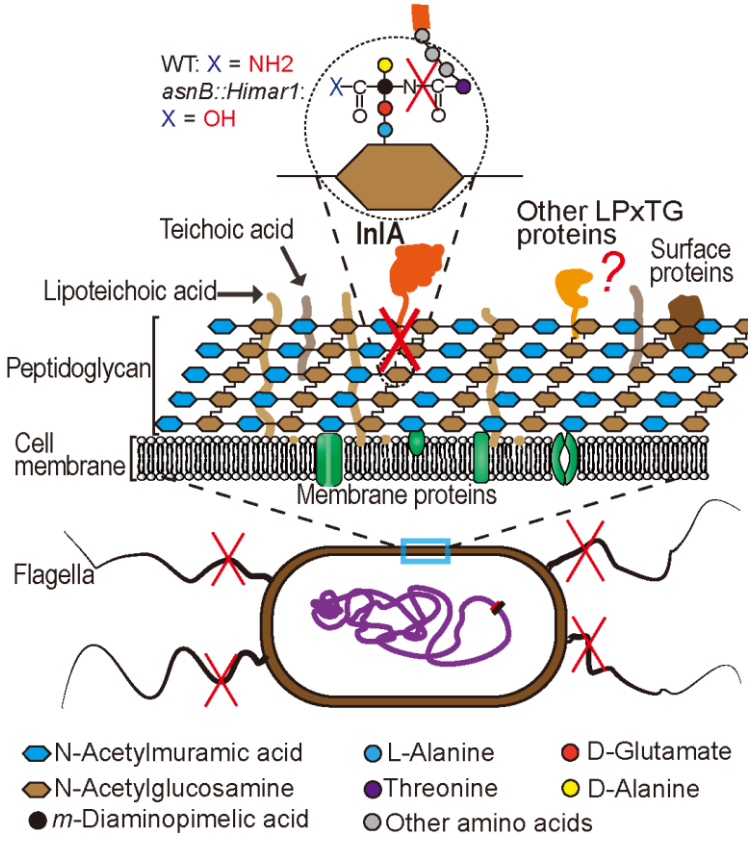

Figure 3.9 Schematic representation of cell surface changes resulting from AsnB deficiency in *L. monocytogenes*. The direct effect of loss of AsnB activity is the absence of amidation of the *m*DAP ε-carboxyl group (shown in the inset at top of the figure). Indirect consequences include inefficient InlA display at the cell surface, probably because it can no longer be cross-linked to the ε-amino group of *m*DAP, and the loss of flagella (indicated by red cross over the structure). Other surface proteins which, like InlA, are exported and cross-linked via an LPXTG motif, may also fail to be anchored to the cell surface (red question mark).

3.5 Discussion

In this work, we demonstrate that the *asnB* gene of *L. monocytogenes* is required for amidation of the ε-carboxyl group of *m*DAP in the peptidoglycan stem peptide (Fig. 3.6; Table S3.2). Based on amino acid sequence similarity, the predicted gene product AsnB belongs to a family of Gln-hydrolyzing amidotransferases designated as asparagine synthases (E.C. 6.3.5.4). While AsnB proteins are indeed involved in Asn synthesis in several bacteria,

representatives in an increasing number of Gram-positive bacteria, including *L. plantarum* [214], *C. glutamicum* [216], *B. subtilis* [213] and *C. difficile* [215], have been shown to catalyze amidotransfer from Gln to the ε-carboxyl group of *m*DAP in the stem peptide of bacterial peptidoglycan rather than to Asp. Although the role of AsnB had not been studied in *L. monocytogenes*, there were at least two reasons to anticipate that it would also have *m*DAP modifying activity. Firstly, structural analysis had already revealed *m*DAP residues to be amidated in two *L. monocytogenes* serotype 1/2a strains [206,220]. Secondly, *L. monocytogenes* AsnB shares most sequence similarity to AsnB from *B. subtilis* and other homologs known to amidate *m*DAP (Fig. 3.5). Furthermore, *L. monocytogenes* AsnB lacks the conserved Asp binding residues (D and R) of enzymes with Asn synthesizing activity, and it has the extra loop in the substrate-binding region that is characteristic of the *m*DAP amidating enzymes[228]. We did not analyze whether AsnB from *L. monocytogenes* can restore Asn auxotrophy in an *E. coli asnB* mutant, and thus cannot exclude that it is a promiscuous enzyme similar to its *B. subtilis* counterpart [212]. However, since neither t-CIN tolerance nor normal cell morphology was restored in the *asnB* mutant by supplying additional Asn in the growth medium, it seems unlikely that these phenotypes result from Asn deficiency and that AsnB plays a role in Asn synthesis in *L. monocytogenes*. Besides the AsnB-catalyzed amidotransfer from Gln to Asp, two alternative Asn biosynthesis routes have been documented in bacteria. One is the direct amidation of Asp with ammonium by an AsnA-type asparagine synthetase. The other one is a tRNA-dependent transamidation, in which a $tRNA^{Asn}$ is first 'mischarged' with Asp by a nondiscriminating aspartyl tRNA synthetase (AspS), and Asp is subsequently amidated by a Gln-hydrolyzing asparaginyl-tRNA synthase (GatABC). Based on its genome sequence, it is predicted that *L. monocytogenes* does not produce an AsnA-like enzyme, but can synthesize Asn via the tRNA-dependent pathway, like many other Gram-positive bacteria.

Like in *B. subtilis*, *L. plantarum* and *C. glutamicum* [213,214,216], the loss of AsnB-dependent *m*DAP amidation resulted in altered cell morphology and growth defects in *L. monocytogenes*. Such effects were not seen in *C. difficile*, but this may be because AsnB is expressed only upon induction with vancomycin in this organism [215]. Given the key role of peptidoglycan in cell shape determination and the complexity of bacterial cell morphogenesis, it is not surprising that chemical modifications of peptidoglycan have an impact on cell shape, cell division, and growth. Nevertheless, the mutational elimination of peptidoglycan O-acetylation by OatA, peptidoglycan N-deacetylation by PgdA, or both

simultaneously, did not affect growth and was not reported to affect cell morphology [222]. One possible explanation for this different impact is that O-acetylation and N-deacetylation do not modify the electrostatic charge of peptidoglycan in the normal pH range of growth, whereas amidation of the ε-carboxyl group of *m*DAP reduces the number of negatively charged carboxylate groups. Similarly, the amidation of D-Glu in the peptidoglycan stem peptide that occurs in some bacteria also reduces negative charges on peptidoglycan, and was found to be essential for normal growth in *S. aureus* [233]. A phenotype of the AsnB mutant that can be directly related to (loss of) peptidoglycan modification is its lysozyme sensitivity. This phenotype was already reported for *asnB* mutants of *B. subtilis* and *C. glutamicum* [213,216]. Besides N-deacetylation and O-acetylation [206,220,222], *m*DAP amidation is therefore the third peptidoglycan modification implicated in lysozyme resistance in *L. monocytogenes*. How the different modifications interact, and their precise contribution and hierarchy in conferring lysozyme resistance is not entirely clear, and may vary among strains and environmental conditions. For example, deletion of *oatA* caused lysozyme sensitivity in *L. monocytogenes* strain EGDe [221] but not in strain 10403S although it exacerbated lysozyme sensitivity of a *pgdA* mutant in this strain [220,222]. *L. monocytogenes* is known to also infect and even cause listeriosis in several other vertebrates, including birds and fish, some of which produce additional or different types of lysozymes with different substrate specificity [234–236], and the presence and ability to modulate the activity of different peptidoglycan modifying enzymes may be an adaptation to this promiscuous lifestyle.

In several bacterial pathogens, modifications that render peptidoglycan resistance to lysozyme support the ability to establish infections [237], and at least two different mechanisms may explain this. First, peptidoglycan modification protects the bacteria from the direct action of lysozyme as a first-line antibacterial defense actor of the innate immune system in those parts of the body where it is abundant, such as the blood, saliva, tears, milk, phagocytes, and mucosal surfaces. Additionally, peptidoglycan modification also suppresses the lysozyme-mediated release of peptidoglycan fragments that modulate the host immune response upon binding to a range of pattern recognition receptors. Among these, the cytosolic receptor NOD1 is of particular importance here because it recognizes peptidoglycan fragments containing the D-Glu-*m*DAP stem peptide residues [238], and amidated *m*DAP significantly blocks the recognition of peptidoglycan fragments by NOD1 while enhances the recognition by NOD2 [239]. Therefore, it can be anticipated that *L. monocytogenes* AsnB

deficient mutants will be recognized differently by the immune system which could affect the innate immune defense process against the bacteria.

In the present work, we found that AsnB is required for *Listeria* invasion of epithelial cells, which is mainly mediated by the bacterial surface protein InlA through its interaction with the host receptor E-cadherin [230,231]. InlA plays a critical role in the ability of *L. monocytogenes* to cross epithelial barriers, such as the intestinal and placental barriers [240]. Here, we showed a reduced presence of InlA on the surface of the *asnB* mutant, which can explain the invasion deficiency in human intestinal Caco-2 cells and placental JEG-3 cells. InlA contains both an N-terminal signal peptide and a C-terminal LPXTG sorting signal [232]. After translation, InlA is secreted across the bacterial membrane via the Sec secretory pathway, which recognizes and cleaves off the N-terminal signal peptide of the protein [241]. Subsequently, SrtA cleaves the protein after the threonine residue of the LPXTG motif in its C-terminal part, and covalently links the protein to the peptidoglycan lipid intermediate II, by forming a new peptide bond between the carboxyl group of Thr and the free ε-amino group of *m*DAP [226,232]. The lipid-linked protein is subsequently incorporated into the mature cell wall through the transglycosylation and transpeptidation reactions [241]. Although the ε-amino group of *m*DAP remains available, our results indicate that deamidation of the ε-carboxyl group may prevent the cross-linking of InlA. However, the *m*DAP was indicated to be unamidated in the study conducted by Dhar et al. [232], which is the only study to characterize the molecular mechanism of bounding of InlA to *m*DAP in *L. monocytogenes*. This can be explained by the insufficient accuracy of the MS data presented at that time (2000) as deviations between observed mass and calculated mass obtained with mass spectrometers in that work were larger (many are above 1) [232]. Thus, amidation of *m*DAP could not be clearly assigned (amidation results in a loss of 1 Da of mass!). While our MS/MS results (Fig. S3.1) showed no ambiguity that the *m*DAP residue is amidated whereas iGlu is not in the peptidoglycan of *L. monocytogenes*.

Several possible reasons for the reduced anchoring of InlA to the *m*DAP caused by the deamination can be conceived. First, the increased negative charge of deamidated *m*DAP may reduce the binding affinity or even cause repulsion between the SrtA-InlA complex and peptidoglycan precursor lipid II. Second, deamidation may induce a conformational change that prevents the correct positioning of the SrtA-InlA complex and the peptidoglycan precursor lipid II [232]. It should be noted that besides InlA, the *in-silico* genome analysis of

several *L. monocytogenes* species unraveled more than 40 genes (41 in strain EGD-e, more than 1% of the genome) encoding proteins bearing an LPXTG motif [111,202,242,243]. Hitherto, only several of these proteins, including InlH, InlI, InlJ, InlK, InlF, Vip, and LapB, have been characterized functionally and/or biochemically [202,241,244–252], and their anchoring to the peptidoglycan might be impaired by the absence of amidation modification on *m*DAP as well (Fig. 3.9). Like InlA, Vip and LapB were revealed to be positively controlled by the master virulence regulator PrfA and needed for adhesion to and entry into some mammalian cells as well as the *in vivo* infection of mice [246,247]. InlJ and InlK were shown to specifically contribute to the bacterial *in vivo* invasion by facilitating bacterial adherence to host tissues and escape from host autophagy, respectively [249–252]. In addition, InlF was shown to promote bacterial entry into endothelial cells and facilitate bacterial colonization of the brain by interacting with vimentin on the host cell surface [244]. In contrast, InlI and InlH were both shown to be nonessential for either *in vitro* invasion of cultured cells or *in vivo* invasion of intestinal cells [248,249]. Apart from the implication in bacterial pathogenesis, some LPXTG motif-containing proteins such as InlL and InlA were indicated to be involved in the adhesion of *L. monocytogenes* to the abiotic surface and affect the biofilm formation [253–255]. The impact of LPXTG proteins on biofilm formation is better elucidated in other Gram-positive bacteria such as *Streptococcus gordonii* and *Enterococci* [256,257]. Unlike many bacteria species in Firmicutes, the peptidoglycan of *Listeria* is quite original as no peptide crossbridges are utilized to link adjacent wall peptides, instead, an *m*DAP is present in the wall peptides (like in most Gram-negative species) for cross-linking the wall peptides [258]. Thus, the LPXTG motif-containing proteins are directly bound to the free ε-amino group of *m*DAP residue. In contrast, in *S aureus* (the paradigm model for LPTXG proteins), LPXTG proteins are linked to a peptide crossbridge in the peptidoglycan, and not to the wall peptides [259]. Therefore, the amidation of *m*DAP could be particularly important for the anchoring of LPXTG peptides in the pathogen *Listeria*.

AsnB deficiency was also accompanied by a loss of bacterial motility due to the inability to produce flagella in *L. monocytogenes* (Fig. 3.3 and Fig. 3.9). Remarkably, this phenotype has not been reported previously in *asnB* mutants of other bacteria including the closely related *B. subtilis*. The flagellar apparatus is embedded in the bacterial cell wall, where it interacts directly with the peptidoglycan layer via several components of its basal body [260]. Its assembly is a complex and highly coordinated process that requires local and controlled peptidoglycan hydrolase activity to mediate the passage of the flagellar rod through

the peptidoglycan layer [260]. As such, it is easy to envision that the increased negative charge of the non-amidated peptidoglycan, or the absence of one or more peptidoglycan-linked proteins, may compromise flagellar assembly. However, the precise reason for the lack of flagella remains to be elucidated. The lack of flagella and flagellum-mediated motility may also explain the reduced biofilm formation of the *asnB* mutant [72], although other changes in surface properties may also contribute.

In conclusion, this work demonstrates that AsnB of *L. monocytogenes* is a Gln-hydrolyzing amidotransferase that amidates *m*DAP residues in the stem peptide of *L. monocytogenes* peptidoglycan. Loss of AsnB does not affect growth in BHI broth at 30°C, but causes sensitivity to *trans*-cinnamaldehyde and lysozyme, reduced epithelial cell invasion, and thus probably reduced virulence, loss of flagella and motility, and reduced biofilm formation. These results indicate the importance of peptidoglycan amidation both for host infection and for life in the non-host environment.

3.6 Supplementary materials

Table S3.1 List of protein sequences used in the phylogeny tree construction (Fig. 3.5).

GenBank acc. no.	Organism	Protein name	Length, a.a
WP_019046170.1	*Nocardia asteroides*	AsnB1	647
WP_022565516.1	*Nocardia asteroides*	AsnB2	613
P22106	*Escherichia coli*	AsnB	554
WP_053414543.1	*Geobacillus stearothermophilus*	AsnB1	635
WP_013523091.1	*Geobacillus stearothermophilus*	AsnB2	615
WP_004398625	*Bacillus subtilis 168*	AsnB	632
WP_003233080	*Bacillus subtilis 168*	AsnO	614
WP_003244103	*Bacillus subtilis 168*	AsnH	747
WP_011729689	*Mycolicibacterium smegmatis*	AsnB1	658
WP_011728459	*Mycolicibacterium smegmatis*	AsnB2	601
WP_003436426	*Clostridioides difficile 630*	AsnB1	624
WP_011860775	*Clostridioides difficile 630*	AsnB2	527
WP_057717704.1	*Lactobacillus plantarum*	AsnB2	633
WP_054399562.1	*Lactobacillus plantarum*	AsnB1	633
WP_003731601	*Listeria monocytogenes Scott A*	AsnB	621
WP_005296050	*Corynebacterium jeikeium*	AsnB	645
BAA89484	*Corynebacterium glutamicum*	LtsA	640
WP_055372007	*Mycobacterium tuberculosis*	AsnB	652
WP_020908107.1	*Rhodococcus erythropolis*	LtsA	641
WP_160875722.1	*Rhodococcus rhodochrous*	AsnB	641

Table S3.2 Mass spectrometry analysis of major muropeptide peaks in the chromatogram of *WT/pIMK2* and *asnB/pIMK2* strain (Fig. 3.6). The deduced muropeptide structures and their corresponding m/z values are shown in the Table. The presence of amidation on the muropeptides is indicated with red color.

WT/pIMK2				***asnB/pIMK2***			
Peak#*	**Muropeptide****	**Observed m/z $[M+Na]^+$**	**Calculated m/z $[M+Na]^+$**	**Peak#***	**Muropeptide****	**Observed m/z $[M+Na]^+$**	**Calculated m/z $[M+Na]^+$**
	Monomers				**Monomers**		
a	Tri(NH_2)-Ac	850.25	850.37	1	Tri	893.19	893.36
b	Tri(NH_2)	892.21	892.38		Tri-Ac	850.92	851.35
c	Di	720.96	721.27	2	Tetra	964.26	964.4
	Tetra(NH_2)-Ac	921.25	921.40	3	Tetra-Ac	922.25	922.39
d	Tetra(NH_2)	963.30	963.41	4	Tri+Ac	935.25	935.37
	Tetra(NH_2)-Ac	921.25	921.40	5	Penta	1035.25	1035.43
e	Tri(NH_2)+Ac	934.21	934.39	6	Tri Anh	873.12	873.33
	Dimers				**Dimers**		
f	TriTetra(NH_2)	1815.93	1815.77	7	TriTetra-Glc	1613.83	1613.68
	TetraTetra(NH_2)-GM	1406.73	1406.62	8	TriTetra-Ac-Glc	1571.82	1571.67
g	TriTetra(NH_2)	1815.93	1815.77	9	TriTetra	1816.88	1816.76
	ds4a4	1406.73	1406.62	10	TriTetra-Ac	1774.86	1774.75
h	TriTetra(2 NH_2)	1814.91	1814.79	11	TriTetra-2Ac	1732.88	1732.74
	TriTetra(2 NH_2)-Ac -Glc	1569.83	1569.70	12	TetraTetra	1887.94	1887.79
	TriTetra(NH_2)-Ac	1773.90	1773.76	13	TriTetra+Ac	1858.95	1858.77
i	TriTetra(2 NH_2)-Ac	1772.95	1772.78				
	TriTetra(2 NH_2)-2Ac	1730.94	1730.77				
j	TetraTetra(2 NH_2)	1886.04	1885.83				
k	TetraTetra(2 NH_2)+Ac	1856.96	1856.80				
	Trimers						
l	TriTetraTetra(3 NH_2)	2736.94	2737.20				
m	TriTetraTetra(3 NH_2)-Ac	2695.01	2695.19				
n	TriTetraTetra(3 NH_2)+Ac	2778.96	2779.21				
	TriTetra(2 NH_2)Anh-Ac	1752.89	1752.75				

Following the Table S3.2:

*: Peak # was assigned based on RP-HPLC chromatography (Fig. 3.6).

**: Di, disaccharide dipeptide (L-Ala-D-iGlu); Tri: disaccharide tripeptide (L-Ala-D-iGlu-*m*DAP); Tetra: disaccharide tetrapeptide (L-Ala-D-iGlu-*m*DAP-D-Ala); Penta: disaccharide pentapeptide (L-Ala-D-iGlu-*m*DAP-D-Ala-D-Ala); disaccharide, GlcNAc-MurNAc; (x NH_2): number of amidated residues; (-Ac): deacetylation of GlcNAc; (+Ac): O-acetylation on MurNAc; -Glc: loss of 1 GlcNAc; -GM: loss of disaccharide GlcNAc-MurNAc; Anh: anhydroMurNAc.

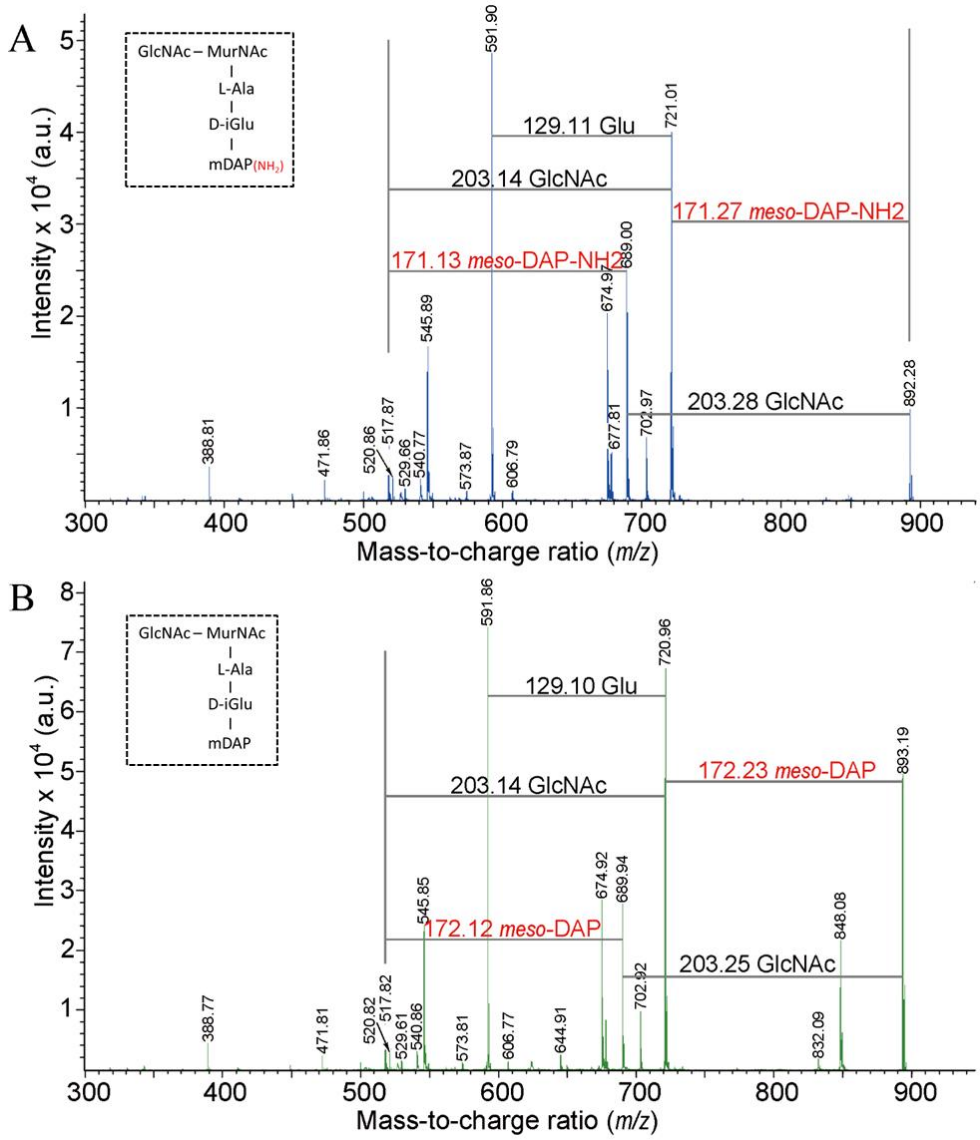

Figure S3.1 The disaccharide tripeptides contained in (A) peak b of *WT/pIMK2* (Fig. 3.6) and (B) peak 1 of *asnB/pIMK2* (Fig. 3.6) were analyzed with MS-MS analysis. Fragmentation of the parental ion at m/z 892.21 for the upper panel and 893.19 for the lower panel. The inferred ions obtained by fragmentation of peptidic or glycosidic bonds and their corresponding m/z value are indicated.

3.7 Author Contributions

Conceptualization: Lei Sun[1] and Chris W. Michiels[1]; investigation: Lei Sun and Gil Rogers[1]; writing—original draft preparation: Lei Sun; writing—review and editing: Lei Sun, Chris W. Michiels, Marie-Pierre Chapot-Chartier[2], and Hélène Bierne[2]; supervision and administration: Chris W. Michiels; bacterial peptidoglycan structure analysis: Pascal Courtin[2] and Marie-Pierre Chapot-Chartier; bacteria invasion assays and immunostaining: Hélène Bierne; All authors have read and agreed to the published version of the manuscript.

Affiliations:

[1] Laboratory of Food Microbiology, Department of Microbial and Molecular Systems (M2S) and Leuven Food Science and Nutrition Research Center (LFoRCe), KU Leuven, Leuven, Belgium.

[2] INRAE, AgroParisTech, Micalis Institute, Université Paris-Saclay, Jouy-en-Josas, France.

3.8 Funding

This work was funded by research grants from the Research Foundation-Flanders (FWO) (G.0C77.14N), from the KU Leuven Research Fund (METH/14/03), and from the French National Research Agency (ANR PERMALI (# ANR-20-CE35-0001-01).

3.9 Acknowledgments

We thank Sanne Wolput, Ines Staes, Wubishet Mengistu Tadesse, and Julien Mortier for assistance with the microscopy and image analysis, and Sreeprasanth Pulinthanathu Sree for conducting the HR SEM analysis.

Chapter 4 Experimental Evolution Reveals a Novel Ene-Reductase that Detoxifies α,β-Unsaturated Aldehydes in *L. monocytogenes*

4.1 Abstract

The plant essential oil component t-CIN exhibits antibacterial activity against a broad range of food-borne pathogenic bacteria including *L. monocytogenes*, but the knowledge of its antimicrobial mechanism is limited. In this study, several t-CIN resistant mutants of *L. monocytogenes* were obtained by experimental evolution. WGS analysis revealed single-nucleotide-variation mutations in the *yhfK* gene, encoding an oxidoreductase of the short-chain dehydrogenases/reductases superfamily, in each mutant. Deletion of *yhfK* conferred increased sensitivity to t-CIN and several other α,β-unsaturated aldehydes, including *trans*-2-hexenal, citral, and 4-hydroxy-2-nonenal. Thet-CIN tolerance was restored by genetic complementation with *yhfK*. Based on GC-MS analysis of culture supernatants, it is proposed that YhfK is an ene reductase that converts t-CIN to 3-phenylpropanal by reducing the conjugated C=C double bond of the α,β-unsaturated aldehyde moiety. YhfK homologs are widely distributed in Bacteria, and deletion of the corresponding homolog in *B. subtilis* caused increased sensitivity to t-CIN and *trans*-2-hexenal, suggesting that this protein may have a conserved function to protect bacteria against toxic α,β-unsaturated aldehydes in their environment.

4.2 Introduction

L. monocytogenes is a Gram-positive foodborne pathogen that causes severe invasive listeriosis and meningitis among susceptible persons such as immunocompromised individuals, pregnant women, and elderly persons [150,152]. This pathogen thrives well in a wide range of natural environments including soil, freshwater, decaying plant material, and the gastrointestinal tract of various animals, but also as a member of the resident house microbiota of food production facilities. It is therefore a common contaminant during food production and storage processes [150,156]. Furthermore, the ability of *L. monocytogenes* to grow under adverse conditions such as high salt concentration (up to 10% NaCl) and low temperature (as low as 0°C) make this pathogen a major concern in refrigerated, ready-to-eat foods. Preservatives such as nitrites, benzoates, and sorbates are commonly used to prevent its outgrowth to high numbers. However, these compounds are increasingly under scrutiny for possible adverse health effects, and food producers are exploring more natural alternatives to replace them [2,4].

Plant essential oil compounds have received much attention in this respect, and a well-studied one is t-CIN, one of the major components of cinnamon essential oil [4,5]. Previous work in our laboratory showed that the growth inhibition by t-CIN against *L. monocytogenes* is typically characterized by a dose-dependent elongation of the lag phase and reduction of growth rate [17]. Many different effects of t-CIN on bacterial cells have been reported, including an increased cell membrane permeability [29], inhibition of the membrane-associated ATPase activity [31], elevated intracellular redox stress [11,39], inhibition of cell division [22], repression of quorum sensing systems [37,47], and disrupted cell wall homeostasis [261]. However, these may be indirect effects that depend on factors such as the concentration and the incubation time, and the primary cellular targets of t-CIN remain unknown [14]. Besides t-CIN, also other α,β-unsaturated carbonyl compounds from plant origin exhibit a broad and promising antimicrobial activity, such as *trans*-2-hexenal (t-HEX) and citral [3,4]. The α,β-unsaturated carbonyl moiety shared by these compounds is electrophilic and accounts for the reactivity with a wide range of nucleophilic nitrogen and sulfur atoms in biomolecules including proteins, glutathione, and cysteine, primarily by the Michael-type addition reaction [84]. Proteins containing active Cys residues (e.g., glyceraldehyde-3-phosphate dehydrogenase, thioredoxins, and glutaredoxins) in particular represent important intracellular targets of various electrophilic α, β-unsaturated carbonyls in human and animal cells, but the targets in bacteria have not been elucidated [85].

Apart from conjugation with cellular nucleophiles, α,β-unsaturated aldehydes can be detoxified by enzymatic transformation to less electrophilic molecules in at least some microbes. It has been demonstrated that t-CIN can be reduced to the less toxic 3-phenyl-2-propenol by *E. coli* O157:H7 [7]. and by the fungi *Aspergillus ochraceus* and *Penicillium expansum* [58,60]. A predicted NADPH-dependent aldehyde reductase, YqhD, was anticipated to catalyze this reaction in *E. coli* because the transcription of *yqhD* was significantly induced by t-CIN and the inactivation of the gene significantly reduced the tolerance of *E. coli* to t-CIN [7,11]. A broad range of short-chain aldehydes, including acrolein, isobutyraldehyde, glycolaldehyde, butanaldehyde, malondialdehyde, and propanaldehyde, were previously demonstrated to be reduced by purified YqhD from *E. coli in vitro* [126,127]. Besides, the Old Yellow Enzyme family of flavin-dependent NADPH dehydrogenases, which are widely distributed in bacteria and fungi, comprises several ene reductases that facilitate hydrogenation of the C=C double bond of a wide spectrum of α,β-unsaturated aldehydes in the presence of cofactors [132,133]. Examples are YqjM from *B. subtilis* [140], XenA from *P. putida*, KYE1 from *K. lactis*, and Yers-ER from *Y. bercovieri* [144], which exhibited versatile substrate specificity towards a set of α,β-unsaturated carbonyl compounds including t-CIN as shown by *in vitro* enzymatic assays. However, no enzymes able to transform α,β-unsaturated carbonyl compounds have been reported in *L. monocytogenes* so far.

In an attempt to generate novel insights into the antibacterial mechanisms of t-CIN, *L. monocytogenes* Scott A was subjected to experimental evolution to develop increased tolerance to t-CIN, and the mutations responsible for this increased tolerance were identified in this work. The results led to the identification of an ene reductase of the short-chain dehydrogenases/reductases (SDRs) superfamily that reduces t-CIN and several other α,β-unsaturated aldehydes, thereby protecting *L. monocytogenes* against the toxic activity of these compounds.

4.3 Material and methods

4.3.1 Bacterial strains and growth conditions

Bacterial strains and plasmids used in this work are listed in Table 4.1. *L. monocytogenes* strains were grown at 30°C in Brain Heart Infusion (Oxoid, Hampshire, UK)

medium, while *E. coli* and *B. subtilis* strains were grown in Luria-Bertani (LB; 10 g/L tryptone, 5 g/L yeast extract, 5 g/L NaCl) medium at 37°C. Agar was added at 1.5% for solid media. Media were supplemented with kanamycin (Km; AppliChem, Darmstadt, Germany), erythromycin (Ery; Acros Organics, New Jersey, USA), ampicillin (Amp; Thermo Fisher Scientific), and anhydrotetracycline (ATc; CaymanChem, Michigan, USA) when appropriate. Antimicrobials used in this work include *trans*-cinnamaldehyde (Acros Organics), *trans*-2-hexenal (Sigma Aldrich, Saint Louis, MO, USA), and 4-hydroxy-2-nonenal (Abcam, Cambridge, GB).

4.3.2 Isolation of t-CIN resistant strains by experimental evolution

Experimental evolution of WT *L. monocytogenes* for increased t-CIN tolerance was performed using six independent parallel lineages according to the selection scheme shown in Fig. 4.1. Briefly, six colonies were grown overnight in 4 mL BHI broth with shaking and then diluted 1000-fold in fresh BHI broth with 3 or 4 mM t-CIN. An additional culture with only the equivalent amount of the solvent (ethanol without t-CIN) was included as the control without selection pressure. Two hundred µL portions of the diluted cultures were transferred into a 96-well microplate, covered with a foil (Greiner Bio-One EASYseal™ Adhesive Microplate Sealer, Thermo Fisher Scientific), and incubated at 30°C with continuous shaking (250 rpm). When the turbidity reached the level of a stationary phase culture, cultures were again diluted 1:1000 in the same (but fresh) medium in a new microplate for another round of growth, and this cycle was repeated nine times with a t-CIN concentration of 3 mM or seven times with a t-CIN concentration of 4 mM. After each round, a portion of the cultures was diluted 10^5-fold and 100 µL was spread on BHI agar. A 6-mm sterile Whatman® filter paper disc impregnated with 10 µL pure t-CIN was then placed in the center of the agar plates. After incubation at 30°C for two days, 16 colonies that had formed near the edge of the inhibition halo were picked and streaked on BHI agar. The resistance of one colony from each of the 16 isolates against t-CIN was evaluated by a microplate growth assay (see below). The evolution experiment was continued until isolates with enhanced t-CIN resistance emerged. A selection of these isolates from independent cultures was sent for whole genome sequencing to analyze the presence of mutations.

Table 4.4 Strains and plasmids in this work.

Bacterial species	Designation in this work	Description	Reference
L. monocytogenes	*WT*	wild-type strain Scott A, obtained from ILSI strain collection	[166]
	WT/pIMK2	WT with pIMK2 integrated, Km^R	This work
	Δ*yhfK*	WT with in-frame deletion of *yhfK*	This work
	Δ*yhfK/pIMK2*	Δ*yhfK* with pIMK2 integrated, Km^R	This work
	Δ*yhfK/pIMK2::yhfK*	Δ*yhfK* with *pIMK2::yhfK* integrated, Km^R	This work
	Δ*yhfK/pIMK2::yhfK* (M1)	Δ*yhfK* with *pIMK2::yhfK* (M1) integrated, Km^R	This work
	Δ*yhfK/pIMK2::yhfK* (M2)	Δ*yhfK* with *pIMK2::yhfK* (M2) integrated, Km^R	This work
	Δ*yhfK/pIMK2::yhfK* (M3)	Δ*yhfK* with *pIMK2::yhfK* (M3) integrated, Km^R	This work
	Δ*yhfK/pIMK2::yhfK* (M4)	Δ*yhfK* with *pIMK2::yhfK* (M4) integrated, Km^R	This work
E. coli	S17-1 λpir	Donor for plasmid conjugation	[168]
	DH5-α	Host strain for plasmid constructs	[167]
B. subtilis	WT	Strain 168, obtained from BGSC	
	BKK 10260 or *ΔyhfK::km*	WT with *yhfK* replaced by a kanamycin resistance cassette, Km^R	[262]
	BKE 10260 or *ΔyhfK::erm*	WT with *yhfK* replaced by an erythromycin resistance cassette, Em^R	[262]
Plasmids	Description		Reference
pIMK2	Site-specific listerial integrative vector, Phelp promoter for constitutive overexpression, 6.2 kb, Km^R		[170]
pIMK2::yhfK	pIMK2 with *yhfK* gene from Scott A under control of pHelp promotor		This work
pHoss1	Plasmid for gene deletion in *L. monocytogenes*, negative selection based on *secY* antisense RNA, 8995 bp, Amp^R, Ery^R		[263]
pHoss::yhfK-LR	pHoss1 with 1 kb flanking fragments upstream and downstream of *yhfK* inserted		This work

* BGSC: Bacillus Genetic Stock Centre (http://www.bgsc.org/).

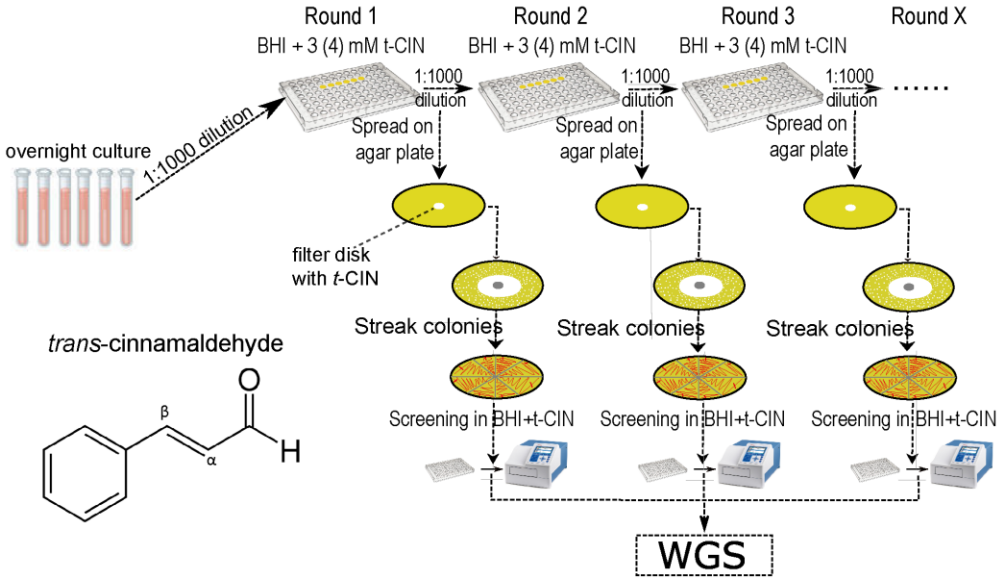

Figure 4.1 Selection scheme of the experimental evolution for increased t-CIN tolerance in *L. monocytogenes* Scott A. Isolates with enhanced t-CIN tolerance emerged in seven independent lineages with t-CIN supplementation after nine (in 3 mM t-CIN) or seven (in 4 mM t-CIN) or more rounds of subculture, but not in control cultures without t-CIN.

4.3.3 Whole-genome sequencing

Genomic DNA was extracted from overnight cultures in BHI at 30°C with the GeneJET Genomic DNA purification kit (Thermo Fisher Scientific). The quality and concentration of genomic DNA were quantified by gel electrophoresis and spectrophotometric NanoDrop™ and Qubit (Thermo Fisher Scientific) analysis. Paired-end libraries were constructed with the NEBNext Ultra DNA Library Prep Kit (NEB, Ipswich, Massachusetts, USA) and sequenced at VIB Nucleomics Core (Leuven, Belgium) with an Illumina MiSeq sequencer (Illumina, San Diego, California, USA). Sequence assembly and analysis was done with CLC Genomic Workbench software (QIAGEN, Hilden, Germany) to identify mutations acquired in evolved strains compared to the parental strain, and these mutations were subsequently verified by PCR and Sanger sequencing (Macrogen Europe, Amsterdam, Netherlands).

4.3.4 Deletion and genetic complementation of *yhfK*

The pHoss1 plasmid was utilized to generate a markerless in-frame deletion mutant of *yhfK* (NCBI accession number: CM001159, locus tag: LMOSA_3600) in *L.*

monocytogenes Scott A as described [263]. First, approximately 1 kb fragments from the upstream and downstream of *yhfK* were amplified separately with the yhfK-KO-A/B and yhfK-KO-C/D primer pairs, respectively (Table 4.2). The purified products were merged by overlapping extension PCR with primers yhfK-KO-A and yhfK-KO-D, and the resulting ~2 kb fragment and pHoss1 were then digested with BspHI/PstI and NcoI/PstI restriction enzymes, respectively, ligated, and transformed into *E. coli* DH5α, and the construct was verified by PCR and Sanger sequencing with pHO-CK-F/pHO-CK-R primers. The plasmid was subsequently electroporated into *L. monocytogenes* ScottA using the procedure of [170], and purified clones were then restreaked three successive times on BHI agar with 10 μg/ml Ery at 42°C to enforce plasmid integration, and then passed two times overnight in BHI broth without Ery at 30°C. Reversal of plasmid integration was then enforced by spreading a diluted culture on BHI agar plates with 2 μg/mL ATc to induce the *secY* antisense RNA counterselection system of pHoss1. Clones in which *yhfK* was successfully deleted were identified by colony PCR with yhfK-KO-A and yhfK-KO-D primers and Sanger sequencing.

For genetic complementation of *ΔyhfK* mutant, WT and evolved *yhfK* alleles were amplified using the yhfK_BspHI/yhfK_SalI primer pair (Table 4.2), the products were cleaved with BspHI and SalI and cloned into the integrational pIMK2 plasmid opened with NcoI and SalI, and introduced in the *L. monocytogenes ΔyhfK* mutant by conjugation from *E. coli* S17-1 λpir. Successful integration was confirmed via PCR with primer yhfK_BspHI and NC16(II) (Table 4.2) (which anneals near, and points towards, the chromosomal plasmid integration site) and Sanger sequencing with primers pIMK_FW and pIMK_REV, which point towards the *yhfK* gene from both sides of the pIMK2 cloning site. The complemented strain was designated *ΔyhfK /pIMK2::yhfK*. WT and *ΔyhfK L. monocytogenes* strains carrying an empty integrated pIMK2 plasmid were constructed in a similar way to serve as controls.

Table 4.5 Primers used in this work.

Primer	Sequence (5' – 3')*	Reference
yhfK_BspHI	ATATATTCATGAATGTACTCGTAATTGGCGCAAA	This work
yhfK_SalI	ATATATGTCGACATGAGCGCGTAATTTGGCTCAT	This work
yhfK-KO-A	ATATGGTACCCATAGGGAAATTACGAACTAG	This work
yhfK-KO-B	ATTCATTGCTAATCTCCTCCTA	This work
yhfK-KO-C	TAGGAGGAGATTAGCAATGAATGACACACCCATTAA ACATTT	This work
yhfK-KO-D	ATATCTGCAGCTGGTAAGGTTGAAAGACAA	This work
pIMK_REV	CCTATCACCTCAAATGGTTCG	[17]
pIMK_FW	GAGTCAGTGAGCGAGGAAGC	[17]
NC16(II)	GTCAAAACATACGCTCTTATCGATTC	This work
pHO-CK-F	ACGATTGATGCAGTGATGTAGG	This work
pHO-CK-R	CGGTCCAATGATCGAAGTTAGG	This work

*Restriction sites are underlined: NcoI (CCATGG), SalI (GTCGAC), BspHI (TCATGA) and PstI (CTGCAG), NdeI (CATATG), XhoI (CTCGAG).

4.3.5 Growth assays

Growth curves were established with an automated microplate reader (Multiskan Ascent® or Multiskan™ FC, Thermo Fisher Scientific). Briefly, overnight cultures were adjusted to the same OD_{600} value in each experiment, diluted 1000-fold in appropriately supplemented BHI broth, and 200 µL aliquots were transferred into a 96-well microplate, which was sealed with a cover foil and incubated at 30°C in an automated microplate reader with shaking at 960 rpm and reading of OD_{600} every 15 or 30 min. The Excel add-in package DMFit (Quadram Institute Bioscience, Norwich, United Kingdom) was used to determine the maximum growth rate (μ_{max}), the lag phase time (λ), and the maximal OD (OD_{max}) value at stationary phase through the Baranyi and Roberts model [169].

4.3.6 Analysis of t-CIN and its metabolites

Headspace solid phase micro-extraction gas chromatography mass spectrometry (HS-SPME-GC-MS) analysis was used to monitor the concentrations of t-CIN and its metabolites in bacterial cultures following the procedure described previously with minor modifications [17]. First, overnight cultures adjusted to the same OD_{600} were 1000-fold diluted in 70 mL fresh BHI broth with 1 mM t-CIN in 250 mL glass flasks with caps tightly screwed to avoid evaporation of the compounds. An uninoculated flask was included as a control. Flasks were

incubated at 30°C with continuously shaking (250 rpm) and 2 mL samples were taken every 3 h. A small portion was used to determine a plate count, and the supernatant obtained after clearing the remainder of the sample by centrifugation (6000 rpm, 5 min) was flush frozen with liquid nitrogen and stored at -80°C. Immediately before the GC-MS analysis, 1 ml saturated NaCl solution, 100 µl 0.01 mM ethyl benzoate (internal standard) (≥ 99%, Sigma Aldrich), and 1 mL unfrozen sample were pipetted into a 10 mL amber glass vial, that was screw-capped with a PTFE/silicon septum seal and additionally sealed with parafilm. The quantification of t-CIN concentration by HS-SPME-GC-MS was conducted as described in [17] with the same setup and parameters. The presence of t-CIN, the degradation products, and ethyl benzoate in the deconvoluted mass spectrum were recognized with the NIST 14 Mass Spectral Library and NIST Mass Spectral Search Program Version 2.2 (National Institute of Standards and technology, Gaithersburg, MD, USA). The MS ions listed in the Table S4.1 were monitored for the quantification and qualification of t-CIN, ethyl benzoate, and t-CIN degradation products. Every sample was analyzed duplicately (technical repetitions).

4.3.7 Survival assay of *L. monocytogenes* in the presence of 4-hydroxy-2-nonenal

Overnight cultures were diluted to OD_{600} ~ 1, washed twice, resuspended and diluted 1:1000 in 10 mM PPB pH 7.0 in PCR tubes, and 4-HNE solution (10 mM in PPB) was added to a final concentration of 2 mM. A control cell suspension to which the equivalent amount of sterile PPB (without 4-HNE) was added was included. After incubation at 30°C for 6 h, the cell suspensions were serially diluted and plated on BHI plates to count the survivors.

4.3.8 Phylogenetic analysis of YhfK homologs

The NCBI (National Centre for Biotechnology Information database) BLASTP algorithm was used to search the amino acid sequences using YhfK from *L. monocytogenes* Scott A as the query. Only hits in prokaryotes that are listed in KEGG (Kyoto Encyclopedia of Genes and Genomes) Organisms database are retrieved. Sequences with amino acid sequence identity ≥ 30% over at least 90% of the entire sequence and having an e-value ≤ $1e^{-10}$ were aligned with MUSCLE [224] and visualized with CLC Genomic Workbench (QIAGEN). A phylogenic tree was then constructed in CLC Genomic Workbench using the Neighbour-joining approach with 300 bootstrap replicates with. For a simplified visualization, the phylogeny tree only displays 104 representative sequences (Table S4.2) with higher

identity value from different genus and species. Finally, the constructed phylogenetic tree was edited and annotated with the Interactive Tree of Life (https://itol.embl.de/) web server tool.

4.3.9 Statistical analysis

Data from the growth assay and GC-MS experiment are presented as means ± standard deviation (SD) from three independent cultures (biological replicates) for each strain. The significance of mean differences was calculated by the Tukey's honestly significant difference (Tukey's HSD) test for growth parameters (λ, μmax, and OD_{max}) or Student's t-test (two-tailed) for the survival assay in the presence of 4-HNE using GraphPad PRISM 7.0 (GraphPad, San Diego, CA, USA). *p* values < 0.05 were considered statistically significant.

4.4 Results

4.4.1 Evolution of *L. monocytogenes* for increased t-CIN resistance selects for YhfK variant proteins

After being sub-cultured for nine rounds in 3 mM t-CIN or seven rounds in 4 mM t-CIN, mutants with significantly elevated t-CIN resistance appeared in seven independent lineages (Fig. 4.2), while this was not the case in the control lineages without t-CIN. Four evolved mutants were selected and further characterized. Their lag phase in BHI with 3 mM t-CIN was reduced to 62 - 72% of that of the WT strain, while their exponential growth rate and OD_{max} were unaffected (with the exception of a slightly lower OD_{max} for mutant M3 (Fig. 4.2). All the mutants showed WT growth in the absence of t-CIN. Interestingly, WGS analysis revealed that the mutants had each acquired only a single base change, in a different position in the coding region of the *yhfK* gene (NCBI locus CRH05_RS12830), resulting in four single amino acid variants of YhfK (Fig. 4.2). YhfK is predicted to be an oxidoreductase of the very large and diverse SDR enzyme family.

Further evidence implicating YhfK in t-CIN tolerance was obtained when *yhfK* was deleted, since this resulted in an almost doubling of the lag phase (50 h for Δ*yhfK* versus 28 h for WT strain) in the presence of 3 mM t-CIN, while no growth attenuation was noted in absence of t-CIN (Fig. 4.3). Complementation of the Δ*yhfK* strain with the WT *yhfK* gene (strain Δ*yhfK/pIMK2::yhfK*) again reduced the lag phase, making it even 3 h shorter than that

of the WT, possibly because the gene is under control of a strong constitutive promotor in pIMK2 [170]. Complementation of Δ*yhfK* with each of the four mutant *yhfK* genes reduced the lag times even further, by 7-8 h relative to WT, in line with their ability to confer t-CIN resistance in the evolved mutants. Complementation with neither of the *yhfK* alleles affected the growth of Δ*yhfK* strain in BHI (Fig. S4.1). However, very little is known about the function of YhfK or its homologs in bacteria except that it is part of Sigma B regulon in *L. monocytogenes* [264–266]. In addition there are studies indicating that the gene was induced in acidic conditions and its deletion conferred moderate sensitivity of *L. monocytogenes* to severe acid shock (pH 2.5) [264,267]. Here, we compared the growth of the WT and Δ*yhfK* strains in BHI acidified with HCl to pH = 4.0, but no difference was observed (Fig. S4.2), suggesting that YhfK plays only a role in lethal acid shock.

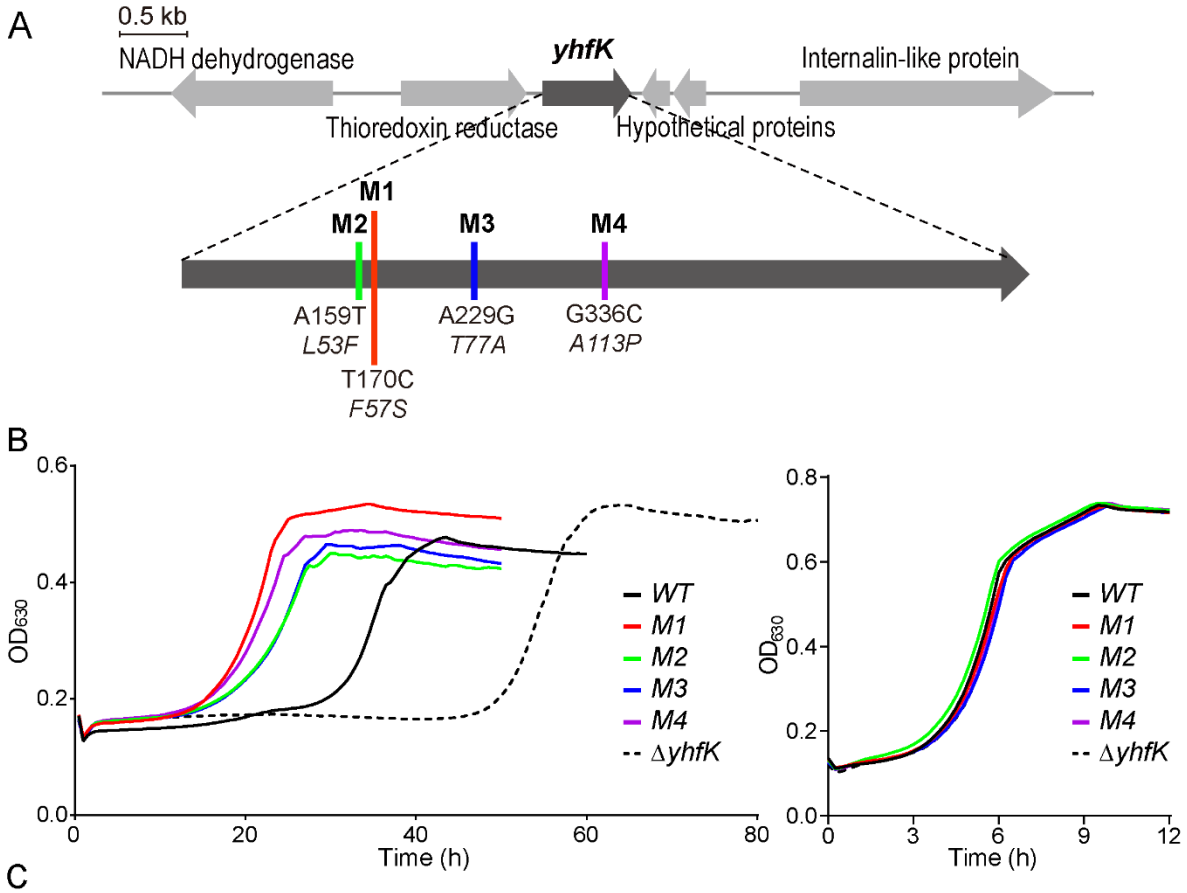

C

Strain	*WT*	*M1*	*M2*	*M3*	*M4*	*ΔyhfK*
Medium	BHI + 3 mM t-CIN					
lag phase (h)	23.2 ± 0.6^{A}	14.3 ± 1.0^{B}	16.2 ± 0.3^{C,D,E}	16.7 ± 0.4^{D}	14.9 ± 0.5^{B,E}	45.1 ± 0.5^{F}
OD_{max}	0.62 ± 0.01^{A}	0.64 ± 0.02^{A}	0.60 ± 0.03^{A,B}	0.55 ± 0.03^{B}	0.59 ± 0.03^{A,B}	0.61 ± 0.01^{A,B}
μ_{max} (/h)	0.034 ± 0.010^{A}	0.052 ± 0.009^{A}	0.034 ± 0.012^{A}	0.037 ± 0.014^{A}	0.043 ± 0.004^{A}	0.048 ± 0.012^{A}
Medium	BHI					
lag phase (h)	3.8 ± 0.0^{A}	3.9 ± 0.2^{A}	3.6 ± 0.5^{A}	4.0 ± 0.1^{A}	4.0 ± 0.1^{A}	4.0 ± 0.0^{A}
OD_{max}	0.71 ± 0.01^{A}	0.71 ± 0.01^{A}	0.72 ± 0.01^{A}	0.71 ± 0.01^{A}	0.72 ± 0.00^{A}	0.71 ± 0.00^{A}
μ_{max} (/h)	0.180 ± 0.003^{A}	0.180 ± 0.002^{A}	0.176 ± 0.002^{A}	0.175 ± 0.003^{A}	0.183 ± 0.004^{A}	0.181 ± 0.004^{A}

Figure 4.2 *L. monocytogenes* Scott A mutants with increased t-CIN resistance have mutations in *yhfK* resulting in single amino acid changes. (**A**) *yhfK g*ene context and mutations in each of four selected mutants (M1, M2, M3, M4). Colored vertical lines show positions of the mutations, with specific base changes (straight font type) and corresponding amino acid changes (italic) specified under each line. (**B**) Growth curves of WT strain and t-CIN resistant mutants in BHI with (left) and without (right) 3 mM t-CIN (**C**) Growth parameters (λ, μmax, and OD_{max}), represented as mean ± SD (n = 3). Values followed by a common letter are not significantly different at the 5% level of significance.

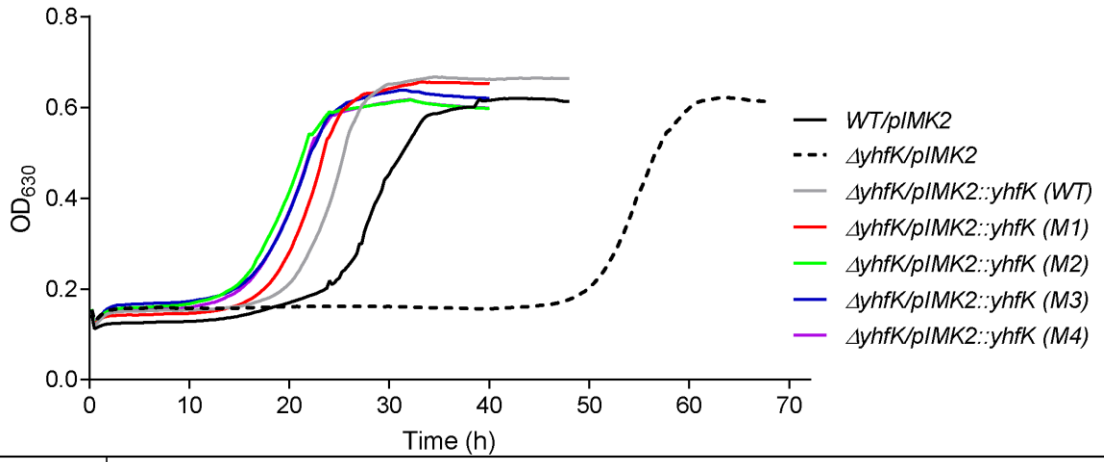

Strain	*WT/pIMK2*	*ΔyhfK/pIMK2*	*ΔyhfK/pIMK2::yhfK (WT)*	*ΔyhfK/pIMK2::yhfK (M1)*	*ΔyhfK/pIMK2::yhfK (M2)*	*ΔyhfK/pIMK2::yhfK (M3)*	*ΔyhfK/pIMK2::yhfK (M4)*
lag phase (h)	23.2 ± 0.6^{A}	50.8 ± 0.5^{B}	19.4 ± 0.6^{C}	16.2 ± 0.2^{D,F,G}	14.7 ± 0.1^{E}	15.0 ± 0.5^{E,F}	15.4 ± 0.1^{E,G}
ODmax	0.62 ± 0.02^{A}	0.62 ± 0.01^{A}	0.66 ± 0.02^{A}	0.65 ± 0.03^{A}	0.59 ± 0.01^{A}	0.64 ± 0.01^{A}	0.61 ± 0.00^{A}
μmax (/h)	0.045 ± 0.014^{A}	0.054 ± 0.001^{A}	0.058 ± 0.006^{A}	0.036 ± 0.004^{A}	0.051 ± 0.000^{A}	0.047 ± 0.010^{A}	0.053 ± 0.010^{A}

Figure 4.3 Complementation analysis of *L. monocytogenes* Δ*yhfK* with WT or mutant *yhfK* alleles, based on growth curves recorded at 30ºC in BHI with 3 mM t-CIN. Control strains had an empty pIMK2 plasmid. Standard deviations are not shown in the graphs for clarity. The growth parameters (λ, μ_{max}, and OD_{max}) are represented in the table as mean ± SD (n = 3). Values followed by a common letter are not significantly different at the 5% level of significance.

4.4.2 YhfK provides tolerance to multiple α,β-unsaturated aldehydes but not to other thiol-reactive electrophiles

The evolved t-CIN resistant strains and the Δ*yhfK* deletion strain and its various complemented derivatives were used to assess the role of YhfK in tolerance of *L. monocytogenes* to α,β-unsaturated aldehydes other than t-CIN, and to thiol-reactive compounds with other electrophilic functional groups (Fig. 4.4, Fig. 4.5, and Fig. S4.3). Six mM t-HEX induced a considerable lag phase extension in the Δ*yhfK* strain (42 h) relative to WT (15 h) and the complemented strain *ΔyhfK/pIMK2::yhfK* (WT) (16 h) (Fig. 4.4B). Surprisingly, the evolved t-CIN resistant strains were more sensitive to t-HEX than the WT strain, with lag times lengthened by 10 - 18 h (Fig. 4.4A), and we speculate that the opposite effect of the amino acid replacement mutations on tolerance to t-CIN and t-HEX may reflect an altered YhfK substrate specificity. The Δ*yhfK* strain also showed increased sensitivity, again reflected by an extended lag phase, to citral (Fig. S4.3). A fourth α,β-unsaturated aldehyde that was tested is 4-HNE, a degradation product of polyunsaturated fatty acids that are formed during the oxidative burst as part of the cellular immunity [268,269]. Since the

compound is bactericidal at low concentrations and may play a role in pathogen elimination during infection, we tested its activity in a cell inactivation assay rather than a growth inhibition assay (Fig. 4.5). Upon incubation with 2 mM 4-HNE for 6 h, survival was only 25% for the Δ*yhfK* strain compared to 40% and 53% for the WT and the complemented strains, respectively. Finally, allyl isothiocyanate and diamide, two antimicrobials that are also thiol-reactive but that lack an α,β-unsaturated aldehyde moiety, were also tested but did not have a different activity against the Δ*yhfK* and the WT strain (Fig. S4.3). Overall, the above findings indicate a role of YhfK in the tolerance of *L. monocytogenes* to antimicrobial α,β-unsaturated aldehydes.

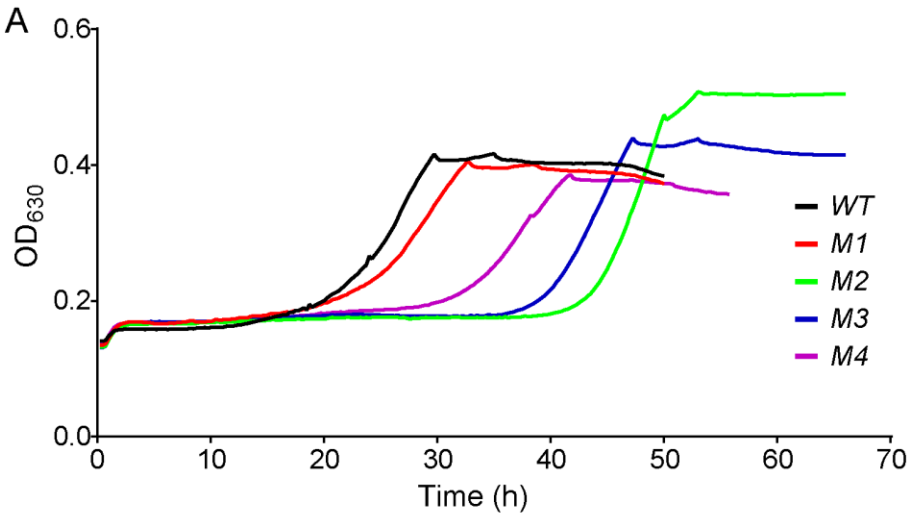

Strain	*WT*	*M1*	*M2*	*M3*	*M4*
lag phase (h)	19.0 ± 2.9^{A}	17.9 ± 3.4^{A}	37.2 ± 6.5^{B}	34.0 ± 7.1^{B}	29.1 ± 1.9^{A,B}
ODmax	0.41 ± 0.01^{A}	0.35 ± 0.01^{A}	0.40 ± 0.01^{A}	0.42 ± 0.05^{A}	0.36 ± 0.05^{A}
μmax (/h)	0.024 ± 0.004^{A}	0.017 ± 0.003^{A}	0.028 ± 0.010^{A}	0.029 ± 0.006^{A}	0.018 ± 0.001^{A}

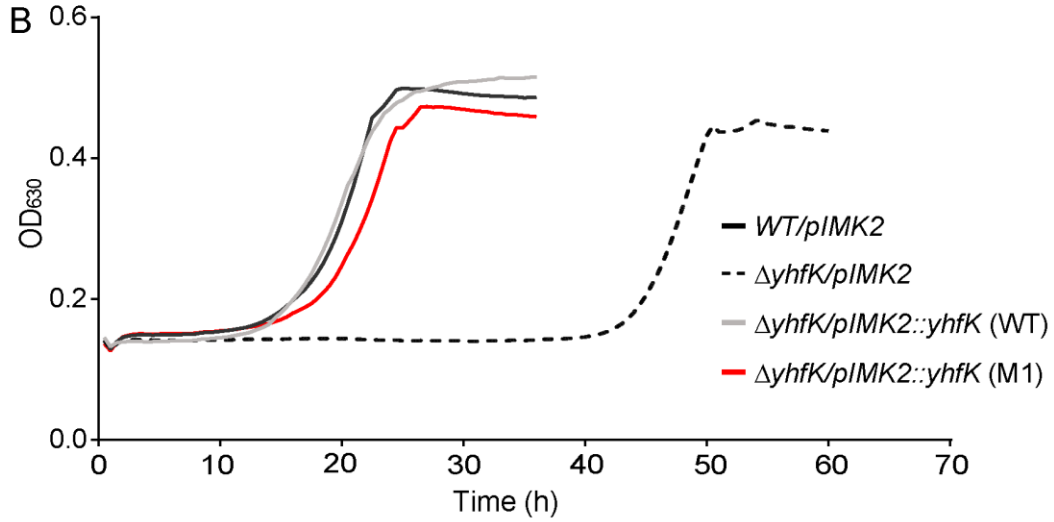

Strain	*WT/pIMK2*	*ΔyhfK/pIMK2*	*ΔyhfK/pIMK2::yhfK (WT)*	*ΔyhfK/pIMK2::yhfK (M1)*
lag phase (h)	15.0 ± 1.1^{A}	42.7 ± 1.1^{B}	15.8 ± 0.2^{A}	16.9 ± 0.6^{A}
ODmax	0.51 ± 0.02^{A}	0.45 ± 0.00^{B}	0.51 ± 0.00^{A}	0.48 ± 0.02^{A}
μmax (/h)	0.042 ± 0.012^{A}	0.041± 0.010^{A}	0.047 ± 0.000^{A}	0.042 ± 0.011^{A}

Figure 4.4 Growth curves showing the involvement of YhfK in t-HEX tolerance of *L. monocytogenes.* (**A**) Comparison of WT strain with different t-CIN-tolerant evolved mutants. (**B**) Comparison of WT /pIMK2, Δ*yhfK/pIMK2* and Δ*yhfK* complemented with different variants of the YhfK protein. Cultures were grown in BHI broth with 6 mM t-HEX at 30ºC. The curve represents the mean value of measurements of three independent cultures. The growth parameters (λ, μmax, and ODmax) are represented as mean ± SD (n = 3). Values followed by a common letter are not significantly different at the 5% level.

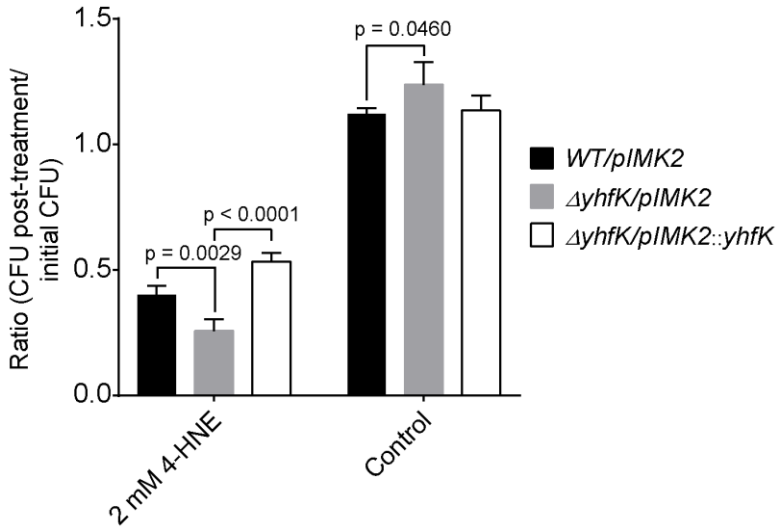

Figure 4.5 Survival assay of *WT/pIMK2, ΔyhfK/pIMK2 and ΔyhfK/pIMK2::yhfK* treated with 2 mM 4-HNE at 30°C for 6 h. The y-axis represents the fraction of survivors after 6 h. The data are represented as mean ± SD (*n* = 3). P-values from a two-tailed Student's t-test are indicated.

4.4.4 YhfK reduces the C=C double bond in t-CIN

Since YhfK is a predicted oxidoreductase of the SDR family, and given its role in the tolerance to α,β-unsaturated aldehydes, we speculated that it could possibly catalyze the reduction of either the ene or the carbonyl group of t-CIN. To investigate this, the degradation of t-CIN and the formation of the three possible reduction products were analyzed using GC-MS in cultures of *WT/pIMK2*, Δ*yhfK/pIMK2* and Δ*yhfK/pIMK2::yhfK* strains grown with 1 mM t-CIN (Fig. 4.6). Analysis of a sterile medium control indicated that the concentration of t-CIN declined to about 0.7 mM in the first six hours, and then stayed more or less constant until the end of the measurements (24 h). Since the same initial decline occurred in all the cultures, it is probably the result of reactions of t-CIN with nucleophiles in BHI broth. Similar losses of t-CIN during culture preparation and the first hours of incubation have been reported previously [7]. In the culture of the WT strain (*WT/pIMK2*), the t-CIN concentration started to drop further at the end of the exponential growth phase (18 h), to reach 0.28 mM in the early stationary phase (24 h). At the same time, the three t-CIN reduction products appear in the culture, suggesting that *L. monocytogenes* can reduce both the aldehyde and the ene group of t-CIN. It should be noted that the reduction products are reported as relative concentrations because we did not make standard curves for these compounds. Therefore, a quantitative analysis of the formation of the reduction products is not possible. The Δ*yhfK/pIMK2* strain also degraded t-CIN during the transition from exponential to stationary phase, but slower

than *WT/pIMK2*, resulting in a final concentration of 0.43 mM after 24 h. The most remarkable difference with the WT strain, however, was that the deletion strain only produced 3-phenyl-2-propenol, but not the two other reduction products, indicating that it could still reduce the aldehyde group but not the ene group. The complemented deletion strain (Δ*yhfK/pIMK2::yhfK*), finally, degraded t-CIN earlier and more rapidly than both other strains, and produced the three reduction products, but in different relative amounts than the WT. 3-phenylpropanal is already detected at 6 h and peaks at 12h, at a much higher level than in the WT culture. Later it declined to an almost undetectable level at 24 h, while 3-phenylpropanol started to appear and reached a maximal level at 24 h. 3-phenyl-2-propenol was also formed, but at clearly lower levels than in the WT strain. The higher production of 3-phenylpropanal and lower production of 3-phenyl-2-propenol in the culture of the complemented strain compared to the WT can be explained by the strong expression of YhfK by the pIMK2 promotor. These data show that *L. monocytogenes* can metabolize t-CIN by a combination of ene reduction and aldehyde reduction without a strict order for both reactions. They also strongly indicate that YhfK is an ene-reductase that reduces the C=C double bond in t-CIN (Fig. 4.7).

The antimicrobial activity of the three t-CIN metabolites was also tested. Both alcohols showed no activity up to 50 mM (data not shown), while 3-phenylpropanal retained some activity but was less potent than t-CIN (Fig. S4.4, and comparison with Fig. 4.2 for t-CIN). Furthermore, the antimicrobial activity of 3-phenylpropanal was not affected by deletion or overexpression of YhfK. As a result, the sensitivity of the strains for t-CIN (as reflected by their growth curves in Fig. 4.6) correlated with their capacity to metabolize t-CIN. The fastest and most complete conversion of t-CIN was by the complemented strain, and this strain also showed the fastest growth in the presence of t-CIN. Conversely, the *yhfK* deletion strain had the slowest metabolism of t-CIN and also the slowest growth with t-CIN. The t-CIN metabolism and growth with t-CIN of the WT strain were intermediate. Taken together, these data suggest that a possible function of YhfK in *L. monocytogenes* is to detoxify t-CIN and other α,β-unsaturated aldehydes.

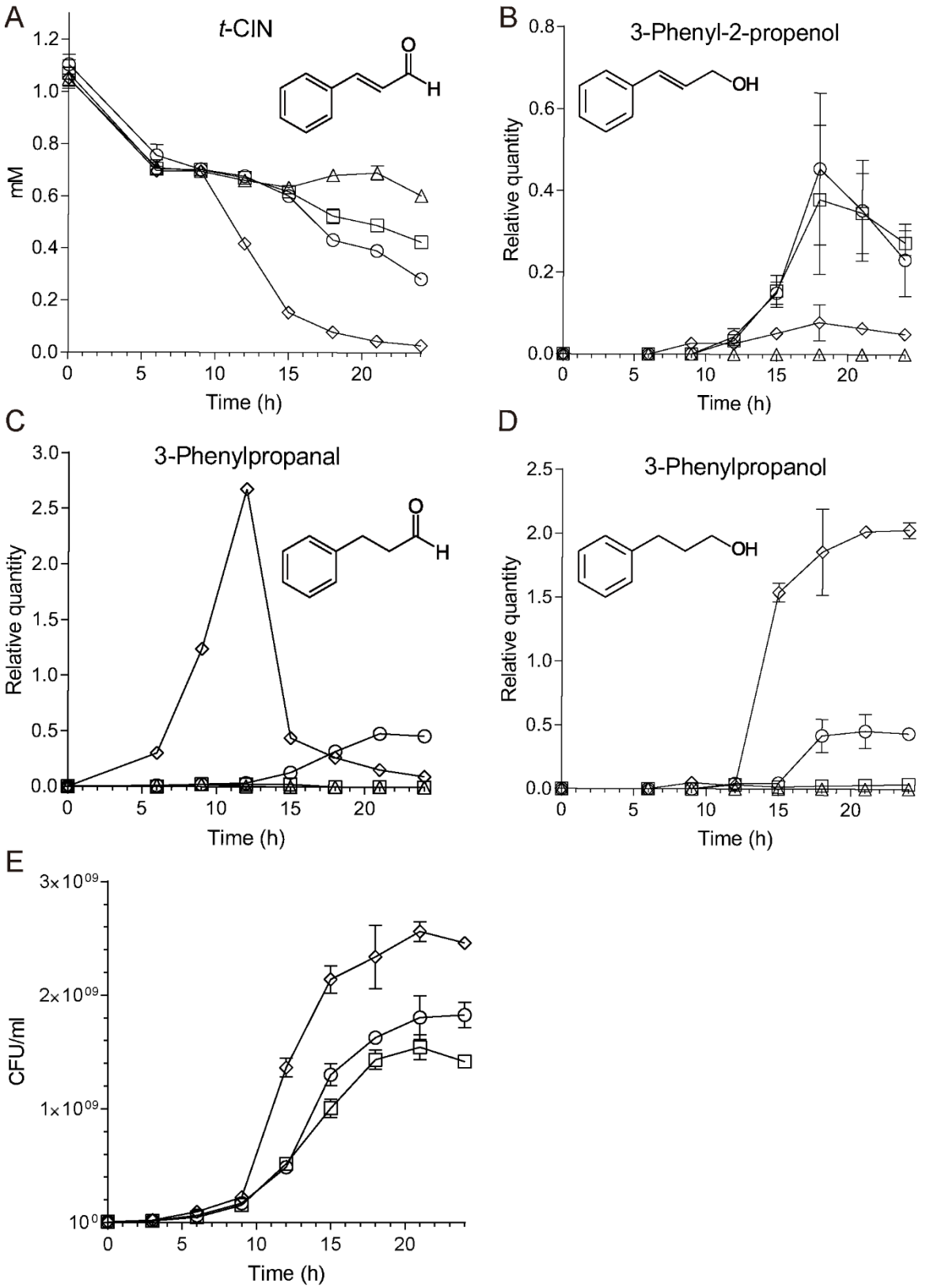

Figure 4.6 GC-MS analysis of t-CIN degradation in cultures of *L. monocytogenes WT/pIMK2* (⊖), Δ*yhfK/pIMK2* (⊟), Δ*yhfK/pIMK2::yhfK* (⊷) grown in BHI with 1 mM t-CIN at 30°C. Sterile BHI medium with 1 mM t-CIN was included as the control (⏃). (**A**) the concentration of t-CIN. (**B**)

relative concentration of 3-phenyl-2-propenol. (**C**) relative concentration of 3-phenylpropanal. (**D**) relative concentration of 3-phenylpropanol. (**E**) CFU enumeration. For plot B-D, Y-axis represents the ratio of the peak area of the corresponding t-CIN degradation product in the chromatogram to the peak area of the ethyl benzoate internal standard and should therefore be regarded as a relative concentration. All data represent the mean value of three independent cultures ± SD.

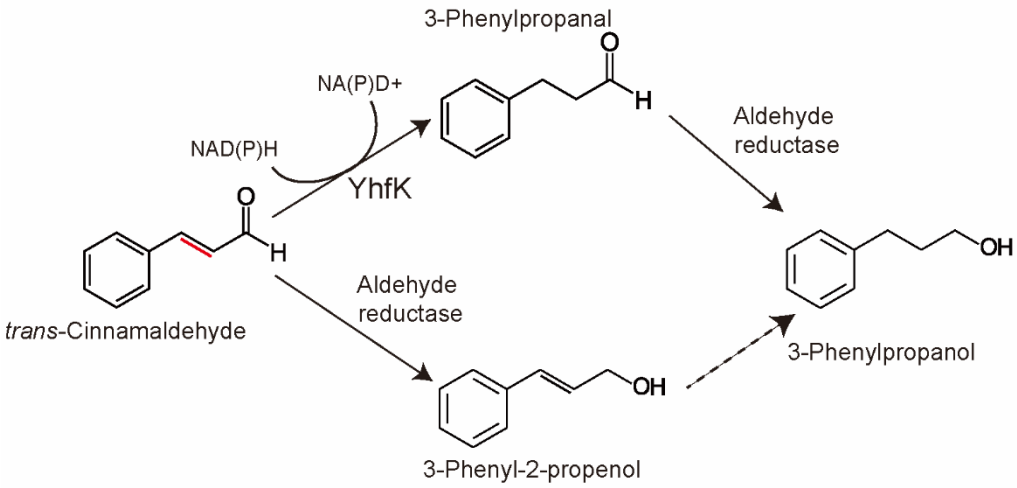

Figure 4.7 Proposed scheme of t-CIN metabolism in *L. monocytogenes*. YhfK is suggested to be an ene reductase converting t-CIN to 3-phenylpropanal. Since both 3-phenyl-2-propenol and 3-phenylpropanol are produced by WT *L. monocytogenes*, the organism must also have one or more aldehyde reductases.

4.4.5 YhfK homolog in *B. subtilis* also confers tolerance to t-CIN and t-HEX

B. subtilis has a putative homolog that shares 43% amino acid sequence identity with YhfK of *L. monocytogenes*, and like in *L. monocytogenes*, deletion of the *yhfK* gene strongly increased the sensitivity of *B. subtilis* to t-CIN and t-HEX (Fig. 4.8), thus suggesting that YhfK has a conserved function in both bacteria. Attenuated growth was exhibited by both mutant strains when incubating with t-CIN and t-HEX in comparison with the parental strain. In the presence of 3 mM t-CIN, both Δ*yhfK* strains failed to resume growth while their parental strain was still able to grow (Fig. 4.8). When grown in the medium supplemented with 2 mM t-HEX, only the growth of *B. subtilis* WT boomed after 12 h, while the mutant strains failed to proliferate (Fig. 4.8). On the contrary, no growth deviation was observed when they are grown in the absence of t-CIN and t-HEX. This evidence suggests that YhfK

in *B. subtilis* might also exhibit substrate specificity towards some α,β-unsaturated aldehydes, suggesting a conserved function of YhfK homologs in bacteria.

A

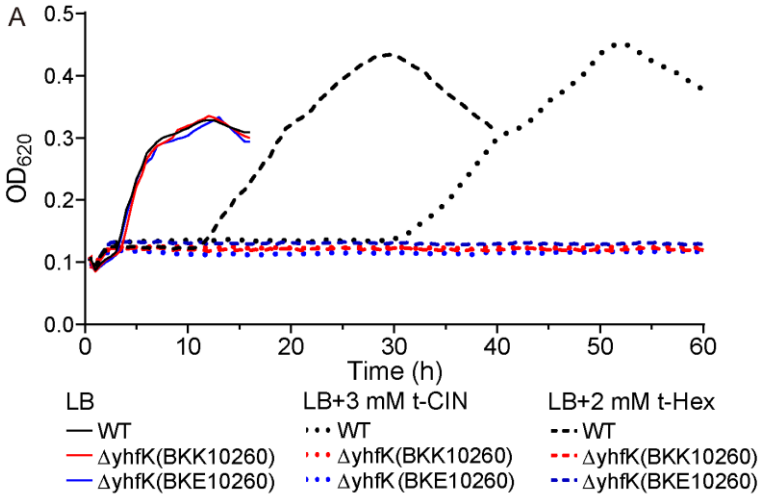

B

Strain	WT	BKK 10260	BKE 10260
Medium		LB	
lag phase (h)	2.1 ± 0.2^{A}	2.4 ± 0.1^{A}	2.1 ± 0.5^{A}
OD_{max}	0.32 ± 0.01^{A}	0.32 ± 0.01^{A}	0.33 ± 0.01^{A}
μ_{max} (/h)	0.061 ± 0.002^{A}	0.053 ± 0.002^{B}	0.064 ± 0.003^{A}
Medium		LB + 3 mM *t*-CIN	
lag phase (h)	36.1 ± 4.2	n.d.	n.d.
OD_{max}	0.46 ± 0.01	n.d.	n.d.
μ_{max} (/h)	0.020 ± 0.004	n.d.	n.d.
Medium		LB + 2 mM *t*-Hex	
lag phase (h)	12.1 ± 1.3	n.d.	n.d.
OD_{max}	0.42 ± 0.02	n.d.	n.d.
μ_{max} (/h)	0.023 ± 0.002	n.d.	n.d.

Figure 4.8 (**A**) Growth curves of *B. subtilis* 168 and its mutants ΔyhfK::Km and ΔyhfK::Erm in the absence and presence of t-CIN and t-HEX at 37°C. Each curve represents a single culture but is representative of three independent cultures. (**B**) Growth parameters (λ, μ_{max}, and OD_{max}) were calculated from the growth curves and represented as mean ± SD; $n = 3$. Values followed by a common letter are not significantly different at the 5% level.

4.5 Discussion

Like many other plant essential oil compounds, t-CIN and t-HEX have antimicrobial activity towards several foodborne pathogens including *L. monocytogenes*, and may therefore find application in natural food preservative systems [4,5]. In the present study, increased tolerance towards t-CIN was evolved in *L. monocytogenes* and shown to be associated with

single nucleotide variants of *yhfK*, a gene coding for a putative oxidoreductase of the SDR family with unknown function. Deletion of *yhfK* did not affect the normal growth of *L. monocytogenes*, but caused increased sensitivity to α,β-unsaturated aldehyde compounds, including t-CIN, t-HEX, citral, and 4-HNE. GC-MS analysis of culture supernatants indicated that YhfK is required for the reduction of t-CIN to 3-phenylpropanal, which is then further converted to 3-phenyl-1-pronanol, indicating that YhfK is a NAD(P)H-dependent ene reductase.

Interestingly, low concentrations of 3-phenyl-2-propenol were also detected in the culture supernatants of *L. monocytogenes* grown with t-CIN (Fig. 4.6B). This compound was in fact a major degradation product when *E. coli* O157:H7 was incubated with t-CIN [7]. Although these authors did not analyze 3-phenylpropanal, it can be deduced from their data that 3-phenylpropanal was either absent or produced at very low amounts [7]. Correspondingly, we could not find a YhfK homolog (identity ≥ 30%) in *E. coli* O157:H7 (data not shown). Two dehydrogenase/reductase enzymes, YqhD and DkgA, were speculated to possibly convert t-CIN to 3-phenyl-2-propenol in *E. coli* because transcriptional analysis showed the corresponding genes to be induced by t-CIN [7,11]. Furthermore, the inactivation of *yqhD* significantly increased the sensitivity of *E. coli* to t-CIN [11]. The purified YqhD of *E. coli* had been previously found to catalyze the reduction of a broad range of short-chain aldehydes, including acrolein, isobutyraldehyde, glycolaldehyde, butanaldehyde, malondialdehyde, and propanaldehyde, to the corresponding alcohols in an NADPH-dependent manner *in vitro* [126,127]. DkgA, on the other hand, is an aldo-keto reductase family enzyme using NADPH as the preferred cofactor and shows substrate specificity towards a variety of aldehydes or ketones such as methylglyoxal [128]. However, direct evidence showing that YqhD or DkgA are active on t-CIN or other α,β-unsaturated aldehydes is still lacking. A close homolog of *E. coli* O157:H7 YqhD, sharing a 57.47% identity (coverage: 99%, e-value: $2e^{-153}$) exists in *L. monocytogenes* Scott A (NCBI accession: EGJ25272). As for DkgA of *E. coli* O157:H7, four homologs (NCBI accession: EGJ26117.1 (e-value: $3e^{-68}$), EGJ25830.1 (e-value: $7e^{-72}$), EGJ26226.1 (e-value: $1e^{-80}$) and EGJ24325.1 (e-value: $2e^{-90}$)) exist in *L. monocytogenes* Scott A with identities ranging from 40.61% to 45.39% (coverage ≥ 93%). However, none of these homologs in *L. monocytogenes* have been characterized, and mutations in the corresponding genes were not found in our evolutionary experiments, so it remains unclear whether they play a role in the detoxification of t-CIN or other aldehydes. Several fungal species, including *A. ochraceus* [58] and *P. expansum* [60],

were reported to transform t-CIN to 3-phenyl-2-propenol as well, presumably by means of aldehyde reductase enzymes, suggesting that the conversion to 3-phenyl-2-propenol might be a common detoxification mechanism of t-CIN in many microbes. Versatile aldehyde reductase enzymes are widely distributed in virtually all organisms, and since some of them have a relaxed substrate selectivity they can be anticipated to detoxify exogenous aldehydes.

Deletion of *yhfK* also resulted in increased sensitivity to 4-HNE in *L. monocytogenes* (Fig. 4.5). 4-HNE is commonly generated during the oxidative deterioration of polyunsaturated fatty acids, together with some other α,β-unsaturated aldehydes including acrolein and 4-hydroxy-2-hexenal [268]. The α,β-unsaturated aldehyde of 4-HNE easily undergoes a Michael-type addition reaction with thiol and amino groups of proteins to generate protein adducts, and this reactivity is held responsible for the antibacterial activity [268,270,271]. A recent study found that two NADPH-dependent oxidoreductases, the flavin-dependent enone reductase Rha1 and the alcohol/quinone reductase Rha2, played pivotal roles in the resistance of *L. monocytogenes* against 4-HNE [269]. Recombinant Rha1 and Rha2 reduced the C=C double bond of 4-HNE, generating 4-hydroxynonanal in an NADPH-dependent manner. Against 4-hydroxy-2-hexenal, however, Rha1 and Rha2 exhibited no and only modest activity respectively [269], indicating a narrow substrate spectrum of both enzymes. Expression of both Rha1 and Rha2 was highly induced (238- and 180-fold respectively) in response to 640 µM of 4-HNE as revealed by the transcriptome analysis. Interestingly, *yhfK* was also found to be induced 19-fold in the same study, but its involvement in 4-HNE degradation was not investigated or suggested. Since our work shows that the absence of YhfK completely abolished the production of 3-phenylpropanal from t-CIN, it can be concluded neither Rha1 or Rha2, nor any other ene-reductases reduce t-CIN in *L. monocytogenes*. Rha1 and Rha2 were shown to be important for *L. monocytogenes* pathogenicity by neutralizing 4-HNE generated during the infection of the pathogen in mice and tissue culture [269]. Since our present work shows that YhfK also protects *L. monocytogenes* against 4-HNE, it would be worthwhile to investigate whether this enzyme also contributes to pathogenicity.

Microbial ‘ene-reductases’ acting on α,β-unsaturated carbonyl compounds commonly belong to the flavin-dependent OYEs, which are renowned for containing a non-covalently bound FMN cofactor [132,133]. These flavoenzymes catalyze the *trans*-hydrogenation of the C=C double bond of α,β-unsaturated carbonyl compounds through the

so-called reductive half-reaction, using NAD(P)H as the reductant of FMN [133,134]. YqjM of *B. subtilis*, one of the most intensively studied OYEs, exhibits activities towards an array of α,β-unsaturated aldehydes and ketones including t-CIN, t-HEX, and cyclohexenone [136,137,140]. An additional OYE from *B. subtilis* (YqiG) also showed considerable activity towards alpha-methyl cinnamaldehyde, citral, and cyclohexenone [141]. Unlike in *B. subtilis*, no OYEs in *L. monocytogenes* have been reported as far as we know, but BLASTP analysis identified two homologs of YqjM and YqiG in *L. monocytogenes* EGD-e, namely lmo2471 (NCBI accession: WP_003732493, identity: 63% and 30% for YqjM and YqiG respectively) and lmo0489 (NCBI accession: WP_010989492, identity: 35% and 33% for YqjM and YqiG respectively).

Several strains with increased t-CIN tolerance were obtained by experimental evolution, which all contained mutations in *yhfK* resulting in amino acid substitutions (L53F, F57S, T77A, A113P) (Fig. 4.2). Since we demonstrated that YhfK is an 'ene-reductase' that detoxifies t-CIN, it seems likely that the increased t-CIN tolerance of the evolved mutants stems from a higher t-CIN conversion rate by the variant YhfK proteins. Remarkably, the tolerance of the mutant strains towards t-HEX was unaltered or reduced (Fig. 4.4), suggesting unaltered ($YhfK_{F57S}$) or reduced ($YhfK_{L53F}$, $YhfK_{T77A,}$ and $YhfK_{A113P}$) t-HEX conversion rates by the corresponding YhfK variants. To understand how the amino acid substitutions affect the structure and catalytic function of YhfK, crystal structures of YhfK in complex with and without cofactors and substrates will be needed. Nevertheless, even without this detailed insight, our results imply the feasibility to improve the enzymatic activity of YhfK towards specific substrates by natural evolution or by rational mutagenesis. The increased sensitivity of a Δ*yhfK* mutant to not only t-CIN, but also t-HEX, citral, and 4-HNE, indicates that YhfK has a relatively relaxed substrate scope. Because of their ability to stereoselectively reduce activated C=C double bonds, several ene reductases, mostly OYEs, have been investigated for application in the biosynthesis of valuable and arduously amenable chemicals [133,272–274]. YhfK may represent an interesting new scaffold of the SDR superfamily for developing novel biocatalysts reducing α,β-unsaturated carbonyl compounds.

BLASTP analysis shows that YhfK-like enzymes are widely distributed in many phyla of Bacteria, although most homologs show only a low to moderate amino acid identity (30% to 53%) (Fig. 4.9A, Table S4.2). They are particularly abundant in the Firmicutes, more specifically in the Bacilli class to which also *L. monocytogenes* belongs, and for two Bacilli

members, the crystal structure has been determined: *Alkalihalobacillus halodurans* (PDB: 3E8X; identity: 50%; e-value: $6e^{-55}$) and *Lactococcus lactis* (PDB: 3DQP; identity: 31%; e-value, $3e^{-19}$). Both are members of the NADP(H)-dependent SDRs, and adopt the conserved SDR-typical Rossmann-fold architecture, featuring seven parallel stranded β-sheet with three α-helices fringed on both sides [275]. Phyre2 analysis of $YhfK_{L.\ mono}$ predicted high structural homology to the *A. halodurans* and *L. lactis* homologs. A sequence alignment of these three proteins is depicted in Fig. 4.9B. A pattern analysis [276] of YhfK from *A. halodurans*, *L. monocytogenes*, *B. subtilis* and *L. lactis* further classified them into the SDR_a5 (atypical SDR, subgroup 5) subgroup, which is hallmarked by the glycine-rich NAD(P)-binding motif, Gly-X-X-Gly-X-X-Gly, and the putative active site including the highly-conserved Tyr-X-X-X-Lys motif, an upstream Ser residue and a highly conserved Asp residue [275], and are highlighted in Fig. 4.9B. The cellular functions of most proteins in the SDR_a5 subgroup remain unexplored except for the anaerobilin reductase ChuY of *E. coli* [277,278] and the divinyl chlorophyllide a 8-vinyl-reductases in some plants and bacteria [279,280]. ChuY is an NADPH-dependent reductase catalyzing the reduction of anaerobilin, a linear tetrapyrrole produced by the ChuW-mediated breakdown of heme [278]. In addition, FMN can also be reduced by ChuY utilizing NADPH as a cofactor [277]. Aligning the crystal structure of $YhfK_{A.\ halodurans}$ against *E. coli* ChuY (PDB: 5FFQ) in complex with NADP using TM-align [281] suggests a high structural homology with RMSD values = 2.01 Å (188 amino acid residues were used for the superimposing), given the moderate sequence homology (identity, 31.47%) between them. Thus, it would be interesting to see whether YhfK in bacteria including *L. monocytogenes* also participates in heme homeostasis. Like in many Gram-positive bacteria, an IsdG-type protein (Lmo2213) was previously reported to degrade heme in *L. monocytogenes* [282].

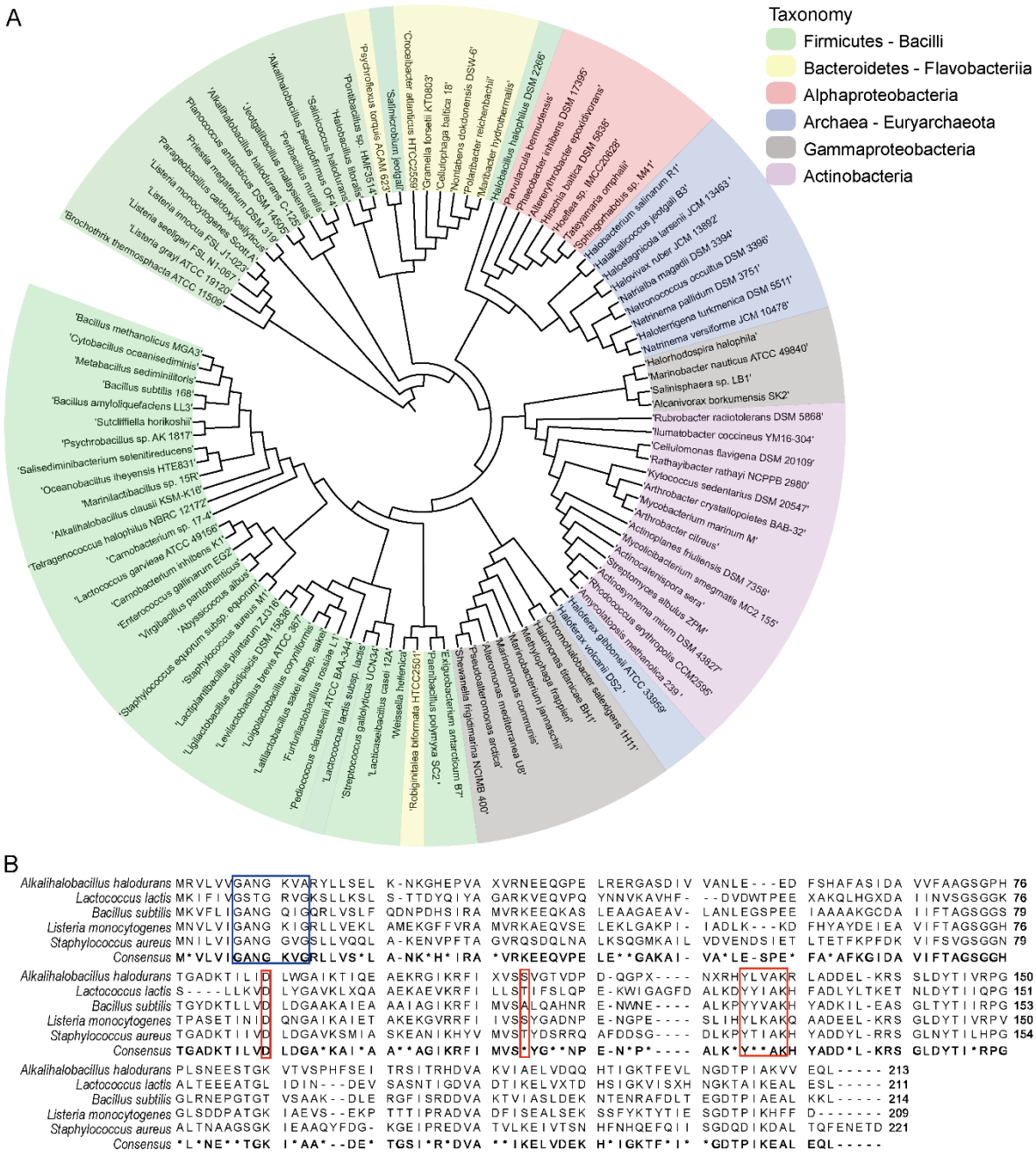

Figure 4.9 (**A**) Phylogenetic analysis of YhfK. The phylogenetic tree was constructed with YhfK homologs in bacteria (Firmicutes, Actinobacteria, Bacteroidetes, Alphaproteobacteria, Gammaproteobacteria) and archaeal microbes using the Neighbour-joining approach with 300 bootstrap replicates. The taxonomy of microbes is indicated with a different color. (**B**) Amino acids sequence alignment of YhfK homologs in *Alkalihalobacillus halodurans*, *Lactococcus lactis*, *L. monocytogenes*, *B. subtilis*, and *Staphylococcus aureus* with MUSCLE alignment program [224]. The position of the conserved atypical SDR domains [275], including a Gly-rich dinucleotide binding site motif (Gly-X-X-Gly-X-X-Gly) (blue box) and the active site motif including the Tyr-X-X-X-Lys

motif, the upstream Ser and Asp residues (red box), are marked. Non-conserved amino acids are indicated by asterisks. Accession numbers of amino acid sequences are listed in Table S4.2.

YhfK$_{L.\ mono}$ possesses the highly conserved active site typical of the majority of SDRs, with a triad of Ser110-Tyr126-Lys130 residues (numbering based on YhfK$_{L.mono}$) that is critical for the protonation and hydride transfer processes [275,283] (Fig. 4.9B). Tyr serves as the critical catalytic residue forming a hydrogen bond with both the substrate carbonyl-oxygen or nicotinamide ribose to provide/accept a hydride, whereas the adjacent Lys stabilizes the cofactor nicotinamide ribose through hydrogen bonds and lowers the Tyr hydroxyl pKa together with positively charged nicotinamide to promote the proton transfer. The Ser residue stabilizes the proton delivery network by forming a hydrogen bond with the carbonyl oxygen of the substrate. Besides the catalytic site, YhfK also contains several residues predicted to constitute an NADP(H)-binding domain, including a conserved Gly-rich segment (Gly7-Gly12) (participates in interactions with the adenine ribose and the central diphosphate group of NADP+), Arg33 and Ala51-Leu53 (adenine-binding moiety), Thr70-Ser73 (ribose-binding moiety), and Pro149-Leu152 (nicotinamide-binding moiety). Interestingly, Leu53 was found to be replaced by Phe in one of our t-CIN tolerant mutants, which might have an effect on the coenzyme binding. The residues of the active site or the NAD(P)H binding site were not affected in the other YhfK variants.

In conclusion, by isolating and characterizing t-CIN tolerant mutants, we have identified the SDR superfamily enzyme YhfK of *L. monocytogenes* to be an 'ene-reductase' catalyzing the reduction of the C=C bond of α,β-unsaturated aldehydes. To our knowledge, this is the first bacterial SDR enzyme exhibiting this specificity, and these enzymes may be of interest for biocatalytic applications. The function of YhfK and its catalytic mechanism can be further investigated by enzyme kinetic studies utilizing purified recombinant YhfK, and by analysis of crystal structures of YhfK in complexes with and without cofactors and substrates. The physiological or ecological function of YhfK in *L. monocytogenes* remains an open question. Our work showed the enzyme to be able to detoxify reactive α,β-unsaturated aldehydes that are generated not only by the host during the infection process (4-HNE), but also by plants on which the bacteria may reside outside the host (t-CIN, t-HEX, citral). However, also a role in a metabolic pathway such as heme degradation can also not be

excluded. The wide distribution and conservation of YhfK-like enzymes in bacteria suggests an important role and warrants further investigation.

4.6 Supplementary information

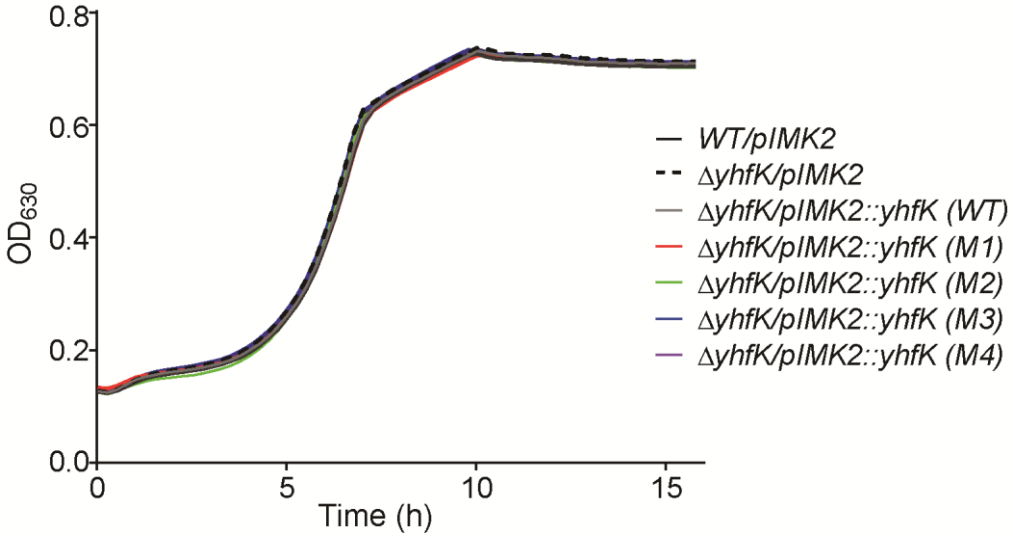

Figure S4.1 Growth of *L. monocytogenes* Δ*yhfK* complemented with WT or mutated *yhfK* alleles at 30ºC in BHI. The data represent the average of measurements of three independent cultures. The SD is omitted for clarity.

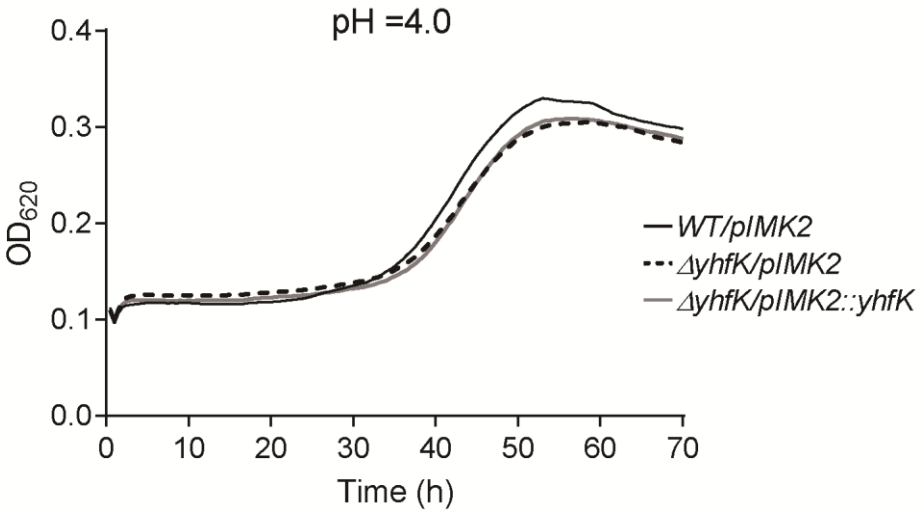

Figure S4.2 Growth of *L. monocytogenes* strains at 30ºC in BHI at pH = 4.0. The data represent the average of measurements of three independent cultures. The standard deviation is omitted for clarity.

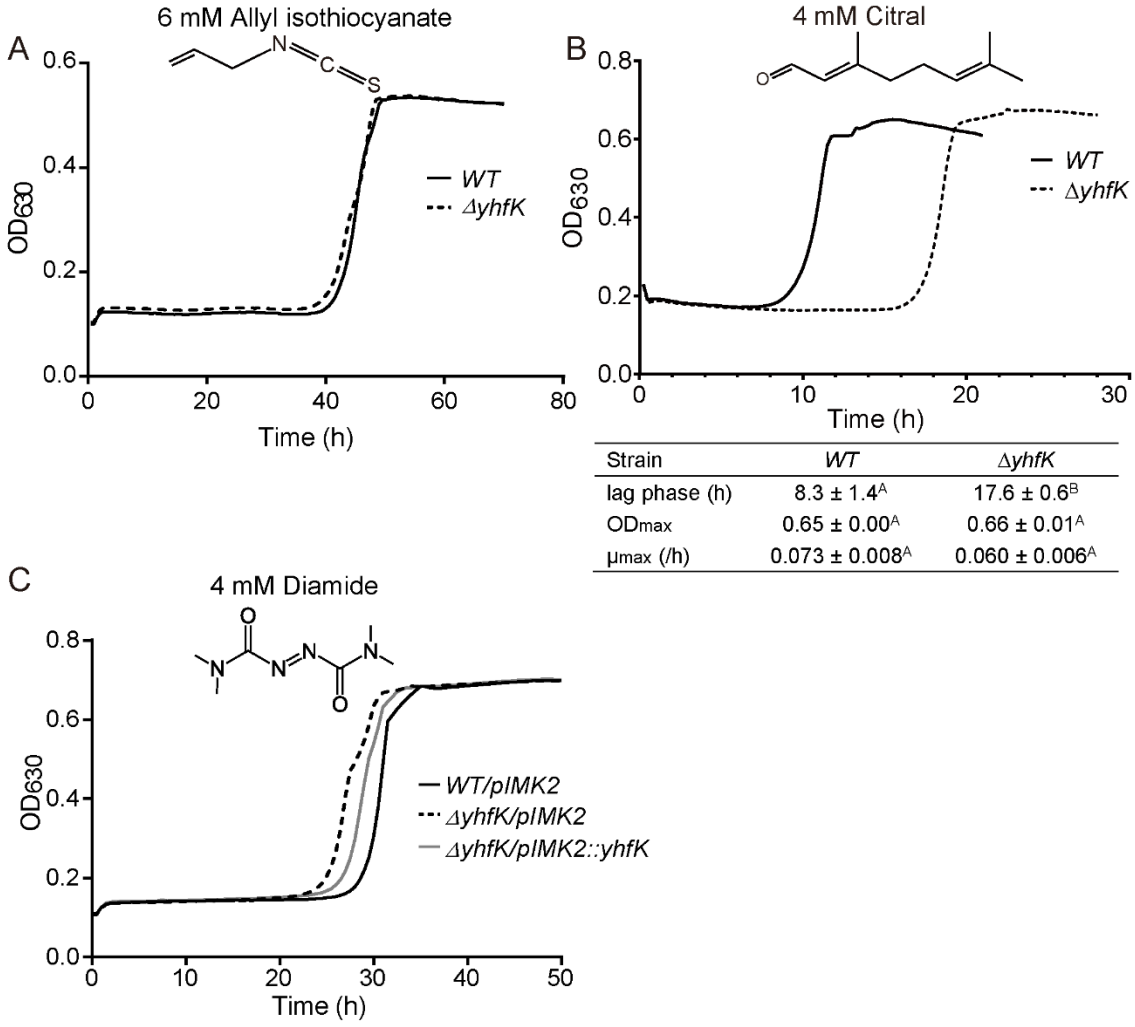

Strain	*WT*	Δ*yhfK*
lag phase (h)	8.3 ± 1.4^{A}	17.6 ± 0.6^{B}
OD_{max}	0.65 ± 0.00^{A}	0.66 ± 0.01^{A}
μ_{max} (/h)	0.073 ± 0.008^{A}	0.060 ± 0.006^{A}

Figure S4.3 Growth of *L. monocytogenes* in BHI supplemented with 6 mM allyl isothiocyanate (**A**), 4 mM citral (**B**), and 4 mM diamide (**C**). All growth curves represent the average of measurements of three independent cultures, but the standard deviation is omitted for clarity. The growth parameters (λ, μ_{max}, and OD_{max}) are represented in the table as mean ± SD; n = 3. Values followed by a common letter are not significantly different at the 5% level. The molecular structures of allyl isothiocyanate, citral (E-isomer), and diamide are shown.

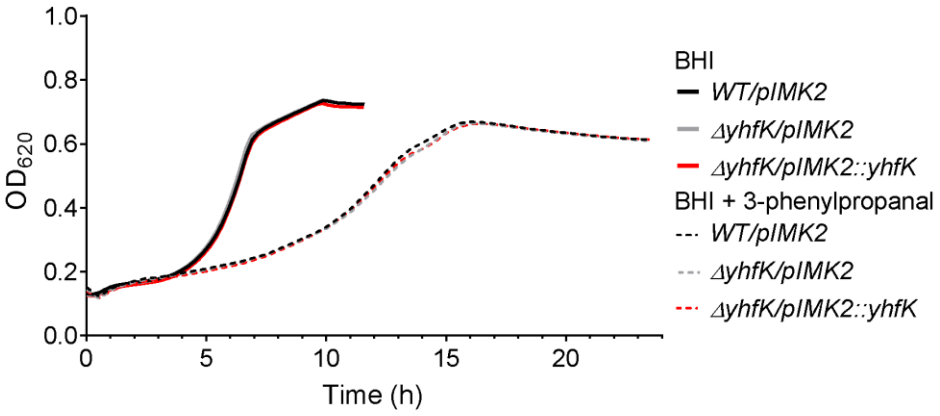

Figure S4.4 The growth of *L. monocytogenes WT/pIMK2*, Δ*yhfK/pIMK2*, and Δ*yhfK/pIMK2::yhfK* in BHI and BHI supplemented with 4 mM 3-phenylpropanal. The curve represents the average of measurements of three independent cultures. The standard deviation is omitted for clarity.

Table S4.1 List of MS ions used to quantify and qualify t-CIN, ethyl benzoate, and t-CIN metabolites from the HS-SPME-GC-MS analysis in Figure 4.6.

Compound	Quantification (m/z)	Qualification (m/z)
trans-Cinnamaldehyde	131	103, 77
Ethyl benzoate	105	77, 122, 150
3-Phenyl-2-propenol	92	91, 134
3-Phenylpropanal	91	92, 134
3-Phenylpropanol	91	92, 117, 118

Table S4.2 Selection of homologs of *L. monocytogenes* YhfK retrieved by BLASTP analysis and represented in a phylogeny tree shown in Figure 4.9.

Organism	GenBank acc.	E-value	Identity
Listeria monocytogenes str. Scott A	EGJ25920	na	100%
Abyssicoccus albus	WP_077139846	2.0E-44	39.71%
Acinetobacter calcoaceticus DSM 30006	WP_005047009	5.0E-25	35.62%
Actinocatenispora sera	WP_051802873	5.0E-23	34.27%
Actinoplanes friuliensis DSM 7358	WP_023561358	3.0E-36	40.85%
Actinosynnema mirum DSM 43827	WP_012782666	1.0E-26	34.76%
Alcanivorax borkumensis SK2	WP_011588187	8.0E-54	47.83%
Alkalihalobacillus clausii KSM-K16	WP_035201633	1.0E-50	43.27%
Alkalihalobacillus halodurans C-125	WP_010897685	6.0E-55	49.51%
Alkalihalobacillus pseudofirmus OF4	WP_012958351	3.0E-54	45.75%
Altererythrobacter epoxidivorans	WP_061925926	3.0E-34	39.71%
Alteromonas mediterranea U8	WP_020743433	3.0E-36	38.28%
Amycolatopsis methanolica 239	WP_017986042	3.0E-27	35.21%
Arthrobacter citreus	WP_152228138	1.0E-33	36.79%
Arthrobacter crystallopoietes BAB-32	WP_005269228	9.0E-32	34.74%
Bacillus amyloliquefaciens LL3	WP_068444393	1.0E-52	44.50%
Bacillus methanolicus MGA3	WP_003349462	2.0E-50	42.03%
Bacillus subtilis 168	WP_003245344	1.0E-38	43.00%
Brochothrix thermosphacta ATCC 11509	WP_029091388	5.0E-54	45.19%
Carnobacterium inhibens K1	WP_034537835	1.0E-34	36.97%
Carnobacterium sp. 17-4	WP_013709813	3.0E-47	42.79%
Cellulomonas flavigena DSM 20109	WP_013118449	1.0E-28	35.03%
Cellulophaga baltica 18	WP_029444924	4.0E-41	40.00%
Chromohalobacter salexigens 1H11	WP_035410475	1.0E-38	37.56%
Croceibacter atlanticus HTCC2559	WP_013187612	3.0E-44	42.16%
Cytobacillus oceanisediminis	WP_019383485	4.0E-47	41.18%
Enterococcus gallinarum EG2	WP_003127925	5.0E-40	40.00%
Exiguobacterium antarcticum B7	WP_014970171	1.0E-47	42.65%
Furfurilactobacillus rossiae L1	WP_017260448	2.0E-36	37.16%
Gramella forsetii KT0803	WP_011709802	1.0E-37	40.39%
Halalkalicoccus jeotgali B3	WP_008415754	2.0E-45	42.23%
Halobacillus halophilus DSM 2266	WP_224895793	3.0E-56	47.32%
Halobacillus litoralis	WP_160916865	2.0E-58	49.28%
Halobacterium salinarum R1	WP_012289566	8.0E-49	42.44%
Haloferax gibbonsii ATCC 33959	WP_004975949	5.0E-44	40.28%
Haloferax volcanii DS2	WP_004041980	3.0E-43	43.62%
Halomonas titanicae BH1	WP_039859619	2.0E-43	39.51%
Halorhodospira halophila	WP_011813864	2.0E-42	41.26%
Halostagnicola larsenii JCM 13463	WP_049953373	3.0E-47	40.58%
Haloterrigena turkmenica DSM 5511	WP_012942372	3.0E-48	43.33%
Halovivax ruber JCM 13892	WP_015299416	2.0E-49	41.43%
Hirschia baltica DSM 5838	WP_012778037	1.0E-34	38.24%
Hoeflea sp. IMCC20628	WP_197078399	3.0E-35	41.58%

Ilumatobacter coccineus YM16-304	WP_015441337	2.0E-27	36.41%
Jeotgalibacillus malaysiensis	WP_039810704	7.0E-65	52.38%
Kytococcus sedentarius DSM 20547	WP_012801883	1.0E-34	35.55%
Lacticaseibacillus casei 12A	WP_087911616	6.0E-32	38.79%
Lactiplantibacillus plantarum ZJ316	WP_063488272	1.0E-38	39.90%
Lactococcus garvieae ATCC 49156	WP_213433223	1.0E-36	37.85%
Lactococcus lactis subsp. lactis	WP_010905761	1.0E-38	43.00%
Latilactobacillus sakei subsp. sakei	WP_094365887	3.0E-19	30.52%
Levilactobacillus brevis ATCC 367	WP_039106899	1.0E-29	37.56%
Ligilactobacillus acidipiscis DSM 15836	WP_010494836	1.0E-28	38.46%
Listeria grayi ATCC 19120	WP_036108203	1.0E-81	60.00%
Listeria innocua FSL J1-023	WP_003768174	1.0E-142	93.78%
Listeria seeligeri FSL N1-067	WP_003749357	9.0E-122	81.34%
Loigolactobacillus coryniformis subsp. torquens	WP_003678857	1.0E-32	38.71%
Maribacter hydrothermalis	WP_068484818	1.0E-43	41.63%
Marinilactibacillus sp. 15R	WP_072693299	6.0E-46	40.57%
Marinobacter nauticus ATCC 49840	WP_072676559	3.0E-59	47.60%
Marinobacterium jannaschii	WP_027859208	3.0E-41	37.98%
Marinomonas communis	WP_228189941	2.0E-40	37.56%
Metabacillus sediminilitoris	WP_136354179	1.0E-52	44.50%
Methylophaga frappieri	WP_014703251	4.0E-43	41.46%
Mycobacterium marinum M	WP_038580518	7.0E-28	36.67%
Mycolicibacterium smegmatis MC2 155	WP_011728707	3.0E-26	34.88%
Natrialba magadii DSM 3394	WP_004215569	1.0E-43	40.67%
Natrinema pallidum DSM 3751	WP_006185363	1.0E-42	40.19%
Natrinema versiforme JCM 10478	WP_049890524	8.0E-49	43.20%
Natronococcus occultus DSM 3396	WP_015320273	6.0E-51	43.60%
Nonlabens dokdonensis DSW-6	WP_015363198	2.0E-38	37.80%
Oceanobacillus iheyensis HTE831	WP_011067527	9.0E-56	45.93%
Paenibacillus polymyxa SC2	WP_013373679	2.0E-59	48.31%
Parageobacillus caldoxylosilyticus	WP_042411246	1.0E-53	48.10%
Parvularcula bermudensis	WP_013300417	2.0E-36	40.10%
Pediococcus claussenii ATCC BAA-344	WP_014214583	4.0E-36	37.98%
Peribacillus muralis	WP_057912132	1.0E-59	44.08%
Phaeobacter inhibens DSM 17395	WP_014873834	7.0E-36	41.29%
Planococcus antarcticus DSM 14505	WP_006828158	6.0E-55	47.37%
Polaribacter reichenbachii	WP_068360023	1.0E-41	41.95%
Pontibacillus sp. HMF3514	WP_160098489	7.0E-57	47.09%
Priestia megaterium DSM 319	WP_214985613	1.0E-63	50.72%
Pseudoalteromonas arctica	WP_010554646	3.0E-32	40.20%
Psychrobacillus sp. AK 1817	WP_151109713	1.0E-50	43.96%
Psychroflexus torquis ACAM 623	WP_015022789	2.0E-37	39.81%
Rathayibacter rathayi NCPPB 2980	WP_097165845	4.0E-34	35.71%
Rhodococcus erythropolis CCM2595	WP_020970330	5.0E-26	34.74%
Robiginitalea biformata HTCC2501	WP_015755446	4.0E-41	41.55%
Rubrobacter radiotolerans DSM 5868	WP_038680084	3.0E-32	40.19%

Salimicrobium jeotgali	WP_008591040	2.0E-52	46.34%
Salinicoccus halodurans	WP_046789033	6.0E-46	38.76%
Salinisphaera sp. LB1	WP_109994268	1.0E-44	41.75%
Salisediminibacterium selenitireducens	WP_013171998	6.0E-51	42.92%
Shewanella frigidimarina NCIMB 400	WP_011635783	6.0E-41	42.16%
Sphingorhabdus sp. M41	WP_067201614	3.0E-34	39.71%
Staphylococcus aureus M1	WP_001024094	3.0E-38	37.91%
Staphylococcus equorum subsp. equorum	WP_046466170	3.0E-34	38.86%
Streptococcus gallolyticus	WP_061459807	1.0E-28	35.02%
Streptomyces albulus ZPM	AKA04559	6.0E-23	33.18%
Sutcliffiella horikoshii	WP_088017909	1.0E-43	40.19%
Tateyamaria omphalii	WP_076626432	4.0E-37	41.50%
Tetragenococcus halophilus NBRC 12172	WP_014124834	2.0E-45	42.33%
Virgibacillus pantothenticus	WP_082240849	2.0E-47	41.90%
Weissella hellenica	WP_074427066	2.0E-43	40.89%

4.7 Author Contributions

Conceptualization: Lei Sun[1] and Chris Michiels[1]; investigation: Lei Sun; writing—original draft preparation: Lei Sun; writing—review and editing: Lei Sun and Chris Michiels; supervision and administration: Chris Michiels; GC-MS analysis: Carolien Buvé[2] and Ann Van Loey[2].

Affiliations:

[1] Laboratory of Food Microbiology, Department of Microbial and Molecular Systems (M2S) and Leuven Food Science and Nutrition Research Center (LFoRCe), KU Leuven, Leuven, Belgium.

2. Laboratory of Food Technology, Department of Microbial and Molecular Systems (M2S) and Leuven Food Science and Nutrition Research Center (LFoRCe), KU Leuven, Leuven, Belgium.

4.8 Funding

This work was funded by research grants from the Research Foundation-Flanders (FWO) (G.0C77.14N) and from the KU Leuven Research Fund (METH/14/03).

4.9 Acknowledgement

We thank Abram Aertsen, Kristof Vanoirbeek, and Maarten Goedseels for their critical advice on the project and experiments.

Chapter 5 General Conclusions and Future perspectives

Plant EO constituents like t-CIN and t-HEX, which contain an α,β-unsaturated aldehyde moiety, are of interest as possible natural food antimicrobials to inhibit the growth of pathogens like *L. monocytogenes* [4,5]. These compounds typically exert a dose-dependent growth inhibition of *L. monocytogenes* characterized by a lag phase elongation in BHI broth [17] (Fig. 1.3), and they induce cell shape deformations at the sub-lethal concentration (Fig. 2.3). Although the lag phase extension implies only temporary inhibition of growth, it still provides a perspective of the compounds to prolong the shelf-life of food products, especially refrigerated ready-to-eat foods, by delaying the outgrowth of foodborne pathogens. As such, these compounds may help to provide more flexibility in the food distribution chain and reduce food losses. The utilization of EO constituents as natural food preservatives also accommodates the demand of consumers for artificial-preservative-free foods and may comply with the 'clean label' concept.

In this thesis, attempts to clarify the antimicrobial mode of action of t-CIN were made by characterizing *L. monocytogenes* mutants with altered sensitivity to t-CIN. First, *yvcK::Himar1* and *asnB::Himar1*, two t-CIN hypersensitive mutants isolated previously in a screening of a genome-wide random *Himar1* transposon mutant library were studied in Chapter 2 and 3. Both mutants are also sensitive to several other EO constituents, including t-HEX, citral, allyl isothiocyanate, and phenethyl isothiocyanate (Fig. S5.1 & S5.2). Then, *yhfK* mutants with increased t-CIN tolerance were obtained by experimental evolution and further investigated in Chapter 4. Although we mainly address pathways and processes underlying the t-CIN tolerance in *L. monocytogenes*, the findings can also benefit or inspire the research on other EOs or EO constituents, especially α,β-unsaturated aldehydes such as t-HEX and citral. Here, t-CIN was selected as a representative compound for a collection of small lipophilic and thiol-reactive compounds extracted from plant EOs. As food microbiologists, we are not only interested in t-CIN, but also in many other antimicrobial EO constituents that can be hopefully applied in food preservation.5.1 Cell wall integrity as a determinant of t-CIN sensitivity

At the start of this work, the function of *yvcK* and *asnB* had not or only partly been studied in *L. monocytogenes.* Our work shows that both genes play an important role in cell

wall homeostasis, and thereby suggests the importance of cell wall integrity to the resistance of *L. monocytogenes* to thiol-reactive EO constituents.

In particular, the vulnerability to t-CIN resulting from the loss of YvcK was accompanied by a significantly elevated bacterial lysis as a result of impaired cell wall integrity (Fig. 2.3). Experimental evolution of the *yvcK:Himar1* mutant in sublethal t-CIN concentrations led to the emergence of suppression mutations in genes involved in the UDP-GlcNAc biosynthesis, including the small RNA rli73 [174] that locates immediate upstream of the *glmU-prs* operon and *nagR* (Fig. 2.6). GlmU catalyzes the last two steps of UDP-GlcNAc biosynthesis [164] and NagR represses the uptake and utilization of GlcNAc [177–179]. Increasing the production of UDP-GlcNAc biosynthetic enzymes including GlmS, GlmM and GlmU or supplying GlcNAc in the medium reduced the impact of YvcK loss on t-CIN tolerance. These findings suggest a pivotal role of YvcK in UDP-GlcNAc biosynthesis in *L. monocytogenes*, similar to what was previously shown in *B. subtilis* [162,165], and that t-CIN interferes with the UDP-GlcNAc homeostasis, probably by limiting the availability of the precursor Fru-6-P. Nevertheless, how the suppression mutations modulated the transcription of *glmU-prs* operon and the function of NagR are unclear and need to be further investigated. Crystal structure analysis of the *B. subtilis* NagR-ligand complex showed that multiple residues including Thr90, Ser165, Ile166, Tyr167, Arg 133, and Arg135, all of which are conserved in *L. monocytogenes* NagR (considering the substitution of the Ile by a Leu residue as conservative), coordinated the interaction with the phosphate group of the ligand (GlcN-P or GlcNAc-P) [196,197]. With this in mind, the Ile-Lys insertion between Leu165-Tyr166 in NagR of one of the evolved suppression mutants of the *yvcK* mutant is likely to modify the interaction of NagR with its ligands, and thus modulate the expression of targeted genes including *nagP* and the *nagABR* operon, thereby affecting the uptake and utilization of extracellular GlcNAc.

AsnB, on the other hand, was shown to amidate *m*DAP residues in the peptidoglycan of *L.* monocytogenes, like several of its homologs in a range of other Gram-positive bacteria, (Chapter 3). Deficiency in *m*DAP amidation caused several peptidoglycan- and cell surface-related phenotypes in *asnB* mutants, including susceptibility to lysozyme, loss of flagellation and motility, and a strong reduction in biofilm formation. Moreover, AsnB inactivation also abrogated the proper cell wall anchoring of InlA, a virulence protein that mediates entry into

the host cells and that normally gets cross-linked to *m*DAP. Nevertheless, how the absence of peptidoglycan amidation relates to increased t-CIN sensitivity remains unclear.

In light of these insights, we anticipate that thiol-reactive essential oil compounds like t-CIN would act synergistically with bacterial cell wall targeting antibiotics, offering a perspective for reducing antibiotic usage or increasing their effectiveness. Significant synergistic effects of t-CIN with (cell wall targeting) vancomycin and amoxicillin at sub-inhibitory concentrations were indeed revealed against methicillin-resistant *S. aureus* strains [33]. Karumathil et al. [79] also found that t-CIN decreased the resistance of multi-drug-resistant *Acinetobacter baumannii* to a range of β-lactam antibiotics.

5.2 The role of YvcK in maintaining UDP-GlcNAc homeostasis

The findings reported in Chapter 2 support a role for YvcK to divert glycolytic intermediates into the UDP-GlcNAc biosynthesis pathway especially when the glycolytic intermediate Fru-6-P is running low (Chapter 2). An insufficient substrate to feed into the UDP-GlcNAc biosynthesis pathway and the ensuing peptidoglycan synthesis defect may be the reason behind the t-CIN hypersensitivity of *yvcK* mutant. In the absence of t-CIN, the mutant showed normal growth in BHI broth, indicating that YvcK is dispensable under these conditions, possibly because this medium has a high glucose content (> 2g/L) and hence sufficient glycolytic metabolites are accessible for UDP-GlcNAc biosynthesis in this medium. The importance of YvcK for t-CIN tolerance in BHI broth may thus indicate that t-CIN targets one or more steps of the glycolysis, thus reducing the availability of intermediates that can be diverted to GlcNAc biosynthesis. One such possible target of t-CIN is GAPDH, a glycolytic enzyme that is sensitive to electrophilic attack because of the highly conserved Cys active site (Cys151 for GAPDH of *L. monocytogenes* EGD-e) [62]. Reaction with t-CIN may abrogate the activity of the enzyme and hence block the glycolytic and gluconeogenetic flux. NADPH, which fuels the regeneration of GSH and diverse enzymatic antioxidant systems, plays a critical role in maintaining bacterial intracellular redox homeostasis [104,184]. When cells are exposed to oxidative stress, the cellular NADPH is predominantly replenished via the oxidative pentose phosphate pathway into which the glycolytic carbon flux will be rerouted [62,185,186]. Thus, *L. monocytogenes* might respond to an oxidative t-CIN challenge by driving glycolytic substrates to the oxidative pentose phosphate pathway to stabilize the intracellular redox state. Proteomic analysis of *E. coli* treated with a sublethal

concentration of t-CIN indeed showed that the expression of genes involved in the pentose phosphate pathway is highly upregulated [11]. In general, we hypothesize that t-CIN induces the reallocation of carbon flux and decreases the glycolytic production of Fru-6-P, which is the basis of the UDP-GlcNAc biosynthetic reactions (Fig. 2.6). Further confirmation of this hypothesis can be obtained by analyzing carbon fluxes using ^{14}C-labeled compounds.

Evolutionary experiments of *yvcK* mutant also identified suppressor mutations in genes involved in glycolysis and the pentose phosphate pathway. Specifically, the PRPP synthetase, which mediates the reversible conversion of Ribose-5-P to PRPP, thereby connecting the pentose phosphate pathway with nucleotide biosynthesis [176], was found to be mutated (Fig. 2.6). Ribose-5-P is a key metabolite of the pentose phosphate pathway that can be reversibly converted to Fru-6-P and glyceraldehyde-3-phosphate through different reactions of the nonoxidative pentose phosphate pathway without NADPH generation [198] (Fig. 2.6B). Of note, a fructose-biphosphate aldolase that might impact the central carbon flux and the cellular content of Fru-6-P was also mutated in one of the suppressor mutants (Table 2.3). Likewise, suppressor mutations of a *B. subtilis yvcK* null mutant were found in genes of the glycolysis, pentose phosphate, or gluconeogenesis pathways when bacteria were grown on nonpreferred carbon sources, including the glycolytic gene regulator CggR and glucose-6-phosphate dehydrogenase [162,163]. These suppression mutations might all drive the flux of cellular Fru-6-P into UDP-GlcNAc biosynthesis, thereby alleviating the metabolic defect of a *yvcK* null mutant.

5.3 AsnB mediates peptidoglycan amidation in *L. monocytogenes*

As noted above, we demonstrated in this work that AsnB of *L. monocytogenes*, like several of its homologs in Gram-positive bacteria, functions as a Gln-hydrolyzing amidotransferase that amidates the ε-carboxyl group of *m*DAP in the peptidoglycan stem peptide and, in this way, affects several cell wall and cell surface-related properties, including the formation of shorter but thicker cells, susceptibility to lysozyme, loss of flagellation and motility, the reduced presence of InlA in the cell surface and a strong reduction in biofilm formation (Chapter 3). AsnB was annotated as a glutamine-dependent asparagine synthase based on the function of some of its well-studied homologs (e.g. from *E. coli*), but an increasing number of AsnB representatives in Gram-positive bacteria catalyze amidotransfer from Gln to *m*DAP in bacterial peptidoglycan rather than to Asp [213–216]. We did not

analyze whether AsnB from *L. monocytogenes* can restore Asn auxotrophy in an *E. coli asnB* mutant, and thus cannot exclude that it is a promiscuous enzyme similar to its *B. subtilis* counterpart [212]. However, since neither t-CIN tolerance nor normal cell morphology was restored in the *asnB* mutant by supplying additional Asn in the growth medium, it seems unlikely that these phenotypes result from Asn deficiency and that AsnB plays a role in Asn synthesis in *L. monocytogenes*.

In general, the loss of peptidoglycan amidation due to the absence of AsnB renders the bacteria sensitive to lysozyme and cell wall-targeting antibiotics [213,216]. A possible explanation for these effects is the elevated number of negatively charged carboxylate groups in the peptidoglycan at the unamidated ε-carboxyl group of *m*DAP. Similarly, we speculate that the reduced anchoring of InlA to the unamidated *m*DAP may also be related to the increased negative charge that may prevent the coordinated positioning of the SrtA-InlA complex and the peptidoglycan precursor lipid II [232]. InlA is a so-called LPXTG motif-containing surface-exposed protein, that gets covalently linked to the free ε-amino group of *m*DAP in the peptidoglycan stem peptide [232]. Besides InlA, *L. monocytogenes* produces many other LPXTG motif-containing proteins (40 in strain EGD-e) that may covalently bind to the free ε-amino group of *m*DAP residue [202,241,245], and the binding of these proteins to non-amidated peptidoglycan may be affected as well.

AsnB deficiency was also accompanied by a loss of bacterial motility due to the inability to produce flagella in *L. monocytogenes* (Fig. 3.3). Remarkably, this phenotype has not been reported previously in *asnB* mutants of other bacteria including the closely related *B. subtilis*. The flagellar apparatus is embedded in the bacterial cell wall, where it interacts directly with the peptidoglycan layer via several components of its basal body [260]. Its assembly is a complex and highly coordinated process that requires local and controlled peptidoglycan hydrolase activity to mediate the passage of the flagellar rod through the peptidoglycan layer [260]. As such, it is easy to envision that the increased negative charge of the non-amidated peptidoglycan, or the absence of one or more peptidoglycan-linked proteins, may compromise flagellar assembly. However, the precise reason for the lack of flagella remains to be elucidated. The lack of flagella and flagellum-mediated motility may also explain the reduced biofilm formation of the *asnB* mutant [72], although other changes in surface properties may also contribute.

5.4 Identification of YhfK oxidoreductase for catalyzing t-CIN degradation

While the screening of a genome-wide random transposon mutant library yielded only mutants with increased t-CIN sensitivity, mutants with increased t-CIN tolerance could be successfully isolated in evolutionary experiments. Remarkably, all isolated t-CIN resistant mutants contained amino acid substitution mutations in *yhfK*, a gene encoding a putative oxidoreductase (Fig. 4.2), which was subsequently proven to be essential for the tolerance of *L. monocytogenes* to multiple antimicrobial α,β-unsaturated aldehydes. Further, it could be concluded from GC-MS analysis of culture supernatants of WT and mutant strains that YhfK is an ene reductase that reduces the C=C double bond of t-CIN. Hitherto, no enzyme-mediated detoxification of antimicrobial α,β-unsaturated carbonyl compounds in pathogenic *L. monocytogenes* has been reported and this work is the first study to unmask the presence of such an enzyme in foodborne pathogens. Loss of YhfK activity did not only result in sensitivity toward t-CIN, but also to t-HEX, citral, and 4-HNE, indicating that the enzyme has a relaxed substrate specificity. Since 4-HNE is produced by host cells as part of their antibacterial defense during the infection process, it would be worthwhile to investigate whether YhfK plays a role in virulence in *L. monocytogenes*.

Attenuation of YhfK also sensitized *B. subtilis* to both t-CIN and t-HEX, suggesting a conserved function of YhfK in many pathogenic and nonpathogenic bacteria. Also, plants produce α,β-unsaturated aldehydes as part of their defense against invading microbes or upon tissue damage, but the compounds are somewhat different than those produced by animal cells. It would be interesting to investigate whether the substrate specificity of YhfK in bacteria colonizing or infecting animals or plants is tuned to the spectrum of α,β-unsaturated produced by their respective hosts. Finally, it should be noted that our work so far has provided only indirect evidence that YhfK has ene reductase activity, and that definitive confirmation with the purified enzyme is required.

From an application perspective, the findings of the evolutionary experiments in this work imply the feasibility to improve the enzymatic activity of YhfK towards specific substrates by enzyme engineering [272]. The engineering of ene-reductases, which are known for stereo-selectively reducing the activated C=C double bond, has been intensively explored for industrial applications in the biosynthesis of valuable and arduously amenable chemicals [133,272,273]. For example, an ene-reductase from the yeast *Pichia anomala*, together with an esterase and a ketoreductase from the same species, were employed by Contente et al. [284]

to chemoenzymatically synthesize the prostaglandin analogue Latanoprost, a valuable pharmaceutical for glaucoma treatment. The potential of some OYEs to be implemented in the production of non-steroidal anti-inflammatory profens was also described [285]. For example, XenA from *P. putida* and GYE from *Gluconobacter oxydans* were demonstrated to efficiently mediate the chemoenzymatic synthesis of Naproxen and analogues (2-phenylpropionic acid and 2-(4-propylphenyl)propanoic acid) from α,β-unsaturated carboxylic acids [285]. However, engineered ene-reductases of SDR-type have been rarely reported [272]. YhfK may therefore possibly serve as a new SDR scaffold for engineering novel biocatalysts typical of the SDR superfamily for challenging industrial biotransformations.

The incubation of *L. monocytogenes* with t-CIN also generated 3-phenyl-2-propenol (Fig. 4.6), indicating a capacity to reduce the aldehyde group of t-CIN. In *E. coli*, YqhD and DkgA were speculated to catalyze this conversion [7,11], although direct evidence is missing. Homologs of YqhD and DkgA exist in *L. monocytogenes*, but neither of them has been characterized yet and efforts are thus needed to investigate their contribution to t-CIN tolerance in *L. monocytogenes*. In many microbes, the most prominent ene-reductases that exhibit substrate specificity towards α,β-unsaturated carbonyl compounds belong to the flavin-dependent OYEs [132,133]. YqjM of *B. subtilis*, one of the most intensively studied OYEs, was reported to exhibit versatile activities towards an array of α,β-unsaturated aldehydes and ketones including t-CIN and t-HEX [136,137,140]. Unlike in *B. subtilis*, the enzymatic activities of OYEs in *L. monocytogenes* are undetermined and it will therefore be interesting to investigate whether they contribute to the tolerance of *L. monocytogenes* to antimicrobial α,β-unsaturated aldehydes, in particular t-CIN.

5.5 Potential of t-CIN as a food preservative

As the major component of cinnamon bark EO, t-CIN is classified as GRAS by U.S. FDA for use in foods and registered by the European Commission for use as a food flavoring agent [14,286]. The acceptable daily intake of t-CIN proposed by some authorities is in the range of 0.7 - 1.25 mg/kg body weight [286]. Yet, no prominent risk to human health has been acknowledged in view of the present levels of usage other than being a potent skin sensitizer as an ingredient of cosmetics and perfumes [14,286–289]. Mammalian studies have disclosed no acute or chronic toxicity, carcinogenicity, and genotoxicity of t-CIN at the tested

concentrations (200 - 550 mg/kg body weight per day in oral studies with rats and mice) as far as we know [286,290–292]. Detoxification processes including the conjugation with GSH, the aldehyde dehydrogenase mediated oxidation and the aldose reductase mediated reduction were shown to efficiently lower t-CIN concentrations in rats [92,290]. Nevertheless, it cannot be excluded that high concentrations of t-CIN may still cause adverse health effects. Further research should be undertaken to determine the maximum concentration of t-CIN that is safe for human consumption and to define acceptable maximum concentrations if the compound is to be used for food preservation. The concentrations of t-CIN used in this work are in the range of 1 to 4 mM, which is too high to apply to foodstuffs taking the acceptable daily intake into account. Therefore, it is important to explore the utilization of t-CIN at lower concentrations in an approach based on the hurdle concept.

Like for many other EO compounds, the undesirable sensory side-effects of t-CIN may impede its acceptance by consumers. The other obstacle to the adoption of t-CIN as a food preservative is that it loses much of its activity in real food matrices and therefore lacks potency when used alone at low doses [3,4]. Another complication is the low solubility of t-CIN in water (approximately 8.3 mM at 20 °C) [14]. As aforementioned, the hurdle technology concept may offer a solution. Several electrophilic EO compounds including t-CIN were previously shown to act synergistically with high-pressure treatment against several bacteria species in our laboratory [76]. Aside from that information on effective combinations of t-CIN with other (potential) food preservatives and/or food preservation methods to suppress food spoilage is scarce.

The insights obtained in this work could provide some rational basis for developing hurdle technology concepts with EO constituents such as t-CIN and t-HEX. Given the essentiality of cell wall integrity to bacterial resistance toward t-CIN and t-HEX, we speculate that the combined use of certain bacterial cell wall targeting compounds with t-CIN (or t-HEX) may significantly reduce the concentrations needed to effectively inhibit food spoilage. Applying t-CIN at low concentrations can also slow down the appearance of t-CIN-resistant mutants among foodborne pathogens based on our experience. It will be interesting to undertake a systematic investigation of which food preservation methods interact synergistically with t-CIN to inhibit or inactivate foodborne microbes. Potential methods that can be examined include low temperature, low water activity, mild heat, low pH, anaerobic packaging, and food additives such as sodium chloride, sodium nitrite, and nisin.

Another important challenge that needs to be addressed is the oxidation of t-CIN to cinnamic acid when exposed to oxygen and light for prolonged periods [14]. The stability of t-CIN can be effectively enhanced by methods such as encapsulation in emulsions, vacuum packaging, inert gas packaging, and lightproof packaging.

Finally, the emergence of mutations resulting in elevated tolerance is also a potential issue for the use of t-CIN as a food preservative. However, interestingly, the mutations in the ene reductase YhfK that led to t-CIN tolerance in the evolution experiment in Chapter 4 resulted in unaltered or reduced tolerance towards t-HEX (Fig. 4.4), suggesting that it may be difficult (or impossible) for the enzyme to increase its affinity for multiple different α,β-unsaturated aldehydes. This implies that the evolution of resistance of the bacteria against a combination of α,β-unsaturated carbonyl compounds is likely to be much more infrequent than resistance to a single compound. If this can be confirmed in evolution experiments with combinations of compounds, the use of cocktails of two or more natural α,β-unsaturated carbonyl compounds (e.g. t-HEX, citral, carvone, and perillaldehyde) could be a convenient and effective approach to suppress the emergence of resistance among food spoilage microorganisms.

5.6 Conclusion

In summary, the mutant-driven analysis of t-CIN tolerance adopted in this work has generated novel findings on several pathways and processes that are important for the tolerance of α,β-unsaturated aldehydes in *L. monocytogenes*. In particular, YvcK was demonstrated to play a critical role in diverting the glycolytic intermediates into peptidoglycan precursor biosynthesis pathway especially when the glycolytic intermediate Fru-6-P is running low (Chapter 2). An insufficient substrate to feed into the UDP-GlcNAc biosynthesis pathway and the subsequent severe peptidoglycan synthesis defect was speculated to be the underlying reason for the hypersensitivity of *yvcK* mutant to t-CIN. AsnB, on the other hand, was found to be a Gln-hydrolyzing amidotransferase that modifies peptidoglycan and, in this way, affects a broad range of cell wall and cell surface-related properties, including the formation of shorter but thicker cells, susceptibility to lysozyme, loss of flagellation and motility, reduced presence of cell surface proteins and a strong reduction in biofilm formation (Chapter 3). Additionally, we further characterized t-CIN mutants with increased t-CIN tolerance isolated from evolutionary experiments for a more

comprehensive understanding of the antimicrobial mechanism of t-CIN against *L. monocytogenes*. YhfK oxidoreductase was identified as an ene-reductase capable of detoxifying a wide range of α,β-unsaturated aldehydes, and thereby providing tolerance to these compounds in *L. monocytogenes*.

5.6 Supplementary information

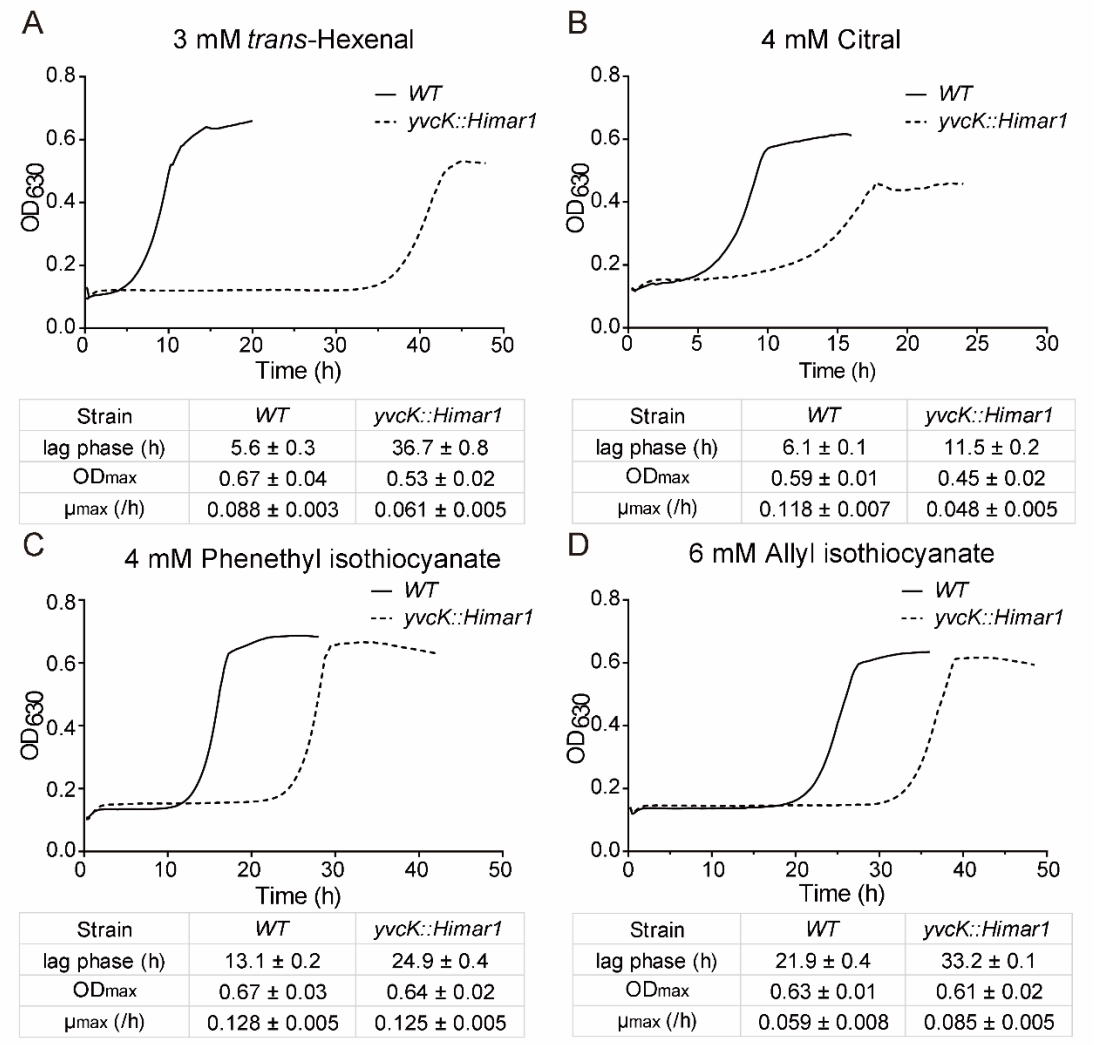

Strain	*WT*	*yvcK::Himar1*
lag phase (h)	5.6 ± 0.3	36.7 ± 0.8
OD_{max}	0.67 ± 0.04	0.53 ± 0.02
μ_{max} (/h)	0.088 ± 0.003	0.061 ± 0.005

Strain	*WT*	*yvcK::Himar1*
lag phase (h)	6.1 ± 0.1	11.5 ± 0.2
OD_{max}	0.59 ± 0.01	0.45 ± 0.02
μ_{max} (/h)	0.118 ± 0.007	0.048 ± 0.005

Strain	*WT*	*yvcK::Himar1*
lag phase (h)	13.1 ± 0.2	24.9 ± 0.4
OD_{max}	0.67 ± 0.03	0.64 ± 0.02
μ_{max} (/h)	0.128 ± 0.005	0.125 ± 0.005

Strain	*WT*	*yvcK::Himar1*
lag phase (h)	21.9 ± 0.4	33.2 ± 0.1
OD_{max}	0.63 ± 0.01	0.61 ± 0.02
μ_{max} (/h)	0.059 ± 0.008	0.085 ± 0.005

Figure S5.1 Growth of WT and *yvcK::Himar1* mutant in BHI supplemented with 3 mM *trans*-2-hexenal (**A**), 4 mM citral (**B**), 4 mM phenethyl isothiocyanate (**C**), and 6 mM allyl isothiocyanate (**D**). All growth curves represent the average of measurements of three independent cultures, but the standard deviation is omitted for clarity. The growth parameters (λ, $\mu_{max,}$ and OD_{max}) are represented in the table as mean ± SD; $n = 3$.

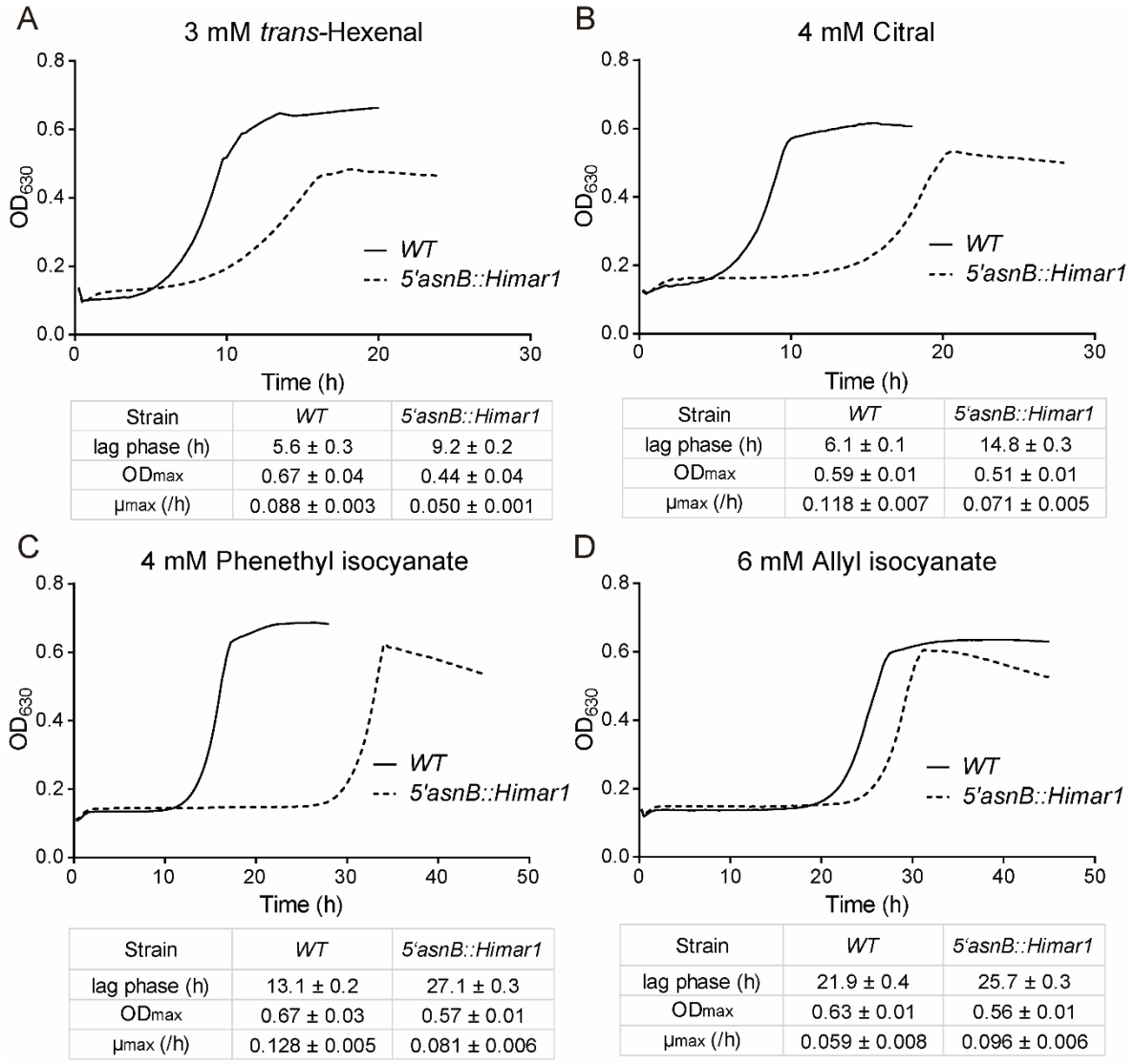

Strain	*WT*	*5'asnB::Himar1*
lag phase (h)	5.6 ± 0.3	9.2 ± 0.2
OD_{max}	0.67 ± 0.04	0.44 ± 0.04
μ_{max} (/h)	0.088 ± 0.003	0.050 ± 0.001

Strain	*WT*	*5'asnB::Himar1*
lag phase (h)	6.1 ± 0.1	14.8 ± 0.3
OD_{max}	0.59 ± 0.01	0.51 ± 0.01
μ_{max} (/h)	0.118 ± 0.007	0.071 ± 0.005

Strain	*WT*	*5'asnB::Himar1*
lag phase (h)	13.1 ± 0.2	27.1 ± 0.3
OD_{max}	0.67 ± 0.03	0.57 ± 0.01
μ_{max} (/h)	0.128 ± 0.005	0.081 ± 0.006

Strain	*WT*	*5'asnB::Himar1*
lag phase (h)	21.9 ± 0.4	25.7 ± 0.3
OD_{max}	0.63 ± 0.01	0.56 ± 0.01
μ_{max} (/h)	0.059 ± 0.008	0.096 ± 0.006

Figure S5.2 Growth of WT and *5'asnB::Himar1* mutant in BHI supplemented with 3 mM *trans*-2-hexenal (**A**), 4 mM citral (**B**), 4 mM phenethyl isothiocyanate (**C**), and 6 mM allyl isothiocyanate (**D**). All growth curves represent the average of measurements of three independent cultures, but the standard deviation is omitted for clarity. The growth parameters (λ, μ_{max}, and OD_{max}) are represented in the table as mean ± SD; $n = 3$.

Reference

1. Carocho, M.; Barreiro, M.F.; Morales, P.; Ferreira, I.C.F.R. Adding molecules to food, pros and cons: A review on synthetic and natural food additives. *Comprehensive Reviews in Food Science and Food Safety* **2014**, *13*, 377–399. 10.1111/1541-4337.12065.
2. Karwowska, M.; Kononiuk, A. Nitrates/nitrites in food-risk for nitrosative stress and benefits. *Antioxidants* **2020**, *9*. 10.3390/antiox9030241.
3. Burt, S. Essential oils: Their antibacterial properties and potential applications in foods-A review. *International Journal of Food Microbiology* **2004**, *94*, 223–253. 10.1016/j.ijfoodmicro.2004.03.022.
4. Hyldgaard, M.; Mygind, T.; Meyer, R.L. Essential oils in food preservation: Mode of action, synergies, and interactions with food matrix components. *Frontiers in Microbiology* **2012**, *3*, 12. 10.3389/fmicb.2012.00012.
5. Maurya, A.; Prasad, J.; Das, S.; Dwivedy, A.K. Essential oils and their application in food safety. *Frontiers in Sustainable Food Systems* **2021**, *5*, 133. 10.3389/fsufs.2021.653420.
6. Santos, M.I.S.; Martins, S.R.; Veríssimo, C.S.C.; Nunes, M.J.C.; Lima, A.I.G.; Ferreira, R.M.S.B.; Pedroso, L.; Sousa, I.; Ferreira, M.A.S.S. Essential oils as antibacterial agents against food-borne pathogens: Are they really as useful as they are claimed to be? *Journal of Food Science and Technology* **2017**, *54*, 4344–4352. 10.1007/s13197-017-2905-0.
7. Visvalingam, J.; Hernandez-Doria, J.D.; Holley, R.A. Examination of the genome-wide transcriptional response of *Escherichia coli* O157: H7 to cinnamaldehyde exposure. *Applied and Environmental Microbiology* **2013**, *79*, 942–950. 10.1128/AEM.02767-12.
8. Basak, S.; Guha, P. A review on antifungal activity and mode of action of essential oils and their delivery as nano-sized oil droplets in food system. *Journal of Food Science and Technology* **2018**, *55*, 4701–4710. 10.1007/s13197-018-3394-5.
9. Wang, P.; Ma, L.; Jin, J.; Zheng, M.; Pan, L.; Zhao, Y.; Sun, X.; Liu, Y.; Xing, F. The anti-aflatoxigenic mechanism of cinnamaldehyde in *Aspergillus flavus*. *Scientific Reports* **2019**, *9*, 10499. 10.1038/s41598-019-47003-z.
10. Zheng, S.; Jing, G.; Wang, X.; Ouyang, Q.; Jia, L.; Tao, N. Citral exerts its antifungal activity against *Penicillium digitatum* by affecting the mitochondrial morphology and function. *Food Chemistry* **2015**, *178*, 76–81. 10.1016/j.foodchem.2015.01.077.
11. Du, G.-F.; Yin, X.-F.; Yang, D.-H.; He, Q.-Y.; Sun, X. Proteomic investigation of the antibacterial mechanism of *trans*-cinnamaldehyde against *Escherichia coli*. *Journal of Proteome Research* **2021**, *20*, 2319–2328. 10.1021/acs.jproteome.0c00847.
12. Alizadeh Behbahani, B.; Falah, F.; Lavi Arab, F.; Vasiee, M.; Tabatabaee Yazdi, F. Chemical composition and antioxidant, antimicrobial, and antiproliferative activities of *Cinnamomum zeylanicum* bark essential oil. *Evidence-Based Complementary and Alternative Medicine* **2020**, *2020*, 1–8. 10.1155/2020/5190603.
13. Vasconcelos, N.G.; Croda, J.; Simionatto, S. Antibacterial mechanisms of cinnamon and its constituents: A review. *Microbial Pathogenesis* **2018**, *120*, 198–203. 10.1016/j.micpath.2018.04.036.
14. Doyle, A.A.; Stephens, J.C. A review of cinnamaldehyde and its derivatives as antibacterial agents. *Fitoterapia* **2019**, *139*, 104405. 10.1016/j.fitote.2019.104405.

15. Shi, C.; Sun, Y.; Liu, Z.; Guo, D.; Sun, H.; Sun, Z.; Chen, S.; Zhang, W.; Wen, Q.; Peng, X.; et al. Inhibition of *Cronobacter sakazakii* virulence factors by citral. *Scientific Reports* **2017**, *7*, 43243. 10.1038/srep43243.
16. Wakai, J.; Kusama, S.; Nakajima, K.; Kawai, S.; Okumura, Y.; Shiojiri, K. Effects of *trans*-2-hexenal and *cis*-3-hexenal on post-harvest strawberry. *Scientific Reports* **2019**, *9*, 10112. 10.1038/s41598-019-46307-4.
17. Rogiers, G.; Kebede, B.T.; Van Loey, A.; Michiels, C.W. Membrane fatty acid composition as a determinant of *Listeria monocytogenes* sensitivity to *trans*-cinnamaldehyde. *Research in Microbiology* **2017**, *168*, 536–546. 10.1016/j.resmic.2017.03.001.
18. He, T.-F.; Wang, L.-H.; Niu, D.; Wen, Q.; Zeng, X.-A. Cinnamaldehyde inhibit *Escherichia coli* associated with membrane disruption and oxidative damage. *Archives of Microbiology* **2019**, *201*, 451–458. 10.1007/s00203-018-1572-5.
19. Rogiers, G. Antimicrobial mechanism of *trans*-cinnalmaldehyde and other essential oil compounds in *Listeria monocytogenes*. *PhD Dissertation (KU Leuven)* **2017**.
20. Kowalska-Krochmal, B.; Dudek-Wicher, R. The minimum inhibitory concentration of antibiotics: methods, interpretation, clinical relevance. *Pathogens* **2021**, *10*, 165. 10.3390/pathogens10020165.
21. Kwon, J.A.; Yu, C.B.; Park, H.D. Bacteriocidal effects and inhibition of cell separation of cinnamic aldehyde on *Bacillus cereus*. *Letters in Applied Microbiology* **2003**, *37*, 61–65. 10.1046/j.1472-765X.2003.01350.x.
22. Domadia, P.; Swarup, S.; Bhunia, A.; Sivaraman, J.; Dasgupta, D. Inhibition of bacterial cell division protein FtsZ by cinnamaldehyde. *Biochemical Pharmacology* **2007**, *74*, 831–840. 10.1016/j.bcp.2007.06.029.
23. Shen, S.; Zhang, T.; Yuan, Y.; Lin, S.; Xu, J.; Ye, H. Effects of cinnamaldehyde on *Escherichia coli* and *Staphylococcus aureus* membrane. *Food Control* **2015**, *47*, 196–202. 10.1016/j.foodcont.2014.07.003.
24. Kot, B.; Sytykiewicz, H.; Sprawka, I.; Witeska, M. Effect of *trans*-cinnamaldehyde on methicillin-resistant *Staphylococcus aureus* biofilm formation: Metabolic activity assessment and analysis of the biofilm-associated genes expression. *International Journal of Molecular Sciences* **2019**, *21*, 102. 10.3390/ijms21010102.
25. Zhang, Y.; Liu, X.; Wang, Y.; Jiang, P.; Quek, S. Antibacterial activity and mechanism of cinnamon essential oil against *Escherichia coli* and *Staphylococcus aureus*. *Food Control* **2016**, *59*, 282–289. 10.1016/j.foodcont.2015.05.032.
26. Wagle, B.R.; Upadhyay, A.; Upadhyaya, I.; Shrestha, S.; Arsi, K.; Liyanage, R.; Venkitanarayanan, K.; Donoghue, D.J.; Donoghue, A.M. *Trans*-cinnamaldehyde, eugenol and carvacrol reduce *Campylobacter jejuni* biofilms and modulate expression of select genes and proteins. *Frontiers in Microbiology* **2019**, *10*, 1837. 10.3389/fmicb.2019.01837.
27. Silva, A.F.; dos Santos, A.R.; Coelho Trevisan, D.A.; Ribeiro, A.B.; Zanetti Campanerut-Sá, P.A.; Kukolj, C.; de Souza, E.M.; Cardoso, R.F.; Estivalet Svidzinski, T.I.; de Abreu Filho, B.A.; et al. Cinnamaldehyde induces changes in the protein profile of *Salmonella* Typhimurium biofilm. *Research in Microbiology* **2018**, *169*, 33–43. 10.1016/j.resmic.2017.09.007.
28. Liu, Y.; Wu, L.; Han, J.; Dong, P.; Luo, X.; Zhang, Y.; Zhu, L. Inhibition of biofilm formation and related gene expression of *Listeria monocytogenes* in response to four natural antimicrobial compounds and sodium hypochlorite. *Frontiers in Microbiology* **2021**, *11*, 3523. 10.3389/fmicb.2020.617473.
29. Di Pasqua, R.; Hoskins, N.; Betts, G.; Mauriello, G. Changes in membrane fatty acids composition of microbial cells induced by addiction of thymol, carvacrol, limonene,

cinnamaldehyde, and eugenol in the growing media. *Journal of Agricultural and Food Chemistry* **2006**, *54*, 2745–9. 10.1021/jf052722l.

30. Upadhyay, A.; Johny, A.K.; Amalaradjou, M.A.R.; Ananda Baskaran, S.; Kim, K.S.; Venkitanarayanan, K. Plant-derived antimicrobials reduce *Listeria monocytogenes* virulence factors *in vitro*, and down-regulate expression of virulence genes. *International Journal of Food Microbiology* **2012**, *157*, 88–94. 10.1016/j.ijfoodmicro.2012.04.018.
31. Gill, A.O.; Holley, R.A. Inhibition of membrane bound ATPases of *Escherichia coli* and *Listeria monocytogenes* by plant oil aromatics. *International Journal of Food Microbiology* **2006**, *111*, 170–174. 10.1016/j.ijfoodmicro.2006.04.046.
32. Oussalah, M.; Caillet, S.; Lacroix, M. Mechanism of action of Spanish oregano, Chinese cinnamon, and savory essential oils against cell membranes and walls of *Escherichia coli* O157:H7 and *Listeria monocytogenes*. *Journal of Food Protection* **2006**, *69*, 1046–1055. 10.4315/0362-028X-69.5.1046.
33. Wang, S.; Kang, O.H.; Kwon, D.Y. *Trans*-cinnamaldehyde exhibits synergy with conventional antibiotic against methicillin-resistant *Staphylococcus aureus*. *International Journal of Molecular Sciences* **2021**, *22*, 1–9. 10.3390/ijms22052752.
34. Ferro, T.A.F.; Araújo, J.M.M.; Pinto, B.L. do. S.; dos Santos, J.S.; Souza, E.B.; da Silva, B.L.R.; Colares, V.L.P.; Novais, T.M.G.; Filho, C.M.B.; Struve, C.; et al. Cinnamaldehyde inhibits *Staphylococcus aureus* virulence factors and protects against infection in a galleria mellonella model. *Frontiers in Microbiology* **2016**, *7*, 2052. 10.3389/fmicb.2016.02052.
35. Di Pasqua, R.; Betts, G.; Hoskins, N.; Edwards, M.; Ercolini, D.; Mauriello, G. Membrane toxicity of antimicrobial compounds from essential oils. *Journal of Agricultural and Food Chemistry* **2007**, *55*, 4863–4870. 10.1021/jf0636465.
36. Shahverdi, A.R.; Monsef-Esfahani, H.R.; Tavasoli, F.; Zaheri, A.; Mirjani, R. *Trans*-cinnamaldehyde from *Cinnamomum zeylanicum* bark essential oil reduces the clindamycin resistance of *Clostridium difficile in vitro*. *Journal of Food Science* **2007**, *72*, S055–S058. 10.1111/j.1750-3841.2006.00204.x.
37. Li, T.; Wang, D.; Liu, N.; Ma, Y.; Ding, T.; Mei, Y.; Li, J. Inhibition of quorum sensing-controlled virulence factors and biofilm formation in *Pseudomonas fluorescens* by cinnamaldehyde. *International Journal of Food Microbiology* **2018**, *269*, 98–106. 10.1016/j.ijfoodmicro.2018.01.023.
38. Yuan, W.; Seng, Z.; Kohli, G.S.; Yang, L.; Yuk, H.-G. Stress resistance development and genome-wide transcriptional response of *Escherichia coli* O157:H7 adapted to sublethal thymol, carvacrol, and *trans*-cinnamaldehyde. *Applied and Environmental Microbiology* **2018**, *84*. 10.1128/AEM.01616-18.
39. Mousavi, F.; Bojko, B.; Bessonneau, V.; Pawliszyn, J. Cinnamaldehyde characterization as an antibacterial agent toward *E. coli* metabolic profile using 96-Blade solid-phase microextraction coupled to liquid chromatography-mass spectrometry. *Journal of Proteome Research* **2016**, *15*, 963–975. 10.1021/acs.jproteome.5b00992.
40. Sun, Q.; Shang, B.; Wang, L.; Lu, Z.; Liu, Y. Cinnamaldehyde inhibits fungal growth and aflatoxin B1 biosynthesis by modulating the oxidative stress response of *Aspergillus flavus*. *Applied Microbiology and Biotechnology* **2016**, *100*, 1355–1364. 10.1007/s00253-015-7159-z.
41. Qu, S.; Yang, K.; Chen, L.; Liu, M.; Geng, Q.; He, X.; Li, Y.; Liu, Y.; Tian, J. Cinnamaldehyde, a promising natural preservative against *Aspergillus flavus*. *Frontiers in Microbiology* **2019**, *10*, 2895. 10.3389/fmicb.2019.02895.
42. Liang, D.; Xing, F.; Selvaraj, J.N.; Liu, X.; Wang, L.; Hua, H.; Zhou, L.; Zhao, Y.;

Wang, Y.; Liu, Y. Inhibitory effect of cinnamaldehyde, citral, and eugenol on aflatoxin biosynthetic gene expression and aflatoxin B1 biosynthesis in *Aspergillus flavus*. *Journal of Food Science* **2015**, *80*, M2917-24. 10.1111/1750-3841.13144.

43. Huang, F.; Kong, J.; Ju, J.; Zhang, Y.; Guo, Y.; Cheng, Y.; Qian, H.; Xie, Y.; Yao, W. Membrane damage mechanism contributes to inhibition of *trans*-cinnamaldehyde on *Penicillium italicum* using Surface-Enhanced Raman Spectroscopy (SERS). *Scientific Reports* **2019**, *9*, 490. 10.1038/s41598-018-36989-7.
44. OuYang, Q.; Duan, X.; Li, L.; Tao, N. Cinnamaldehyde exerts its antifungal activity by disrupting the cell wall integrity of *Geotrichum citri-aurantii*. *Frontiers in Microbiology* **2019**, *10*, 55. 10.3389/fmicb.2019.00055.
45. Kollanoor Johny, A.; Frye, J.G.; Donoghue, A.; Donoghue, D.J.; Porwollik, S.; McClelland, M.; Venkitanarayanan, K. Gene expression response of *Salmonella enterica* serotype Enteritidis phage type 8 to subinhibitory concentrations of the plant-derived compounds *trans*-cinnamaldehyde and eugenol. *Frontiers in Microbiology* **2017**, *8*, 1828. 10.3389/fmicb.2017.01828.
46. Niu, C.; Afre, S.; Gilbert, E.S. Subinhibitory concentrations of cinnamaldehyde interfere with quorum sensing. *Letters in Applied Microbiology* **2006**, *43*, 489–494. 10.1111/j.1472-765X.2006.02001.x.
47. Ahmed, S.A.K.S.; Rudden, M.; Smyth, T.J.; Dooley, J.S.G.; Marchant, R.; Banat, I.M. Natural quorum sensing inhibitors effectively downregulate gene expression of *Pseudomonas aeruginosa* virulence factors. *Applied Microbiology and Biotechnology* **2019**, *103*, 3521–3535. 10.1007/s00253-019-09618-0.
48. Topa, S.H.; Subramoni, S.; Palombo, E.A.; Kingshott, P.; Rice, S.A.; Blackall, L.L. Cinnamaldehyde disrupts biofilm formation and swarming motility of *Pseudomonas aeruginosa*. *Microbiology* **2018**, *164*, 1087–1097. 10.1099/mic.0.000692.
49. Sun, Q.; Li, J.; Sun, Y.; Chen, Q.; Zhang, L.; Le, T. The antifungal effects of cinnamaldehyde against *Aspergillus niger* and its application in bread preservation. *Food Chemistry* **2020**, *317*, 126405. 10.1016/j.foodchem.2020.126405.
50. Wang, L.; Jin, J.; Liu, X.; Wang, Y.; Liu, Y.; Zhao, Y.; Xing, F. Effect of cinnamaldehyde on morphological alterations of *Aspergillus ochraceus* and expression of key genes involved in ochratoxin a biosynthesis. *Toxins* **2018**, *10*. 10.3390/toxins10090340.
51. Lenardon, M.D.; Munro, C.A.; Gow, N.A. Chitin synthesis and fungal pathogenesis. *Current Opinion in Microbiology* 2010, *13*, 416–423. 10.1016/j.mib.2010.05.002.
52. Bang, K.H.; Lee, D.W.; Park, H.M.; Rhee, Y.H. Inhibition of fungal cell wall synthesizing enzymes by *trans*-cinnamaldehyde. *Bioscience, Biotechnology, and Biochemistry* **2000**, *64*, 1061–3. 10.1271/bbb.64.1061.
53. Nikaido, H. Molecular basis of bacterial outer membrane permeability revisited. *Microbiology and Molecular Biology Reviews : MMBR* **2003**, *67*, 593–656. 10.1128/MMBR.67.4.593-656.2003.
54. Sun, J.; Rutherford, S.T.; Silhavy, T.J.; Huang, K.C. Physical properties of the bacterial outer membrane. *Nature Reviews Microbiology* **2021**, 1–13. 10.1038/s41579-021-00638-0.
55. Nowotarska, S.W.; Nowotarski, K.J.; Friedman, M.; Situ, C. Effect of structure on the interactions between five natural antimicrobial compounds and phospholipids of bacterial cell membrane on model monolayers. *Molecules* **2014**, *19*, 7497–7515. 10.3390/molecules19067497.
56. Patrignani, F.; Iucci, L.; Belletti, N.; Gardini, F.; Guerzoni, M.E.; Lanciotti, R. Effects of sub-lethal concentrations of hexanal and 2-*(E)*-hexenal on membrane fatty acid composition and volatile compounds of *Listeria monocytogenes*, *Staphylococcus*

aureus, *Salmonella enteritidis* and *Escherichia coli*. *International Journal of Food Microbiology* **2008**, *123*, 1–8. 10.1016/j.ijfoodmicro.2007.09.009.

57. Douglas, L.M.; Konopka, J.B. Fungal membrane organization: the eisosome concept. *Annual Review of Microbiology* **2014**, *68*, 377–93. 10.1146/annurev-micro-091313-103507.
58. Hua, H.; Xing, F.; Selvaraj, J.N.; Wang, Y.; Zhao, Y.; Zhou, L.; Liu, X.; Liu, Y. Inhibitory effect of essential oils on *Aspergillus ochraceus* growth and ochratoxin A production. *PloS one* **2014**, *9*, e108285. 10.1371/journal.pone.0108285.
59. Chen, L.; Wang, Z.; Liu, L.; Qu, S.; Mao, Y.; Peng, X.; Li, Y.; Tian, J. Cinnamaldehyde inhibits *Candida albicans* growth by causing apoptosis and its treatment on vulvovaginal candidiasis and oropharyngeal candidiasis. *Applied Microbiology and Biotechnology* **2019**, *103*, 9037–9055. 10.1007/s00253-019-10119-3.
60. Wang, Y.; Feng, K.; Yang, H.; Yuan, Y.; Yue, T. Antifungal mechanism of cinnamaldehyde and citral combination against: *Penicillium expansum* based on FT-IR fingerprint, plasma membrane, oxidative stress and volatile profile. *RSC Advances* **2018**, *8*, 5806–5815. 10.1039/c7ra12191a.
61. Wang, Y.; Feng, K.; Yang, H.; Zhang, Z.; Yuan, Y.; Yue, T. Effect of cinnamaldehyde and citral combination on transcriptional profile, growth, oxidative damage and patulin biosynthesis of *Penicillium expansum*. *Frontiers in Microbiology* **2018**, *9*, 597. 10.3389/fmicb.2018.00597.
62. Ralser, M.; Wamelink, M.M.; Kowald, A.; Gerisch, B.; Heeren, G.; Struys, E.A.; Klipp, E.; Jakobs, C.; Breitenbach, M.; Lehrach, H.; et al. Dynamic rerouting of the carbohydrate flux is key to counteracting oxidative stress. *Journal of Biology* **2007**, *6*, 10. 10.1186/jbiol61.
63. Mullarky, E.; Cantley, L.C. Diverting glycolysis to combat oxidative stress. In *Innovative Medicine*; Springer Japan: Tokyo, 2015; pp. 3–23 ISBN 9784431556503. 10.1007/978-4-431-55651-0_1.
64. Zorov, D.B.; Juhaszova, M.; Sollott, S.J. Mitochondrial reactive oxygen species (ROS) and ROS-induced ROS release. *Physiological Reviews* 2014, *94*, 909–950. 10.1152/physrev.00026.2013.
65. Auten, R.L.; Davis, J.M. Oxygen toxicity and reactive oxygen species: The devil is in the details. *Pediatric Research* 2009, *66*, 121–127. 10.1203/PDR.0b013e3181a9eafb.
66. OuYang, Q.; Tao, N.; Zhang, M. A damaged oxidative phosphorylation mechanism is involved in the antifungal activity of citral against *Penicillium digitatum*. *Frontiers in Microbiology* **2018**, *9*, 239. 10.3389/fmicb.2018.00239.
67. Abisado, R.G.; Benomar, S.; Klaus, J.R.; Dandekar, A.A.; Chandler, J.R. Bacterial quorum sensing and microbial community interactions. *mBio* **2018**, *9*. 10.1128/mBio.02331-17.
68. Zetzmann, M.; Sánchez-Kopper, A.; Waidmann, M.S.; Blombach, B.; Riedel, C.U. Identification of the agr Peptide of *Listeria monocytogenes*. *Frontiers in Microbiology* **2016**, *7*, 989. 10.3389/fmicb.2016.00989.
69. Rieu, A.; Weidmann, S.; Garmyn, D.; Piveteau, P.; Guzzo, J. *agr* system of *Listeria monocytogenes* EGD-e: Role in adherence and differential expression pattern. *Applied and Environmental Microbiology* **2007**, *73*, 6125–33. 10.1128/AEM.00608-07.
70. Riedel, C.U.; Monk, I.R.; Casey, P.G.; Waidmann, M.S.; Gahan, C.G.M.; Hill, C. AgrD-dependent quorum sensing affects biofilm formation, invasion, virulence and global gene expression profiles in *Listeria monocytogenes*. *Molecular Microbiology* **2009**, *71*, 1177–1189. 10.1111/j.1365-2958.2008.06589.x.
71. Flemming, H.-C.; Wingender, J.; Szewzyk, U.; Steinberg, P.; Rice, S.A.; Kjelleberg,

S. Biofilms: an emergent form of bacterial life. *Nature Reviews Microbiology* **2016**, *14*, 563–575. 10.1038/nrmicro.2016.94.

72. Lemon, K.P.; Higgins, D.E.; Kolter, R. Flagellar motility is critical for *Listeria monocytogenes* biofilm formation. *Journal of Bacteriology* **2007**, *189*, 4418–4424. 10.1128/JB.01967-06.
73. Upadhyay, A.; Upadhyaya, I.; Kollanoor-Johny, A.; Venkitanarayanan, K. Antibiofilm effect of plant derived antimicrobials on *Listeria monocytogenes*. *Food Microbiology* **2013**, *36*, 79–89. 10.1016/j.fm.2013.04.010.
74. He, Z.; Huang, Z.; Jiang, W.; Zhou, W. Antimicrobial activity of cinnamaldehyde on *Streptococcus mutans* biofilms. *Frontiers in Microbiology* **2019**, *10*, 2241. 10.3389/fmicb.2019.02241.
75. Kim, Y.-G.; Lee, J.-H.; Kim, S.-I.; Baek, K.-H.; Lee, J. Cinnamon bark oil and its components inhibit biofilm formation and toxin production. *International Journal of Food Microbiology* **2015**, *195*, 30–39. 10.1016/j.ijfoodmicro.2014.11.028.
76. Feyaerts, J.; Rogiers, G.; Corthouts, J.; Michiels, C.W. Thiol-reactive natural antimicrobials and high pressure treatment synergistically enhance bacterial inactivation. *Innovative Food Science & Emerging Technologies* **2015**, *27*, 26–34. 10.1016/j.ifset.2014.12.005.
77. Langeveld, W.T.; Veldhuizen, E.J.A.; Burt, S.A. Synergy between essential oil components and antibiotics: a review. *Critical Reviews in Microbiology* **2014**, *40*, 76–94. 10.3109/1040841X.2013.763219.
78. Liu, Q.; Niu, H.; Zhang, W.; Mu, H.; Sun, C.; Duan, J. Synergy among thymol, eugenol, berberine, cinnamaldehyde and streptomycin against planktonic and biofilm-associated food-borne pathogens. *Letters in Applied Microbiology* **2015**, *60*, 421–430. 10.1111/lam.12401.
79. Karumathil, D.P.; Nair, M.S.; Gaffney, J.; Kollanoor-Johny, A.; Venkitanarayanan, K. *Trans*-cinnamaldehyde and eugenol increase *Acinetobacter baumannii* sensitivity to beta-lactam antibiotics. *Frontiers in Microbiology* **2018**, *9*, 1011. 10.3389/fmicb.2018.01011.
80. Kennepohl, D.; Farmer, S.; Morsch, L. Conjugate nucleophilic addition to α,β-unsaturated aldehydes and ketones. Available online: https://chem.libretexts.org/@go/page/36393 (accessed on Nov 18, 2021).
81. Doyle, A.A.; Krämer, T.; Kavanagh, K.; Stephens, J.C. Cinnamaldehydes: Synthesis, antibacterial evaluation, and the effect of molecular structure on antibacterial activity. *Results in Chemistry* **2019**, *1*, 100013. 10.1016/j.rechem.2019.100013.
82. Böhme, A.; Laqua, A.; Schüürmann, G. Chemoavailability of organic electrophiles: Impact of hydrophobicity and reactivity on their aquatic excess toxicity. *Chemical Research in Toxicology* **2016**, *29*, 952–962. 10.1021/acs.chemrestox.5b00398.
83. Sikkema, J.; de Bont, J.A.; Poolman, B. Mechanisms of membrane toxicity of hydrocarbons. *Microbiological Reviews* **1995**, *59*, 201–222. 10.1128/mr.59.2.201-222.1995.
84. Sauerland, M.; Mertes, R.; Morozzi, C.; Eggler, A.L.; Gamon, L.F.; Davies, M.J. Kinetic assessment of Michael addition reactions of α,β-unsaturated carbonyl compounds to amino acid and protein thiols. *Free Radical Biology and Medicine* **2021**, *169*, 1–11. 10.1016/j.freeradbiomed.2021.03.040.
85. Jackson, P.A.; Widen, J.C.; Harki, D.A.; Brummond, K.M. Covalent modifiers: A chemical perspective on the reactivity of α,β-unsaturated carbonyls with thiols via Hetero-Michael addition reactions. *Journal of Medicinal Chemistry* **2017**, *60*, 839–885. 10.1021/acs.jmedchem.6b00788.
86. Mayer, R.J.; Ofial, A.R. Nucleophilicity of glutathione: A link to Michael acceptor

reactivities. *Angewandte Chemie International Edition* **2019**, *58*, 17704–17708. 10.1002/anie.201909803.

87. Loi, V. Van; Rossius, M.; Antelmann, H. Redox regulation by reversible protein S-thiolation in bacteria. *Frontiers in Microbiology* **2015**, *6*, 187. 10.3389/fmicb.2015.00187.
88. Gopal, S.; Borovok, I.; Ofer, A.; Yanku, M.; Cohen, G.; Goebel, W.; Kreft, J.; Aharonowitz, Y. A multidomain fusion protein in *Listeria monocytogenes* catalyzes the two primary activities for glutathione biosynthesis. *Journal of Bacteriology* **2005**, *187*, 3839–3847. 10.1128/JB.187.11.3839-3847.2005.
89. Reniere, M.L.; Whiteley, A.T.; Hamilton, K.L.; John, S.M.; Lauer, P.; Brennan, R.G.; Portnoy, D.A. Glutathione activates virulence gene expression of an intracellular pathogen. *Nature* **2015**, *517*, 170–173. 10.1038/nature14029.
90. Boyland, E.; Chasseaud, L.F. Enzymes catalysing conjugations of glutathione with α,β-unsaturated carbonyl compounds. *Biochemical Journal* **1968**, *109*, 651–661. 10.1042/bj1090651.
91. Janzowski, C.; Glaab, V.; Mueller, C.; Straesser, U.; Kamp, H.G.; Eisenbrand, G. α,β-unsaturated carbonyl compounds: Induction of oxidative DNA damage in mammalian cells. *Mutagenesis* **2003**, *18*, 465–70. 10.1093/mutage/geg018.
92. Kiwamoto, R.; Ploeg, D.; Rietjens, I.M.C.M.; Punt, A. Dose-dependent DNA adduct formation by cinnamaldehyde and other food-borne α,β-unsaturated aldehydes predicted by physiologically based *in silico* modelling. *Toxicology in Vitro* **2016**, *31*, 114–125. 10.1016/j.tiv.2015.11.014.
93. Kiwamoto, R.; Spenkelink, A.; Rietjens, I.M.C.M.; Punt, A. An integrated QSAR-PBK/D modelling approach for predicting detoxification and DNA adduct formation of 18 acyclic food-borne α,β-unsaturated aldehydes. *Toxicology and Applied Pharmacology* **2015**, *282*, 108–117. 10.1016/j.taap.2014.10.014.
94. Kiwamoto, R.; Rietjens, I.M.C.M.; Punt, A. A physiologically based *in silico* model for *trans*-2-hexenal detoxification and DNA adduct formation in rat. *Chemical Research in Toxicology* **2012**, *25*, 2630–2641. 10.1021/tx3002669.
95. Böhme, A.; Thaens, D.; Paschke, A.; Schüürmann, G. Kinetic glutathione chemoassay to quantify thiol reactivity of organic electrophiles—application to α,β-unsaturated ketones, acrylates, and propiolates. *Chemical Research in Toxicology* **2009**, *22*, 742–750. 10.1021/tx800492x.
96. Böhme, A.; Thaens, D.; Schramm, F.; Paschke, A.; Schüürmann, G. Thiol reactivity and its impact on the ciliate toxicity of α,β-Unsaturated aldehydes, ketones, and esters. *Chemical Research in Toxicology* **2010**, *23*, 1905–1912. 10.1021/tx100226n.
97. Hayes, J.D.; Flanagan, J.U.; Jowsey, I.R. Glutathione transferase. *Annual Review of Pharmacology and Toxicology* **2005**, *45*, 51–88. 10.1146/annurev.pharmtox.45.120403.095857.
98. Allocati, N.; Federici, L.; Masulli, M.; Di Ilio, C. Glutathione transferases in bacteria. *FEBS Journal* **2009**, *276*, 58–75. 10.1111/j.1742-4658.2008.06743.x.
99. Allocati, N.; Federici, L.; Masulli, M.; Di Ilio, C. Distribution of glutathione transferases in Gram-positive bacteria and archaea. *Biochimie* **2012**, *94*, 588–96. 10.1016/j.biochi.2011.09.008.
100. Amslinger, S.; Al-Rifai, N.; Winter, K.; Wörmann, K.; Scholz, R.; Baumeister, P.; Wild, M. Reactivity assessment of chalcones by a kinetic thiol assay. *Org. Biomol. Chem.* **2013**, *11*, 549–554. 10.1039/C2OB27163J.
101. Autelitano, A.; Minassi, A.; Pagani, A.; Taglialatela-Scafati, O.; Appendino, G. The reaction of cinnamaldehyde and cinnam(o)yl derivatives with thiols. *Acta Pharmaceutica Sinica B* **2017**, *7*, 523–526. 10.1016/j.apsb.2017.06.005.

102. Winterbourn, C.C.; Hampton, M.B. Thiol chemistry and specificity in redox signaling. *Free Radical Biology and Medicine* **2008**, *45*, 549–561. 10.1016/j.freeradbiomed.2008.05.004.
103. Seidler, N.W. Basic biology of GAPDH. In *Advances in Experimental Medicine and Biology*; Advances in Experimental Medicine and Biology; Springer Netherlands: Dordrecht, 2013; Vol. 985, pp. 1–36 ISBN 9789400747159. 10.1007/978-94-007-4716-6_1.
104. Ezraty, B.; Gennaris, A.; Barras, F.; Collet, J.-F. Oxidative stress, protein damage and repair in bacteria. *Nature Reviews Microbiology* **2017**, *15*, 385–396. 10.1038/nrmicro.2017.26.
105. Carmel-Harel, O.; Storz, G. Roles of the glutathione- and thioredoxin-dependent reduction systems in the *Escherichia coli* and *Saccharomyces cerevisiae* responses to oxidative stress. *Annual Review of Microbiology* **2000**, *54*, 439–461. 10.1146/annurev.micro.54.1.439.
106. Uchida, K.; Stadtman, E.R. Covalent attachment of 4-hydroxynonenal to glyceraldehyde-3-phosphate dehydrogenase: A possible involvement of intra- and intermolecular cross-linking reaction. *Journal of Biological Chemistry* **1993**, *268*, 6388–6393. 10.1016/S0021-9258(18)53264-6.
107. Martyniuk, C.J.; Fang, B.; Koomen, J.M.; Gavin, T.; Zhang, L.; Barber, D.S.; LoPachin, R.M. Molecular mechanism of glyceraldehyde-3-phosphate dehydrogenase inactivation by α,β-unsaturated carbonyl derivatives. *Chemical Research in Toxicology* **2011**, *24*, 2302–2311. 10.1021/tx200437y.
108. Chew, E.-H.; Nagle, A.A.; Zhang, Y.; Scarmagnani, S.; Palaniappan, P.; Bradshaw, T.D.; Holmgren, A.; Westwell, A.D. Cinnamaldehydes inhibit thioredoxin reductase and induce Nrf2: Potential candidates for cancer therapy and chemoprevention. *Free Radical Biology and Medicine* **2010**, *48*, 98–111. 10.1016/j.freeradbiomed.2009.10.028.
109. Lu, J.; Holmgren, A. The thioredoxin antioxidant system. *Free Radical Biology and Medicine* 2014, *66*, 75–87. 10.1016/j.freeradbiomed.2013.07.036.
110. McCarver, A.C.; Lessner, D.J. Molecular characterization of the thioredoxin system from *Methanosarcina acetivorans*. *FEBS Journal* **2014**, *281*, 4598–4611. 10.1111/febs.12964.
111. Glaser, P.; Frangeul, L.; Buchrieser, C.; Rusniok, C.; Amend, A.; Baquero, F.; Berche, P.; Bloecker, H.; Brandt, P.; Chakraborty, T.; et al. Comparative genomics of *Listeria* species. *Science* **2001**, *294*, 849–852. 10.1126/science.1063447.
112. Gopal, S.; Srinivas, V.; Zameer, F.; Kreft, J. Prediction of proteins putatively involved in the thiol: disulfide redox metabolism of a bacterium (*Listeria*): The CXXC motif as query sequence. *In Silico Biology* **2009**, *9*, 407–414. 10.3233/ISB-2009-0409.
113. Cheng, C.; Dong, Z.; Han, X.; Wang, H.; Jiang, L.; Sun, J.; Yang, Y.; Ma, T.; Shao, C.; Wang, X.; et al. Thioredoxin a is essential for motility and contributes to host infection of *Listeria monocytogenes* via redox interactions. *Frontiers in Cellular and Infection Microbiology* **2017**, *7*, 287. 10.3389/fcimb.2017.00287.
114. van Iersel, M.L.P..; Ploemen, J.-P.H.T..; Lo Bello, M.; Federici, G.; van Bladeren, P.J. Interactions of α, β-unsaturated aldehydes and ketones with human glutathione S-transferase P1-1. *Chemico-Biological Interactions* **1997**, *108*, 67–78. 10.1016/S0009-2797(97)00096-3.
115. Chien, C.; Kirollos, K.S.; Linderman, R.J.; Dauterman, W.C. α,β-Unsaturated carbonyl compounds: inhibition of rat liver glutathione S-transferase isozymes and chemical reaction with reduced glutathione. *Biochimica et Biophysica Acta (BBA) - Protein Structure and Molecular Enzymology* **1994**, *1204*, 175–180. 10.1016/0167-

4838(94)90006-X.
116. Kiwamoto, R.; Spenkelink, A.; Rietjens, I.M.C.M.; Punt, A. A physiologically based in silico model for *trans*-2-hexenal detoxification and DNA adduct formation in human including interindividual variation indicates efficient detoxification and a negligible genotoxicity risk. *Archives of Toxicology* **2013**, *87*, 1725–1737. 10.1007/s00204-013-1091-8.
117. Srivastava, S.; Watowich, S.J.; Petrash, J.M.; Srivastava, S.K.; Bhatnagar, A. Structural and kinetic determinants of aldehyde reduction by aldose reductase. *Biochemistry* **1999**, *38*, 42–54. 10.1021/bi981794l.
118. bander Jagt, D.L.; Kolb, N.S.; bander Jagt, T.J.; Chino, J.; Martinez, F.J.; Hunsaker, L.A.; Royer, R.E. Substrate specificity of human aldose reductase: identification of 4-hydroxynonenal as an endogenous substrate. *Biochimica et Biophysica Acta (BBA) - Protein Structure and Molecular Enzymology* **1995**, *1249*, 117–126. 10.1016/0167-4838(95)00021-L.
119. Shen, Y.; Zhong, L.; Johnson, S.; Cao, D. Human aldo–keto reductases 1B1 and 1B10: A comparative study on their enzyme activity toward electrophilic carbonyl compounds. *Chemico-Biological Interactions* **2011**, *191*, 192–198. 10.1016/j.cbi.2011.02.004.
120. de Smidt, O.; du Preez, J.C.; Albertyn, J. The alcohol dehydrogenases of *Saccharomyces cerevisiae*: a comprehensive review. *FEMS Yeast Research* **2008**, *8*, 967–978. 10.1111/j.1567-1364.2008.00387.x.
121. Klibanov, A.M.; Giannousis, P.P. Geometric specificity of alcohol dehydrogenases and its potential for separation of *trans* and *cis* isomers of unsaturated aldehydes. *Proceedings of the National Academy of Sciences* **1982**, *79*, 3462–3465. 10.1073/pnas.79.11.3462.
122. Larroy, C.; Fernández, M.R.; González, E.; Parés, X.; Biosca, J.A. Characterization of the *Saccharomyces cerevisiae* YMR318C (ADH6) gene product as a broad specificity NADPH-dependent alcohol dehydrogenase: relevance in aldehyde reduction. *The Biochemical journal* **2002**, *361*, 163–72. 10.1042/0264-6021:3610163.
123. Larroy, C.; Parés, X.; Biosca, J.A. Characterization of a *Saccharomyces cerevisiae* NADP(H)-dependent alcohol dehydrogenase (ADHVII), a member of the cinnamyl alcohol dehydrogenase family. *European Journal of Biochemistry* **2002**, *269*, 5738–5745. 10.1046/j.1432-1033.2002.03296.x.
124. Pennacchio, A.; Esposito, L.; Zagari, A.; Rossi, M.; Raia, C.A. Role of Tryptophan 95 in substrate specificity and structural stability of *Sulfolobus solfataricus* alcohol dehydrogenase. *Extremophiles* **2009**, *13*, 751–761. 10.1007/s00792-009-0256-0.
125. Liu, X.; Bastian, S.; Snow, C.D.; Brustad, E.M.; Saleski, T.E.; Xu, J.; Meinhold, P.; Arnold, F.H. Structure-guided engineering of *Lactococcus lactis* alcohol dehydrogenase LlAdhA for improved conversion of isobutyraldehyde to isobutanol. *Journal of Biotechnology* **2013**, *164*, 188–195. 10.1016/j.jbiotec.2012.08.008.
126. Pérez, J.M.; Arenas, F.A.; Pradenas, G.A.; Sandoval, J.M.; Vásquez, C.C. *Escherichia coli* YqhD exhibits aldehyde reductase activity and protects from the harmful effect of lipid peroxidation-derived aldehydes. *Journal of Biological Chemistry* **2008**, *283*, 7346–7353. 10.1074/jbc.M708846200.
127. Jarboe, L.R. YqhD: A broad-substrate range aldehyde reductase with various applications in production of biorenewable fuels and chemicals. *Applied Microbiology and Biotechnology* **2011**, *89*, 249–257. 10.1007/s00253-010-2912-9.
128. Jeudy, S.; Monchois, V.; Maza, C.; Claverie, J.M.; Abergel, C. Crystal structure of *Escherichia coli* DkgA, a broad-specificity aldo-keto reductase. *Proteins: Structure, Function, and Bioinformatics* **2005**, *62*, 302–307. 10.1002/prot.20710.

129. Shortall, K.; Djeghader, A.; Magner, E.; Soulimane, T. Insights into aldehyde dehydrogenase enzymes: A structural perspective. *Frontiers in Molecular Biosciences* **2021**, *8*, 410. 10.3389/fmolb.2021.659550.
130. Klyosov, A.A. Kinetics and specificity of human liver aldehyde dehydrogenases toward aliphatic, aromatic, and fused polycyclic aldehydes. *Biochemistry* **1996**, *35*, 4457–4467. 10.1021/bi9521102.
131. Wang, M.; Han, C.; Yin, S. Substrate specificity of human and yeast aldehyde dehydrogenases. *Chemico-Biological Interactions* **2009**, *178*, 36–39. 10.1016/j.cbi.2008.10.002.
132. Winkler, C.K.; Tasnádi, G.; Clay, D.; Hall, M.; Faber, K. Asymmetric bioreduction of activated alkenes to industrially relevant optically active compounds. *Journal of Biotechnology* **2012**, *162*, 381–389. 10.1016/j.jbiotec.2012.03.023.
133. Toogood, H.S.; Scrutton, N.S. New developments in 'ene'-reductase catalysed biological hydrogenations. *Current Opinion in Chemical Biology* **2014**, *19*, 107–115. 10.1016/j.cbpa.2014.01.019.
134. Kohli, R.M.; Massey, V. The oxidative half-reaction of Old Yellow Enzyme. *Journal of Biological Chemistry* **1998**, *273*, 32763–32770. 10.1074/jbc.273.49.32763.
135. Scholtissek, A.; Tischler, D.; Westphal, A.; van Berkel, W.; Paul, C. Old Yellow Enzyme-catalysed asymmetric hydrogenation: linking family roots with improved catalysis. *Catalysts* **2017**, *7*, 130. 10.3390/catal7050130.
136. Fitzpatrick, T.B.; Amrhein, N.; Macheroux, P. Characterization of YqjM, an Old Yellow Enzyme homolog from *Bacillus subtilis* involved in the oxidative stress response. *Journal of Biological Chemistry* **2003**, *278*, 19891–19897. 10.1074/jbc.M211778200.
137. Kitzing, K.; Fitzpatrick, T.B.; Wilken, C.; Sawa, J.; Bourenkov, G.P.; Macheroux, P.; Clausen, T. The 1.3 Å crystal structure of the flavoprotein YqjM reveals a novel class of Old Yellow Enzymes. *Journal of Biological Chemistry* **2005**, *280*, 27904–27913. 10.1074/jbc.M502587200.
138. Toogood, H.S.; Fryszkowska, A.; Hare, V.; Fisher, K.; Roujeinikova, A.; Leys, D.; Gardiner, J.M.; Stephens, G.M.; Scrutton, N.S. Structure-based insight into the asymmetric bioreduction of the C=C double bond of α,β-unsaturated nitroalkenes by pentaerythritol tetranitrate reductase. *Advanced Synthesis & Catalysis* **2008**, *350*, 2789–2803. 10.1002/adsc.200800561.
139. Spiegelhauer, O.; Dickert, F.; Mende, S.; Niks, D.; Hille, R.; Ullmann, M.; Dobbek, H. Kinetic characterization of xenobiotic reductase A from *Pseudomonas putida* 86. *Biochemistry* **2009**, *48*, 11412–20. 10.1021/bi901370u.
140. Lee, S.H.; Choi, D.S.; Pesic, M.; Lee, Y.W.; Paul, C.E.; Hollmann, F.; Park, C.B. Cofactor-free, direct photoactivation of enoate reductases for the asymmetric reduction of C=C bonds. *Angewandte Chemie International Edition* **2017**, *56*, 8681–8685. 10.1002/anie.201702461.
141. Sheng, X.; Yan, M.; Xu, L.; Wei, M. Identification and characterization of a novel Old Yellow Enzyme from *Bacillus subtilis* str.168. *Journal of Molecular Catalysis B: Enzymatic* **2016**, *130*, 18–24. 10.1016/j.molcatb.2016.04.011.
142. Schittmayer, M.; Glieder, A.; Uhl, M.K.; Winkler, A.; Zach, S.; Schrittwieser, J.H.; Kroutil, W.; Macheroux, P.; Gruber, K.; Kambourakis, S.; et al. Old Yellow Enzyme-catalyzed dehydrogenation of saturated ketones. *Advanced Synthesis & Catalysis* **2011**, *353*, 268–274. 10.1002/adsc.201000862.
143. Buckman, J.; Miller, S.M. Binding and reactivity of *Candida albicans* estrogen binding protein with steroid and other substrates. *Biochemistry* **1998**, *37*, 14326–14336. 10.1021/bi981106y.

144. Chaparro-Riggers, J.F.; Rogers, T.A.; Vazquez-Figueroa, E.; Polizzi, K.M.; Bommarius, A.S. Comparison of three enoate reductases and their potential use for biotransformations. *Advanced Synthesis and Catalysis* **2007**, *349*, 1521–1531. 10.1002/adsc.200700074.
145. Fryszkowska, A.; Toogood, H.; Sakuma, M.; Gardiner, J.M.; Stephens, G.M.; Scrutton, N.S. Asymmetric reduction of activated alkenes by pentaerythritol tetranitrate reductase: Specificity and control of stereochemical outcome by reaction optimisation. *Advanced Synthesis & Catalysis* **2009**, *351*, 2976–2990. 10.1002/adsc.200900574.
146. Opperman, D.J.; Sewell, B.T.; Litthauer, D.; Isupov, M.N.; Littlechild, J.A.; van Heerden, E. Crystal structure of a thermostable Old Yellow Enzyme from *Thermus scotoductus* SA-01. *Biochemical and Biophysical Research Communications* **2010**, *393*, 426–431. 10.1016/j.bbrc.2010.02.011.
147. Buchanan, R.L.; Gorris, L.G.M.; Hayman, M.M.; Jackson, T.C.; Whiting, R.C. A review of *Listeria monocytogenes*: An update on outbreaks, virulence, dose-response, ecology, and risk assessments. *Food Control* **2017**, *75*, 1–13. 10.1016/j.foodcont.2016.12.016.
148. Yin, Y.; Tan, W.; Wang, G.; Kong, S.; Zhou, X.; Zhao, D.; Jia, Y.; Pan, Z.; Jiao, X. Geographical and longitudinal analysis of *Listeria monocytogenes* genetic diversity reveals its correlation with virulence and unique evolution. *Microbiological Research* **2015**, *175*, 84–92. 10.1016/j.micres.2015.04.002.
149. den Bakker, H.C.; Bundrant, B.N.; Fortes, E.D.; Orsi, R.H.; Wiedmann, M. A population genetics-based and phylogenetic approach to understanding the evolution of virulence in the genus *Listeria*. *Applied and Environmental Microbiology* **2010**, *76*, 6085–6100. 10.1128/AEM.00447-10.
150. de Noordhout, C.M.; Devleesschauwer, B.; Angulo, F.J.; Verbeke, G.; Haagsma, J.; Kirk, M.; Havelaar, A.; Speybroeck, N. The global burden of listeriosis: A systematic review and meta-analysis. *The Lancet Infectious Diseases* **2014**, *14*, 1073–1082. 10.1016/S1473-3099(14)70870-9.
151. ECDC Listeriosis, Annual Epidemiological report for 2017. *Surveillance Report* **2018**, 11.
152. Lamont, R.F.; Sobel, J.; Mazaki-Tovi, S.; Kusanovic, J.P.; Vaisbuch, E.; Kim, S.K.; Uldbjerg, N.; Romero, R. Listeriosis in human pregnancy: a systematic review. *Journal of Perinatal Medicine* **2011**, *39*, 227–36. 10.1515/jpm.2011.035.
153. Sauders, B.D.; Overdevest, J.; Fortes, E.; Windham, K.; Schukken, Y.; Lembo, A.; Wiedmann, M. Diversity of *Listeria* species in urban and natural environments. *Applied and Environmental Microbiology* **2012**, *78*, 4420–4433. 10.1128/AEM.00282-12.
154. Schlech, W.F.; Lavigne, P.M.; Bortolussi, R.A.; Allen, A.C.; Haldane, E.V.; Wort, A.J.; Hightower, A.W.; Johnson, S.E.; King, S.H.; Nicholls, E.S.; et al. Epidemic listeriosis — evidence for transmission by food. *New England Journal of Medicine* **1983**, *308*, 203–206. 10.1056/nejm198301273080407.
155. Matle, I.; Mbatha, K.R.; Madoroba, E. A review of *Listeria monocytogenes* from meat and meat products: Epidemiology, virulence factors, antimicrobial resistance and diagnosis. *Onderstepoort Journal of Veterinary Research* **2020**, *87*, e1–e20. 10.4102/ojvr.v87i1.1869.
156. Bucur, F.I.; Grigore-Gurgu, L.; Crauwels, P.; Riedel, C.U.; Nicolau, A.I. Resistance of *Listeria monocytogenes* to stress conditions encountered in food and food processing environments. *Frontiers in Microbiology* **2018**, *9*, 2700. 10.3389/fmicb.2018.02700.
157. Wiktorczyk-Kapischke, N.; Skowron, K.; Grudlewska-Buda, K.; Wałecka-Zacharska,

E.; Korkus, J.; Gospodarek-Komkowska, E. Adaptive response of *Listeria monocytogenes* to the stress factors in the food processing environment. *Frontiers in Microbiology* **2021**, *12*, 710085. 10.3389/fmicb.2021.710085.

158. Tasara, T.; Stephan, R. Cold stress tolerance of *Listeria monocytogenes*: A review of molecular adaptive mechanisms and food safety implications. *Journal of food protection* **2006**, *69*, 1473–84. 10.4315/0362-028x-69.6.1473.
159. Vollmer, W.; Blanot, D.; De Pedro, M.A. Peptidoglycan structure and architecture. *FEMS Microbiology Reviews* **2008**, *32*, 149–167. 10.1111/j.1574-6976.2007.00094.x.
160. Pensinger, D.A.; Boldon, K.M.; Chen, G.Y.; Vincent, W.J.B.; Sherman, K.; Xiong, M.; Schaenzer, A.J.; Forster, E.R.; Coers, J.; Striker, R.; et al. The *Listeria monocytogenes* PASTA kinase PrkA and its substrate YvcK are required for cell wall homeostasis, metabolism, and virulence. *PLOS Pathogens* **2016**, *12*, e1006001. 10.1371/journal.ppat.1006001.
161. Mir, M.; Prisic, S.; Kang, C.M.; Lun, S.; Guo, H.; Murry, J.P.; Rubin, E.J.; Husson, R.N. Mycobacterial gene *cuvA* is required for optimal nutrient utilization and virulence. *Infection and Immunity* **2014**, *82*, 4104–4117. 10.1128/IAI.02207-14.
162. Patel, V.; Wu, Q.; Chandrangsu, P.; Helmann, J.D. A metabolic checkpoint protein GlmR is important for diverting carbon into peptidoglycan biosynthesis in *Bacillus subtilis*. *PLoS Genetics* **2018**, *14*, e1007689. 10.1371/journal.pgen.1007689.
163. Görke, B.; Foulquier, E.; Galinier, A. YvcK of *Bacillus subtilis* is required for a normal cell shape and for growth on Krebs cycle intermediates and substrates of the pentose phosphate pathway. *Microbiology* **2005**, *151*, 3777–3791. 10.1099/mic.0.28172-0.
164. Barreteau, H.; Kovač, A.; Boniface, A.; Sova, M.; Gobec, S.; Blanot, D. Cytoplasmic steps of peptidoglycan biosynthesis. *FEMS Microbiology Reviews* **2008**, *32*, 168–207. 10.1111/j.1574-6976.2008.00104.x.
165. Foulquier, E.; Pompeo, F.; Byrne, D.; Fierobe, H.P.; Galinier, A. Uridine diphosphate N-acetylglucosamine orchestrates the interaction of GlmR with either YvcJ or GlmS in *Bacillus subtilis*. *Scientific Reports* **2020**, *10*, 1–13. 10.1038/s41598-020-72854-2.
166. Fugett, E.; Fortes, E.; Nnoka, C.; Wiedmann, M. International Life Sciences Institute North America *Listeria monocytogenes* strain collection: Development of standard *Listeria monocytogenes* strain sets for research and validation studies. *Journal of Food Protection* **2006**, *69*, 2929–2938. 10.4315/0362-028X-69.12.2929.
167. Grant, S.G.N.; Jessee, J.; Bloom, F.R.; Hanahan, D. Differential plasmid rescue from transgenic mouse DNAs into *Escherichia coli* methylation-restriction mutants. *Proceedings of the National Academy of Sciences of the United States of America* **1990**, *87*, 4645–4649. 10.1073/pnas.87.12.4645.
168. Simon, R.; Priefer, U.; Pühler, A. A broad host range mobilization system for *in vivo* genetic engineering: Transposon mutagenesis in Gram-negative bacteria. *Bio/Technology* **1983**, *1*, 784–791. 10.1038/nbt1183-784.
169. Baranyi, J.; Roberts, T.A. A dynamic approach to predicting bacterial growth in food. *International Journal of Food Microbiology* **1994**, *23*, 277–294. 10.1016/0168-1605(94)90157-0.
170. Monk, I.R.; Gahan, C.G.M.; Hill, C. Tools for functional postgenomic analysis of *Listeria monocytogenes*. *Applied and Environmental Microbiology* **2008**, *74*, 3921–3934. 10.1128/AEM.00314-08.
171. Smith, K.; Youngman, P. Use of a new integrational vector to investigate compartment-specific expression of the *Bacillus subtilis spoIIM* gene. *Biochimie* **1992**, *74*, 705–711. 10.1016/0300-9084(92)90143-3.
172. Camilli, A.; Tilney, L.G.; Portnoy, D.A. Dual roles of plcA in *Listeria monocytogenes* pathogenesis. *Molecular Microbiology* **1993**, *8*, 143–157. 10.1111/j.1365-

2958.1993.tb01211.x.
173. Sliusarenko, O.; Heinritz, J.; Emonet, T.; Jacobs-Wagner, C. High-throughput, subpixel precision analysis of bacterial morphogenesis and intracellular spatio-temporal dynamics. *Molecular Microbiology* **2011**, *80*, 612–627. 10.1111/j.1365-2958.2011.07579.x.
174. Wurtzel, O.; Sesto, N.; Mellin, J.R.; Karunker, I.; Edelheit, S.; Bécavin, C.; Archambaud, C.; Cossart, P.; Sorek, R. Comparative transcriptomics of pathogenic and non-pathogenic *Listeria* species. *Molecular Systems Biology* **2012**, *8*, 583. 10.1038/msb.2012.11.
175. Cooper, S.J.; Leonard, G.A.; McSweeney, S.M.; Thompson, A.W.; Naismith, J.H.; Qamar, S.; Plater, A.; Berry, A.; Hunter, W.N. The crystal structure of a class II fructose-1,6-bisphosphate aldolase shows a novel binuclear metal-binding active site embedded in a familiar fold. *Structure* **1996**, *4*, 1303–1315. 10.1016/S0969-2126(96)00138-4.
176. Hove-Jensen, B.; Andersen, K.R.; Kilstrup, M.; Martinussen, J.; Switzer, R.L.; Willemoës, M. Phosphoribosyl diphosphate (PRPP): Biosynthesis, enzymology, utilization, and metabolic significance. *Microbiology and Molecular Biology Reviews* **2017**, *81*. 10.1128/MMBR.00040-16.
177. Bertram, R.; Rigali, S.; Wood, N.; Lulko, A.T.; Kuipers, O.P.; Titgemeyer, F. Regulon of the N -acetylglucosamine utilization regulator NagR in *Bacillus subtilis*. *Journal of Bacteriology* **2011**, *193*, 3525–3536. 10.1128/JB.00264-11.
178. Gaugué, I.; Oberto, J.; Plumbridge, J. Regulation of amino sugar utilization in *Bacillus subtilis* by the GntR family regulators, NagR and GamR. *Molecular Microbiology* **2014**, *92*, 100–115. 10.1111/mmi.12544.
179. Zeng, L.; Burne, R.A. NagR differentially regulates the expression of the *glmS* and *nagAB* genes required for amino sugar metabolism by *Streptococcus mutans*. *Journal of Bacteriology* **2015**, *197*, 3533–3544. 10.1128/JB.00606-15.
180. Reizer, J..; Bachem, S..; Reizer, A..; Arnaud, M..; Saier Jr, M.H..; Stülke, J.. Novel phosphotransferase system genes revealed by genome analysis – the complete complement of PTS proteins encoded within the genome of *Bacillus subtilis*. *Microbiology* **1999**, *145*, 3419–3429. 10.1099/00221287-145-12-3419.
181. Vincent, F.; Yates, D.; Garman, E.; Davies, G.J.; Brannigan, J.A. The three-dimensional structure of the N-acetylglucosamine-6-phosphate deacetylase, NagA, from *Bacillus subtilis*. *Journal of Biological Chemistry* **2004**, *279*, 2809–2816. 10.1074/jbc.M310165200.
182. Vincent, F.; Davies, G.J.; Brannigan, J.A. Structure and kinetics of a monomeric glucosamine 6-phosphate deaminase: Missing link of the NagB superfamily? *Journal of Biological Chemistry* **2005**, *280*, 19649–19655. 10.1074/jbc.M502131200.
183. Huang, T.-C.; Fu, H.-Y.; Ho, C.-T.; Tan, D.; Huang, Y.-T.; Pan, M.-H. Induction of apoptosis by cinnamaldehyde from indigenous cinnamon *Cinnamomum osmophloeum* Kaneh through reactive oxygen species production, glutathione depletion, and caspase activation in human leukemia K562 cells. *Food Chemistry* **2007**, *103*, 434–443. 10.1016/j.foodchem.2006.08.018.
184. Staerck, C.; Gastebois, A.; Vandeputte, P.; Calenda, A.; Larcher, G.; Gillmann, L.; Papon, N.; Bouchara, J.P.; Fleury, M.J.J. Microbial antioxidant defense enzymes. *Microbial Pathogenesis* **2017**, *110*, 56–65. 10.1016/j.micpath.2017.06.015.
185. Nikel, P.I.; Fuhrer, T.; Chavarría, M.; Sánchez-Pascuala, A.; Sauer, U.; de Lorenzo, V. Reconfiguration of metabolic fluxes in *Pseudomonas putida* as a response to sub-lethal oxidative stress. *ISME Journal* **2021**, *15*, 1751–1766. 10.1038/s41396-020-00884-9.
186. Christodoulou, D.; Link, H.; Fuhrer, T.; Kochanowski, K.; Gerosa, L.; Sauer, U.

Reserve flux capacity in the pentose phosphate pathway enables *Escherichia coli*'s rapid response to oxidative stress. *Cell Systems* **2018**, *6*, 569-578.e7. 10.1016/j.cels.2018.04.009.

187. Egan, A.J.F.; Errington, J.; Vollmer, W. Regulation of peptidoglycan synthesis and remodelling. *Nature Reviews Microbiology* **2020**, *18*, 446–460. 10.1038/s41579-020-0366-3.
188. Oliva, G.; Fontes, M.R.; Garratt, R.C.; Altamirano, M.M.; Calcagno, M.L.; Horjales, E. Structure and catalytic mechanism of glucosamine 6-phosphate deaminase from *Escherichia coli* at 2.1 å resolution. *Structure* **1995**, *3*, 1323–1332. 10.1016/S0969-2126(01)00270-2.
189. Isupov, M.N.; Obmolova, G.; Butterworth, S.; Badet-Denisot, M.A.; Badet, B.; Polikarpov, I.; Littlechild, J.A.; Teplyakov, A. Substrate binding is required for assembly of the active conformation of the catalytic site in Ntn amidotransferases: Evidence from the 1.8 Å crystal structure of the glutaminase domain of glucosamine 6- phosphate synthase. *Structure* **1996**, *4*, 801–810. 10.1016/S0969-2126(96)00087-1.
190. Badet, B.; Vermoote, P.; Haumont, P.Y.; Lederer, F.; LeGoffic, F. Glucosamine synthetase from *Escherichia coli*: purification, properties, and glutamine-utilizing site location. *Biochemistry* **1987**, *26*, 1940–8. 10.1021/bi00381a023.
191. Tinsley, R.A.; Furchak, J.R.W.; Walter, N.G. *Trans*-acting *glmS* catalytic riboswitch: Locked and loaded. *Rna* **2007**, *13*, 468–477. 10.1261/rna.341807.
192. Winkler, W.C.; Nahvi, A.; Roth, A.; Collins, J.A.; Breaker, R.R. Control of gene expression by a natural metabolite-responsive ribozyme. *Nature* **2004**, *428*, 281–286. 10.1038/nature02362.
193. Foulquier, E.; Galinier, A. YvcK, a protein required for cell wall integrity and optimal carbon source utilization, binds uridine diphosphate-sugars. *Scientific Reports* **2017**, *7*, 4139. 10.1038/s41598-017-04064-2.
194. Gonzalez, G.M.; Durica-Mitic, S.; Hardwick, S.W.; Moncrieffe, M.C.; Resch, M.; Neumann, P.; Ficner, R.; Görke, B.; Luisi, B.F. Structural insights into RapZ-mediated regulation of bacterial amino-sugar metabolism. *Nucleic Acids Research* **2017**, *45*, 10845–10860. 10.1093/nar/gkx732.
195. Göpel, Y.; Papenfort, K.; Reichenbach, B.; Vogel, J.; Görke, B. Targeted decay of a regulatory small RNA by an adaptor protein for RNase E and counteraction by an anti-adaptor RNA. *Genes and Development* **2013**, *27*, 552–564. 10.1101/gad.210112.112.
196. Resch, M.; Schiltz, E.; Titgemeyer, F.; Muller, Y.A. Insight into the induction mechanism of the GntR/HutC bacterial transcription regulator YvoA. *Nucleic Acids Research* **2010**, *38*, 2485–2497. 10.1093/nar/gkp1191.
197. Fillenberg, S.B.; Grau, F.C.; Seidel, G.; Muller, Y.A. Structural insight into operator *dre*-sites recognition and effector binding in the GntR/HutC transcription regulator NagR. *Nucleic Acids Research* **2015**, *43*, 1283–1296. 10.1093/nar/gku1374.
198. Stincone, A.; Prigione, A.; Cramer, T.; Wamelink, M.M.C.; Campbell, K.; Cheung, E.; Olin-Sandoval, V.; Grüning, N.M.; Krüger, A.; Tauqeer Alam, M.; et al. The return of metabolism: Biochemistry and physiology of the pentose phosphate pathway. *Biological Reviews* **2015**, *90*, 927–963. 10.1111/brv.12140.
199. Doan, T.; Aymerich, S. Regulation of the central glycolytic genes in *Bacillus subtilis*: Binding of the repressor CggR to its single DNA target sequence is modulated by fructose-1,6-bisphosphate. *Molecular Microbiology* **2003**, *47*, 1709–1721. 10.1046/j.1365-2958.2003.03404.x.
200. Zamboni, N.; Fischer, E.; Laudert, D.; Aymerich, S.; Hohmann, H.P.; Sauer, U. The *Bacillus subtilis yqjI* gene encodes the NADP+-dependent 6-P-gluconate dehydrogenase in the pentose phosphate pathway. *Journal of Bacteriology* **2004**, *186*,

4528–4534. 10.1128/JB.186.14.4528-4534.2004.
201. Yadav, A.K.; Espaillat, A.; Cava, F. Bacterial strategies to preserve cell wall integrity against environmental threats. *Frontiers in Microbiology* 2018, *9*, 2064. 10.3389/fmicb.2018.02064.
202. Bierne, H.; Cossart, P. *Listeria monocytogenes* surface proteins: From genome predictions to function. *Microbiology and Molecular Biology Reviews* **2007**, *71*, 377–397. 10.1128/MMBR.00039-06.
203. Gust, A.A. Peptidoglycan perception in plants. *PLOS Pathogens* **2015**, *11*, e1005275. 10.1371/journal.ppat.1005275.
204. Irazoki, O.; Hernandez, S.B.; Cava, F. Peptidoglycan muropeptides: Release, perception, and functions as signaling molecules. *Frontiers in Microbiology* **2019**, *10*. 10.3389/fmicb.2019.00500.
205. Vollmer, W.; Tomasz, A. The *pgdA* gene encodes for a peptidoglycan N-acetylglucosamine deacetylase in *Streptococcus pneumoniae*. *Journal of Biological Chemistry* **2000**, *275*, 20496–20501. 10.1074/jbc.M910189199.
206. Boneca, I.G.; Dussurget, O.; Cabanes, D.; Nahori, M.-A.; Sousa, S.; Lecuit, M.; Psylinakis, E.; Bouriotis, V.; Hugot, J.-P.; Giovannini, M.; et al. A critical role for peptidoglycan N-deacetylation in *Listeria* evasion from the host innate immune system. *Proceedings of the National Academy of Sciences* **2007**, *104*, 997–1002. 10.1073/pnas.0609672104.
207. Fittipaldi, N.; Sekizaki, T.; Takamatsu, D.; de la Cruz Domínguez-Punaro, M.; Harel, J.; Bui, N.K.; Vollmer, W.; Gottschalk, M. Significant contribution of the *pgdA* gene to the virulence of *Streptococcus suis*. *Molecular Microbiology* **2008**, *70*, 1120–1135. 10.1111/j.1365-2958.2008.06463.x.
208. Brott, A.S.; Clarke, A.J. Peptidoglycan O-acetylation as a virulence factor: Its effect on lysozyme in the innate immune system. *Antibiotics* 2019, *8*. 10.3390/antibiotics8030094.
209. Espaillat, A.; Forsmo, O.; El Biari, K.; Björk, R.; Lemaitre, B.; Trygg, J.; Cañada, F.J.; de Pedro, M.A.; Cava, F. Chemometric analysis of bacterial peptidoglycan reveals atypical modifications that empower the cell wall against predatory enzymes and fly innate immunity. *Journal of the American Chemical Society* **2016**, *138*, 9193–9204. 10.1021/jacs.6b04430.
210. Liu, X.; Gallay, C.; Kjos, M.; Domenech, A.; Slager, J.; Kessel, S.P.; Knoops, K.; Sorg, R.A.; Zhang, J.; Veening, J. High-throughput CRISPRi phenotyping identifies new essential genes in *Streptococcus pneumoniae*. *Molecular Systems Biology* **2017**, *13*, 931. 10.15252/msb.20167449.
211. Figueiredo, T.A.; Sobral, R.G.; Ludovice, A.M.; de Almeida, J.M.F.; Bui, N.K.; Vollmer, W.; de Lencastre, H.; Tomasz, A. Identification of genetic geterminants and enzymes involved with the amidation of glutamic acid residues in the peptidoglycan of *Staphylococcus aureus*. *PLoS Pathogens* **2012**, *8*, e1002508. 10.1371/journal.ppat.1002508.
212. Yoshida, K.I.; Fujita, Y.; Ehrlich, S.D. Three asparagine synthetase genes of *Bacillus subtilis*. *Journal of Bacteriology* **1999**, *181*, 6081–6091. 10.1128/jb.181.19.6081-6091.1999.
213. Dajkovic, A.; Tesson, B.; Chauhan, S.; Courtin, P.; Keary, R.; Flores, P.; Marlière, C.; Filipe, S.R.; Chapot-Chartier, M.-P.; Carballido-Lopez, R. Hydrolysis of peptidoglycan is modulated by amidation of *meso*-diaminopimelic acid and Mg^{2+} in *Bacillus subtilis*. *Molecular Microbiology* **2017**, *104*, 972–988. 10.1111/mmi.13673.
214. Bernard, E.; Rolain, T.; Courtin, P.; Hols, P.; Chapot-Chartier, M.-P. Identification of the amidotransferase AsnB1 as being responsible for *meso*-diaminopimelic acid

amidation in *Lactobacillus plantarum* peptidoglycan. *Journal of Bacteriology* **2011**, *193*, 6323–6330. 10.1128/JB.05060-11.

215. Ammam, F.; Patin, D.; Coullon, H.; Blanot, D.; Lambert, T.; Mengin-Lecreulx, D.; Candela, T. AsnB is responsible for peptidoglycan precursor amidation in *Clostridium difficile* in the presence of vancomycin. *Microbiology* **2020**, *166*, 567–578. 10.1099/mic.0.000917.
216. Levefaudes, M.; Patin, D.; de Sousa-d'Auria, C.; Chami, M.; Blanot, D.; Hervé, M.; Arthur, M.; Houssin, C.; Mengin-Lecreulx, D. Diaminopimelic acid amidation in *Corynebacteriales*. *Journal of Biological Chemistry* **2015**, *290*, 13079–13094. 10.1074/jbc.M115.642843.
217. Ren, H.; Liu, J. AsnB is involved in natural resistance of *Mycobacterium smegmatis* to multiple drugs. *Antimicrobial Agents and Chemotherapy* **2006**, *50*, 250–255. 10.1128/AAC.50.1.250-255.2006.
218. Ngadjeua, F.; Braud, E.; Saidjalolov, S.; Iannazzo, L.; Schnappinger, D.; Ehrt, S.; Hugonnet, J.-E.; Mengin-Lecreulx, D.; Patin, D.; Ethève-Quelquejeu, M.; et al. Critical impact of peptidoglycan precursor amidation on the activity of l,d-Transpeptidases from *Enterococcus faecium* and *Mycobacterium tuberculosis*. *Chemistry - A European Journal* **2018**, *24*, 5743–5747. 10.1002/chem.201706082.
219. Radoshevich, L.; Cossart, P. *Listeria monocytogenes*: Towards a complete picture of its physiology and pathogenesis. *Nature Reviews Microbiology* **2018**, *16*, 32–46. 10.1038/nrmicro.2017.126.
220. Burke, T.P.; Loukitcheva, A.; Zemansky, J.; Wheeler, R.; Boneca, I.G.; Portnoy, D.A. *Listeria monocytogenes* is resistant to lysozyme through the regulation, not the acquisition, of cell wall-modifying enzymes. *Journal of Bacteriology* **2014**, *196*, 3756–3767. 10.1128/JB.02053-14.
221. Aubry, C.; Goulard, C.; Nahori, M.A.; Cayet, N.; Decalf, J.; Sachse, M.; Boneca, I.G.; Cossart, P.; Dussurget, O. OatA, a peptidoglycan O-acetyltransferase involved in *Listeria monocytogenes* immune escape, is critical for virulence. *Journal of Infectious Diseases* **2011**, *204*, 731–740. 10.1093/infdis/jir396.
222. Rae, C.S.; Geissler, A.; Adamson, P.C.; Portnoy, D.A. Mutations of the *Listeria monocytogenes* peptidoglycan N-Deacetylase and O-acetylase result in enhanced lysozyme sensitivity, bacteriolysis, and hyperinduction of innate immune pathways. *Infection and Immunity* **2011**, *79*, 3596–3606. 10.1128/IAI.00077-11.
223. Gründling, A.; Burrack, L.S.; Bouwer, H.G.A.; Higgins, D.E. *Listeria monocytogenes* regulates flagellar motility gene expression through MogR, a transcriptional repressor required for virulence. *Proceedings of the National Academy of Sciences* **2004**, *101*, 12318–12323. 10.1073/pnas.0404924101.
224. Edgar, R.C. MUSCLE: Multiple sequence alignment with high accuracy and high throughput. *Nucleic Acids Research* **2004**, *32*, 1792–1797. 10.1093/nar/gkh340.
225. Courtin, P.; Miranda, G.; Guillot, A.; Wessner, F.; Mézange, C.; Domakova, E.; Kulakauskas, S.; Chapot-Chartier, M.-P. Peptidoglycan structure analysis of *Lactococcus lactis* reveals the presence of an l, d-carboxypeptidase involved in peptidoglycan maturation. *Journal of Bacteriology* **2006**, *188*, 5293–5298. 10.1128/JB.00285-06.
226. Bierne, H.; Mazmanian, S.K.; Trost, M.; Pucciarelli, M.G.; Liu, G.; Dehoux, P.; Jänsch, L.; Garcia-del Portillo, F.; Schneewind, O.; Cossart, P. Inactivation of the *srtA* gene in *Listeria monocytogenes* inhibits anchoring of surface proteins and affects virulence. *Molecular Microbiology* **2002**, *43*, 869–881. 10.1046/j.1365-2958.2002.02798.x.
227. Linnett, P.E.; Strominger, J.L. Amidation and cross linking of the enzymatically synthesized peptidoglycan of *Bacillus stearothermophilus*. *Journal of Biological*

Chemistry **1974**, *249*, 2489–2496. 10.1016/s0021-9258(19)42757-9.
228. Ahn, Y.-M. Inhibition and functional characterization of glutamine-dependent asparagine synthetase. *Dissertation Thesis* **2013**, 113–119.
229. Bierne, H.; Sabet, C.; Personnic, N.; Cossart, P. Internalins: a complex family of leucine-rich repeat-containing proteins in *Listeria monocytogenes*. *Microbes and Infection* **2007**, *9*, 1156–1166. 10.1016/j.micinf.2007.05.003.
230. Gaillard, J.L.; Berche, P.; Frehel, C.; Gouln, E.; Cossart, P. Entry of *L. monocytogenes* into cells is mediated by internalin, a repeat protein reminiscent of surface antigens from gram-positive cocci. *Cell* **1991**, *65*, 1127–1141. 10.1016/0092-8674(91)90009-N.
231. Mengaud, J.; Ohayon, H.; Gounon, P.; Mege, R.M.; Cossart, P. E-cadherin is the receptor for internalin, a surface protein required for entry of *L. monocytogenes* into epithelial cells. *Cell* **1996**, *84*, 923–932. 10.1016/S0092-8674(00)81070-3.
232. Dhar, G.; Faull, K.F.; Schneewind, O. Anchor structure of cell wall surface proteins in *Listeria monocytogenes*. *Biochemistry* **2000**, *39*, 3725–3733. 10.1021/bi992347o.
233. Münch, D.; Roemer, T.; Lee, S.H.; Engeser, M.; Sahl, H.G.; Schneider, T. Identification and *in vitro* analysis of the GatD/MurT enzyme-complex catalyzing lipid II amidation in *Staphylococcus aureus*. *PLoS Pathogens* **2012**, *8*, e1002509. 10.1371/journal.ppat.1002509.
234. Callewaert, L.; Michiels, C.W. Lysozymes in the animal kingdom. *Journal of Biosciences* **2010**, *35*, 127–160. 10.1007/s12038-010-0015-5.
235. Miettinen, H.; Wirtanen, G. Prevalence and location of *Listeria monocytogenes* in farmed rainbow trout. *International Journal of Food Microbiology* **2005**, *104*, 135–143. 10.1016/j.ijfoodmicro.2005.01.013.
236. Hellström, S.; Kiviniemi, K.; Autio, T.; Korkeala, H. *Listeria monocytogenes* is common in wild birds in Helsinki region and genotypes are frequently similar with those found along the food chain. *Journal of Applied Microbiology* **2008**, *104*, 883–888. 10.1111/j.1365-2672.2007.03604.x.
237. Davis, K.M.; Weiser, J.N. Modifications to the peptidoglycan backbone help bacteria to establish infection. *Infection and Immunity* 2011, *79*, 562–570. 10.1128/IAI.00651-10.
238. Chamaillard, M.; Hashimoto, M.; Horie, Y.; Masumoto, J.; Qiu, S.; Saab, L.; Ogura, Y.; Kawasaki, A.; Fukase, K.; Kusumoto, S.; et al. An essential role for NOD1 in host recognition of bacterial peptidoglycan containing diaminopimelic acid. *Nature Immunology* **2003**, *4*, 702–707. 10.1038/ni945.
239. Girardin, S.E.; Travassos, L.H.; Hervé, M.; Blanot, D.; Boneca, I.G.; Philpott, D.J.; Sansonetti, P.J.; Mengin-Lecreulx, D. Peptidoglycan molecular requirements allowing detection by Nod1 and Nod2. *Journal of Biological Chemistry* **2003**, *278*, 41702–41708. 10.1074/jbc.M307198200.
240. Lecuit, M. Understanding how *Listeria monocytogenes* targets and crosses host barriers. *Clinical Microbiology and Infection* **2005**, *11*, 430–436. 10.1111/j.1469-0691.2005.01146.x.
241. Bierne, H.; Dramsi, S. Spatial positioning of cell wall-anchored virulence factors in Gram-positive bacteria. *Current Opinion in Microbiology* 2012, *15*, 715–723. 10.1016/j.mib.2012.10.010.
242. Nelson, K.E. Whole genome comparisons of serotype 4b and 1/2a strains of the food-borne pathogen *Listeria monocytogenes* reveal new insights into the core genome components of this species. *Nucleic Acids Research* **2004**, *32*, 2386–2395. 10.1093/nar/gkh562.
243. Cabanes, D.; Dehoux, P.; Dussurget, O.; Frangeul, L.; Cossart, P. Surface proteins and

the pathogenic potential of *Listeria monocytogenes*. *Trends in Microbiology* **2002**, *10*, 238–245. 10.1016/S0966-842X(02)02342-9.

244. Ghosh, P.; Halvorsen, E.M.; Ammendolia, D.A.; Mor-Vaknin, N.; O'Riordan, M.X.D.; Brumell, J.H.; Markovitz, D.M.; Higgins, D.E. Invasion of the brain by *Listeria monocytogenes* is mediated by InlF and host cell vimentin. *mBio* **2018**, *9*. 10.1128/mBio.00160-18.
245. Mariscotti, J.F.; Quereda, J.J.; Graciela Pucciarelli, M. Contribution of sortase A to the regulation of *Listeria monocytogenes* LPXTG surface proteins. *International Microbiology* **2012**, *15*, 43–51. 10.2436/20.1501.01.157.
246. Reis, O.; Sousa, S.; Camejo, A.; Villiers, V.; Gouin, E.; Cossart, P.; Cabanes, D. LapB, a novel *Listeria monocytogenes* LPXTG surface adhesin, required for entry into eukaryotic cells and virulence. *Journal of Infectious Diseases* **2010**, *202*, 551–562. 10.1086/654880.
247. Cabanes, D.; Sousa, S.; Cebriá, A.; Lecuit, M.; García-Del Portillo, F.; Cossart, P. Gp96 is a receptor for a novel *Listeria monocytogenes* virulence factor, Vip, a surface protein. *EMBO Journal* **2005**, *24*, 2827–2838. 10.1038/sj.emboj.7600750.
248. Personnic, N.; Bruck, S.; Nahori, M.A.; Toledo-Arana, A.; Nikitas, G.; Lecuit, M.; Dussurget, O.; Cossart, P.; Bierne, H. The stress-induced virulence protein InlH controls interleukin-6 production during murine listeriosis. *Infection and Immunity* **2010**, *78*, 1979–1989. 10.1128/IAI.01096-09.
249. Sabet, C.; Lecuit, M.; Cabanes, D.; Cossart, P.; Bierne, H. LPXTG protein InlJ, a newly identified internalin involved in *Listeria monocytogenes* virulence. *Infection and Immunity* **2005**, *73*, 6912–6922. 10.1128/IAI.73.10.6912-6922.2005.
250. Sabet, C.; Toledo-Arana, A.; Personnic, N.; Lecuit, M.; Dubrac, S.; Poupel, O.; Gouin, E.; Nahori, M.-A.; Cossart, P.; Bierne, H. The *Listeria monocytogenes* virulence factor InlJ is specifically expressed *in vivo* and behaves as an adhesin. *Infection and Immunity* **2008**, *76*, 1368–1378. 10.1128/IAI.01519-07.
251. Dortet, L.; Mostowy, S.; Samba-Louaka, A.; Gouin, E.; Nahori, M.-A.; Wiemer, E.A.C.; Dussurget, O.; Cossart, P. Recruitment of the major vault protein by InlK: a *Listeria monocytogenes* strategy to avoid autophagy. *PLoS pathogens* **2011**, *7*, e1002168. 10.1371/journal.ppat.1002168.
252. Dortet, L.; Mostowy, S.; Cossart, P. *Listeria* and autophagy escape. *Autophagy* **2012**, *8*, 132–134. 10.4161/auto.8.1.18218.
253. Janež, N.; Škrlj, B.; Sterniša, M.; Klančnik, A.; Sabotič, J. The role of the *Listeria monocytogenes* surfactome in biofilm formation. *Microbial Biotechnology* **2021**, *14*, 1269–1281. 10.1111/1751-7915.13847.
254. Popowska, M.; Krawczyk-Balska, A.; Ostrowski, R.; Desvaux, M. InlL from *Listeria monocytogenes* is involved in biofilm formation and adhesion to mucin. *Frontiers in Microbiology* **2017**, *8*, 660. 10.3389/fmicb.2017.00660.
255. Chen, B.Y.; Kim, T.J.; Jung, Y.S.; Silva, J.L. Attachment strength of *Listeria monocytogenes* and its internalin-negative mutants. *Food Biophysics* **2008**, *3*, 329–332. 10.1007/s11483-008-9090-7.
256. Nairn, B.L.; Lee, G.T.; Chumber, A.K.; Steck, P.R.; Mire, M.O.; Lima, B.P.; Herzberg, M.C. Uncovering roles of *Streptococcus gordonii* SrtA-processed proteins in the biofilm lifestyle. *Journal of Bacteriology* **2020**, *203*. 10.1128/JB.00544-20.
257. Hendrickx, A.P.A.; Willems, R.J.L.; Bonten, M.J.M.; van Schaik, W. LPxTG surface proteins of enterococci. *Trends in Microbiology* **2009**, *17*, 423–430. 10.1016/j.tim.2009.06.004.
258. Schleifer, K.H.; Kandler, O. Peptidoglycan types of bacterial cell walls and their taxonomic implications. *Bacteriological Reviews* **1972**, *36*, 407–477.

10.1128/br.36.4.407-477.1972.
259. Navarre, W.W.; Schneewind, O. Surface proteins of Gram-positive bacteria and mechanisms of their targeting to the cell wall envelope. *Microbiology and Molecular Biology Reviews* **1999**, *63*, 174–229. 10.1128/MMBR.63.1.174-229.1999.
260. Macnab, R.M. How bacteria assemble flagella. *Annual Review of Microbiology* **2003**, *57*, 77–100. 10.1146/annurev.micro.57.030502.090832.
261. Sun, L.; Rogiers, G.; Michiels, C.W. The natural antimicrobial *trans*-cinnamaldehyde interferes with UDP-N-acetylglucosamine biosynthesis and cell wall homeostasis in *Listeria monocytogenes*. *Foods* **2021**, *10*, 1666. 10.3390/foods10071666.
262. Koo, B.-M.; Kritikos, G.; Farelli, J.D.; Todor, H.; Tong, K.; Kimsey, H.; Wapinski, I.; Galardini, M.; Cabal, A.; Peters, J.M.; et al. Construction and analysis of two genome-scale deletion libraries for *Bacillus subtilis*. *Cell Systems* **2017**, *4*, 291-305.e7. 10.1016/j.cels.2016.12.013.
263. Abdelhamed, H.; Lawrence, M.L.; Karsi, A. A novel suicide plasmid for efficient gene mutation in *Listeria monocytogenes*. *Plasmid* **2015**, *81*, 1–8. 10.1016/j.plasmid.2015.05.003.
264. Abram, F.; Starr, E.; Karatzas, K.A.G.; Matlawska-Wasowska, K.; Boyd, A.; Wiedmann, M.; Boor, K.J.; Connally, D.; O'Byrne, C.P. Identification of components of the sigma B regulon in *Listeria monocytogenes* that contribute to acid and salt tolerance. *Applied and Environmental Microbiology* **2008**, *74*, 6848–6858. 10.1128/AEM.00442-08.
265. Oliver, H.F.; Orsi, R.H.; Ponnala, L.; Keich, U.; Wang, W.; Sun, Q.; Cartinhour, S.W.; Filiatrault, M.J.; Wiedmann, M.; Boor, K.J. Deep RNA sequencing of *L. monocytogenes* reveals overlapping and extensive stationary phase and sigma B-dependent transcriptomes, including multiple highly transcribed noncoding RNAs. *BMC Genomics* **2009**, *10*, 641. 10.1186/1471-2164-10-641.
266. Liu, Y.; Orsi, R.H.; Gaballa, A.; Wiedmann, M.; Boor, K.J.; Guariglia-Oropeza, V. Systematic review of the *Listeria monocytogenes* σ B regulon supports a role in stress response, virulence and metabolism. *Future Microbiology* **2019**, *14*, 801–828. 10.2217/fmb-2019-0072.
267. Cortes, B.W.; Naditz, A.L.; Anast, J.M.; Schmitz-Esser, S. Transcriptome sequencing of *Listeria monocytogenes* reveals major gene expression changes in response to lactic acid stress exposure but a less pronounced response to oxidative stress. *Frontiers in Microbiology* **2020**, *10*, 3110. 10.3389/fmicb.2019.03110.
268. Schaur, R.J.; Siems, W.; Bresgen, N.; Eckl, P.M. 4-hydroxy-nonenal-A bioactive lipid peroxidation product. *Biomolecules* **2015**, *5*, 2247–337. 10.3390/biom5042247.
269. Tabakh, H.; McFarland, A.P.; Thomason, M.K.; Pollock, A.J.; Glover, R.C.; Zaver, S.A.; Woodward, J.J. 4-hydroxy-2-nonenal antimicrobial toxicity is neutralized by an intracellular pathogen. *eLife* **2021**, *10*. 10.7554/eLife.59295.
270. Esterbauer, H.; Schaur, R.J.; Zollner, H. Chemistry and biochemistry of 4-hydroxynonenal, malonaldehyde and related aldehydes. *Free Radical Biology and Medicine* **1991**, *11*, 81–128. 10.1016/0891-5849(91)90192-6.
271. LoPachin, R.M.; Gavin, T.; Petersen, D.R.; Barber, D.S. Molecular mechanisms of 4-hydroxy-2-nonenal and acrolein toxicity: Nucleophilic targets and adduct formation. *Chemical Research in Toxicology* **2009**, *22*, 1499–1508. 10.1021/tx900147g.
272. Toogood, H.S.; Scrutton, N.S. Discovery, characterization, engineering, and applications of ene-reductases for industrial biocatalysis. *ACS Catalysis* **2018**, *8*, 3532–3549. 10.1021/acscatal.8b00624.
273. Reich, S.; Nestl, B.M.; Hauer, B. Loop-grafted Old Yellow Enzymes in the bienzymatic cascade reduction of allylic alcohols. *ChemBioChem* **2016**, *17*, 561–565.

10.1002/cbic.201500604.
274. Kumar Roy, T.; Sreedharan, R.; Ghosh, P.; Gandhi, T.; Maiti, D. Ene-reductase: A multifaceted biocatalyst in organic synthesis. *Chemistry – A European Journal* **2022**, *28*, e202103949. 10.1002/chem.202103949.
275. Kavanagh, K.L.; Jörnvall, H.; Persson, B.; Oppermann, U. Medium- and short-chain dehydrogenase/reductase gene and protein families. *Cellular and Molecular Life Sciences* **2008**, *65*, 3895. 10.1007/s00018-008-8588-y.
276. Lu, S.; Wang, J.; Chitsaz, F.; Derbyshire, M.K.; Geer, R.C.; Gonzales, N.R.; Gwadz, M.; Hurwitz, D.I.; Marchler, G.H.; Song, J.S.; et al. CDD/SPARCLE: the conserved domain database in 2020. *Nucleic Acids Research* **2020**, *48*, D265–D268. 10.1093/nar/gkz991.
277. Kim, H.; Chaurasia, A.K.; Kim, T.; Choi, J.; Ha, S.C.; Kim, D.; Kim, K.K. Structural and functional study of ChuY from *Escherichia coli* strain CFT073. *Biochemical and Biophysical Research Communications* **2017**, *482*, 1176–1182. 10.1016/j.bbrc.2016.12.008.
278. LaMattina, J.W.; Delrossi, M.; Uy, K.G.; Keul, N.D.; Nix, D.B.; Neelam, A.R.; Lanzilotta, W.N. Anaerobic heme degradation: ChuY is an anaerobilin reductase that exhibits kinetic cooperativity. *Biochemistry* **2017**, *56*, 845–855. 10.1021/acs.biochem.6b01099.
279. Nagata, N.; Tanaka, R.; Satoh, S.; Tanaka, A. Identification of a vinyl reductase gene for chlorophyll synthesis in *Arabidopsis thaliana* and implications for the evolution of *Prochlorococcus* species. *The Plant Cell* **2005**, *17*, 233–240. 10.1105/tpc.104.027276.
280. Chew, A.G.M.; Bryant, D.A. Characterization of a plant-like protochlorophyllide a divinyl reductase in green sulfur bacteria. *Journal of Biological Chemistry* **2007**, *282*, 2967–2975. 10.1074/jbc.M609730200.
281. Zhang, Y. TM-align: a protein structure alignment algorithm based on the TM-score. *Nucleic Acids Research* **2005**, *33*, 2302–2309. 10.1093/nar/gki524.
282. Duong, T.; Park, K.; Kim, T.; Kang, S.W.; Hahn, M.J.; Hwang, H.-Y.; Kim, K.K. Structural and functional characterization of an Isd-type haem-degradation enzyme from *Listeria monocytogenes*. *Acta Crystallographica Section D Biological Crystallography* **2014**, *70*, 615–626. 10.1107/S1399004713030794.
283. Filling, C.; Berndt, K.D.; Benach, J.; Knapp, S.; Prozorovski, T.; Nordling, E.; Ladenstein, R.; Jörnvall, H.; Oppermann, U. Critical residues for structure and catalysis in short-chain dehydrogenases/reductases. *Journal of Biological Chemistry* **2002**, *277*, 25677–25684. 10.1074/jbc.M202160200.
284. Contente, M.L.; Zambelli, P.; Galafassi, S.; Tamborini, L.; Pinto, A.; Conti, P.; Molinari, F.; Romano, D. A new chemoenzymatic approach to the synthesis of Latanoprost and Bimatoprost. *Journal of Molecular Catalysis B: Enzymatic* **2015**, *114*, 7–12. 10.1016/j.molcatb.2014.05.022.
285. Waller, J.; Toogood, H.S.; Karuppiah, V.; Rattray, N.J.W.; Mansell, D.J.; Leys, D.; Gardiner, J.M.; Fryszkowska, A.; Ahmed, S.T.; Bandichhor, R.; et al. Structural insights into the ene-reductase synthesis of profens. *Organic & Biomolecular Chemistry* **2017**, *15*, 4440–4448. 10.1039/C7OB00163K.
286. Shreaz, S.; Wani, W.A.; Behbehani, J.M.; Raja, V.; Irshad, M.; Karched, M.; Ali, I.; Siddiqi, W.A.; Hun, L.T. Cinnamaldehyde and its derivatives, a novel class of antifungal agents. *Fitoterapia* **2016**, *112*, 116–131. 10.1016/j.fitote.2016.05.016.
287. European Food Safety Authority Flavouring Group Evaluation 214: alpha,beta-unsaturated aldehydes and precursors from chemical subgroup 3.1 of FGE.19: Cinnamyl derivatives[1]. *The EFSA Journal* **2009**, 1–27. https://doi.org/10.2903/j.efsa.2009.880.

288. Smith, C.K.; Moore, C.A.; Elahi, E.N.; Smart, A.T.S.; Hotchkiss, S.A.M. Human skin absorption and metabolism of the contact allergens, cinnamic aldehyde, and cinnamic alcohol. *Toxicology and Applied Pharmacology* **2000**, *168*, 189–199. 10.1006/taap.2000.9025.
289. Bickers, D.; Calow, P.; Greim, H.; Hanifin, J.M.; Rogers, A.E.; Saurat, J.H.; Sipes, I.G.; Smith, R.L.; Tagami, H. A toxicologic and dermatologic assessment of cinnamyl alcohol, cinnamaldehyde and cinnamic acid when used as fragrance ingredients. *Food and Chemical Toxicology* **2005**, *43*, 799–836. 10.1016/j.fct.2004.09.013.
290. Yuan, J.H.; Dieter, M.P.; Bucher, J.R.; Jameson, C.W. Toxicokinetics of cinnamaldehyde in F344 rats. *Food and Chemical Toxicology* **1992**, *30*, 997–1004. https://doi.org/10.1016/0278-6915(92)90109-X.
291. Honma, M.; Yamada, M.; Yasui, M.; Horibata, K.; Sugiyama, K.; Masumura, K. *In vivo* and *in vitro* mutagenicity of perillaldehyde and cinnamaldehyde. *Genes and Environment* **2021**, *43*, 30. 10.1186/s41021-021-00204-3.
292. National Toxicology Program NTP toxicology and carcinogenesis studies of *trans*-cinnamaldehyde (CAS No. 14371-10-9) in F344/N rats and B6C3F1 mice (feed studies). *National Toxicology Program technical report series* **2004**, 1–281.

Curriculum

Lei Sun

Birth Date: January 1992
Address: Tervuursevest 119/00/11, 3001 Leuven, Belgium
Mobile:+8613872898639
Email: lei.sun@kuleuven.be

EDUCATION

09/2017-	Doctoral training in Laboratory of Food Microbiology, Bioscience Engineering Faculty, ***KU Leuven***, Leuven, Belgium **Ph.D. Thesis**: Isolation and Characterization of Mutants with Altered Sensitivity to the Natural Antimicrobial *trans*-Cinnamaldehyde in *Listeria monocytogenes* **Promoter**: **Prof**. Dr. Ir. Chris Michaels, email: chris.michiels@kuleuven.be
09/2016-09/2017	Internship in Stem Cell Institute, ***KU Leuven***, Leuven, Belgium **Supervisor: Prof**. Dr. Kian Peng Koh, email: kian.koh@med.kuleuven.be
09/2015-07/2016	Master of Biochemical Engineering, ***KU Leuven***, Leuven, Belgium Master thesis performed at Stem Cell Institute, ***KU Leuven***, Leuven, Belgium **Supervisor**: **Prof**. Dr. Inge Holsbeeks, email: inge.holsbeeks@kuleuven.be **Co-supervisor**: **Prof**. Dr. Kian Peng Koh, email: kian.koh@med.kuleuven.be Grades: 75%, cum laude
09/2013-07/2015	Bachelor of Chemical Engineering, ***KU Leuven***, Leuven, Belgium Grade: cum laude (Results: 75%; efficiency: 100%).
09/2011-07/2015	Bachelor of Biology Engineering, ***Southwestern Jiaotong University***, Chengdu, P.R.China GPA: 3.85; average grade: 88.59, top 1%.

RESEARCH EXPERIENCE

09/2017- Doctoral training, Laboratory of Food Microbiology, ***KU Leuven***, Belgium

- Investigated the antimicrobial mechanisms of natural essential oil constituents against foodborne pathogens by screening a self-constructed transposon mutant library to obtain sensitive mutants;
- Genetically characterized multiple *trans*-cinnamaldehyde sensitive mutants of *Listeria monocytogenes* at the molecular level;
- Characterized *trans*-cinnamaldehyde resistant mutants of *Listeria monocytogenes* generated from the evolutionary experiments at the genetic and molecular level;
- Identify an unprecedented oxidoreductase that was manifested to metabolize a bunch of natural compounds with α,β-unsaturated aldehyde moiety with the recombinant protein from *Escherichia coli*.

09/2016-09/2017	Internship, Stem Cell Institute, ***KU Leuven***, Belgium ➢ Performed mouse breeding, mouse embryo dissections, mouse stem cell cultivation, and some experiments in molecular biology.
09/2015-07/2016	Master thesis project, Stem Cell Institute, ***KU Leuven***, Belgium Topic: The interaction of master transcriptional factors with *Tet1 cis*-regulatory elements. ➢ Examined the interaction of Oct4 and Sox2 transcriptional factors with *Tet1 cis*-regulating elements by dual-luciferase assay and Tet-Off gene expression system; ➢ Utilized Crispr-Cas9 technique to specifically delete *Tet1 cis*-regulating elements in mouse embryonic stem cells.
10/2014-06/2015	EE5 Project, Faculty of Engineering Technology, ***KU Leuven***, Belgium Project: Optimizing anaerobic bio-hydrogen fermentation process with *Clostridium acetobutylicum*. ➢ Maintained the hydrogen production with a self-designed small-scale multifunctional fermenter utilizing *Clostridium acetobutylicum*; ➢ Optimized the fermentation process and fermenter design for an escalated hydrogen yield and production efficiency.
01/2013-05/2014	EE4 Project, Faculty of Engineering Technology, ***KU Leuven***, Belgium Project: Optimizing enzyme-catalyzed starch to the glucose conversion process. ➢ Determined the enzyme kinetics of amyloglucosidase to improve the biotransformation efficiency of starch to glucose; ➢ Optimized a small-scale starch to glucose biotransformation system.
10/2012-05/2013	Student research training program, ***Southwestern Jiaotong University***, P.R.China Project: Exploring an efficient system to detect sewer oil with gas chromatography. ➢ Acquired the know-how on gas chromatography and high-performance liquid chromatography; ➢ Sewer oil components analysis (chemical reactions, gas chromatography, and high-performance liquid chromatography) to design a fast and efficient system to identify sewer oil.

SCIENTIFIC SKILLS

Research abilities:

- Molecular cloning, bacteria transposon mutant library construction, recombinant protein production and purification, SDS-PAGE, RT-qPCR, ChIP-qPCR, Western blot, and Crispr-Cas9 technique;
- Bacteria cultivation and manipulation, mouse embryonic stem cells culture and manipulation, mouse embryo dissection techniques, and sufficient animal working experience;
- Microbial whole-genome sequencing library preps and analysis, RNA-seq analysis;
- Programming skills: R (basic), Linux Shell (basic);
- Excellent scientific writing skills.

Computer skill:

- Statistical software: GraphPad, MATLAB, Maple
- Microsoft Office

Language:

- Mother language: Chinese
- English: good (2-year bachelor's, 1-year master and 4-year doctoral training in English)

HONORS

2020-2021	Ph.D. Scholarship, ***KU Leuven***, Belgium
2016-2020	Ph.D. Scholarship, **Chinese Scholarship Council**, P.R.China
2013-2016	Hongzhi Scholarship, ***KU Leuven***, Belgium
2013	National Scholarship of China, ***Southwestern Jiaotong University***, P.R.Ch
2011-2013	First Class Scholarship of School four times in a row, ***Southwestern Jiaoto University***, P.R.China

CONFERENCES

Lei Sun, Maarten Goedseels, Gil Rogiers, Chris Michiels. “Transposon mutagenesis and laboratory evolution to investigate the mode of action of *trans*-cinnamaldehyde against *Lis monocytogenes*.” Poster presentation at the 26th International ICFMH Conference (FoodM 2018) in Berlin, Germany.

Lei Sun, Maarten Goedseels, Gil Rogiers, Chris Michiels. “Transposon mutagenesis and laboratory evolution to investigate the mode of action of *trans*-cinnamaldehyde against *Lis monocytogenes*.” Poster presentation **at** the 24th National Symposium for Applied Biologi Sciences (NSABS 2019) in Ghent, Belgium.

PUBLICATIONS

Sun, L., Rogiers, G., Courtin, P., Chapot-Chartier, M-P., Bierne, H., Michiels, C.W. (2021) Mediates Amidation of *Meso*-Diaminopimelic Acid Residues in the Peptidoglycan of *Listeri monocytogenes* and Affects Bacterial Surface Properties and Host Cell Invasion. *FRONTI MICROBIOLOGY*, *12*, Art.No. ARTN 760253. DOI: 10.3389/fmicb.2021.760253

Sun, L., Rogiers, G., Michiels, C.W. (2021). The Natural Antimicrobial *trans*-Cinnamaldehyde Interferes with UDP-N-Acetylglucosamine Biosynthesis and Cell Wall Homeostasis in *Listeria monocytogenes*. *FOODS*, *10* (7), Art.No. ARTN 1666. DOI: 10.3390/foods10071666

Luo, X., van der Veer, B., **Sun, L.**, Bartoccetti, M., Boretto, M., Vankelecom, H., Khoueiry, R., Koh, K.P. (2020). Coordination of germ-layer lineage choice by TET1 during primed pluripotency. *Genes & Development*, *34(7-8)*, 598-618. DOI: 10.1101/gad.329474.119

Publications

Sun, L., Rogiers, G., Courtin, P., Chapot-Chartier, M-P., Bierne, H., Michiels, C.W. (2021). AsnB Mediates Amidation of Meso-Diaminopimelic Acid Residues in the Peptidoglycan of Listeria monocytogenes and Affects Bacterial Surface Properties and Host Cell Invasion. *FRONTIERS IN MICROBIOLOGY*, *12*, Art.No. ARTN 760253. doi: 10.3389/fmicb.2021.760253

Sun, L., Rogiers, G., Michiels, C.W. (2021). The Natural Antimicrobial trans-Cinnamaldehyde Interferes with UDP-N-Acetylglucosamine Biosynthesis and Cell Wall Homeostasis in Listeria monocytogenes. *FOODS*, *10* (7), Art.No. ARTN 1666. doi: 10.3390/foods10071666

Luo, X., van der Veer, B., Sun, L., Bartoccetti, M., Boretto, M., Vankelecom, H., Khoueiry, R., Koh, K.P. (2020). Coordination of germ-layer lineage choice by TET1 during primed pluripotency. *Genes & Development*, *34(7-8)*, 598-618. doi: 10.1101/gad.329474.119